

England, Jennifer Katherine (2005) *Calcium carbonate biomineralisation in disparate systems - common mechanisms?*

PhD thesis

<http://theses.gla.ac.uk/4024/>

Copyright and moral rights for this thesis are retained by the author

A copy can be downloaded for personal non-commercial research or study, without prior permission or charge

This thesis cannot be reproduced or quoted extensively from without first obtaining permission in writing from the Author

The content must not be changed in any way or sold commercially in any format or medium without the formal permission of the Author

When referring to this work, full bibliographic details including the author, title, awarding institution and date of the thesis must be given

Calcium Carbonate Biomineralisation in Disparate Systems - Common Mechanisms?

Jennifer Katherine England

A thesis submitted for the degree of Doctor of Philosophy

Division of Earth Sciences, Centre for Geosciences,
University of Glasgow

March 2005

© Jennifer England 2005

Abstract

Biominerals are composite materials in which organic components control mineral nucleation and structure. Calcium minerals account for over 50% of biominerals, with calcium carbonate being the most common type.

This study considers the extent to which four calcium carbonate biomineral systems share common characteristics. Within the sample set, there is a range of ultrastructures and two types of calcium carbonate polymorph (calcite and aragonite). The mini survey includes three invertebrate systems: two members of the Phylum Brachiopoda; the articulated brachiopod *Terebratulina retusa* (Subphylum Rhynchonelliformea) and the inarticulated brachiopod *Novocrania anomala* (Subphylum Craniiformea), and a member of the Mollusca, the bivalve *Mytilus edulis*. The fourth, outlying vertebrate system, is the eggshell of the domestic fowl, *Gallus gallus*.

The minor element composition of each of the four systems is considered in the context of mineral ultrastructure. The shell of *T. retusa* comprises two layers; a primary layer of acicular calcite and an underlying secondary layer composed of calcite fibres. In thin section, a variation between the upper and lower portions of the secondary layer is evident. The concentration of magnesium, sulphur and strontium are significantly greater in the primary layer of the shell. Magnesium concentration also differs between the upper and lower regions of the secondary layer with higher concentration in the upper portion of the secondary layer.

The shell of *N. anomala* consists of two layers; a primary layer of acicular calcite and a secondary layer of calcite semi-nacre. *N. anomala* has a high magnesium calcite shell. The concentration of minor elements does not differ significantly between the primary and secondary layers.

Two calcium carbonate polymorphs occur in the *M. edulis* shell with an outer calcite layer and an inner aragonite layer. Magnesium concentration is higher in the calcite layer while strontium concentrations are greater in the aragonite layer. Sodium concentration gradually decreases across the calcite layer from the outer surface to the calcite/aragonite boundary and increases in the aragonite layer.

The eggshell of *G. gallus* contains shell membranes, mammillary caps, a palisade layer, a vertical crystal layer and an outer organic cuticle. The concentration of magnesium is high

in the mammillary caps, and decreases as the mammillary caps fuse and then gradually increases through the palisade and vertical crystal layers to the outer cuticle. The concentration of phosphorus and potassium is low in the mammillary caps and gradually increases through the shell to reach maximum concentration in the cuticle.

Variation in the concentration of minor elements in the shells of *T. retusa* and *N. anomala* do not relate to changes in mineral ultrastructure. Differences in shell chemistry between these two brachiopods may be related to differences in physiology. The principal control on the distribution of minor elements in *M. edulis* is crystal structure. In *G. gallus* the concentration of minor elements changes as ultrastructure changes. However, ultrastructure is unlikely to be the main control on shell chemistry, as abrupt changes in shell ultrastructure contrast to gradual changes in element distribution throughout the shell. While there may be similarities in the mechanisms controlling the minor element composition between some systems e.g. the extent to which some organisms control the ionic composition of the mineralising medium, there does not appear to be a common principal mechanism that governs the chemical composition of these four biominerals.

To some extent, more unity is evident in the biochemical characteristics of the organic matrix that are common to the four systems. The soluble organic matrices of the shells all contain small, acidic proteins. The amino acid composition of the four systems also displays some similarities such as a high glycine concentration. In each case, sulphated sugars are also associated with the soluble organic matrix.

Closer examination of the organic components reveals that the protein profiles are different in each of the four systems.

Acknowledgments

I am extremely grateful to the Engineering and Physical Sciences Research Council for funding for this three year studentship (Grant number GR/R23107/01).

I would firstly like to thank Dr. Maggie Cusack for her help, support and guidance over the past three years and Dr. Martin Lee for his advice and encouragement. I am indebted to Sandra Tierney who has not only provided me with exceptional technical knowledge but has been a great friend. A special thankyou is required for Robert McDonald for his assistance with EPMA and SEM, Kenny Roberts for his help with IT, Bill Higgison for assistance with XRD and John Gilleece for preparation of samples. Many thanks to Eddie for driving myself and Big Dave to Oban to collect brachiopods. I am also grateful to the crew of the RV Calanus for their assistance with brachiopod collection and making me welcome on board. I would also like to thank Dr Rob Martin and Dr Paul Edwards from the Department of Physics, University of Strathclyde for their advice on CL spectroscopy.

I would like to thank the late Sir Alwyn Williams FRS, FRSE for his help and guidance with interpretation of brachiopod shell structure.

I am extremely grateful to all the postgraduates for keeping me sane, in particular to Sarah and Davie for being good friends over the last three years. A special thankyou goes to Liz Campbell for her friendship and enthusiasm for running 10K races and to Big Dave for being a bad influence (RC now). Thanks also to Wolfie for being a great friend and listener.

Finally and most importantly I would like to thank my Mum, Dad and Bob for their love, support and encouragement.

Declaration

The material presented in this thesis summarises the results of three years of independent research carried out in the Division of Earth Sciences, University of Glasgow. The research was supervised by Dr. Maggie Cusack (University of Glasgow) and Dr. Martin Lee (University of Glasgow).

This thesis is a result of my own research and any published or unpublished work of other researchers has been given full acknowledgment in the text.

Jennifer K England

Jennifer K. England

March 2005

Table of Contents

	Page
Abstract	i
Acknowledgments	iii
Declaration	iv
Table of contents	v
List of Figures	ix
List of Tables	xiv

Chapter 1 Introduction

1.1	Introduction	1
1.2	Biominerals	1
1.2.1	<i>Inorganic Composition</i>	2
1.2.2	<i>Organic Composition</i>	3
1.2.3	<i>Biominalisation Mechanisms</i>	4
1.3	Emergence and Early Evolution of Biominerals	5
1.4	Aims of the Study	6
1.5	The Four Biomineral Systems	7
1.5.1	<i>Terebratulina retusa</i>	7
1.5.2	<i>Novocrania anomala</i>	8
1.5.3	<i>Mytilus edulis</i>	9
1.5.4	<i>Avian Eggshell (Gallus gallus)</i>	10

Chapter 2 Materials and Methods

2.1	Materials	12
2.2	Sample Collection and Preparation	12
2.3	X-ray Diffraction (XRD)	13
2.4	Examination of Shell Ultrastructure	13
2.5	Thin Section Preparation	13
2.6	Minor Element Analysis	14
2.6.1	<i>Sample Preparation</i>	14
2.6.2	<i>Electron Microprobe Analysis</i>	14
2.6.3	<i>Element Mapping</i>	16
2.6.4	<i>Cathodoluminescence (CL) Microscopy</i>	17
2.6.5	<i>Cathodoluminescence (CL) Spectroscopy</i>	17

2.7	Determination of Total Organic Concentration and Distribution	17
2.7.1	<i>Loss On Ignition</i>	17
2.7.2	<i>Scanning Electron Microscope Backscatter (BSE) Imaging</i>	18
2.8	Extraction, purification and visualisation of shell protein	18
2.8.1	<i>Extraction of intercrystalline protein</i>	18
2.8.2	<i>Extraction of intracrystalline protein</i>	18
2.8.3	<i>Purification of intercrystalline and intracrystalline protein</i>	19
2.8.4	<i>Sodium dodecyl sulphate polyacrylamide gel electrophoresis (SDS PAGE)</i>	19
2.8.5	<i>Coomassie Brilliant Blue Staining</i>	22
2.8.6	<i>Silver Staining</i>	22
2.8.7	<i>Acridine Orange Staining</i>	22
2.88	<i>Isoelectric Focusing (IEF)</i>	22
2.9	Amino Acid Analysis	23
2.9.1	<i>Manual Hydrolysis</i>	24
2.9.2	<i>Amino Acid Analysis</i>	24
2.9.3	<i>Summary of Steps for Amino Acid Analysis</i>	24
2.10	N-terminal Sequencing	25
2.10.1	<i>Transfer of Protein to Problott Membrane</i>	25
2.10.2	<i>N-terminal Sequencing</i>	25
2.11	Calcium Carbonate Crystal Growth	26
2.11.1	<i>Kitano Protocol</i>	26
2.11.2	<i>Calcite Grown in the Presence of Protein Extract</i>	27

Chapter 3 Ultrastructure and Minor Element Concentration

3.1	Introduction	28
3.2	Previous Work	29
3.2.1	<i>Magnesium</i>	29
3.2.2	<i>Strontium</i>	31
3.2.3	<i>Cathodoluminescence</i>	32
3.3	Results	34
3.3.1	<i>Terebratulina retusa Ultrastructure and Minor Elements</i>	34
3.3.1.1	Ultrastructure	34
3.3.1.2	Minor Element Composition-Electron Microprobe Analysis	34
3.3.1.3	Cathodoluminescence Spectroscopy	46
3.3.2	<i>Novocrania anomala Ultrastructure and Minor Elements</i>	47
3.3.2.1	Ultrastructure	47

3.3.2.2 Minor Element Composition-Electron Microprobe Analysis	50
3.3.2.3 Cathodoluminescence Imaging and Spectroscopy	57
3.3.3 <i>Mytilus edulis Ultrastructure and Minor Elements</i>	59
3.3.3.1 Ultrastructure	59
3.3.3.1 Minor Element Composition-Electron Microprobe Analysis	63
3.3.3.3 Cathodoluminescence Imaging and Spectroscopy	69
3.3.4 <i>Avian Eggshell (Gallus gallus) Ultrastructure and Minor Elements</i>	71
3.3.4.1 Ultrastructure	71
3.3.4.2 Minor Element Composition-Electron Microprobe Analysis	74
3.3.4.3 Cathodoluminescence Microscopy and Cathodoluminescence Spectroscopy	79
3.4 Discussion	81
3.4.1 <i>Terebratulina retusa and Novocrania anomala</i>	81
3.4.2 <i>Mytilus edulis</i>	85
3.4.3 <i>Eggshell (Gallus gallus)</i>	86
 Chapter 4 Organic Matrix Composition	
4.1 Introduction	88
4.2 Previous Work	89
4.2.1 <i>Organic Matrix Structure and Control of the Mineral Phase</i>	89
4.2.2 <i>Insoluble Matrix Composition</i>	90
4.2.3 <i>Soluble Matrix Composition</i>	91
4.3 Results	93
4.3.1 <i>Concentration and Distribution of Organic Matrix</i>	93
4.3.2 <i>Molecular Weight of Intercrystalline and Intracrystalline Proteins</i>	95
4.3.3 <i>Protein Charge</i>	101
4.3.4 <i>Organic Sulphate</i>	102
4.3.5 <i>Distribution of amino acids in T. retusa, N. anomala, M. edulis and G. gallus</i>	107
4.3.6 <i>N-Terminal Sequencing</i>	116
4.3.7 <i>Calcite Growth in the Presence of Intracrystalline Proteins</i>	116
4.4 Discussion	123
4.4.1 <i>Intercrystalline and intracrystalline organic matrix composition</i>	123
4.4.1.1 Comparison of the intercrystalline and intracrystalline organic matrix of <i>T. retusa, N. anomala, M. edulis</i> and the avian eggshell (<i>G. gallus</i>)	123
4.4.2 <i>Organic Matrix Carbohydrate</i>	127

Chapter 5 Discussion and Further Work

5.1	Aims of the Study	130
5.2	The Four Biomineral Systems	130
5.2.1	<i>Mineral Ultrastructure and Polymorph Type</i>	131
5.3	Minor Element Concentration and Distribution in Relation to Mineral Ultrastructure	131
5.4	Minor Element Distribution in Relation to the Distribution of Organic Matrix	136
5.5	Organic Matrix Composition	136
5.6	Calcium Carbonate Biomineralisation in Disparate Systems-Common Mechanisms?	137
5.8	Suggestions for Further Work	139

References

Appendices

Appendix A	Materials	xvi
Appendix B	Electron microprobe data	xvii
Appendix C	Gel protein data	xlvi

List of Figures

		Page
Figure 1.1	Specimen of the articulated brachiopod <i>Terebratulina retusa</i> collected from the Firth of Lorne, NW Scotland	8
Figure 1.2	Dorsal valve of a specimen of the inarticulated brachiopod <i>Novocrania anomala</i>	9
Figure 1.3	Interior of specimen of the Bivalve Mollusc <i>Mytilus edulis</i>	10
Figure 1.4 (a)	Eggshell formation in the domestic fowl <i>Gallus gallus</i>	11
Figure 1.4 (b)	Cross-section of the eggshell of <i>G. gallus</i>	
Figure 2.1	Plot of concentration of Na against percentage error for <i>N. anomala</i> electron microprobe analyses	16
Figure 2.2	Calibration curve of electrophoretic mobility as a function of the log molecular weight of proteins of known molecular weight	21
Figure 2.3	Edman degradation chemistry	26
Figure 3.1	Secondary electron image of the primary (PL) and secondary (SL) layers of <i>Terebratulina retusa</i>	35
Figure 3.2	Secondary electron image of the primary (PL) and secondary (SL) layers of <i>Terebratulina retusa</i>	35
Figure 3.3	Secondary electron image of the secondary layer fibres of <i>Terebratulina retusa</i>	36
Figure 3.4	Plane-polarised transmitted light image of <i>Terebratulina retusa</i> in thin section	36
Figure 3.5	Cross-polarised light image of <i>Terebratulina retusa</i> thin section	37
Figure 3.6 (a-c)	Electron microprobe spot analyses across three specimens of <i>Terebratulina retusa</i>	40
Figure 3.7 (a-e)	Boxplots of element concentration in the primary and secondary layers of <i>T. retusa</i>	41

Figure 3.8 (a-j)	Scatter plots of element concentration in the primary and secondary layers of <i>Terebratulina retusa</i>	43
Figure 3.9 (a-d)	X-ray maps of element concentration in <i>Terebratulina retusa</i> acquired by SEM	44
Figure 3.10 (a-c)	X-ray maps of element concentration in <i>Terebratulina retusa</i> acquired by electron probe	45
Figure 3.11(a)	Hyperspectral image showing the intensity and wavelength of CL emission from a specimen of <i>Terebratulina retusa</i>	46
Figure 3.11 (b)	CL emission spectrum acquired from <i>Terebratulina retusa</i>	46
Figure 3.12	Secondary electron image of primary (PL) and secondary (SL) layers of <i>Novocrania anomala</i>	48
Figure 3.13	Secondary electron image of the inner surface of the shell of <i>Novocrania anomala</i>	48
Figure 3.14	Secondary electron image of screw dislocations in the secondary layer of <i>Novocrania anomala</i>	49
Figure 3.15	Transmitted light image of <i>Novocrania anomala</i> in thin section	49
Figure 3.16 (a-c)	Electron microprobe spot analyses across the shell of <i>Novocrania anomala</i>	52
Figure 3.17 (a-e)	Boxplots of element concentration in the primary and secondary layers of <i>Novocrania anomala</i>	53
Figure 3.18 (a-j)	Scatter plots of element concentration in the primary and secondary layers of <i>Novocrania anomala</i>	55
Figure 3.19	X-ray maps of element concentration in <i>Novocrania anomala</i>	56
Figure 3.20	Cathodoluminescence image of <i>Novocrania anomala</i>	57
Figure 3.21 (a)	Hyperspectral image showing the intensity and wavelength of CL emission from a specimen of <i>Novocrania anomala</i>	58
Figure 3.21 (b)	CL emission spectrum acquired from <i>Novocrania anomala</i>	58
Figure 3.22	The periostracum (P), prismatic calcite layer (PC) and aragonite layer (A) of a specimen of <i>Mytilus edulis</i>	60

Figure 3.23	The prismatic calcite layer of <i>Mytilus edulis</i>	60
Figure 3.24	Boundary between the prismatic calcite layer (PC) and aragonite layer (A) in <i>Mytilus edulis</i>	61
Figure 3.25	Aragonite layer of a specimen of <i>Mytilus edulis</i>	61
Figure 3.26	Transmitted light image of <i>Mytilus edulis</i> in thin section	62
Figure 3.27	Cross-polarised light image of <i>Mytilus edulis</i> in thin section	62
Figure 3.28	Electron microprobe spot analyses of <i>Mytilus edulis</i>	66
Figure 3.29	Scatterplots of element concentration in <i>Mytilus edulis</i>	67
Figure 3.30	X-ray maps of element distribution in a specimen of <i>Mytilus edulis</i>	68
Figure 3.31	Cathodoluminescence image of a specimen of <i>Mytilus edulis</i>	69
Figure 3.32 (a)	Map of cathodoluminescence emission from a specimen of <i>Mytilus edulis</i>	70
Figure 3.32 (b)	Cathodoluminescence spectra from the calcite and aragonite layers of <i>M. edulis</i>	70
Figure 3.33	Secondary electron image of a section through a specimen of an avian eggshell (<i>Gallus gallus</i>)	72
Figure 3.34	Secondary electron image of the membrane fibres covering the base of the mammillary caps in an avian eggshell (<i>Gallus gallus</i>)	72
Figure 3.35	Secondary electron image of the mammillary caps in a specimen of an avian eggshell (<i>Gallus gallus</i>)	73
Figure 3.36	Secondary electron image of the mammillary caps displaying a normal growth pattern (MC) and Type B mammillary bodies (B)	73
Figure 3.37 (a & b)	Electron microprobe spot analyses across the avian eggshell	76
Figure 3.38	Scatterplots of element concentration in the avian eggshell (<i>Gallus gallus</i>)	77
Figure 3.39	X-ray maps of element concentration in an avian eggshell	78

	(<i>Gallus gallus</i>)	
Figure 3.40	Optical CL image of a specimen of the avian eggshell (<i>Gallus gallus</i>)	79
Figure 3.41 (a)	Map of cathodoluminescence emission from a specimen of an eggshell (<i>Gallus gallus</i>),	80
Figure 3.41 (b)	Spectrum of luminescence emission from an eggshell (<i>Gallus gallus</i>)	80
Figure 4.1	Backscattered electron images of <i>T. retusa</i> , <i>N. anomala</i> , <i>M. edulis</i> and the <i>G. gallus</i>	95
Figure 4.2	Silver stained, 15% polyacrylamide gel of the intercrystalline and intracrystalline protein fractions of <i>T. retusa</i>	96
Figure 4.3	Silver stained, 15% polyacrylamide gel of the intercrystalline and intracrystalline protein fractions extracted from <i>N. anomala</i>	97
Figure 4.4	Silver stained, 15% polyacrylamide gel of the intercrystalline and intracrystalline protein fractions of <i>M. edulis</i>	98
Figure 4.5	Coomassie Blue stained, 20% polyacrylamide gel of protein within the extrapallial fluid of <i>M. edulis</i>	99
Figure 4.6	Silver stained, 15% polyacrylamide gel of eggshell (<i>Gallus gallus</i>) intracrystalline protein	100
Figure 4.7	Intracrystalline proteins separated by isoelectric focusing	101
Figure 4.8	Acridine Orange stained, 15% polyacrylamide gel of <i>T. retusa</i> intercrystalline and intracrystalline protein fractions	103
Figure 4.9	Acridine Orange stained, 15% polyacrylamide gel of <i>N. anomala</i> intracrystalline protein fraction	104
Figure 4.10	Acridine orange stained, 10% polyacrylamide gel of <i>M. edulis</i> intracrystalline fraction	105
Figure 4.11	Acridine orange stained, 15% polyacrylamide gel of <i>G. gallus</i> eggshell intracrystalline protein fraction	106
Figure 4.12	Distribution of amino acids in <i>T. retusa</i> , <i>N. anomala</i> , <i>M. edulis</i> and an avian eggshell (<i>Gallus gallus</i>)	108

Figure 4.13	Amino acid composition of the total protein fraction of <i>T. retusa</i> , <i>N. anomala</i> , <i>M. edulis</i> and <i>G. gallus</i>	113
Figure 4.14	Amino acid composition of the intercrystalline protein fraction of <i>T. retusa</i> , <i>N. anomala</i> , <i>M. edulis</i> and <i>G. gallus</i>	114
Figure 4.15	Amino acid composition of the intracrystalline fraction of <i>T. retusa</i> , <i>N. anomala</i> , <i>M. edulis</i> and <i>G. gallus</i>	115
Figure 4.16	Histograms of Crystal Number vs. Crystal Size for calcite growth <i>in vitro</i>	119
Figure 4.17 (a-e)	Histograms of Crystal number vs. Crystal Size for calcite growth with the addition of intracrystalline proteins	120
Figure 4.18	Scanning electron micrographs of calcite crystals after 48 hours growth with addition of intracrystalline organic matrix extracts	121
Figure 4.19	X-ray Diffraction pattern from crystals grown in the presence of <i>M. edulis</i> intracrystalline proteins	122
Figure 5.1	Summary Diagram	140

List of Tables

		Page
Table 2.1	Solution composition for 20%, 15% gels and stacking gels for SDS	20
Table 2.2	Molecular weight (M.wt) of proteins of known molecular weight (standards) used for SDS PAGE (expressed in kDa)	21
Table 2.3	Solution composition for IEF gels	23
Table 2.4	Concentration of protein added to crystal growth solution	27
Table 3.1	Summary of electron microprobe results for <i>T. retusa</i>	38
Table 3.2	Pearson correlation coefficients for element concentration in the primary and secondary layers of <i>T. retusa</i>	42
Table 3.3	Summary of electron microprobe results for <i>N. anomala</i>	50
Table 3.4	Results of Analysis of Variance for element concentration in the primary and secondary layers of <i>Novocrania anomala</i>	51
Table 3.5	Pearson correlation coefficients for element concentration in the primary and secondary layers of <i>N. anomala</i>	54
Table 3.6	Summary of electron microprobe results for <i>M. edulis</i>	63
Table 3.7	Pearson correlation coefficients for element concentration in the calcite and aragonite layers of <i>M. edulis</i>	64
Table 3.8	Summary of electron microprobe results for <i>G. gallus</i> eggshell	74
Table 3.9	Pearson correlation coefficients for element concentration in the calcite eggshell of <i>G. gallus</i>	75
Table 4.1	Loss on Ignition Results	93
Table 4.2	One letter codes for amino acids	109
Table 4.3	Amino acid composition (pmol) of the total protein fractions of <i>T. retusa</i> , <i>N. anomala</i> , <i>M. edulis</i> , and <i>G. gallus</i>	110
Table 4.4	Amino acid composition of the total protein fraction of <i>T. retusa</i> , <i>N. anomala</i> , <i>M. edulis</i> and <i>G. gallus</i>	110
Table 4.5	Amino acid composition (pmol) of the intercrystalline protein fractions of <i>T. retusa</i> , <i>N. anomala</i> , <i>M. edulis</i> , and <i>G. gallus</i>	111
Table 4.6	Amino acid composition of the intercrystalline protein fraction of <i>T. retusa</i> , <i>N. anomala</i> , <i>M. edulis</i> and <i>G. gallus</i>	111
Table 4.7	Amino acid composition (pmol) of the intracrystalline protein	112

Table 4.8 Amino acid composition of the intracrystalline protein fraction 112
of *T. retusa*, *N. anomala*, *M. edulis* and *G. gallus*

Chapter 1 Introduction

1.1 Introduction

Biominerals are produced by organisms from all five kingdoms (Lowenstam and Weiner, 1989). They vary in complexity from chains of magnetite crystals produced by magnetotactic bacteria to the intricate structures of bone, tooth enamel and dentine. Biominerals perform a wide range of functions from magnetic sensors to protection and motion. Calcium minerals account for approximately 50% of biogenic minerals (Lowenstam and Weiner, 1989), of which calcium carbonate is the common phase and is frequently present as one or both of the polymorphs of CaCO_3 , calcite and aragonite.

Biominerals are composite materials composed of a mineral phase with an organic matrix. Biomineralisation processes can be considered in two categories: Biologically Induced Mineralisation and Biologically Controlled Mineralisation (Lowenstam and Weiner, 1989). Biologically induced mineralisation takes place by precipitation of minerals commonly from metabolic and cellular processes (Lowenstam and Weiner, 1989 and Mann, 2001). In this case, the organism does not regulate the formation of the biomineral. Biologically controlled mineralisation refers to the interaction of organic macromolecules and ions to regulate the precipitation and growth of the mineral (Lowenstam and Weiner, 1989 and Mann, 1990 and 2001). The products of biologically controlled mineralisation display exquisite morphologies and have physical properties that differ from those of inorganic carbonates (Feng *et al.*, 2000 and Magdams and Gies, 2004).

1.2 Biominerals

Biominerals comprise a mineral phase with an organic matrix of proteins, carbohydrates and lipids. The protein component controls the nucleation, morphology and crystal structure of the mineral (Lowenstam and Weiner, 1989, Belcher *et al.*, 1996 and Falini *et al.*, 1996). The minor and trace element compositions of the skeletons of marine invertebrates have been of interest due to their potential application as seawater palaeothermometers (e.g. Elderfield and Ganssen, 2000 and Martin *et al.*, 2002). The chemical composition of the mineral and the organic matrix can also provide information on the mechanisms that underlie the formation of biominerals. The following sections describe some of the extensive literature on the composition of both the inorganic and organic components of biominerals. For a more detailed review of minor element

composition and organic matrix composition of biominerals refer to Sections 3.2 and 4.2 respectively.

1.2.1 Inorganic Components

The concentration and spatial distribution of minor and trace elements within the skeletons of marine invertebrates is determined by a range of biological and environmental variables (Lorens and Bender, 1977, Dodd, 1965 and Elderfield *et al.*, 1996). Mg/Ca values of calcite skeletons of a variety of marine invertebrates display a positive correlation with the temperature of ambient seawater (Lea *et al.*, 1999, Lowenstam, 1961 and Dickson, 2002). However, this relationship is not consistent between species and biological factors may influence the incorporation of magnesium into marine invertebrate skeletons (Vander Putten *et al.*, 2000 and Lorens and Bender, 1977). Mg/Ca values in shells of *M. edulis* do not display a consistent correlation with water temperature over the year (Vander Putten *et al.*, 2000). Although the influence of temperature is not dismissed, other factors must therefore contribute to controlling the incorporation of magnesium into *M. edulis* calcite (Vander Putten *et al.*, 2000). One suggestion is that variations in growth rates may contribute to variation in element distribution throughout individual CaCO₃ shells. Buening and Carlson (1992) identified two patterns of magnesium distribution in the shells of the articulated brachiopods *Terebratulina unguicula* and *Terebratalia transversa*. Both ontogenetic patterns of magnesium distribution are attributed to variations in growth rate through ontogeny and seasonal variations in the availability of nutrients (Buening and Carlson, 1992). In some cases it is difficult to ascertain the precise controls on incorporation of magnesium into marine biominerals as temperature and growth rate are partially coupled (Mii and Grossman, 1994) and may also influence physiological processes that ultimately control the uptake of magnesium into the shells of some taxa (Nurnberg *et al.*, 1996).

Mg/Ca values also influence crystal morphology (Meldrum and Hyde, 2001), while varying the concentration of magnesium alters the kinetics of calcite growth *in vitro* (Hincke & St Maurice, 1998). Magnesium may therefore have an active role in the development of the biomineral.

Strontium/calcium values of biotic carbonate may be related to a number of factors including temperature, growth rate and the organism's physiology (Stoll *et al.*, 2002,

Vander Putten, 2000, Stecher III *et al.*, 1996, Klein *et al.*, 1996). A positive relationship between strontium concentration and temperature has been found in the aragonite test of the benthic foram, *Hoeglundina elegans* (Reichart *et al.*, 2003). There is also a positive relationship between strontium concentration and temperature in the calcite tests of the benthic foraminifera, *Cibicides wuellerstorfi* and *Cibicides refulgens* (Rathburn and De Deckker, 1997). However, this relationship is not consistent with other species of benthic foraminifera (Rathburn and De Deckker, 1997). Strontium concentration in abiotic and biotic marine carbonate may also be related to precipitation rate (Lorens, 1981; Carpenter and Lohmann, 1992), the concentration of magnesium present in the crystal lattice (Mucci and Morse, 1983) and the concentration of strontium in the seawater (Lorens and Bender, 1980; Hockett *et al.*, 1997).

1.2.2 Organic Components

The organic components of biominerals are extremely important to many aspects of biomineral formation, influencing the nucleation, crystal structure and morphology of the mineral (Lowenstam and Weiner, 1989, Simkiss and Wilbur, 1989, Mann, 2001, Belcher *et al.*, 1996, Wheeler and Sikes, 1984). The organic matrix can be divided into two fractions, the intercrystalline matrix, which surrounds the mineral, and the intracrystalline matrix, which is encased within the mineral. Demineralisation of the biomineral using the calcium chelator, ethylene diamine tetra acetic acid (EDTA) releases the intracrystalline matrix which comprises two fractions: an insoluble and a soluble organic matrix fraction.

The insoluble matrix is composed of hydrophobic macromolecules, which provide a framework for crystal formation and influence the final properties of the biomineral (Feng *et al.*, 2000, Weiner *et al.*, 1983, Weiner, 1984). The concentration of insoluble organic matrix varies considerably between species and in some cases is absent, suggesting that the framework proteins do not have an essential role in the mineralisation of some skeletons (Weiner *et al.*, 1983).

In contrast, the soluble organic matrix is present in all biologically controlled systems (Weiner *et al.*, 1983). It is composed predominantly of acidic macromolecules that have a calcium binding function, which is essential to the nucleation process (Weiner, 1979). A number of soluble matrix proteins are also glycosylated and the carbohydrate groups may

be involved in the biomineralisation process possibly via their sulphate and carboxylic acid groups (Cusack *et al.*, 2000, Ameye *et al.*, 2001, Mann, 2001).

There have been a number of *in vitro* studies on the effect of organic matrix proteins on calcium carbonate crystal growth (e.g. Feng *et al.* 2000b, Zaremba *et al.* 1996, Wheeler *et al.* 1981 and Levi *et al.*, 1998). Soluble matrix proteins exert control over both crystal morphology and polymorph (Belcher *et al.*, 1996, Thompson *et al.*, 2000, Levi *et al.*, 1998 and Falini *et al.*, 1996). Aragonite grew in the presence of macromolecules extracted from the aragonite layers of molluscs which were adsorbed onto a substrate of β -chitin and silk-fibroin (Falini *et al.*, 1996). By contrast, calcite formed with the addition of macromolecules extracted from the calcite layers of the same molluscs. A mixture of proteins extracted from mollusc shell nacre on addition to CaCO_3 induced the formation of aragonite *in vitro* in the absence of a preformed organic matrix (Belcher *et al.*, 1996).

1.2.3 Biomineralisation Mechanisms

The general model for the structure of organic matrices comprises a core framework of hydrophobic macromolecules with surface layers of hydrophilic proteins and polysaccharides (Weiner, 1984). This model is illustrated in the nacreous layer of mollusc shells, in which the surface of a core framework comprising the polysaccharide β -chitin and layers of silk-fibroin-like protein is covered by acidic macromolecules (Weiner and Traub, 1984). Levi-Kalisman *et al.*, (2001) confirmed the presence of ordered interlamellar sheets of organic matrix between layers of nacre in the bivalve *Atrina*. However, the overall structure of the layer is determined by β -chitin, while the other constituent of the organic matrix, silk-fibroin, is not an essential component of the interlamellar sheets (Levi-Kalisman *et al.*, 2001).

The nucleation, morphology and crystal structure of biominerals is controlled by the interaction of organic molecules and ions at the surface of the crystal nucleus (Mann, 1988, 2001). This match of charge, polarity and stereochemistry between organic molecules and ions, termed "molecular recognition", reduces the activation energy required for crystal nucleation (Mann, 1988, 2001).

Ionotropy involves the accumulation of binding sites in localised areas which result in regions of high charge density (Mann, 2001). The accumulation of ionic charge attracts a

large number of ions resulting in the nucleation of the biomineral (Mann, 1988, 2001). With respect to calcium carbonate, the binding sites fixed to the organic matrix framework bind Ca^{2+} ions, which attract carbonate anions (CO_3^{2-}). In turn, the carbonate anions attract Ca^{2+} ions. Nucleation takes place due to the local supersaturation of ions resulting in an amorphous mineral deposit (Greenfield *et al.*, 1984). Amorphous calcium carbonate deposits have been identified as a precursor stage to crystalline deposits in some invertebrate calcium carbonate skeletons, including calcite sea urchin spicules (Beniash *et al.*, 1997, Wilt *et al.*, 2003), spicules from ascidian skeleton (Aizenberg *et al.*, 2002) and the aragonitic larval shells of the bivalves *Mercenaria mercenaria* and *Crassostrea gigas* (Weiss *et al.*, 2002).

The alternative model to ionotropy, the template model (epitaxy) requires that the structural arrangement of the surface of the organic matrix matches that of the structure of the crystal face (Mann, 1988). The soluble organic matrices of the molluscs, *Crassostrea virginica*, *Mercenaria mercenaria*, *Crassostrea irredescens* and *Nautilus pompilius* contain a high concentration of the amino acids glycine and aspartic acid suggesting the presence of proteins with repeat sequences of $(\text{Asp-Y})_n$ where Y is glycine or serine (Weiner and hood, 1975). If this sequence is present in the β -sheet formation then the arrangement of aspartic acid residues would correspond to the crystallographic arrangement of Ca^{2+} in the aragonite lattice (Weiner and Hood, 1975).

This model does not explain the preferential formation of calcite or aragonite owing to the similarities in crystal structure of the (001) faces of calcite and aragonite, it has been suggested that the polymorph may be dependant on the arrangement of CO_3^{2-} anions around Ca^{2+} ions (Mann, 1988 and 2001).

1.3 Emergence and Early Evolution of Biominerals

The relatively sudden emergence of organisms with complex mineralised skeletons together with a radiation of metazoans with complex body plans in the Early Cambrian (545-595Ma) marks one of the major events in the evolution of life. Only a few shelly fossils have been found at the base of the Cambrian but there followed a gradual proliferation of taxa with mineralised skeletons (Knoll, 2003). The abundance of shelly fossils increased over 25Ma from the base of the Cambrian (Knoll, 2003). A number of theories have been suggested for the apparently rapid development of skeletal

mineralisation. These have included environmental factors, such as rising atmospheric oxygen levels (Towe, 1970), and biological factors including an increase in predation pressure (Bengtson, 1994, Simkiss, 1989).

There is no clear evidence to indicate that the evolution of marine animals with mineralised skeletons in the Early Cambrian was principally linked to environmental changes. The diversification of taxa producing mineralised skeletons may have resulted from a combination of biological and environmental factors. Many of the cell mechanisms involved in producing biominerals were present before the appearance of skeletal material in the fossil record (Simkiss, 1989). These cell systems and biochemical pathways that were established before the evolution of eukaryotes predisposed cells to producing biominerals. These cell mechanisms, coupled with the development of complex multicellular organisms and the environmental stresses (i.e. increased predation) that were prevalent in the Early Cambrian, led to the diversification of taxa with skeletons (Simkiss, 1989).

There are some biochemical similarities between the organic matrices of organisms from different phyla, in particular the presence of acidic proteins (Weiner *et al.*, 1983). This suggests that there may be common processes involved in the formation of biominerals (Weiner *et al.*, 1983). Biologically controlled mineralisation could therefore have originated in common Early Precambrian ancestors or evolved following the divergence of phyla (Lowenstam and Weiner, 1983). While phylogenetic evidence indicates that skeletons evolved independently in the Metazoa (Knoll, 2003), the biochemical mechanisms that underlie skeletal formation may have a common origin (Westbroek and Marin, 1998).

1.4 Aims of this Study

In order to establish whether organisms from different phyla employ similar processes in the formation of biominerals it is necessary to establish whether the organic matrix and mineral components of the biominerals share common characteristics. While some comparative studies have been undertaken, few of these have compared organisms from different phyla e.g. Weiner *et al.*, (1983). The aims of this study are to compare the organic and inorganic constituents of biominerals produced by organisms from different

phyla and so determine whether they share common mineralisation components and by implication processes.

As calcium carbonate is the most common biomineral, four calcium carbonate systems from three different phyla were used for the survey. The four systems comprise biominerals produced by three invertebrates and a vertebrate. The invertebrates include two members of the phylum Brachiopoda; the articulated brachiopod *Terebratulina retusa* (Sub-phylum Rhynchonelliformea) and the inarticulated brachiopod *Novocrania anomala* (Sub-phylum Craniata), and a member of the phylum Mollusca (Class Bivalvia); *Mytilus edulis*. The vertebrate system is the eggshell of the domestic fowl, *Gallus gallus*. These four systems comprise two calcium carbonate polymorphs, calcite and aragonite, and a variety of ultrastructures.

The concentration and distribution of minor elements within each is described within the context of ultrastructure in Chapter 3. Chapter 4 compares the organic matrix composition, in particular the protein composition of the four systems in terms of protein molecular weight and charge, amino acid composition and the presence of sulphated sugars.

1.5 The Four Biomineral Systems

The following sections provide a brief introduction to the four systems analysed in this study. For a more detailed description of the ultrastructure of the shells of *T. retusa*, *N. anomala*, *M. edulis* and *G. gallus* refer to Chapter 3, Sections 3.3.1 to 3.3.4 inclusive.

1.5.1 *Terebratulina retusa*

Terebratulina retusa (Figure 1.1) is an articulated brachiopod belonging to the Subphylum Rhynchonelliformea, Class Rhynchonellata (Williams *et al.*, 1996). The Subphylum Rhynchonelliformea is characterised by an organocarbonate shell with a fibrous secondary layer. Rhynchonelliform brachiopods possess a pedicle. The calcite shell comprises two layers; an outer primary layer of acicular calcite and an inner secondary layer of calcite fibres (Figure 3.1), both of which are secreted by the mantle epithelium (Williams, 1968). Specimens of *T. retusa* attached to shells of the bivalve *Modiolus modiolus* were collected from a depth 200m in the Firth of Lorne, NW Scotland.



**Figure 1.1 Specimen of the articulated brachiopod
Terebratulina retusa collected from the Firth
of Lorne, NW Scotland**

Anterior to posterior shell length is approximately 2cm.

1.5.2 Novocrania anomala

Novocrania anomala (Figure 1.2) is an inarticulated brachiopod belonging to the Subphylum Craniiformea, Class Craniida (Williams *et al.*, 1996). The Subphylum Craniiformea is characterised by an organocarbonate shell with a laminar secondary layer lacking teeth and sockets. In contrast to members of the Rhynchonelliformea such as *T. retusa*, Craniiformea lack a pedicle. In *N. anomala*, the ventral valve is cemented to the substrate. Specimens of *N. anomala* were collected from the same location as *T. retusa*.

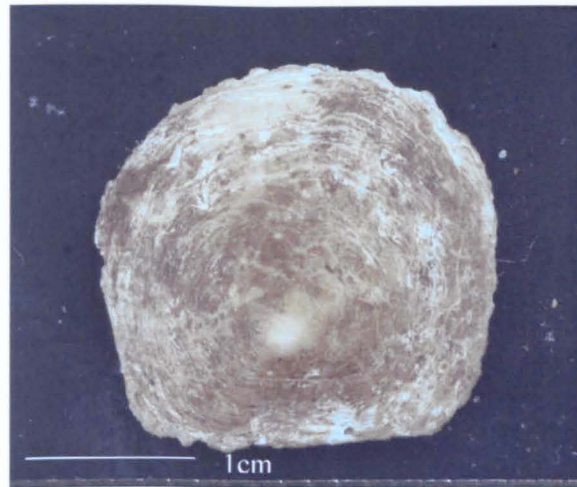


Figure 1.2 Dorsal valve of a specimen of the inarticulated brachiopod *Novocrania anomala*

The width of the dorsal valve is approximately 1.5cm.

1.5.3 *Mytilus edulis*

Mytilus edulis (Figure 1.3) belongs to the Phylum Mollusca, Class Bivalvia, Subclass Pteriomorpha. The bivalve molluscs have soft parts enclosed within an equivalved shell, while the Pteriomorpha encompass a group of byssate bivalves with shells composed of either calcite, aragonite, or both calcium carbonate polymorphs. *Mytilus edulis* has a shell with an outer layer of prismatic calcite and an inner aragonite layer. In bivalve molluscs the shell is separated from the mantle by the extrapallial fluid from which calcium carbonate crystallisation takes place (Simkiss and Wilbur, 1989). The inorganic composition of the extrapallial fluid is regulated by the movement of ions across the mantle and is different to seawater (Simkiss and Wilbur, 1989 and Crenshaw, 1972). Specimens of *M. edulis* were obtained from a mussel farm on the coast of Oban, NW Scotland.



**Figure 1.3 Interior of specimen of the Bivalve
Mollusc *Mytilus edulis***

Length of the shell from anterior to posterior is approximately 7cm.

1.5.4 Avian Eggshell (*Gallus gallus*)

The calcite eggshell of the domestic fowl, *Gallus gallus* comprises six regions; the inner and outer shell membranes, the calcified mammillary caps, the pallisade layer, the vertical crystal layer and the cuticle which is composed of organic material and hydroxyapatite crystals (Dennis *et al.*, 1996 and Fernandez *et al.*, 2001). The egg is produced in the isthmus and uterine sections of the hen oviduct (Nys *et al.*, 1999). The membranes that encompass the yolk and albumen of the egg are produced in the isthmus, which forms the distal part of the oviduct. As the egg moves down the oviduct, initial calcification takes place in the red isthmus where the mammillary caps are formed. A large proportion of calcite deposition and the addition of the eggshell cuticle finally take place in the uterus (Nys *et al.*, 1999, Fernandez *et al.*, 2001 and Solomon, 1991). Eggshell formation is rapid being complete within 24 hours in a constant temperature environment (Simkiss, 1961 and Cusack *et al.*, 2003). Specimens of the eggshell of *G. gallus* were obtained from a commercial source.

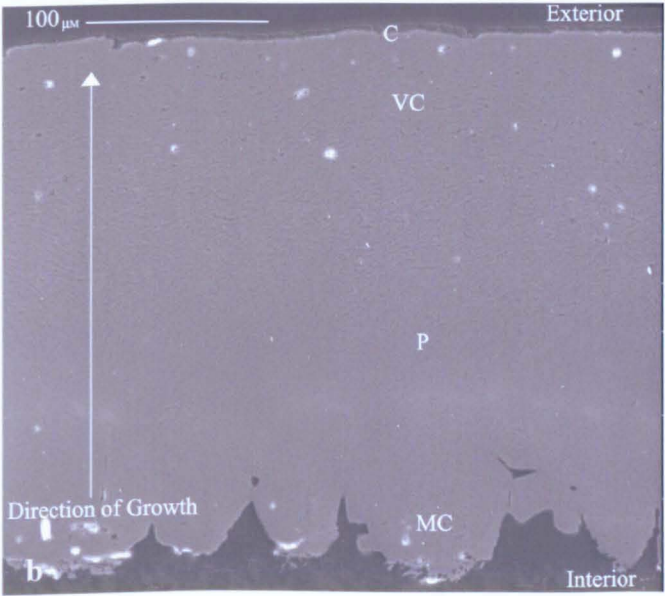
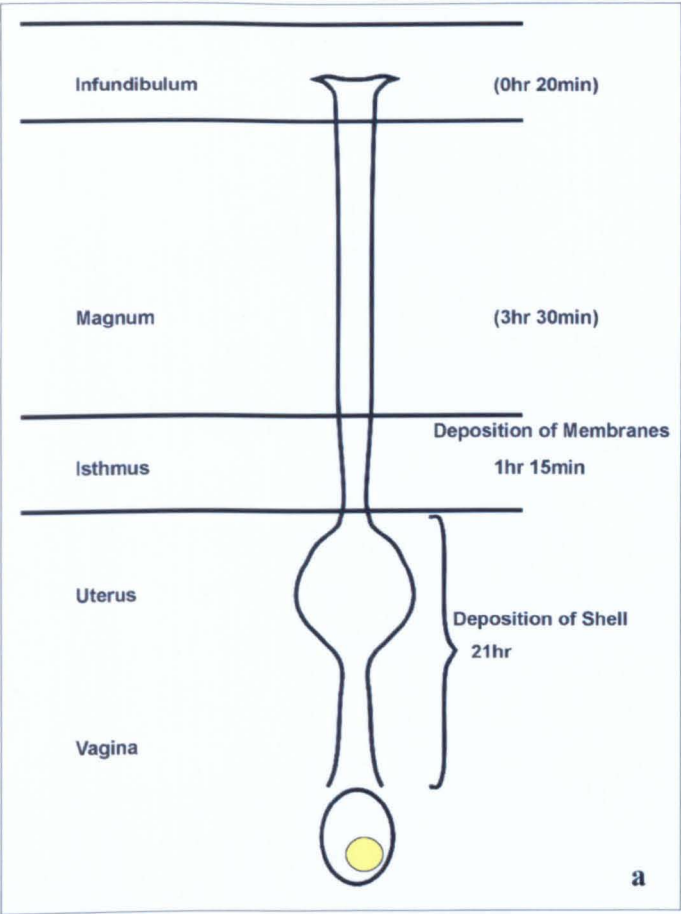


Figure 1.4 (a) Eggshell formation in the domestic fowl *Gallus gallus* (after Gautron, 1994), (b) Cross-section of the eggshell of *G. gallus*

MC mammillary caps, *P* palisade layer, *VC* vertical crystal layer, *C* cuticle.

2 Materials and Methods

2.1 Materials (Appendix A)

2.2 Sample Collection and Preparation

Living specimens of *Terebratulina retusa* and *Novocrania anomala* were collected from the Firth of Lorne, Oban, NW Scotland (56° 24'N, 5°38' 4"W). Samples were obtained from a depth of 200m by dredging, which was carried out by the crew of the research vessel *Calanus* from the Dunstaffnage Marine Laboratory, Oban. Specimens were stored in seawater and transported to the University of Glasgow. Specimens of the bivalve *Mytilus edulis* were collected from a mussel farm on the coast of Oban. Eggshells were obtained from a commercial source.

T. retusa is attached to the substrate via a muscular pedicle. The pedicle was removed, the valves disarticulated and the soft tissues removed using dental tools. In contrast, the ventral valve of *N. anomala* is cemented to the substrate. When removing the ventral valve from the substrate it is therefore difficult to ensure that the base of the valve is not contaminated by substrate material. As a result, only the dorsal valve of *N. anomala* was analysed. The dorsal valve was separated from the ventral valve and the soft tissues removed. *T. retusa* and *N. anomala* valves were cleaned in an aqueous solution of sodium hypochlorite (1% v/v) and rinsed in Milli QTM water.

For *M. edulis*, the left and right valves were prised apart, the soft tissues removed and the valves cleaned in a solution of sodium hypochlorite (1% v/v). The thick periostracum was removed using a hand drill equipped with a grinding wheel tool. The valves were rinsed in Milli QTM water.

To extract extrapallial fluid from specimens of *M. edulis* the shell valves were prised apart and a syringe inserted between the mantle tissues and the shell. To prevent contamination by seawater only live specimens with the mantle tissues fully attached to the inner surface of the shell were used. The fluid was extracted, washed with sodium phosphate buffer and concentrated through Microcon filters under centrifugation at 3000rpm (734.53g) for 15 minutes.

For the three marine invertebrates, only shells obtained from individuals that were alive when collected were analysed.

The eggshells were halved and the contents removed. The membrane covering the inner surface of the shell was removed by incubation in an aqueous solution of sodium hypochlorite (37% v/v) for 20 minutes (Cusack and Fraser, 2002). All specimens were rinsed thoroughly with Milli QTM water.

2.3 X-ray Diffraction (XRD)

X-ray diffraction (XRD) utilises the reflection profile of X-rays from crystal lattice planes for mineral identification. Each mineral has a unique XRD profile (i.e. d spacing and 2θ angle) enabling mineral identification by comparison of the XRD profile with those in the Joint Committee on Powder Diffraction Standards (JCPDS) database.

Each sample was powdered in an agate mortar and pestle and mixed with acetone. The powder was pasted onto a glass slide, allowed to dry and loaded on to A Philips PW 1050/35 X-ray diffractometer.

2.4 Examination of Shell Ultrastructure

Samples were prepared as described in Section 2.2. The shells were fractured and mounted on scanning electron microscope stubs. The samples were gold coated and the fractured edges examined using secondary electrons in a Cambridge Instruments S360 Scanning Electron Microscope (SEM) operated at 20kV.

2.5 Thin Section Preparation

Samples were prepared as described in Section 2.2. The samples were embedded in araldite resin and sectioned. *T. retusa* and *N. anomala* valves were sectioned from anterior to posterior, *M. edulis* shells were sectioned at 90° to the hinge axis, and a square section (approximately 1cm²) from the equator of the eggshell was cut in half. The samples were fixed to glass slides, ground to a thickness of 30µm and polished using diamond compounds (6µm-1/4µm) for reflected light microscopy and cathodoluminescence microscopy and spectroscopy.

2.6 Minor and Trace Element Analysis

2.6.1 Sample Preparation

Samples were prepared as described in Section 2.2, however the *M. edulis* periostracum and the eggshell membrane were not removed for element analysis. *T. retusa* and *N. anomala* valves were sectioned from anterior to posterior, *M. edulis* shells were sectioned at 90° to the hinge axis, and a square section (approximately 1cm²) was taken from the equator of the eggshell. All samples were embedded in araldite resin blocks, polished with diamond compounds (6µm to 1/4µm) and carbon coated for electron microprobe spot analysis (EMPA) and element mapping by wavelength dispersive spectral analysis (WDS). Element mapping was also carried out using a Cambridge Instruments SEM equipped with an energy dispersive spectrometer (EDS).

2.6.2 Electron microprobe analysis (EPMA)

Electron microprobe analysis (EPMA) enables the concentration of minor and trace elements in a polished sample to be quantified. The wavelength dispersive spectrometer (WDS) provides better peak resolution and a lower detection limit than EDS for quantitative analysis of elements that are present in low concentrations. A further advantage of EPMA in relation to other chemical analysis techniques (e.g. atomic absorption) is that micrometre-sized volumes of samples can be analysed.

Analyses in a line perpendicular to the line of section were carried out using a Cameca SX50 Electron Microprobe equipped with three wavelength dispersive spectrometers. The instrument was operated at 15KV with a 10nA current and the spot was defocused to 10µm in order to prevent beam damage. The electron microprobe was calibrated using standards for Na, Mg, S, K, Ca, Mn, Fe and Sr (see Appendix B for calibration standards). Three specimens of *T. retusa*, *N. anomala*, *M. edulis* and *G. gallus* were analysed and each analysis repeated in triplicate. Matrix corrections were carried out using a PAP correction procedure. The detection limit for each element on the SX50 electron microprobe was calculated from:

$$\text{Detection limit} = \frac{3}{m} \sqrt{\frac{R_b}{T_b}}$$

Where

m = counts/second/% element in the standard

R_b = counts per second on the background

T_b = count time on the background

Data errors were calculated from:

$$\% \text{ Error} = \frac{100}{\sqrt{T} (\sqrt{R_p} - \sqrt{R_b})}$$

Where

T = count time on the peak

R_p = counts per second on the peak

R_b = counts per second on the background

The quantitative analysis of carbonates by EPMA can be problematic, especially for elements that are present in low concentration (e.g. Mn). Thus, it is essential to determine both the detection limit of the electron microprobe for each element and the errors related to the data set.

A plot of Na concentration as a function of the percentage error associated with the data is presented in Figure 2.1. The errors shown are calculated for analyses carried out on *N. anomala* under electron microprobe conditions of 15kV with a 10nA defocused beam. There is a clear relationship between the concentration of each element in the sample and the size of the error associated with each data point. Error size is greatest for those elements that are present in low concentration. For sodium analyses, a large proportion of the data falls within a +/-5-10% error limit and is above the detection limit of 0.089 wt %. For magnesium, the error limit is below +/-2 % while errors for Sr data are commonly between +/-10-15%. For analyses of manganese, the data set is unreliable as the errors associated with the data are large and elemental concentration is below the calculated detection limit of 0.055 wt%. Other elements that are present in concentrations below the detection limit of the electron microprobe include iron and, in some instances, potassium

and phosphorus. Plots of Mg, S, Ca, Sr, Mn, Fe, P and K were produced for each system and only elements that are above the detection limit are discussed.

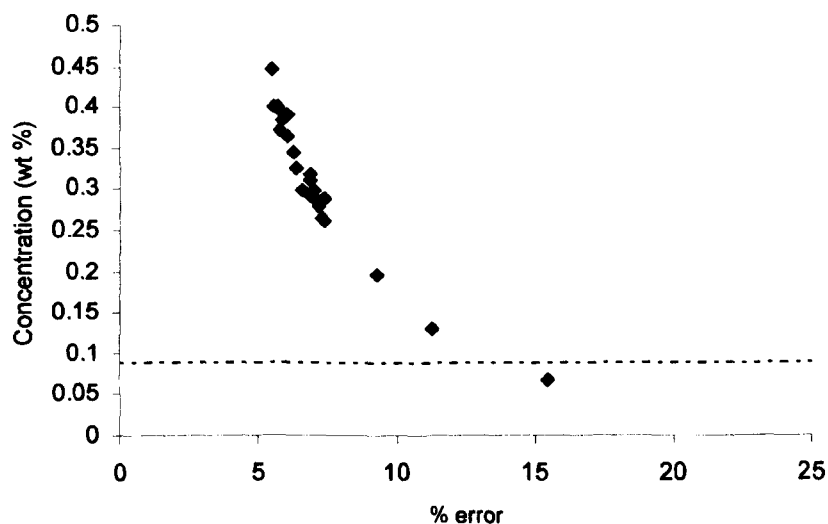


Figure 2.1 Plot of concentration of Na against percentage error for *N. anomala* electron microprobe analyses

*The detection limit and errors for sodium were calculated using the equation presented in Section 2.6.2. The errors on the data set for sodium concentration in *N. anomala* were calculated using the equations in Section 2.6.2. The detection limit of 0.08wt% is shown as a dashed line.*

2.6.3 Element Mapping

EDS element mapping is a qualitative technique that produces an image showing spatial variations in element concentrations. Elemental maps were produced using a Cambridge instruments S360 SEM equipped with an Oxford Instruments Isis Microanalysis System, (operated at 15KeV with a 4nA current). In instances where an element was present in particularly low concentration or a more detailed map was required, element mapping was carried out using the Cameca SX50 electron microprobe operated at 15KV with a 20nA current and a 5 μ m defocused beam.

2.6.4 Cathodoluminescence (CL) Microscopy

The wavelength and intensity of light emitted from a sample when bombarded by electrons can be characteristic of the mineral type and the elements incorporated within it. CL imaging has an advantage over electron probe analysis and EDS mapping because it may reveal the presence of elements in concentrations below analytical detection. CL images of the systems were produced using a CITL Technosyn 8200 MK4 operated at 25kV and mounted on a Zeiss Axioplan petrological microscope.

2.6.5 Cathodoluminescence (CL) Spectroscopy

CL-spectroscopy can be used to determine the presence of certain chemical elements from their CL emission wavelength (Habermann *et al.*, 1999). In cases where an element is below the detection limit for microprobe analyses, the high sensitivity of CL-spectroscopy is an advantage (Habermann, 2002).

Thin sections were prepared as described in Section 2.5. CL spot analyses and CL mapping were carried out using a Cameca SX100 electron microprobe equipped with a CL spectrometer capable of determining the wavelength and intensity of CL emission over the wavelength range of 350-850nm. CL maps and spectra were displayed using the computer software, Cathodoluminescence Hyperspectral Imaging and Manipulation Program (CHIMP).

2.7 Determination of Total Organic Concentration and Distribution

2.7.1 Loss on Ignition

Loss on ignition was employed to determine the total organic content of each of the four biominerals. Each sample was powdered, weighed and heated in an oven at 500°C for two hours then re-weighed. The weight loss following combustion corresponds to the mass of organic material originally present.

2.7.2 Scanning Electron Microscope Backscatter (BSE) Imaging

Backscatter electron (BSE) imaging in the SEM can be used to highlight spatial variations in mean atomic number. Here BSE imaging has been used in an attempt to determine the distribution of organic material within the four biomineral systems. The significant difference in mean atomic number between calcium carbonate and organic components of the shell should enable these two components to be distinguished. BSE images were produced using a Cambridge Instruments S360 SEM operated at 15KV with a range of beam currents.

2.8 Extraction, purification and visualisation of shell protein

2.8.1 Extraction of intercrystalline protein

Shell samples were crushed to a fine powder using a Temer rock crusher (for large quantities) or a ceramic mortar and pestle (for smaller quantities). Powdered samples were incubated in an aqueous solution of guanidine hydrochloride (GnHCL) containing proteinase inhibitors and Tris buffer (4M guanidine, 50mM Tris, 2.5mM Benzamidine-HCl, 50mM N-ethylmaleimide, 1mM Phenyl methyl sulphonyl fluoride), buffered to pH 7.4 under constant agitation for 24 hours. The insoluble fraction was separated from the soluble fraction by centrifugation at 4000rpm (3452g) for 15 minutes. Guanidine incubation and centrifugation were repeated for the remaining sample. The supernatants were pooled and stored at 3°C.

2.8.2 Extraction of intracrystalline protein

The remaining sample was incubated in ethylene diamine tetra acetic acid (EDTA), with proteinase inhibitors (20% EDTA, 50mM Tris, 2.5mM Benzamidine-HCL, 50mM N-ethylmaleimide, 1mM Phenyl methyl sulphonyl fluoride), buffered to pH 7.4 under constant agitation for up to 5 days. The insoluble fraction was removed by centrifugation at 4000 rpm (3452g) for 15 minutes and the supernatant stored at 3°C.

2.8.3 Purification of intercrystalline and intracrystalline protein

The supernatant obtained from both the intercrystalline and intracrystalline fractions was concentrated and residual GnHCl and EDTA removed by filtration through a MinitanTM tangential flow ultrafiltration system (Cusack *et al.*, 1992). Both fractions were filtered using 10kDa cut off filters. Both samples were further concentrated through CentriprepTM concentrators with 10kDa cut off filters under centrifugation at 3000 rpm (1942g) for 20 minutes, and through Microcon filters also with 10kDa filters under centrifugation at 10,000 rpm (8161.4g) for 15 minutes.

2.8.4 Sodium dodecyl sulphate polyacrylamide gel electrophoresis (SDS PAGE)

Sodium dodecyl sulphate polyacrylamide gel electrophoresis (SDS PAGE) involves the separation of proteins based entirely on their molecular weight. One-dimensional discontinuous SDS PAGE was used to analyse the proteins from the four biomineral systems using a modification of the method described by Schagger and Von Jagow (1987).

Acrylamide is crosslinked by the compound N, N'-methylene-bis-acrylamide (Bis-acrylamide) producing a mesh that acts as a "molecular sieve". The pore size of the gel mesh is controlled by the concentration of both acrylamide and Bis-acrylamide. Polymerisation is initiated by ammonium persulphate (APS) and catalysed by the addition of Tetramethylethane (TEMED). Fifteen percent polyacrylamide gels were prepared as described in Table 2.1. In some instances 20% gels were used in order to improve the resolution of low molecular weight proteins. Stacking gels were prepared as described in Table 2.1.

Reagent	Resolving Gel (15%)	Resolving Gel (20%)	Stacking Gel
Acrylamide/Bis	3.6ml	4.8ml	0.42ml
Gel Buffer	3.3ml	3.3ml	1ml
Glycerol	1ml	1ml	n/a
Milli Q	2.1ml	0.9ml	2.53ml
APS	75 μ l	75 μ l	40 μ l
TEMED	7.5 μ l	7.5 μ l	7.5 μ l

Table 2.1 Solution composition for 20%, 15% gels and stacking gels for SDS PAGE

For each sample, the concentrated protein mixture was heated with sample buffer (Tris buffer (50mM), SDS (4% w/v), Glycerol (12% w/v), β -Mercaptoethanol (2% w/v), Bromophenol blue (0.0002% w/v) at 100°C for 4 minutes. Sodium dodecyl sulphate is a denaturing detergent that binds to proteins in a ratio of 1.4g SDS per gram polypeptide (Andrews, 1986). The charge on the polypeptide is overcome by the large negative charge on the SDS resulting in a constant charge to mass ratio. Protein separation through the gel is therefore based solely on protein size.

The molecular weights of proteins of known molecular weight (standards) are presented in Table 2.2. The volume of sample buffer mixture loaded onto the gel differed according to the protein concentration within the sample, which was estimated from UV spectroscopy using $A_{280\text{nm}}$ of 1.0 for 1mg/mL protein. For 15% gels, a voltage of 60V was applied across the gel for three hours, the same voltage was applied for five hours to 20% gels.

Unstained Proteins	Full Range (M.wt) Proteins	Low M.wt ProteinsProteins
66	250	44
45	160	29
36	105	20
29	75	14
24	50	5
20	35	2
14	30	
	25	
	15	
	10	

Table 2.2 Molecular weight (M. wt) of proteins of known molecular weight (standards) used for SDS PAGE (expressed in kDa)

The molecular weights of the unknown proteins are determined from a calibration curve of the electrophoretic mobility (Rf) as a function of the log molecular weight of the proteins of known molecular weight (Figure 2.4).

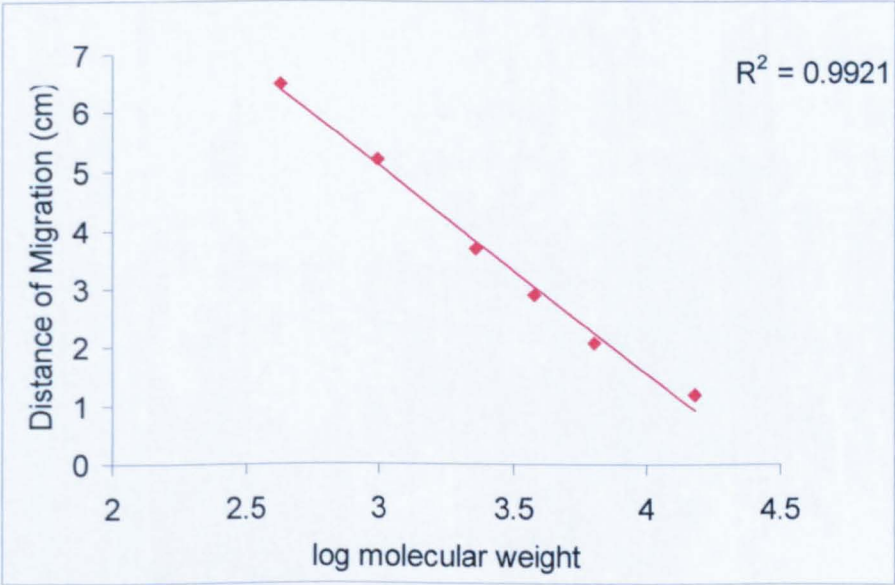


Figure 2.2 Calibration curve of electrophoretic mobility as a function of the log molecular weight of proteins of known molecular weight

Proteins of known molecular weight (unstained protein standards) prepared as described in Section 2.8.4 and electrophoresed in a 15% polyacrylamide gel as described in Section 2.8.4

2.8.5 Coomassie Brilliant Blue Staining

Proteins were fixed and revealed by staining overnight in a solution of Coomassie Brilliant Blue (Coomassie Brilliant Blue (0.5% w/v), methanol (30% v/v) and acetic acid (10% v/v)). Gels were then incubated in destain solution (methanol (30 % v/v) and acetic acid (10% v/v)) to remove background staining.

2.8.6 Silver Staining

Silver staining provides a more sensitive staining technique than Coomassie Blue staining and is able to detect around 1ng of protein (Hames and Rickwood, 1990). Following staining with Coomassie Blue, the gels were rinsed in Milli QTM water for 30 minutes and incubated in DTE solution (0.0005% w/v) for 30 minutes followed by silver solution (0.2% w/v) for 30 minutes. Gels were agitated in developer solution (Na₂CO₃.10H (0.8% w/v), formaldehyde (0.05% v/v)) until staining took place. To stop staining, gels were incubated in an aqueous solution of acetic acid (1% v/v) for 10 minutes.

2.8.7 Acridine Orange Staining

Acridine orange can be used to detect sulphated macromolecules e.g. sulphated sugars in polyacrylamide gels. The staining protocol was carried out as described by Dauphin *et al.*, (2003a). Gels were incubated in a fixing solution of methanol (40%) and acetic acid (10%) for 30 minutes, followed by a stain solution of Acridine orange (0.02 %) in a solution of 5% methanol for 30 minutes. Gels were rinsed in Milli QTM water and destained in a solution of 25% ethanol and 7% acetic acid.

2.8.8 Isoelectric Focusing

Isoelectric focusing can be used to separate proteins based on their overall charges. The method is similar to gel electrophoresis in that a gel medium is used to separate the protein components of the sample. For isoelectric focusing the gel contains ampholytes, which are necessary to establish a pH gradient across the gel. By applying a voltage across the gel the ampholytes migrate to either the anode or the cathode depending on whether they are

acidic or basic. The point at which they stop is dependant on their pI value i.e. the pH at which they are neutral.

Isoelectric focusing (IEF) was undertaken in the Biology Department, University of York. Gels were prepared in accordance with Table 2.3. Isoelectric focusing (IEF) was carried out using a Biorad III IEF cell. The standards and samples were loaded on to the gel using a guide. Two sets of standards were used, a broad range set of standards (pH3-10) and a low range set of standards (pH2.5-6.5). Six samples were loaded onto the gel (mussel aragonite, mussel calcite, eggshell, total mussel, *T. retusa* and *N. anomala* EDTA extracts). An initial voltage of 100V was applied for 15 minutes to set up a pH gradient across the gel. The voltage was increased to 200V for 15 minutes and finally 450V for one hour. On application of a voltage across the gel the proteins migrate towards the point where the pH is equal to their pI (i.e. protein net charge=0). The gel was then washed with a fixer solution (17.3g Sulphosalicylic acid, 57.5g Trichloroacetic acid (TCA)) for 30 minutes, stained with a solution of Coomassie Brilliant Blue (0.92g Coomassie Brilliant Blue/800ml destain solution) and placed in a destain solution (500ml ethanol and 160ml acetic acid). The protein samples were compared to the protein standards with known isoelectric points.

Reagent	Concentration
Ampholine	0.5ml
Glycerol	0.5ml
Acrylamide	1.35ml
Water	7.65ml
Ammonium persulphate (APS)	42µl
Tetramethylethane (TEMED)	7µl

Table 2.3 Solution composition for IEF gels

2.9 Amino Acid Analysis

Amino acid analysis provided a comparison between the amino acid compositions of organic matrix proteins within the four systems. Before amino acid analysis can be carried out, the peptide bonds that link individual amino acids must be hydrolysed. In this case, manual vapour phase hydrolysis was used.

2.9.1 Manual Hydrolysis

Shell samples were cleaned as described in Section 2.2, powdered and weighed. To determine the intracrystalline amino acid composition, samples were powdered, weighed and incubated in an aqueous solution of sodium hypochlorite (1% v/v) for one hour. These samples were washed thoroughly with MilliQTM water until no bleach could be detected by smell. All samples were dissolved in an aqueous solution of HCl (2N), transferred to hydrolysis tubes and vacuum dried. The hydrolysis tubes were placed in hydrolysis vials containing 500µl HCl (6N), purged with argon for 60 seconds and then sealed. Vials were heated at 165°C for one hour. The heated vials were vented in a fume cupboard to release the acid vapour and left to cool. Samples were then reconstituted in K₃EDTA.

2.9.2 Amino Acid Analysis

The Applied Biosystems 420 Amino Acid Analyser employs the first stage of the Edman degradation sequence (described in Section 2.10.2) for derivatization. The free amino acids resulting from hydrolysis are tagged with phenylisothiocyanate (PITC) to produce phenylthiocarbamyl-amino acids (PTC-AA). This increases detection of the amino acids by UV absorbance at a wavelength of 254nm. In the case of the 420A Amino Acid analyser, the derivatization process is automated.

2.9.3 Summary of Steps for Amino Acid Analysis

The samples in aqueous solution are applied to glass frits. The derivatisation jaw clamps to each frit, individually delivering an aliquot of methanol containing K₃EDTA. This step prevents any metal contamination that may interfere with the derivatisation process. Diisopropylethylamine (DIEA) vapour is delivered to the sample in order to neutralise any acid. PITC is delivered to the frit and derivatization takes place resulting in the production of PTC-AAs. The PTC-AAs are transferred to the transfer flask by aqueous buffer where they are mixed. The contents of the flask is delivered to the Model 130A for hplc separation of the derivatised amino acids.

2.10 N-terminal Sequencing

2.10.1 Transfer of Protein to ProBlott Membrane

Electroblotting enables the direct transfer of proteins from a polyacrylamide gel to a Polyvinylidene fluoride membrane (ProBlott membrane) for N-terminal sequencing. To transfer the proteins from the gel to a ProBlott membrane the gel was incubated in transfer buffer (CAPS buffer (10mM, pH 11, methanol (10% v/v)) for five minutes. The ProBlott membrane was dipped in methanol and rinsed in transfer buffer. The proteins were transferred using a BioRad Mini Transblot Electrophoretic Transfer Cell. A voltage of 55V was applied across the cell for one hour.

The Problott membrane was rinsed in Milli QTM water, dipped in methanol and placed in Coomassie Blue stain solution (Coomassie Brilliant Blue-R (0.5% w/v), methanol (30% v/v), and acetic acid (10% v/v)) for one minute. The membrane was then destained by rinsing in 50% methanol and allowed to dry.

2.10.2 N-terminal Sequencing

N-terminal sequencing was carried out using an Applied Biosystems Procise Edman Protein Sequencer at the University of Edinburgh, Proteomics Centre. This automated sequencer employs Edman Degradation Chemistry for protein sequencing (Figure 2.5). The Edman reagent, phenylisothiocyanate (PITC), reacts with the N-terminal amino acid to produce a phenylthiocarbamyl derivative. Breakage of the peptide bond between the first and second amino acid results in the formation of a phenylhydantoin derivative of the first amino acid. The phenylthiohydantoin derivative is then identified by high performance liquid chromatography (hplc). This process is repeated for the subsequent amino acids to determine the N-terminal protein sequence.

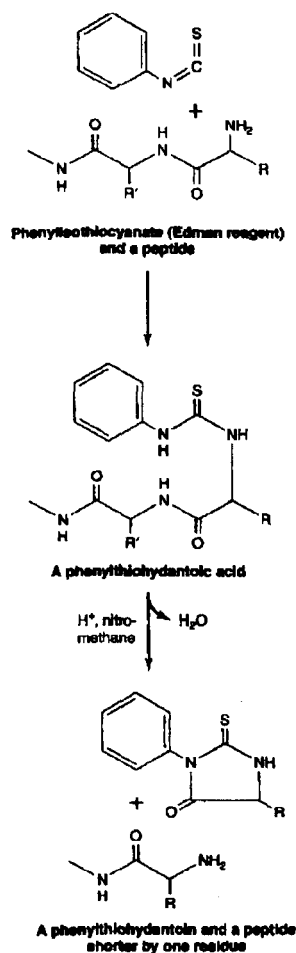


Figure 2.3 Edman degradation chemistry (from Murray *et al.*, 2000)

2.11 Calcium Carbonate Crystal Growth

2.11.1 Kitano Protocol

Calcite crystals were grown according to the Kitano Protocol (Kitano, 1962). Glassware was washed in hot soapy water, followed by 0.1% (v/v) HCl and rinsed with methanol. Between each stage, the glassware was rinsed with Milli QTM water. The reaction solution consisting of 2g CaCO₃/litre Milli QTM water, was prepared in a 5l round bottomed flask and stirred rapidly. CO₂ gas was bubbled through the reaction solution for 1 ½ hours. The solution was filtered through two filter papers into a conical flask to remove any residue, and CO₂ gas bubbled through for a further 30 minutes. In order to determine the optimum conditions for calcite growth, saturated calcium hydrogen carbonate solution was distributed in a well plate and the crystals left to develop under a range crystallisation times (24, 48, and 72 hours).

2.11.2 Calcite Grown in the Presence of Protein Extract

Calcite crystals were grown in the presence of intracrystalline proteins that had been extracted from the four biomineral systems (Sections 2.8.1-2.8.3). Sodium phosphate buffer was removed from the intracrystalline/extrapallial fluid extracts by washing with Milli QTM water through MicroconTM filters. In order to determine the influence of intracrystalline/extrapallial fluid proteins on crystal growth *in vitro*, protein extracts were added to the saturated calcium hydrogen carbonate solution. The effect of sodium phosphate buffer on calcite growth was also determined by addition of 2 μ l of buffer to the calcium hydrogen carbonate solution.

A one centimetre diameter coverslip was placed in each well of a 25 well plate and covered with 1ml of saturated calcium hydrogen carbonate solution. Protein extracts were added to each well. The concentration of each extract was dependant on the availability of intracrystalline/extrapallial fluid protein extracts (Table 2.4). The coverslips were removed after a period of 24 and 48 hours.

Sample	Volume of Protein Solution Added	Final Protein Concentration in 1ml reaction volume (μ g/ml)
<i>T. retusa</i>	2 μ l of 0.8 μ g/ μ l	1.6
<i>N. anomala</i>	2 μ l of 7.4 μ g/ μ l	14.8
<i>M. edulis</i>	2 μ l of 8.8 μ g/ μ l	17.6
Extrapallial Fluid	2 μ l of 1.6 μ g/ μ l	3.2
Eggshell	2 μ l of 0.8 μ g/ μ l	1.6

Table 2.4 Concentration of protein added to crystal growth solution

The coverslips were air dried, attached to SEM stubs and gold-coated in order to examine crystal morphology using the SEM. The mineralogy was determined by X-ray diffraction using a Phillips PW 1050/35 X-ray diffractometer. The number and size of crystals in SEM images was determined using the computer software, Scion Image.

3.Ultrastructure and Minor and Trace Element Concentration

3.1 Introduction

Chemical analysis of modern and fossil carbonate shells is an important tool for both developing our knowledge of the processes involved in the formation of biominerals and increasing our understanding of evolutionary relationships between biomineral systems. By determining the chemical composition of various biomineral systems and the effect of elements on the growth and structure of the biomineral we can begin to understand some of the processes involved in carbonate biomineralisation. The question is complicated however due to the influence of a wide range of mineralogical, biological and environmental factors on the chemical composition of calcium carbonate biominerals.

This chapter provides a detailed account of the crystal ultrastructure of *T. retusa*, *N. anomala*, *M. edulis* and the avian eggshell (*Gallus gallus*) in relation to the distribution and concentration of minor and trace elements throughout each shell. The four systems described here display a range of crystal ultrastructures and two types of calcium carbonate polymorph since the shell of *M. edulis* contains both calcite and aragonite. They have also been subjected to a range of environmental conditions during formation. The two brachiopods *T. retusa* and *N. anomala* were obtained from the same location and therefore have experienced the same water depth and temperature conditions. *M. edulis* is commonly found in shallow coastal zones with warmer, higher salinity seawater conditions than those from which the two brachiopods were obtained. In contrast to the three marine systems the eggshell forms within a regulated, constant temperature environment. By analysing systems that comprise various forms of calcium carbonate with a range of ultrastructural motifs, it is possible to assess the range of variations in chemical composition or the extent to which chemical composition is constant despite differences in structure.

The minor and trace element composition of each system was analysed quantitatively by electron probe. Three sets of spot analyses were carried out in a line perpendicular to the line of section for samples of each system. The data is presented both as line analyses across each shell and as scatter plots in order to determine if there are any relationships

between the concentrations of various elements within each system. Qualitative maps of element distribution in each system were produced by SEM. For some samples where more detailed elemental maps were required the maps were made using the electron probe. As discussed in Section 3.2.3 cathodoluminescence can provide valuable information on the presence of certain chemical elements. Therefore all four systems were analysed by optical cathodoluminescence and cathodoluminescence spectroscopy.

3.2 Previous Work

The skeletons of marine invertebrates are commonly composed of calcium carbonate, as either or both of the polymorphs, calcite and aragonite. The chemical composition of these skeletons has been of much interest due to the information that skeletal chemistry provides about the processes involved in biomineral formation. The use of shell chemistry to determine seawater palaeotemperatures has also been extensively investigated (Elderfield and Ganssen, 2000, Martin *et al.* 2002, Eggins *et al.*, 2003 and Parkinson *et al.*, 2005). As there are a number of biological and environmental factors that affect shell chemistry (e.g. temperature, growth rate and the composition of the mineralising medium), it is a complex task to determine the exact controls on the chemical composition of any one individual organism.

3.2.1 Magnesium

Temperature is thought to be one of the main controls on the incorporation of magnesium in biogenic calcium carbonate (Mii and Grossman, 1994 and Dodd, 1967) and a positive relationship between seawater temperature and the concentration of magnesium in the calcium carbonate exoskeletons of a range of marine invertebrates has been identified (Lowenstam, 1961, Lea *et al.*, 1999 and Dickson, 2002). The magnesium/calcium ratio of calcium carbonate skeletons has frequently been employed as seawater thermometer and palaeothermometer (Watanabe *et al.* 2001, Lear *et al.*, 2002 and Lear *et al.*, 2000). It is therefore important to establish if the temperature-related partitioning of magnesium is consistent between species.

Foraminifera are both geographically widespread and biologically less complex than the Brachiopoda or the Bivalvia and have been of particular interest in determining the controls on calcification and the uptake of minor and trace elements. A positive

exponential relationship between magnesium and temperature has been described for both benthic and planktonic foraminifera (Rosenthal *et al.* 1997, Nurnberg *et al.* 1996 and Lea *et al.* 1999), and a number of studies have attempted to use this relationship to determine past seawater temperatures (Martin *et al.*, 2002, Elderfield and Ganssen, 2000 and Lear *et al.*, 2000). The positive correlation between water temperatures and magnesium concentrations has also been described for the carbonate skeletons of more complex taxa. Lowenstam (1961) identified an increase in the magnesium content of recent brachiopod shells with increasing water temperatures, while Mii and Grossman (1994) also found evidence for a positive trend between magnesium and temperature in a well preserved fossil specimen of *Neospirifer*. A positive relationship between temperature and magnesium content has also been found in some species of echinoderm (Dickson, 2002).

The relationship between temperature and the magnesium concentration of carbonates is however complicated by a number of physical factors including the effect of salinity (Dodd, 1967) and the effect of the size and charge of the magnesium ion on lattice partitioning in different CaCO_3 polymorphs (Rosenberg, 1990), and also biological factors such as the organism's rate of growth throughout ontogeny (Buening and Carlson, 1992). Seawater chemistry alone cannot explain the magnesium content of marine carbonate skeletons as many organisms have skeletons whose magnesium content differs from that predicted from distribution coefficients. In particular, brachiopods live in habitats where fluctuations in seawater chemistry are insufficient to account for measured variations in shell chemistry (Mii and Grossman, 1994). The eggshell of the domestic fowl, *Gallus gallus* is precipitated in a constant temperature environment and so if temperature were the sole control on partitioning, magnesium concentration should be constant throughout the eggshell. However the concentration of magnesium varies through the eggshell, which suggests that it is not a simple relationship between the Mg/Ca ratio and temperature, while other factors may also be involved in controlling the magnesium content of the eggshell (Cusack *et al.*, 2003).

Incorporation of magnesium ions into the calcite mineral lattice inhibits crystal growth (Davis *et al.*, 2000, de Leeuw, 2002 and Wilbur and Bernhardt, 1984). Many organisms exhibit Mg/Ca ratios that are different to values predicted from the composition of the seawater within which the organism lived (Rosenberg, 1990). It has been suggested that many organisms employ mechanisms for controlling the uptake of magnesium from seawater, thus limiting the inhibiting effect of magnesium. Lorens and Bender (1977,

1980) identified a physiological mechanism in the mussel *M. edulis*, which allows the organism to exclude magnesium from the extrapallial fluid. Tests of the planktonic foraminifera *Globigerinoides sacculifer* are undersaturated with magnesium with respect to predicted values (Numberg *et al.*, 1996). They suggest that foraminifera are therefore capable of controlling their uptake of magnesium to some extent. However the physiological processes that ultimately control the uptake of magnesium are temperature controlled.

Mg/Ca ratio may determine the polymorph of calcium carbonate and influence the morphology of the crystals that are formed (Meldrum and Hyde., 2001, Kitamura, 2001, Loste *et al.*, 2003). Evidence from *in vitro* studies suggests that the precipitation of aragonite and high magnesium calcite is favoured by the presence of Mg^{2+} (Kitano and Hood, 1965). Alternations in the Mg/Ca ratio of seawater caused by fluctuations in the spreading rate of midocean ridges may have resulted in the transition between calcite and aragonite seas through the Palaeozoic (Hardie, 1996, Stanley *et al.*, 2002). Stanley *et al.*, (2002) suggest that simple marine invertebrates which precipitate aragonite or high magnesium calcite skeletons in the modern aragonite sea may in fact have produced low magnesium calcite skeletons in past calcite seas when the Mg/Ca ratio of the seawater was low. The simple relationship between the Mg/Ca ratio of the fluid and the resulting mineralogy of abiotic calcium carbonate has however, been questioned (Given and Wilkinson, 1985), while Blackwelder *et al.*, (1976) found that in the case of the coccoliths of the coccolithophorid *Cricosphaera cartarae* the calcium carbonate polymorph produced is not solely dependent on the concentration of magnesium in solution.

3.2.2 Strontium

Within abiotic calcium carbonate systems, the concentration of strontium within calcite may relate to the precipitation rate of the mineral, where an increase in the distribution coefficient of strontium occurs with increased precipitation rate (Lorens, 1981, Major and Wilber, 1991). An increase in precipitation rate also leads to an increase in the strontium content of biotic calcite (Lea *et al.*, 1999). A positive relationship between the calcification rate and the concentration of strontium within calcite tests of benthic foraminifera has been identified (Lea *et al.*, 1999, Rathburn and De Deckker, 1997 and Elderfield *et al.*, 1996). If the incorporation of strontium into the tests of benthic foraminifera is kinetically controlled then the composition of the test may be indirectly

linked to factors such as temperature and water depth/CO₂ levels which influence the rate of calcification (Elderfield *et al.*, 1996). The controls on strontium incorporation into aragonite may be different than those associated with strontium incorporation in calcite.

The potential application of Sr/Ca ratios in the calcium carbonate skeletons of marine invertebrates as environmental indicators has gained much attention (Stoll *et al.*, 2002, Vander Putten, 2000 and Stecher III *et al.*, 1996). Strontium thermometry is based on the inverse relationship between water temperature and the Sr/Ca ratio of aragonitic coral skeletons (Beck *et al.*, 1992 and Weber, 1973). A correlation between strontium concentration and water temperature has also been identified in other species. Reichart *et al.*, (2003) identified a positive correlation between water temperature and the concentration of strontium in the tests of *Hogelundina elegans*. Stecher III *et al.*, (1996) suggested that the Sr/Ca ratio in the aragonite layers of the shells of two molluscs, *Mercenaria mercenaria* and *Spisula solidissima* is kinetically controlled, as low Sr/Ca ratios in the shells of both molluscs correlate with periods of slow growth.

The influence of precipitation rate on the Sr/Ca ratio of some calcite biomineral systems has been questioned. Klein *et al.* (1996) found that the Sr/Ca ratio of the bivalve mollusc *Mytilus trossulus* (*Mytilus edulis*) is primarily controlled by the metabolic activity of the mantle and secondarily by salinity, while the shell growth rate had little effect on the strontium concentrations. Lorens and Bender (1980) also found no evidence of a relationship between Sr/Ca ratio and growth rate in the shell of *Mytilus edulis* but found that the Sr/Ca ratio in both the calcite and aragonite layers of the bivalve shell varied linearly with the Sr/Ca ratio in artificial seawater solutions in which the mussels were grown. Hockett *et al.*, (1997) also found a linear relationship between the incorporation of strontium into the calcium carbonate shells of barnacles and the concentration of strontium in artificial seawater. In comparison Vander Putten *et al.*, (2000) found that the variations in Sr/Ca ratios found in the calcite layer of specimens of *M. edulis* could not be explained simply in terms of the ratio of Sr/Ca in solution, while they also found no evidence for a correlation between Sr/Ca and temperature.

3.2.3 Cathodoluminescence

Cathodoluminescence (CL) is the emission of photons from a material due to bombardment with electrons. In geosciences, cathodoluminescence is commonly used for analysing the

texture and chemical composition of rock samples. Certain chemical elements act as luminescence activators (e.g. Mn), while others act as luminescence quenchers (e.g. Fe). The wavelength of the light emitted is dependent on both the activator element and the identity of the mineral in which it is present. Manganese is the most common activator in carbonates, while Fe^{2+} is the main quencher (Marshall, 1988). The colour of luminescence produced in the presence of manganese differs between calcite and aragonite. In calcite Mn produces an orange-red luminescence while aragonite luminesces green (Sommer, 1972). The intensity of luminescence also varies with the concentration of the activator element, although the concentration of manganese that is needed to activate luminescence in calcite is poorly known. For biogenic carbonate, Richter and Zinkernagel (1981) found that a minimum manganese concentration of 20-40ppm is necessary for visible cathodoluminescence, while Mason and Mariano (1990) suggest that the activation concentration may be as low as 10ppm. Habermann *et al.*, (1998) suggest that caution is required as a sample may still emit luminescence which is not visibly detectable even with very low Mn concentrations.

In palaeontology, cathodoluminescence has principally been used to assess the extent of diagenesis in fossil samples (Samtleben *et al.*, 2001, Popp *et al.*, 1986). It had been previously thought that recent biogenic carbonates do not luminesce and thus fossils that luminesce have been diagenetically altered. However, recent work has shown that modern carbonate skeletons also luminesce and the potential application of cathodoluminescence for the study of recent carbonate shells has been recognised (Barbin, 1991).

Many carbonate shells comprise growth increments between which the chemical composition varies (Lowenstam, 1961, Dodd, 1967, Rosenberg and Hughes, 1991, Barbin, 1992). Luminescence emission may therefore reflect these variations where the concentration of activator elements is above the detection limit (Barbin, 1992). Barbin *et al.*, (1991) detected cathodoluminescence in a range of marine and freshwater organisms. In most cases, manganese was the principal activator and the colour of luminescence produced was related to the mineral in which it occurred. Orange luminescence was detected from the calcite layers of the molluscs, *Pecten maximus*, *Ostrea edulis* and *Mytilus edulis*. The aragonite layers within *P. maximus* and *M. edulis* were non-luminescent while faint green CL bands were apparent in *Ostrea edulis*.

Cathodoluminescence spectroscopy quantifies the information recorded by optical CL. The spectrum produced provides information on the intensity and wavelength of CL that is emitted. CL-spectroscopy is a relatively new method for analysis of biogenic carbonates and, as such, the data available for various species is limited. Barbin *et al.*, (1995a) report the CL spectrum determined from the cephalopod *Nautilus pompilus* in which an emission band resulting from manganese substitution in aragonite is present at 540nm and a band related to intrinsic emission is present within the blue range of the spectrum. For the cephalopod *Nautilus macromphalus*, the main emission was in the blue range of the spectrum.

3.3 Results

3.3.1 *Terebratulina retusa* Ultrastructure and Minor Elements

3.3.1.1 Ultrastructure

The *Terebratulina retusa* shell has three layers; an outer organic periostracum, underlain by a primary layer of acicular calcite and an inner secondary layer composed of calcite fibres (Figure 3.1). The primary layer is approximately 25µm thick and has a sharp boundary with the fibrous secondary layer, which is 350µm thick. The interlocking fibres of the secondary layer show blunt terminations as illustrated in Figures 3.2 and 3.3.

Transmitted light images of thin sections of *T. retusa* are presented in Figures 3.4 and 3.5. The primary and secondary layers of the shell are distinct in both plane polarised light (PPL) (Figure 3.4) and cross-polarised light (XPL) (Figure 3.5), with punctae extending through both the primary and secondary layers (Figure 3.4). Both images indicate that the secondary layer has two distinct regions, which are not resolved in SEM images (Figures 3.1 and 3.2).

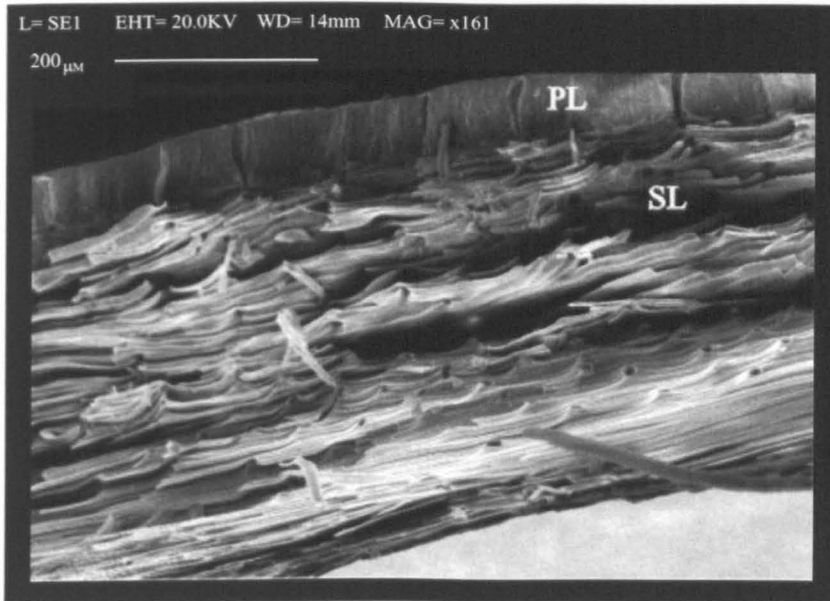


Figure 3.1 Secondary electron image of the primary (PL) and secondary (SL) layers of *Terebratulina retusa*

SEM image of a fractured cross section of a specimen of T. retusa. The outer part of the shell, the primary layer (PL) is to the top of the image.

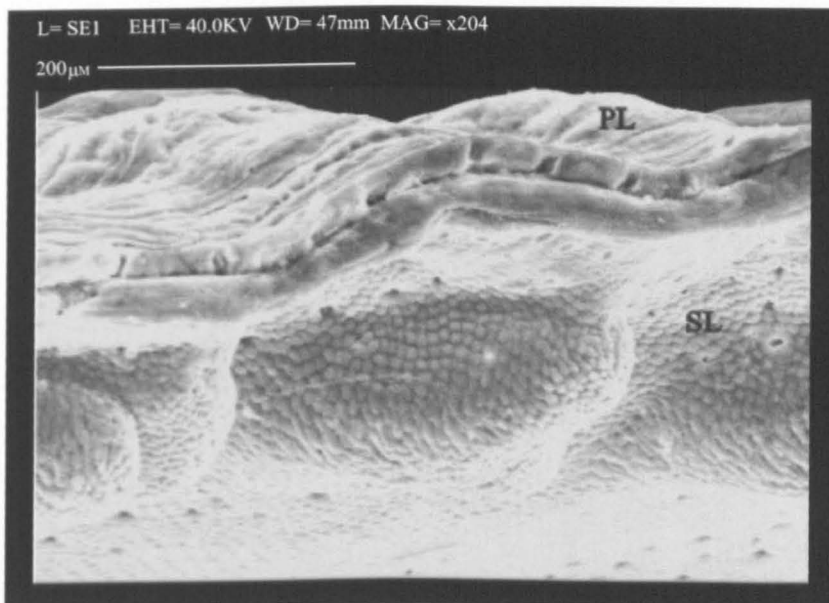


Figure 3.2 Secondary electron image of the primary (PL) and secondary (SL) layers of *Terebratulina retusa*

SEM image of a fractured cross section of a specimen of T. retusa. The image shows the blunt terminations of the secondary layer fibres.

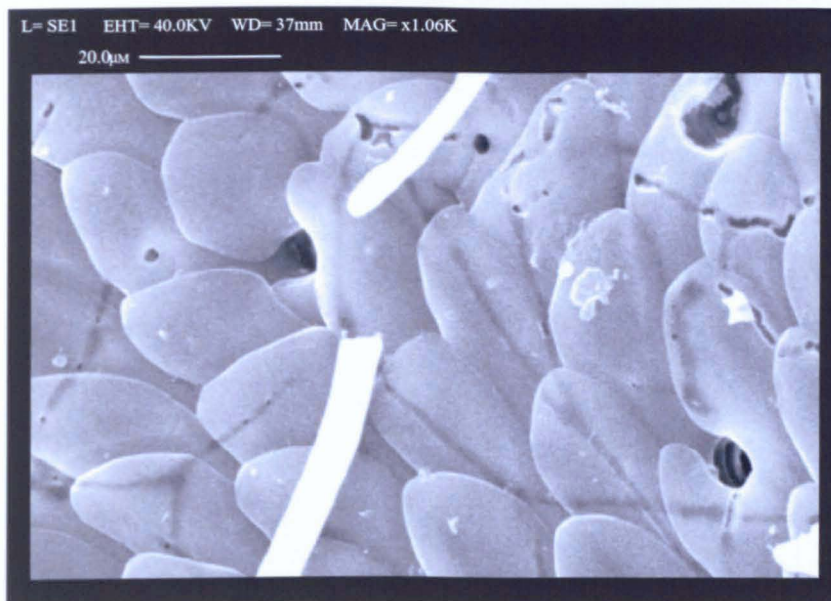


Figure 3.3 Secondary electron image of the secondary layer fibres of *Terebratulina retusa*

SEM image of a specimen of T. retusa illustrating the blunt terminations of the secondary layer fibres.



Figure 3.4 Plane-polarised transmitted light image of *Terebratulina retusa* in thin section

The primary layer (PL) is distinct from the secondary layer (SL). A division between the upper (SL1) and lower (SL2) regions of the secondary layer is also apparent.

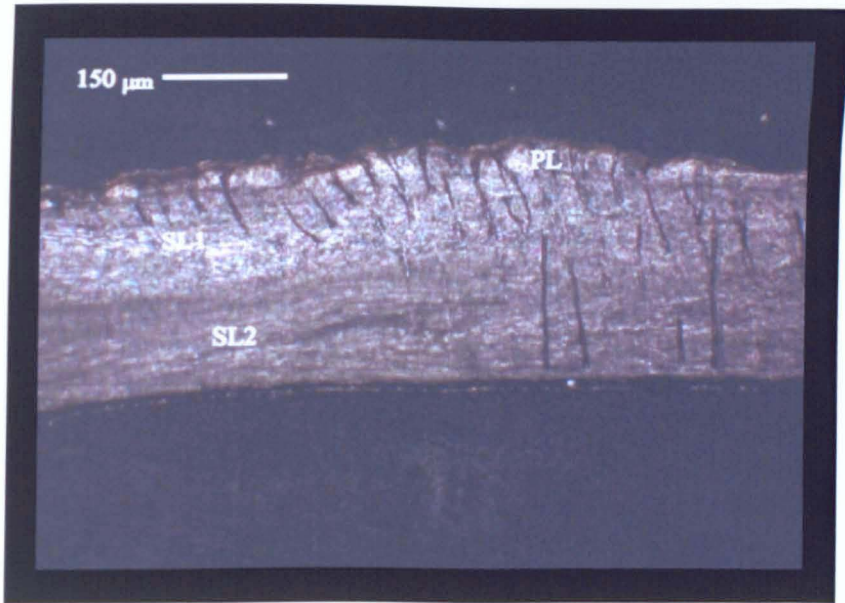


Figure 3.5 Cross-polarised light image of *Terebratulina retusa* in thin section

The primary layer (PL) is distinct from the secondary layer (SL). A division between the upper (SL1) and lower (SL2) regions of the secondary layer is also apparent.

3.3.1.2 Minor Element Composition-Electron Microprobe Analysis

Electron microprobe analyses of magnesium, sulphur, strontium and sodium across the primary and secondary layers of three specimens of *T. retusa* are presented in Figure 3.6 (a-c). Magnesium, sulphur, strontium and sodium are all above the limit of detection. For *T. retusa*, manganese, iron, potassium and phosphorus are below the limit of detection and are therefore not discussed. As some elements may be present in different phases within the shell e.g. magnesium (MgCO_3) in the crystalline phase and sulphur within the organic matrix, data are expressed as wt% element (carbonate weight percentage data is provided in the Appendix). Results are summarised in Table 3.1.

Specimen	Layer	Mg Conc. Range (wt%)	Sr Conc. Range (wt%)	Na Conc. Range (wt%)	S Conc. Range (wt%)	Figure No.
a	Primary	0.99-1.54	0.12-0.15	0.16-0.17	0.26-0.30	3.6a
a	Secondary	0.15-0.89	0.08-0.16	0.10-0.16	0.13-0.33	3.6a
b	Primary	0.28-0.75	0.13-0.15	0.16-0.16	0.21-0.33	3.6b
b	Secondary	0.12-0.34	0.08-0.16	0.11-0.18	0.10-0.24	3.6b
c	Primary	0.26-0.70	0.11-0.16	0.19-0.21	0.21-0.31	3.6c
c	Secondary	0.17-0.47	0.08-0.14	0.16-0.19	0.15-0.23	3.6c

Table 3.1 Summary of electron microprobe results for *T. retusa*

The results displayed in Table 3.1 summarise the concentration range (i.e. the lowest concentration to the highest concentration) of Mg, Sr, Na and S in the primary and secondary layers of T. retusa.

The boundary between the primary and secondary layers of *T. retusa* is marked by distinct changes in shell chemistry. The concentration of magnesium is greater in the primary layer of *T. retusa* than the secondary layer. Magnesium reaches a maximum of 1.54, 0.75 and 0.70 wt% respectively in the primary layers of specimens a, b and c (Figure 3.6a-c and Table 3.1). In all cases there is an abrupt decrease in magnesium concentration across the primary/secondary layer boundary. Within the secondary layer there is some variation in the distribution of magnesium between samples. Data for the specimen a displays an abrupt increase in magnesium concentration in the upper secondary layer (SL1), i.e. around

100µm into the secondary layer (Figure 3.6a), which is not present in the other two specimens. Specimen b contains a greater concentration of magnesium in the upper region of the secondary layer (SL1) compared to the lower region of the secondary layer (SL2) (Figure 3.6b). All three samples exhibit an increase in magnesium concentration at the innermost shell surface, albeit poorly defined for the sample in Figure 3.6(b).

Sulphur and strontium also display a similar pattern of higher concentrations in the primary layer in comparison to the secondary layer. Sulphur attains a maximum concentration of 0.3 wt% in the primary layer of each of the three specimens (Figure 3.6a-c and Table 3.1). Strontium reaches a maximum concentration of 0.16wt% in the three specimens (Figure 3.6a-c and Table 3.1). Sodium attains a maximum concentration of 0.17 wt% in specimen a, 0.18wt% in specimen b and 0.21wt % in specimen c (Figure 3.6a-c and Table 3.1).

One-way ANOVA was carried out on nine sets of analyses from three specimens of *T. retusa* in order to determine if there is a significant difference in the concentration of all four elements between the primary and secondary layers. Figure 3.7 (a-e) presents boxplots of element concentration as a function of the shell layer. Each box represents the inter-quartile range of the data set, while the mean value is displayed as a red circle. The concentration of magnesium (P value 0.001), sulphur (P value 0.000), calcium (P value 0.018) and strontium (P value 0.002) varies significantly between the two shell layers. Sodium concentration (P value 0.228) is not significantly different between the primary and secondary layers.

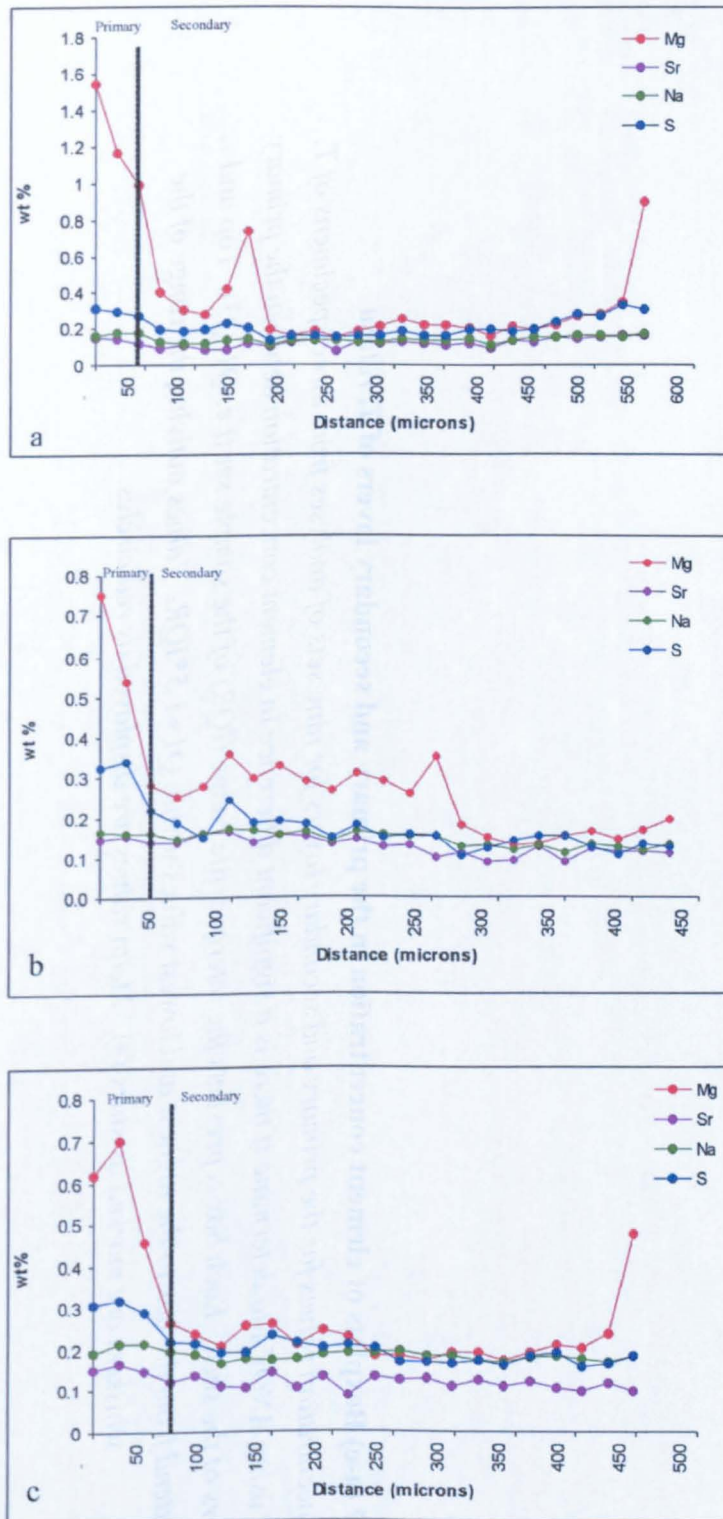
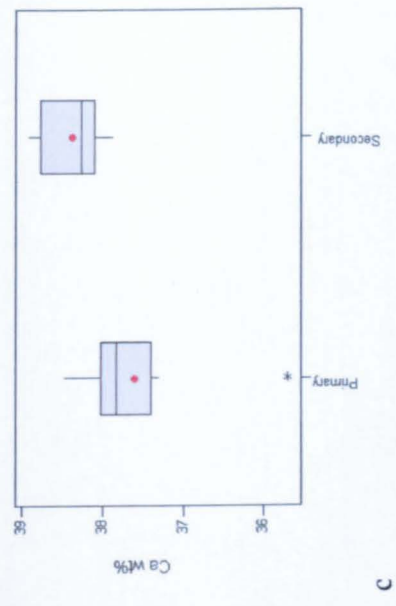
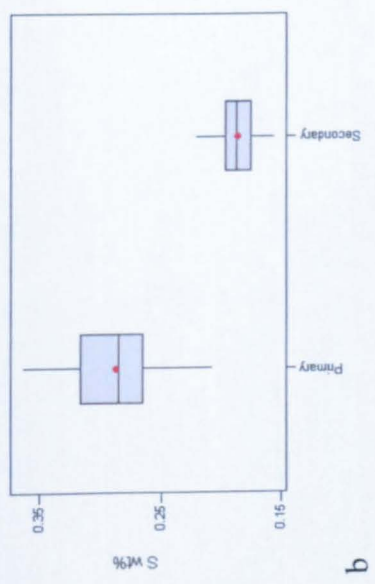
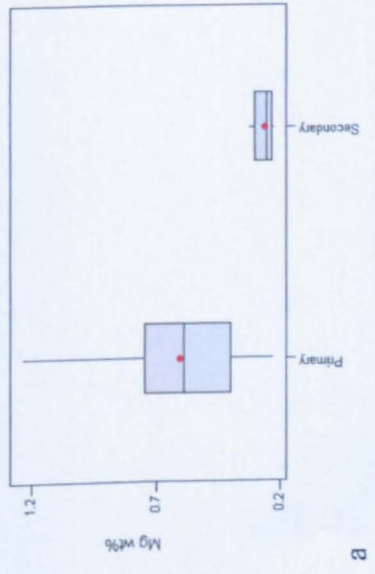
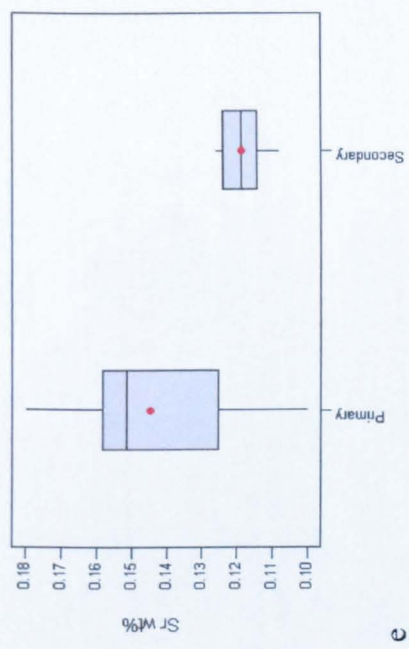
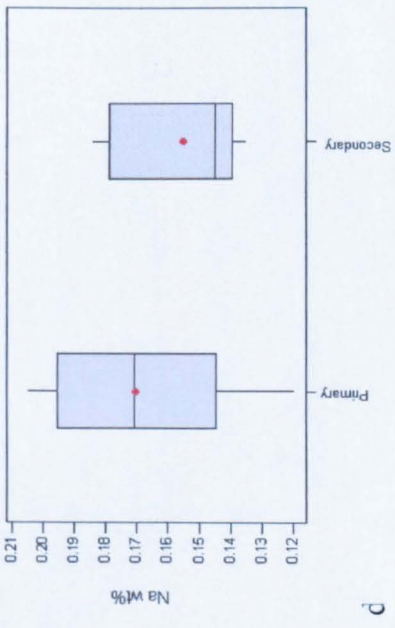


Figure 3.6 (a, b & c) Electron microprobe spot analyses across three specimens of *Terebratulina retusa*

Electron microprobe analyses were carried out as described in Section 2.6.2. Elements displayed are above their limit of detection. The y axis of graph (a) is on a different scale to the y axes of graphs b and c due to variations in overall element concentrations between individuals.

Figure 3.7 (a-e) Boxplots of element concentration in the primary and secondary layers of *T. retusa*

*The mean element concentration values for the primary and secondary layers for nine sets of analyses from three specimens of *T. retusa* were analysed using ANOVA to determine if there is a significant difference in element concentration between the primary and secondary layers of the shell. Each box represents the interquartile range (IQR) of the sample set (i.e. $Q1-Q3$). Top and bottom whiskers extend from the box to the highest and lowest values within $Q1+1.5*IQR$. Values outlying the range of the whiskers are marked as stars (*). Mean values are displayed as red circles.*



The distribution of elements in *T. retusa* (Figure 3.6) implies that there is a positive correlation between magnesium, sodium and sulphur concentration. Scatter plots of element concentration in the primary and secondary layers of *T. retusa* are presented in Figures 3.8 (a-j). Each graph contains data from ten sets of analyses taken across the primary and secondary layers of three specimens of *T. retusa*. Pearson correlation coefficients are shown in Table 3.2.

In the primary and secondary layers the correlation coefficient between sulphur and magnesium is similar. There is a positive correlation between sulphur and strontium, sulphur and sodium and between strontium and sodium in both layers of the shell however the positive trend is stronger in the primary layer in each case. There is a weak negative correlation between calcium and magnesium in the primary and secondary layers, and between calcium and sulphur in the secondary layer.

<i>T. retusa</i>	Primary Layer		Secondary Layer	
Variables	Correlation Coefficient	P-value	Correlation Coefficient	P-value
S/Sr	0.751	0.000	0.350	0.000
S/Na	0.562	0.003	0.415	0.000
Mg/Sr	0.377	0.057	0.339	0.000
Mg/S	0.601	0.001	0.669	0.000
Mg/Na	0.218	0.284	0.288	0.000
Ca/Na	0.053	0.797	-0.170	0.009
Ca/Mg	-0.432	0.027	-0.276	0.000
Ca/S	0.062	0.765	-0.351	0.000
Ca/Sr	0.311	0.122	0.066	0.312
Sr/Na	0.759	0.000	0.367	0.000

Table 3.2. Pearson correlation coefficients with P-values for element concentration in the primary and secondary layers of *T. retusa*

*Pearson correlation coefficients were calculated to determine the linear relationships between element concentrations in the primary and secondary layers of *T. retusa*. Values close to 1 indicate a strong positive linear correlation.*

Figure 3.8 (a-j) Scatter plots of element concentration in the primary and secondary layers of *Terebratulina retusa*

The concentration of minor elements in the primary and secondary layers of three specimens of T. retusa was analysed by electron microprobe as described in Section 2.6.2. The data from three sets of electron microprobe analyses from each specimen are plotted in order to determine any relationships between elements present within the shell.

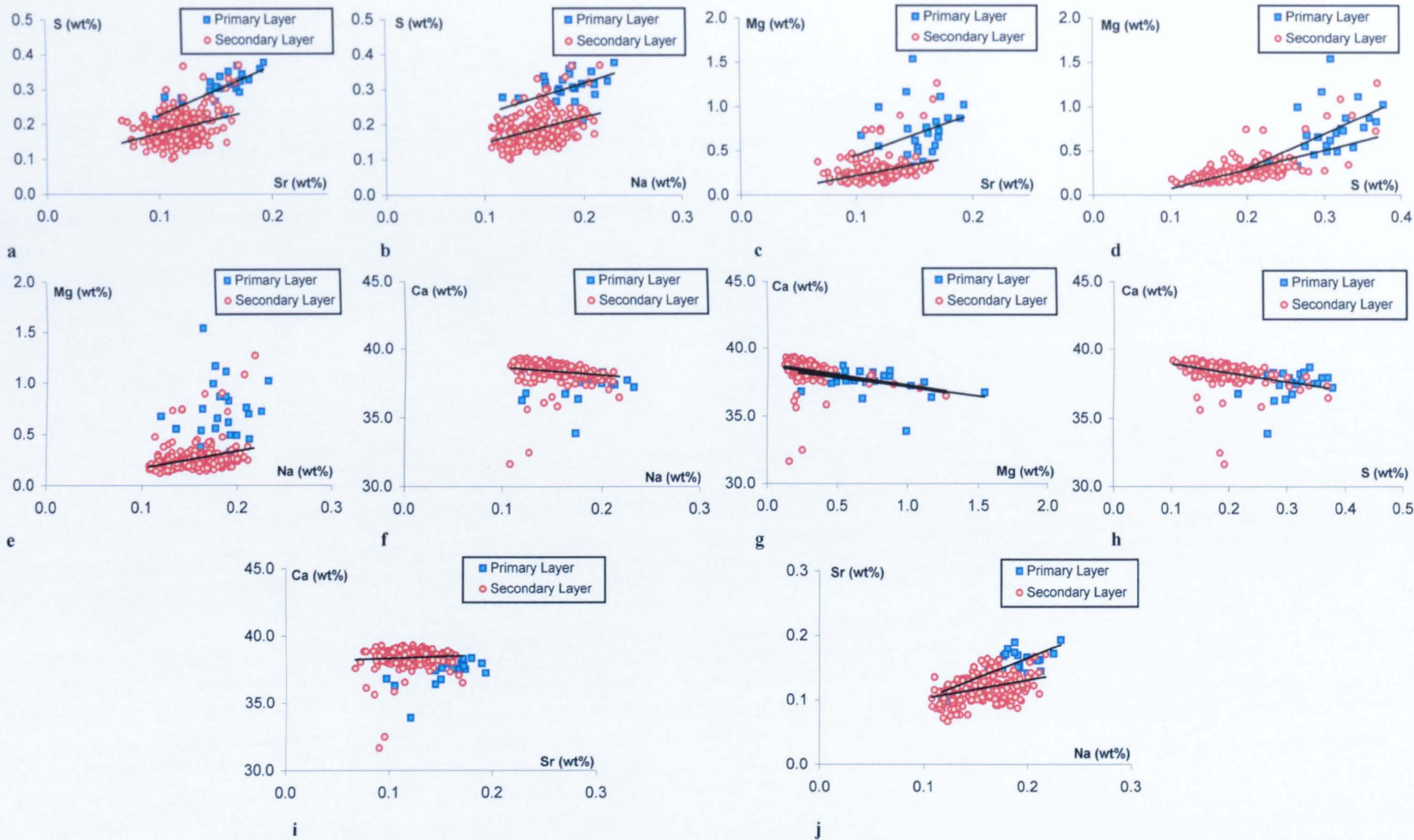


Figure 3.9 (a-d) presents X-ray maps of magnesium, sulphur, sodium and strontium in a specimen of *T. retusa*. X-ray maps of magnesium, sulphur and calcium distribution produced using the electron probe are presented in Figure 3.10 (a-c). The difference in magnesium and sulphur concentration between the primary and secondary layers is illustrated in Figures 3.9 a and b and 3.10 a and b. These maps clearly indicate that there is a higher concentration of magnesium and sulphur in the primary layer of the shell. The maps also display related regions of high concentration of magnesium and sulphur, which extend from the primary layer into the secondary layer. Figure 3.10(c) indicates that the same regions of the shell, which have a high magnesium and sulphur content, are depleted in calcium.

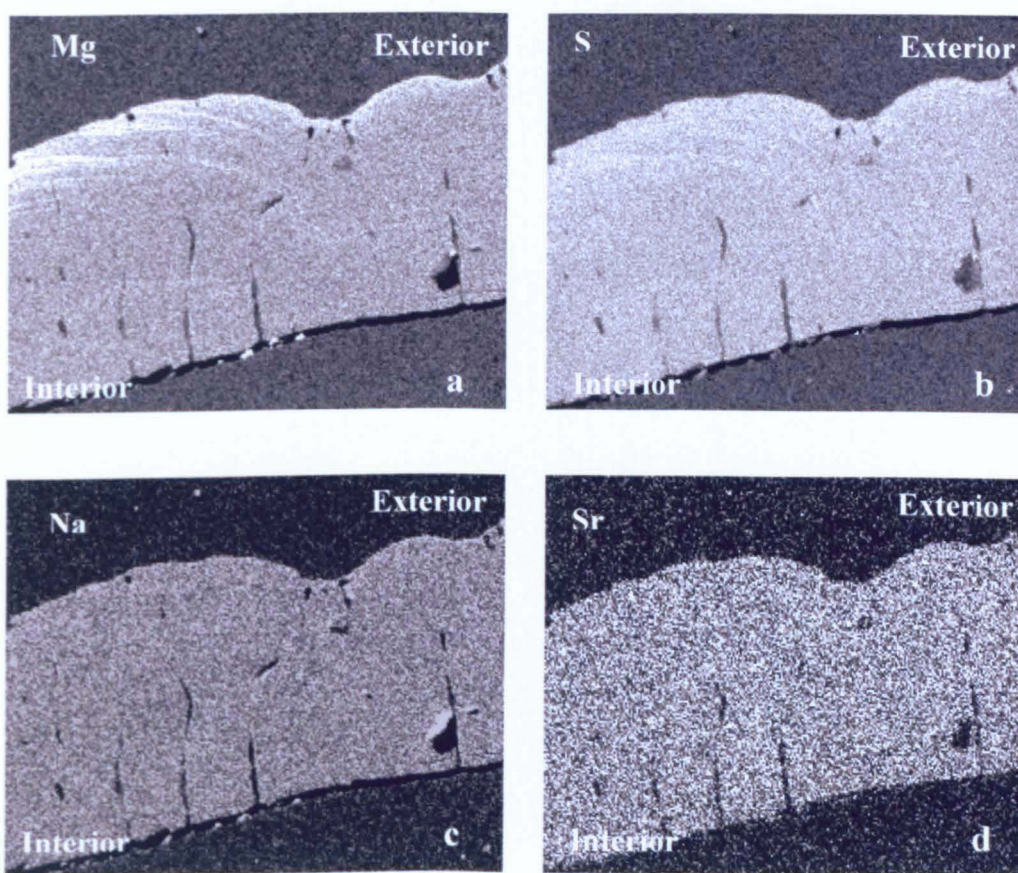


Figure 3.9 (a-d) X-ray maps of element concentration in *Terebratulina retusa* acquired by SEM

a. MgK α , b. SK α , c. NaK α , d. SrK α . For each map light grey areas indicate a greater element concentration while dark grey areas indicate lower element concentration.

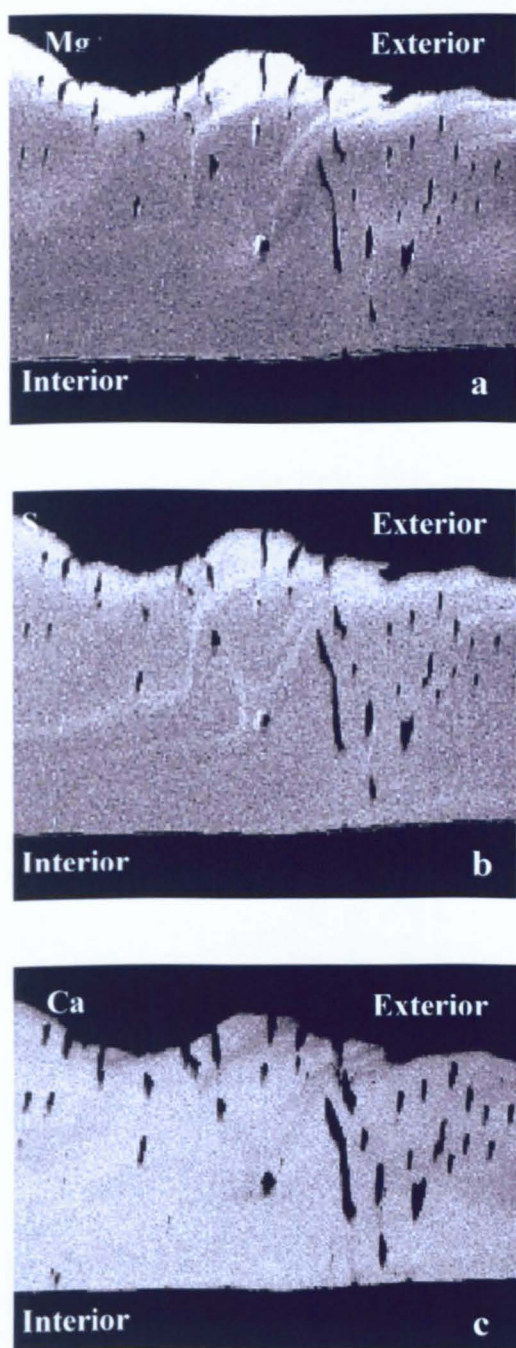


Figure 3.10 (a-c) X-ray maps of element concentration in *Terebratulina retusa* acquired by electron probe

a. Magnesium, b. Sulphur, c. Calcium. For each map, light grey areas indicate a greater element concentration while dark grey areas indicate lower element concentration.

3.3.1.3 Cathodoluminescence Spectroscopy

T. retusa is optically non-luminescent but luminesces blue when studied by CL-spectroscopy (Figure 3.11a and b). Both the wavelength and intensity of luminescence is consistent across the shell (Figure 3.11a). Dark blue/black areas of the map are areas of the sample that have been damaged by the electron probe.

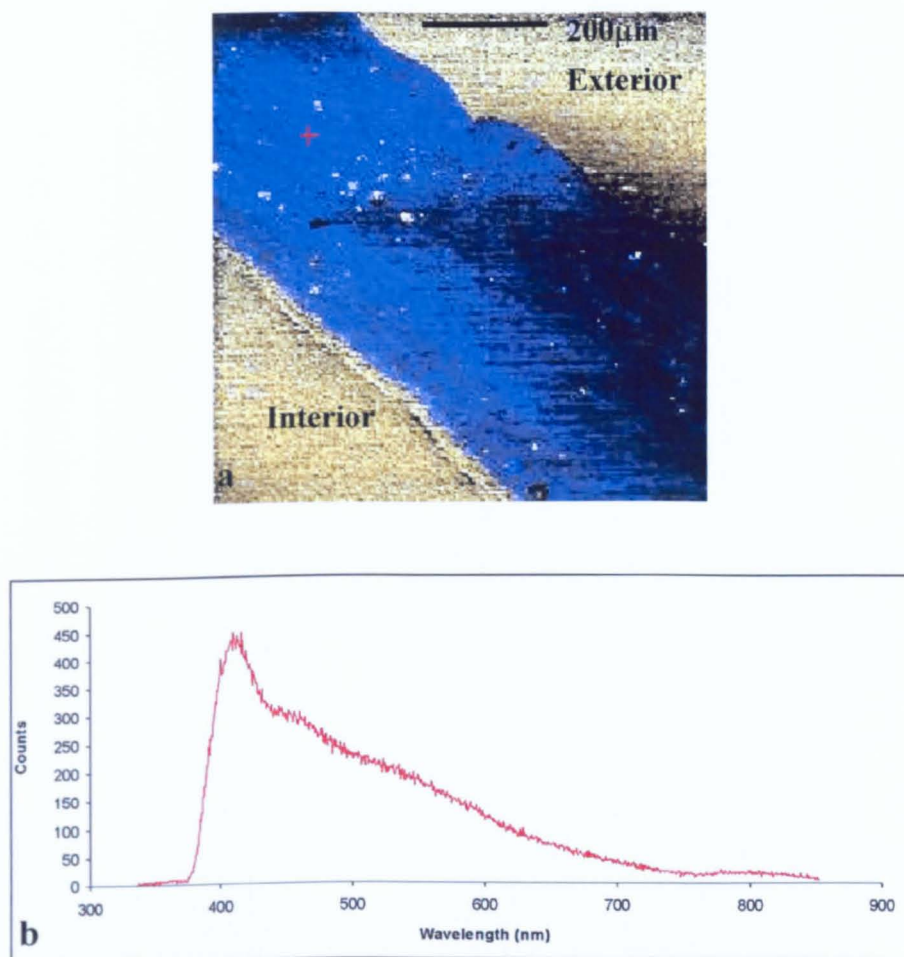


Figure 3.11(a) Hyperspectral image showing the intensity and wavelength of CL emission from a specimen of *Terebratulina retusa*, **(b)** CL emission spectrum acquired from *Terebratulina retusa*

CL spectroscopy was carried out as described in Section 2.6.5. The image and spectrum were produced using the software, CHIMP. The red cross in Figure 3.11(a) marks the point from which the spectrum was obtained. Units on the Y axis of the CL spectrum (Figure 3.11b) are arbitrary.

3.3.2 *Novocrania anomala* Ultrastructure and Minor Elements

3.3.2.1 Ultrastructure

The *N. anomala* shell has three layers; an outer organic periostracum, a primary layer consisting of acicular calcite and a secondary layer composed of calcite semi nacre (Figure 3.12). The shell also contains punctae (Figure 3.13), which branch at the terminus (Williams and Wright, 1970). The primary layer of the shell is composed of needle-like crystals, each of which is orientated at 45° to the isochronous surfaces within the primary layer (Williams and Wright, 1970). The secondary layer is formed from calcite semi-nacre. Semi-nacre exhibits a laminar structure similar to that of aragonite nacre, which is characteristic of mollusc shells. However semi-nacre differs in that it is composed of calcite rather than aragonite and has fewer screw dislocations (Weedon and Taylor, 1995). Steps form on the lattice surface due to dislocation of the lattice planes, the steps rotate producing a spiral growth pattern resulting in the formation of both left and right screw dislocations (Figure 3.14).

A transmitted light (plane polarised light) image is presented in Figures 3.15, in which the boundary between the primary and secondary layer and the laminar structure of the secondary layer are evident.

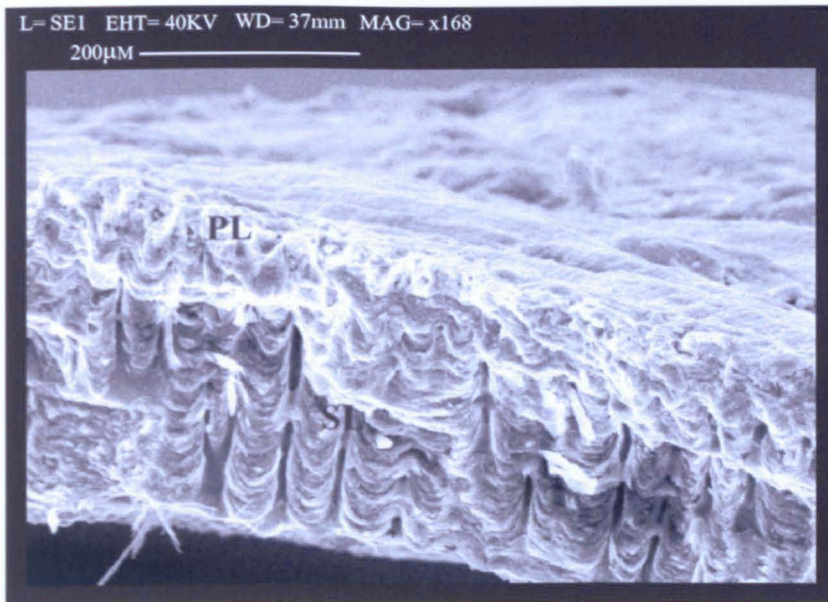


Figure 3.12 Secondary electron image of the primary (PL) and secondary (SL) layers of *Novocrania anomala*

SEM image of a fractured section of a specimen of N. anomala.

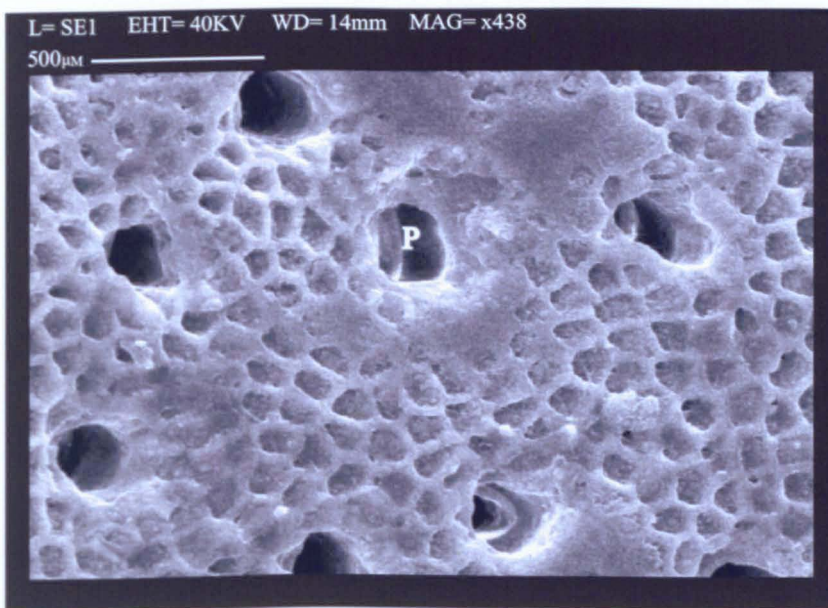


Figure 3.13 Secondary electron image of the inner surface of the shell of *Novocrania anomala*

SEM image of a fractured section of a specimen of N. anomala.

Punctae (P).

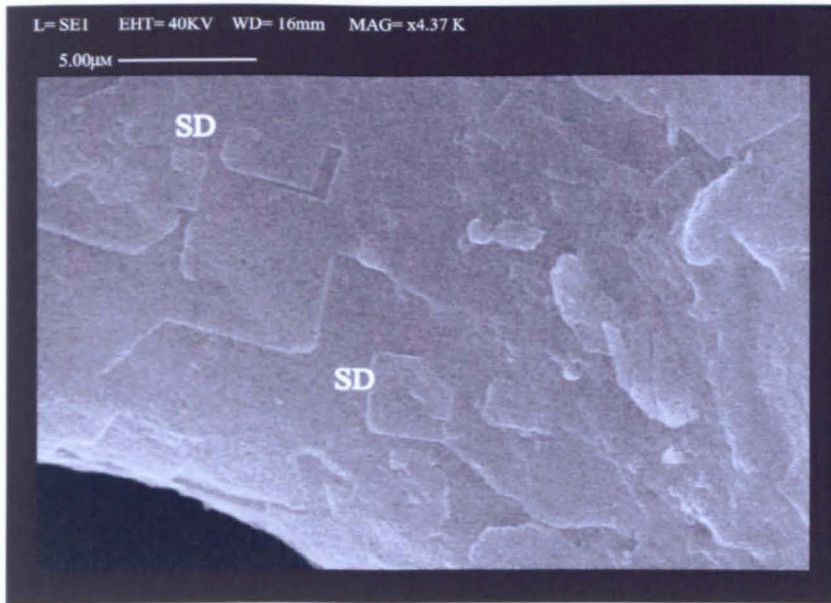


Figure 3.14 Secondary electron image of screw dislocations (SD) in the secondary layer of *Novocrania anomala*

SEM image of a fractured section of a specimen of N. anomala.

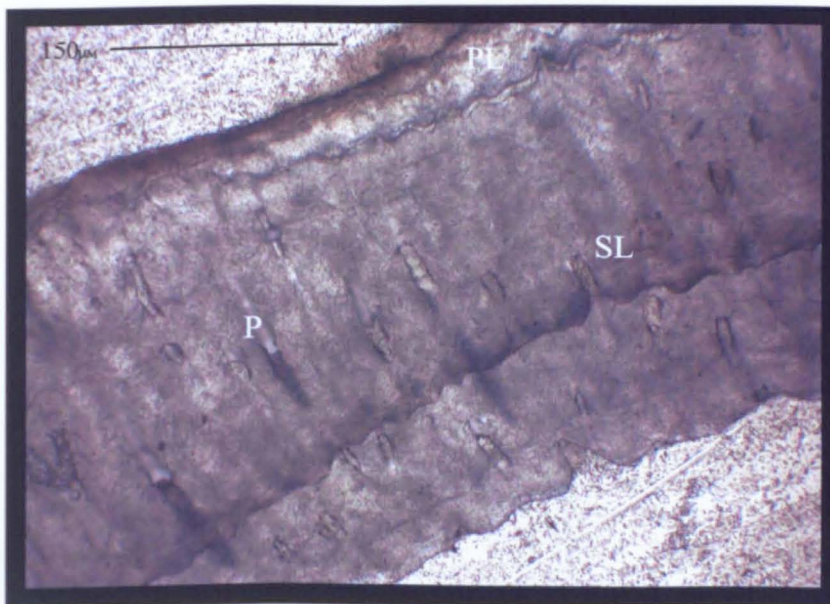


Figure 3.15 Transmitted light image of *Novocrania anomala* in thin section

The primary layer (PL), secondary layer (SL) and punctae (P) are evident in thin section.

3.3.2.2 Minor Element Composition-Electron Microprobe Analysis

Electron microprobe analyses of magnesium, strontium, sodium and sulphur across the shells of three individuals of *N. anomala* are presented in Figure 3.16. Manganese, iron, potassium and phosphorus were all below the limit of detection of the SX 50 electron microprobe and are therefore not discussed. Results are summarised in Table 3.3.

Specimen	Layer	Mg Conc. Range (wt%)	Sr Conc. Range (wt%)	Na Conc. Range (wt%)	S Conc. Range (wt%)	Figure No.
a	Primary	2.09-2.76	0.21-0.22	0.20-0.28	0.28-0.31	3.16a
a	Secondary	1.90-2.65	0.18-0.25	0.15-0.23	0.25-0.44	3.16a
b	Primary	1.90-2.36	0.26-0.28	0.14-0.17	0.31-0.32	3.16b
b	Secondary	1.09-3.73	0.13-0.33	0.08-0.23	0.21-0.34	3.16b
c	Primary	2.37-2.41	0.22-0.26	0.17-0.19	0.26-0.27	3.16c
c	Secondary	2.20-2.68	0.22-0.27	0.15-0.28	0.19-0.29	3.16c

Table 3.3 Summary of electron microprobe results for *N. anomala*

The results displayed in Table 3.3 summarise the concentration range (i.e. the lowest concentration to the highest concentration) of Mg, Sr, Na and S in the primary and secondary layers of N. anomala

In contrast to *T. retusa*, *N. anomala* has a high magnesium calcite shell. Magnesium concentrations attain a maximum of 2.76, 3.73 and 2.68 wt% respectively in the three specimens of *N. anomala* presented in Figure 3.16 (a-c). Magnesium concentrations vary little across the shells and there is no detectable difference in concentration between the primary and secondary layers. Sulphur, strontium and sodium concentrations are also invariant across the primary and secondary layers of the shell.

In common with data obtained for *T. retusa*, the mean values for the concentration of each element in the primary and secondary layers were analysed using ANOVA in order to determine if there are any significant differences in concentration between the two layers. Results indicate that there is no significant difference in element concentration between the primary and secondary layers of the shell (Table 3.4).

Element	P-value
Sulphur	0.785
Magnesium	0.466
Calcium	0.948
Strontium	0.137
Sodium	0.539

Table 3.4 Results of Analysis of Variance for element concentration in the primary and secondary layers of *Novocrania anomala*

Figure 3.17 (a-e) presents boxplots of element concentration as a function of the shell layer. Each box represents the interquartile range of each data set, the mean values are represented as red circles. For the elements discussed here the spread of data for the primary and secondary layers lie within the same range and therefore the concentration of elements in each layer is not significantly different.

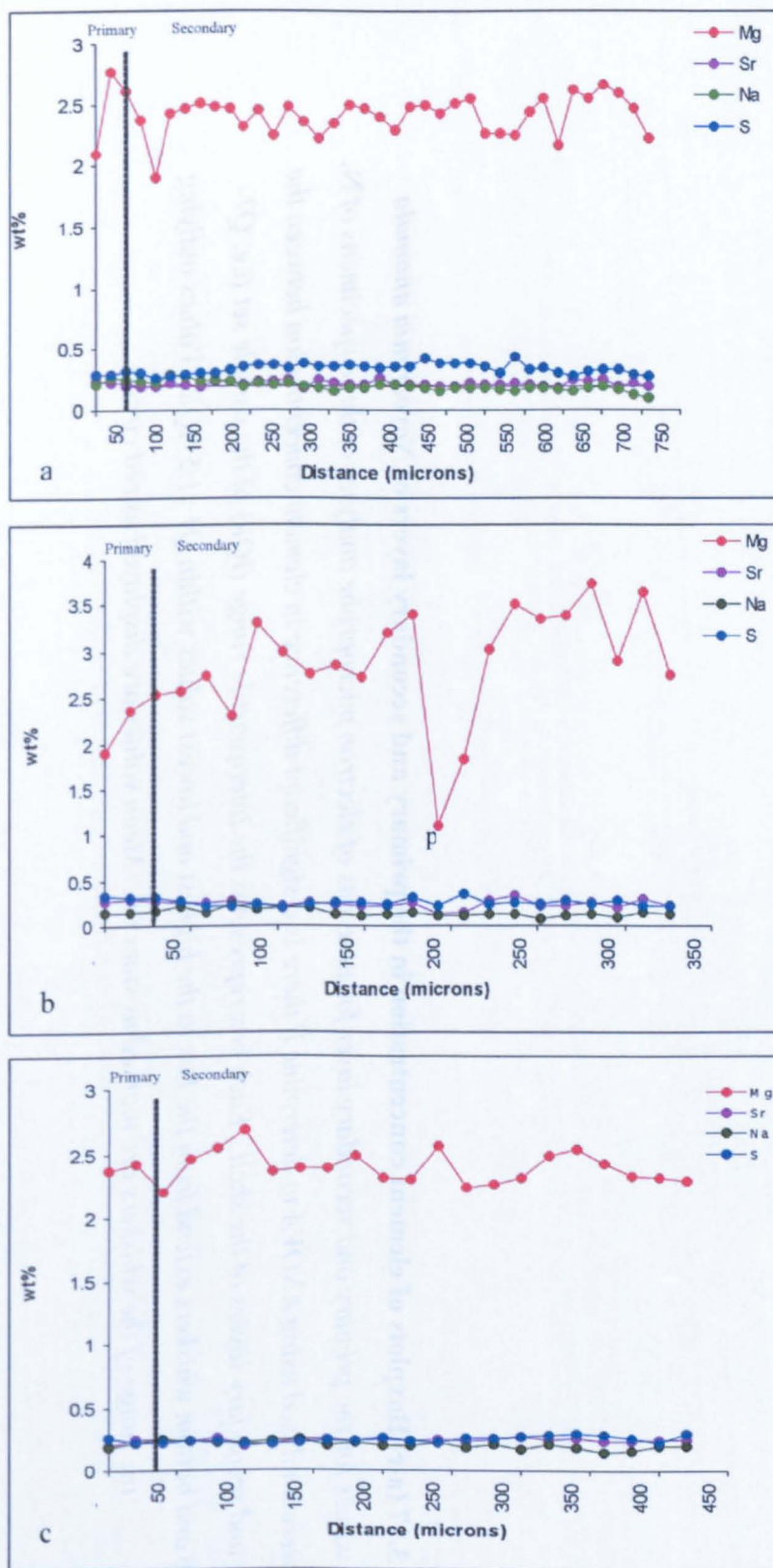


Figure 3.16 (a,b&c) Electron microprobe spot analyses across the shell of *Novocrania anomala*

Electron microprobe analyses were carried out as described in Section 2.6.2.

Elements displayed are above the limit of detection. Punctae (p)

Figure 3.17 (a-e) Boxplots of element concentration in the primary and secondary layers of *Novocrania anomala*
*The mean values for the primary and secondary layer for nine sets of electron microprobe analyses of three specimens of *N. anomala* were analysed using ANOVA to determine if there is a significant difference in element concentration between the primary and secondary layers of the shell. Each box represents the interquartile range (IQR) of the sample set (i.e. Q1-Q3). Top and bottom whiskers extend from the box to the highest and lowest values within $Q1 + 1.5 * IQR$. Values outlying the range of the whiskers are marked as stars (*). Mean values are displayed as red circles.*

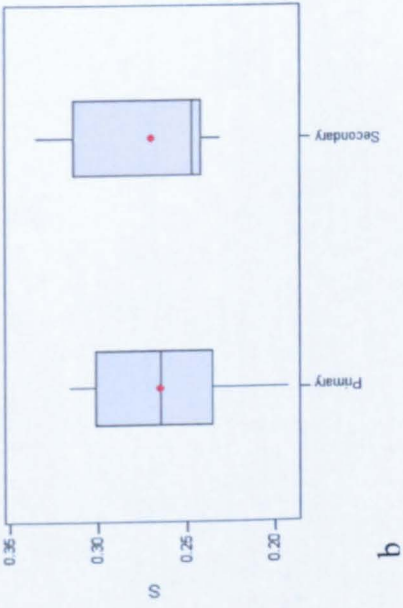
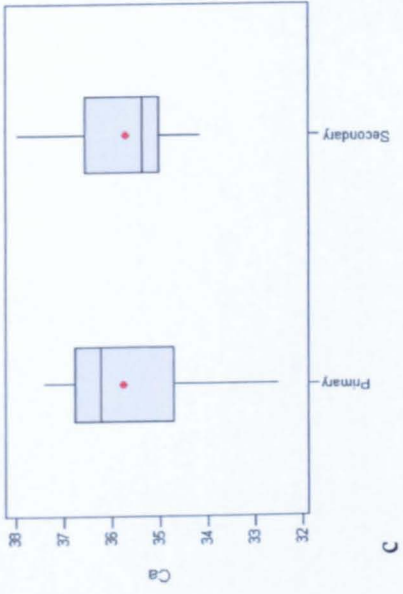
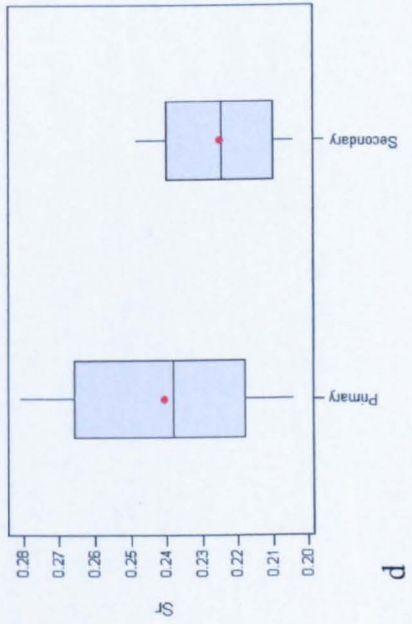
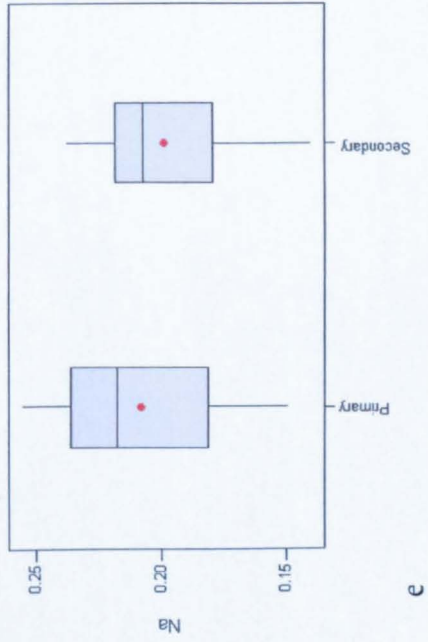


Figure 3.18 displays scatter plots for data comprising three sets of analyses taken across the primary and secondary layers of three individuals of *N. anomala*. Correlation coefficients are presented in Table 3.5. There is some indication of a positive correlation between calcium and magnesium and between calcium and strontium in the secondary layer. There is a negative correlation between calcium and sodium in the primary and secondary layers and between strontium and sodium in the primary layer.

<i>N. anomala</i>	Primary Layer		Secondary Layer	
Variables	Correlation Coefficient	P-value	Correlation Coefficient	P-value
S/Sr	-0.188	0.348	-0.377	0.000
S/Na	-0.375	0.054	-0.052	0.477
Mg/Sr	0.002	0.994	0.303	0.000
Mg/S	-0.141	0.483	-0.158	0.029
Mg/Na	0.322	0.102	-0.333	0.000
Ca/Na	-0.495	0.009	-0.363	0.000
Ca/Mg	0.100	0.619	0.464	0.000
Ca/S	-0.095	0.636	-0.240	0.001
Ca/Sr	0.487	0.010	0.436	0.000
Sr/Na	-0.491	0.009	-0.180	0.014

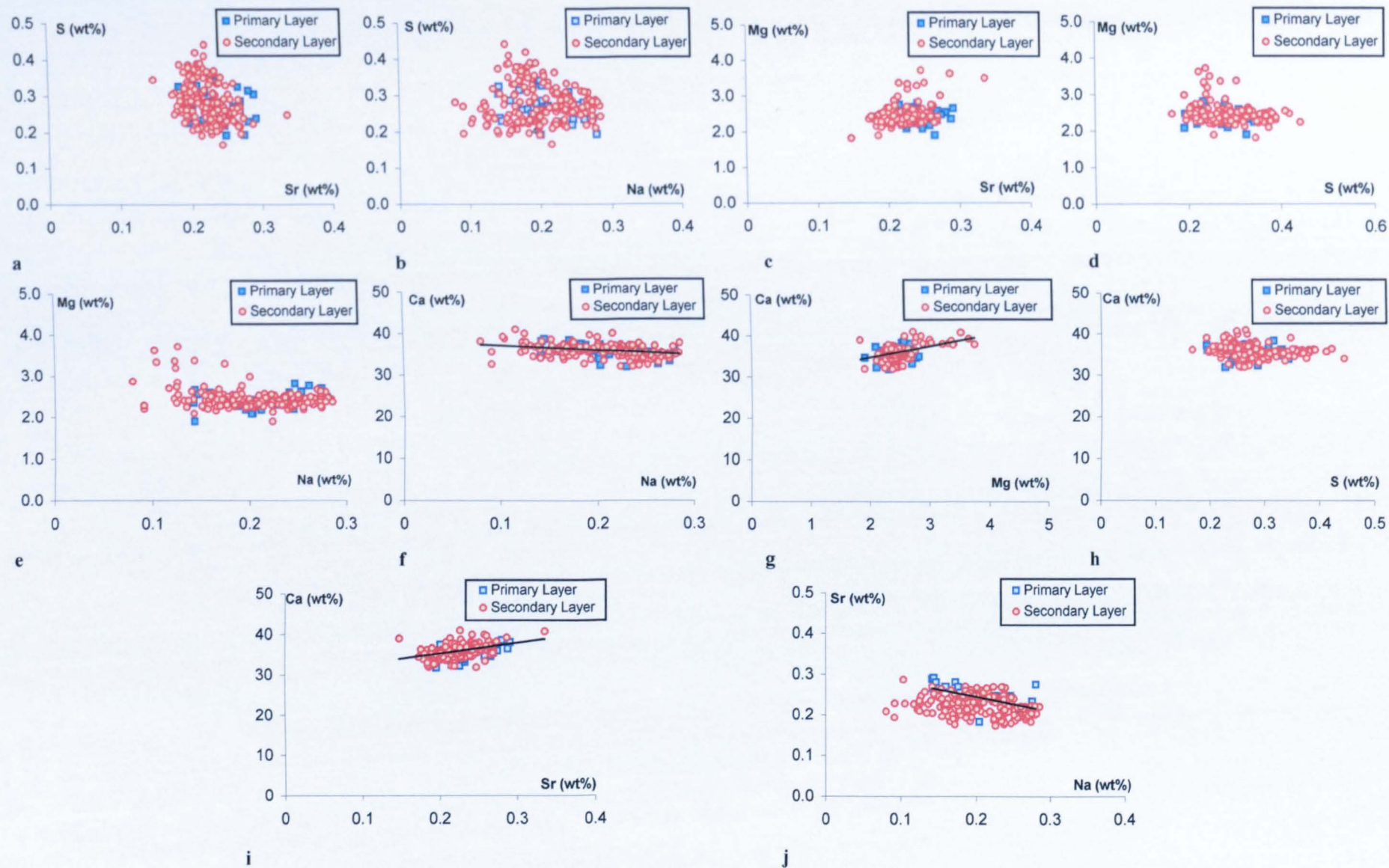
Table 3.5 Pearson correlation coefficients with P-values for element concentration in the primary and secondary layers of *N. anomala*

*Pearson correlation coefficients were calculated to determine the linear relationships between element concentrations in the primary and secondary layers of *N. anomala*. Values close to 1 indicate a strong positive linear correlation.*

Figure 3.19 presents EDS maps of element concentration across a specimen of *N. anomala*. The maps concur with the data obtained from electron microprobe spot analyses (Figure 3.16) in that there is no detectable difference in element concentration between the primary and secondary layers of the shell and little variation across the whole specimen.

Figure 3.18 (a-j) Scatter plots of element concentration in the primary and secondary layers of *Novocrania anomala*

The concentration of minor elements in the primary and secondary layers of three specimens of N. anomala was analysed by electron microprobe as described in Section 2.6.2. The data from three sets of electron microprobe analyses from each specimen are plotted in order to determine any relationships between elements present within the shell.



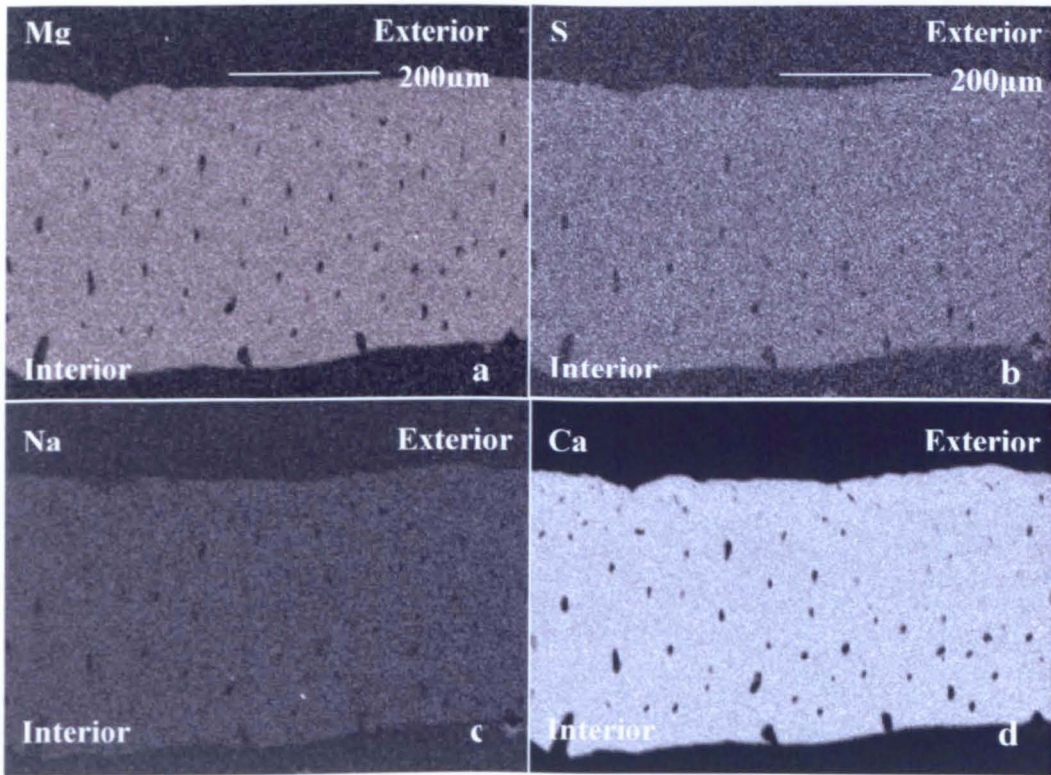


Figure 3.19 X-ray maps of element concentration in *Novocrania anomala*

a. MgK α , b. SK α , c. NaK α , d. CaK α . A specimen of N. anomala was prepared for analysis as described in Section 2.6.1. Mapping was carried out as described in Section 2.6.4. For each map, light grey areas indicate a greater element concentration while dark grey areas indicate lower element concentration.

3.3.2.3 Cathodoluminescence Imaging and Spectroscopy

In optical CL *N. anomala* has an orange-red emission (Figure 3.20), in contrast to *T. retusa*. These images also pick out the laminae that form the secondary layer.

A hyperspectral map of luminescence from a specimen of *N. anomala* differs from the optical CL image (Figure 3.21a). The most intense emission is at blue wavelengths but the innermost area of the secondary layer has a peak at between 600-650nm (Figure 3.21b), which produces the pink emission mixed with the blue (Figure 3.21a)

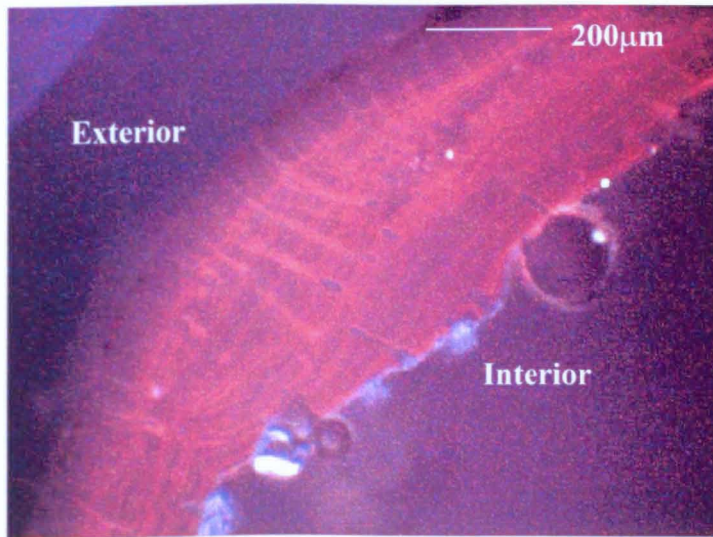
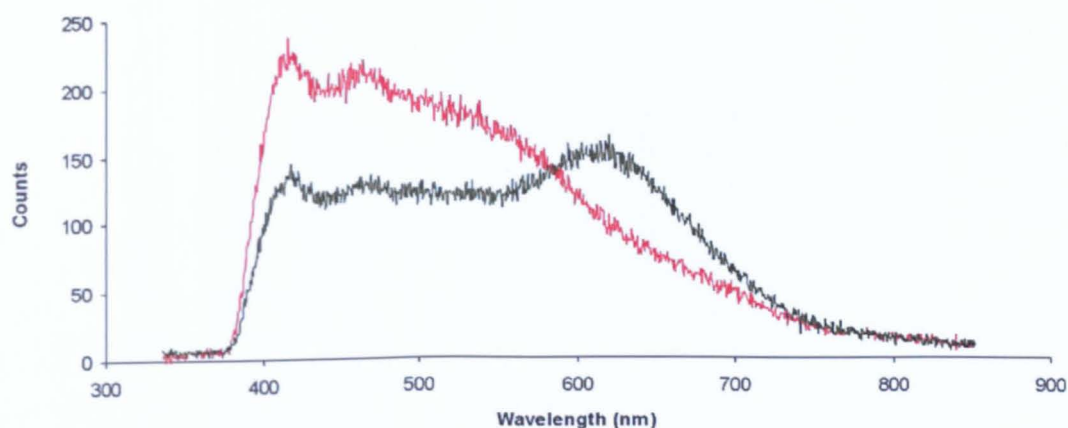


Figure 3.20 Cathodoluminescence image of *Novocrania anomala*

A thin section of a specimen of N. anomala was prepared as described in Section 2.5. The image was captured as described in Section 2.6.5.



(b)

Figure 3.21 (a) Hyperspectral image showing the intensity and wavelength of CL emission from a specimen of *Novocrania anomala* (b) CL emission spectrum acquired from *Novocrania anomala*

Cathodoluminescence spectroscopy was carried out as described in Section 2.6.6. The image was produced using the software, CHIMP. The red cross on the CL map corresponds to the red line spectrum while the green cross corresponds to the green line spectrum. Units on the Y axis of Figure 3.21(b) are arbitrary.

3.3.3 *Mytilus edulis* Ultrastructure and Minor Elements

3.3.3.1 Ultrastructure

The shell of *Mytilus edulis* has three layers; an outer organic periostracum and two inner mineralised layers (Figure 3.22). In contrast to the calcite shells of *T. retusa* and *N. anomala*, the mineralised layers of *M. edulis* are composed of calcite and aragonite. The organic periostracum is composed mainly of sclerotised proteins and acts as a substrate for initial crystal nucleation (Watabe, 1988). The calcite layer comprises prisms that are oriented in the same direction and each is encased in organic matrix (Figure 3.23). Underlying the calcite are layers of tabular aragonite crystals (Figure 3.24 and 3.25). Each crystal is offset from the underlying crystal to form a "brick wall" structure. All the crystals are aligned with the c axis almost perpendicular to the inner surface while the orientation of the a and b axes vary (Watabe, 1988).

Thin section photographs are presented in Figures 3.26 and 3.27. The calcite and aragonite layers and the boundary between the layers can be seen in both plane-polarised light and cross-polarised light images.

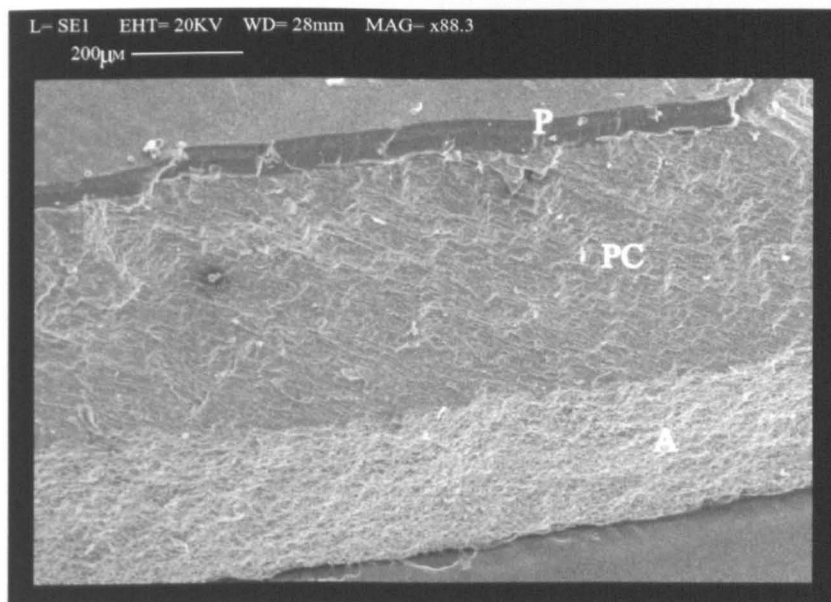


Figure 3.22 The periostracum (P), prismatic calcite layer (PC) and aragonite layer (A) of a specimen of *Mytilus edulis*

Secondary electron image of a fractured section of a specimen of M. edulis.

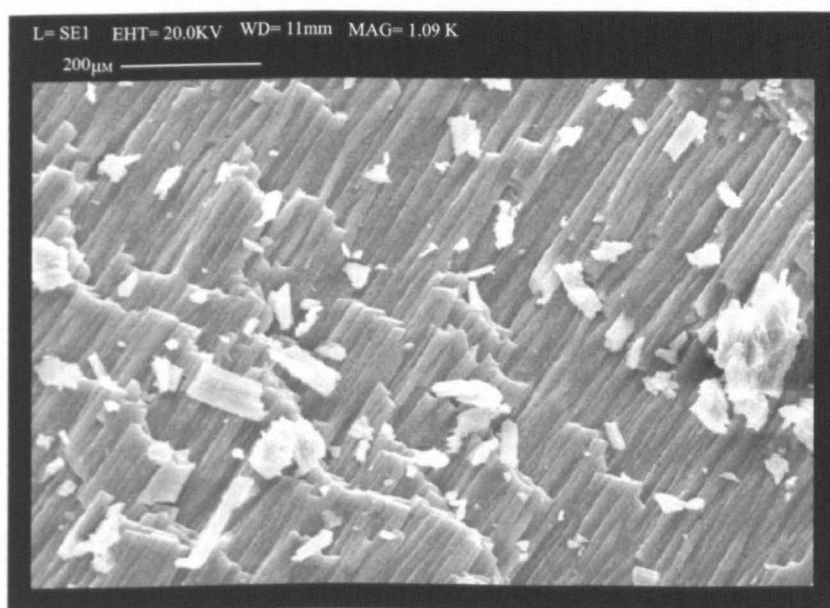


Figure 3.23 The prismatic calcite layer of *Mytilus edulis*

Secondary electron image of a fractured section of a specimen of M. edulis.

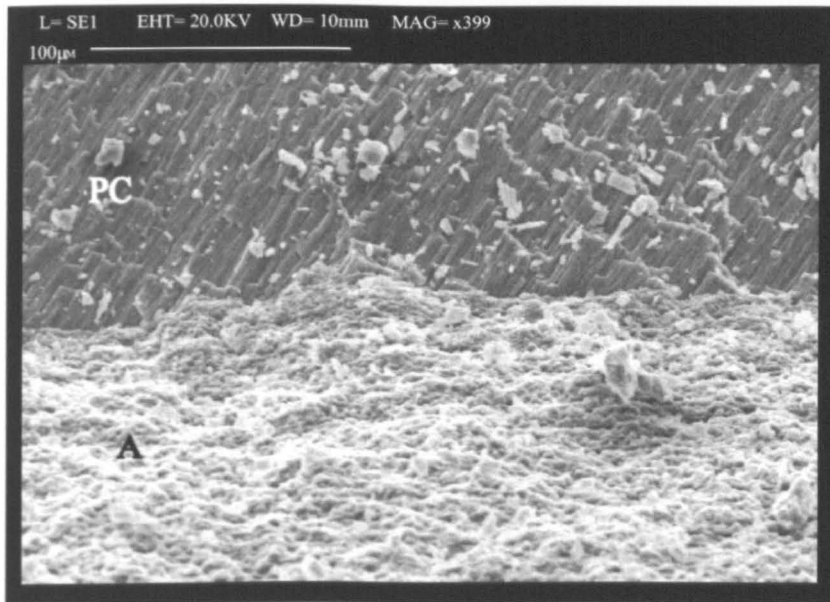


Figure 3.24 Boundary between the prismatic calcite layer (PC) and aragonite layer (A) in *Mytilus edulis*

Secondary electron image of a fractured section of a specimen of M. edulis.

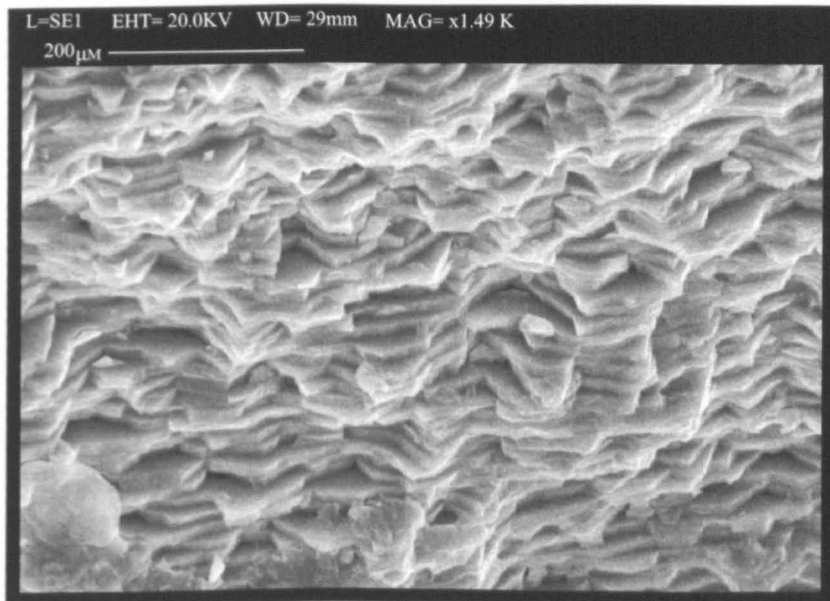


Figure 3.25 Aragonite layer of a specimen of *Mytilus edulis*

Secondary electron image of a fractured section of a specimen of M. edulis.

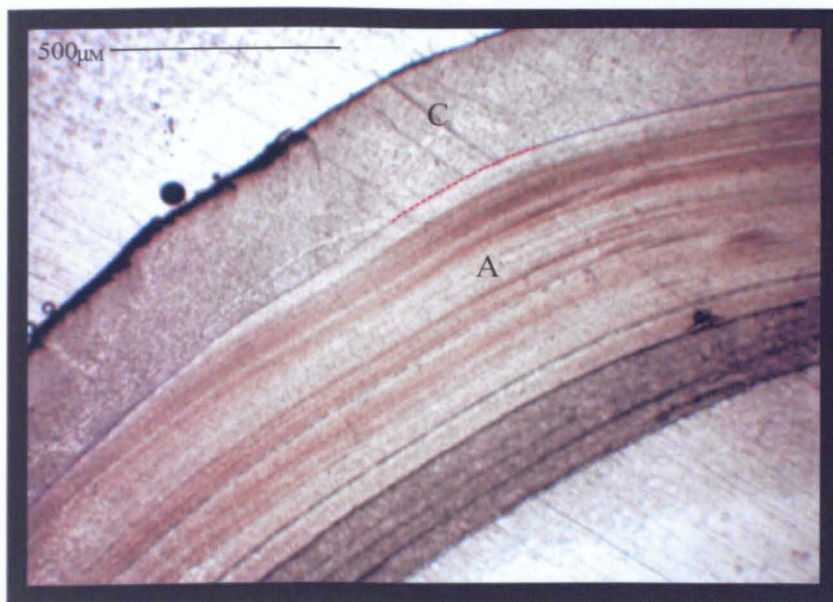


Figure 3.26 Transmitted light image of *Mytilus edulis* in thin section

Calcite (C) and aragonite (A) layers are apparent in thin section. Red dashed line marks the boundary between the calcite and aragonite layers

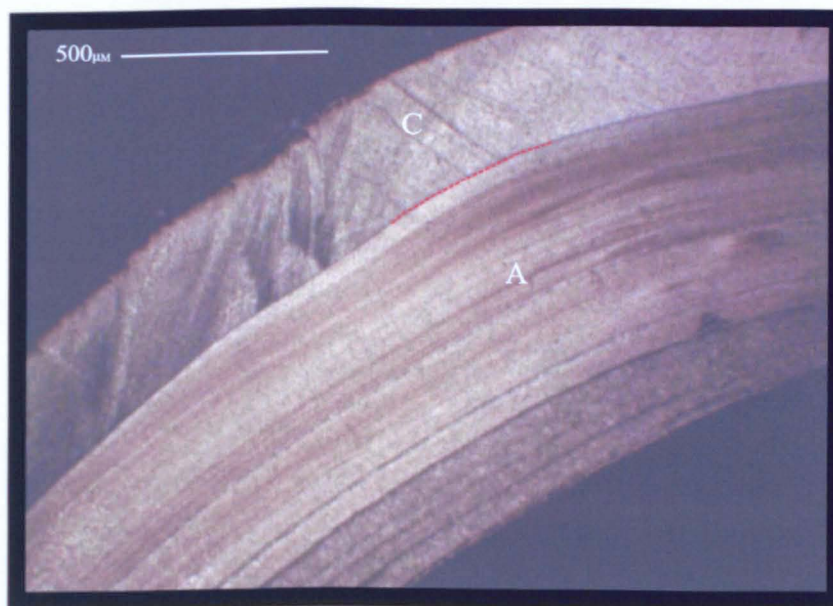


Figure 3.27 Cross-polarised light image of *Mytilus edulis* in thin section

Calcite (C) and aragonite (A) layers are apparent in thin section. Red dashed line marks the boundary between the calcite and aragonite layers

3.3.3.2 Minor Element Composition- Electron Microprobe Analysis

Electron microprobe spot analyses taken across the calcite and aragonite layers of specimens a and b of *M. edulis* are presented in Figure 3.28 a and b respectively. Spot analyses were taken in a line perpendicular to the line of section. Magnesium, strontium, sodium and sulphur are all present in concentrations above detection limits. (Manganese, iron, potassium and phosphorus are below detection limits and therefore not discussed). Results are summarised in Table 3.6.

Specimen	Polymorph	Mg Conc. Range (wt%)	Sr Conc. Range (wt%)	Na Conc. Range (wt%)	S Conc. Range (wt%)	Figure No.
a	Calcite	0.05-0.18	0.06-0.13	0.05-0.22	0.01-0.11	3.28a
a	Aragonite	0-0.04	0.07-0.32	0.19-0.24	0.01-0.06	3.28a
b	Calcite	0.06-0.16	0.04-0.14	0.19-0.30	0.03-0.11	3.28b
b	Aragonite	0-0.01	0-0.15	0.12-0.30	0.02-0.10	3.28b

Table 3.6 Summary of electron microprobe results for *M. edulis*

The results displayed in Table 3.6 summarise the concentration range (i.e. the lowest concentration to the highest concentration) of Mg, Sr, Na and S in the calcite and aragonite layers of M. edulis

There is a difference in chemical composition between the calcite and aragonite in *M. edulis*. Magnesium concentrations are highest in the outer calcite layer (0.05 to 0.18 wt% and 0.06 to 0.16 wt% in specimens a and b respectively (Figure 3.28). The distribution of magnesium within the calcite layer varies between individuals, as is demonstrated by specimens a and b (Figure 3.28).

The maximum concentrations of sodium are comparable between the calcite and aragonite layers. Sodium reaches a maximum of 0.22 wt% and 0.24 wt% respectively in the calcite and aragonite layer of specimen a (Figure 3.28a), and 0.30 wt% in the calcite and aragonite layers of specimen b (Figure 3.28b). In both specimens sodium concentration decreases across the calcite layer from the periostracum towards the polymorph boundary, while sodium concentration is relatively constant throughout the aragonite layer of the shell.

Analyses of specimen a indicate that strontium concentration is slightly greater in the aragonite layer than the calcite layer (Figure 3.28a) but this trend is not apparent in specimen b (Figure 3.29b) where the concentration of strontium is constant across the shell section. There is no evidence for a significant difference in sulphur concentration between the calcite and aragonite.

Figure 3.29 presents scatter plots of element concentration in *M. edulis* from six sets of spot analyses taken across both specimens of *M. edulis*. Correlation coefficients are presented in Table 3.7. Within the calcite layer there is a strong positive correlation between sulphur, strontium and sodium (Table 3.7). Magnesium and sodium display a negative correlation in the aragonite layer. There is a positive correlation between strontium and sodium in the calcite layer while there is a negative correlation in the aragonite layer (Figure 3.29j and Table 3.7).

<i>M. edulis</i>	Calcite Layer		Aragonite Layer	
Variables	Correlation Coefficient	P-value	Correlation Coefficient	P-value
S/Sr	0.608	0.000	0.204	0.219
S/Na	0.826	0.000	-0.220	0.185
Mg/Sr	0.091	0.347	0.089	0.596
Mg/S	0.028	0.774	0.130	0.437
Mg/Na	0.136	0.157	-0.787	0.000
Ca/Na	-0.015	0.873	0.300	0.067
Ca/Mg	0.198	0.040	0.077	0.647
Ca/S	0.041	0.675	-0.068	0.685
Ca/Sr	0.086	0.375	-0.304	0.063
Sr/Na	0.658	0.000	-0.391	0.015

Table 3.7 Pearson correlation coefficients with P-values for element concentration in the calcite and aragonite layers of *M. edulis*

*Pearson correlation coefficients were calculated to determine the linear relationships between element concentrations in the calcite and aragonite layers of *M. edulis*. Values close to 1 indicate a strong positive linear correlation.*

Figure 3.30 displays maps of the distribution of magnesium, sulphur, sodium and calcium in a specimen of *M. edulis*. Magnesium concentration is greater in the calcite layer of the shell (Figure 3.30a). The element maps do not highlight any variation in sulphur, sodium and calcium concentration between the calcite and aragonite layers of the specimen possibly as the X-ray mapping is insensitive to the slight differences in concentration of some elements between the calcite and aragonite.

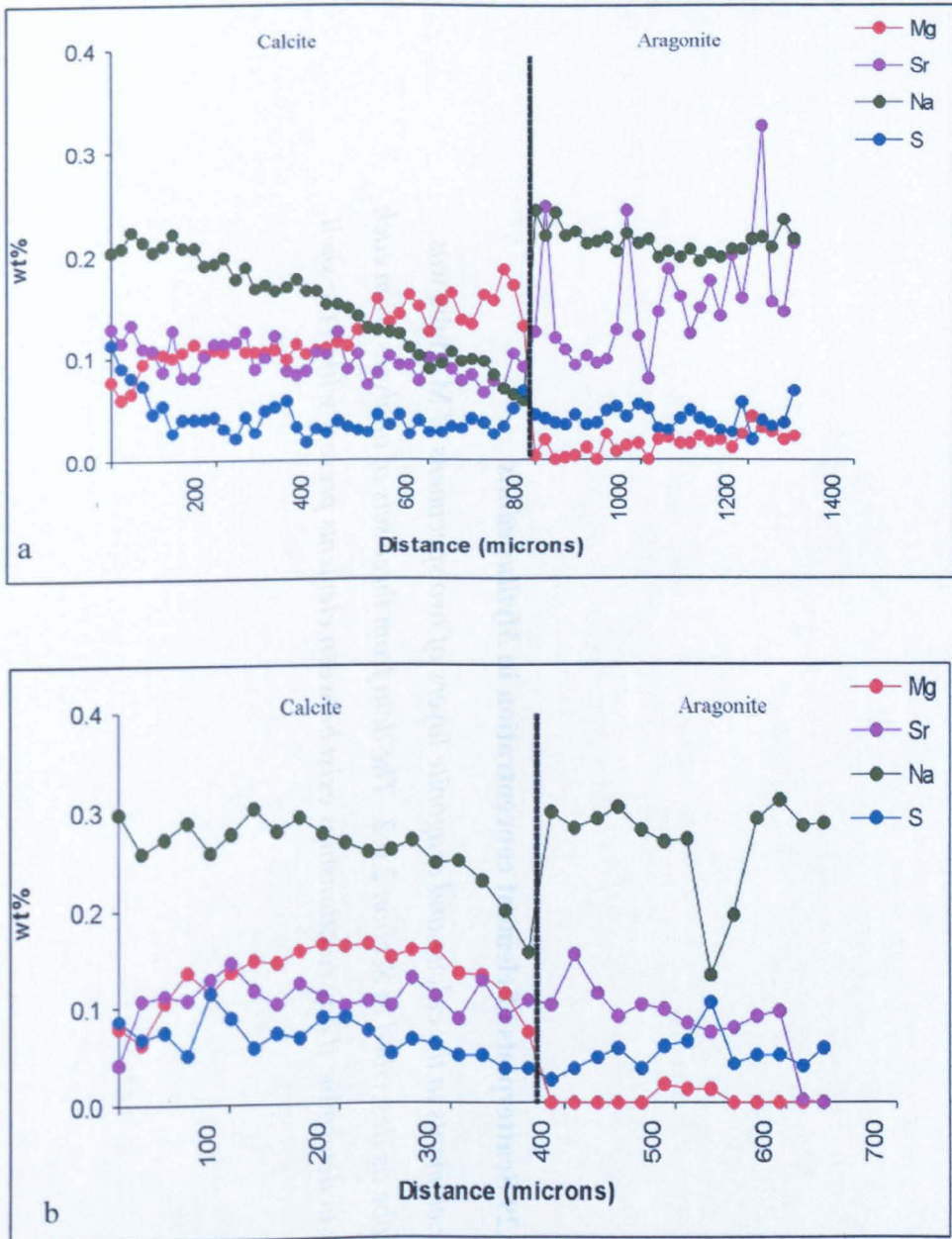
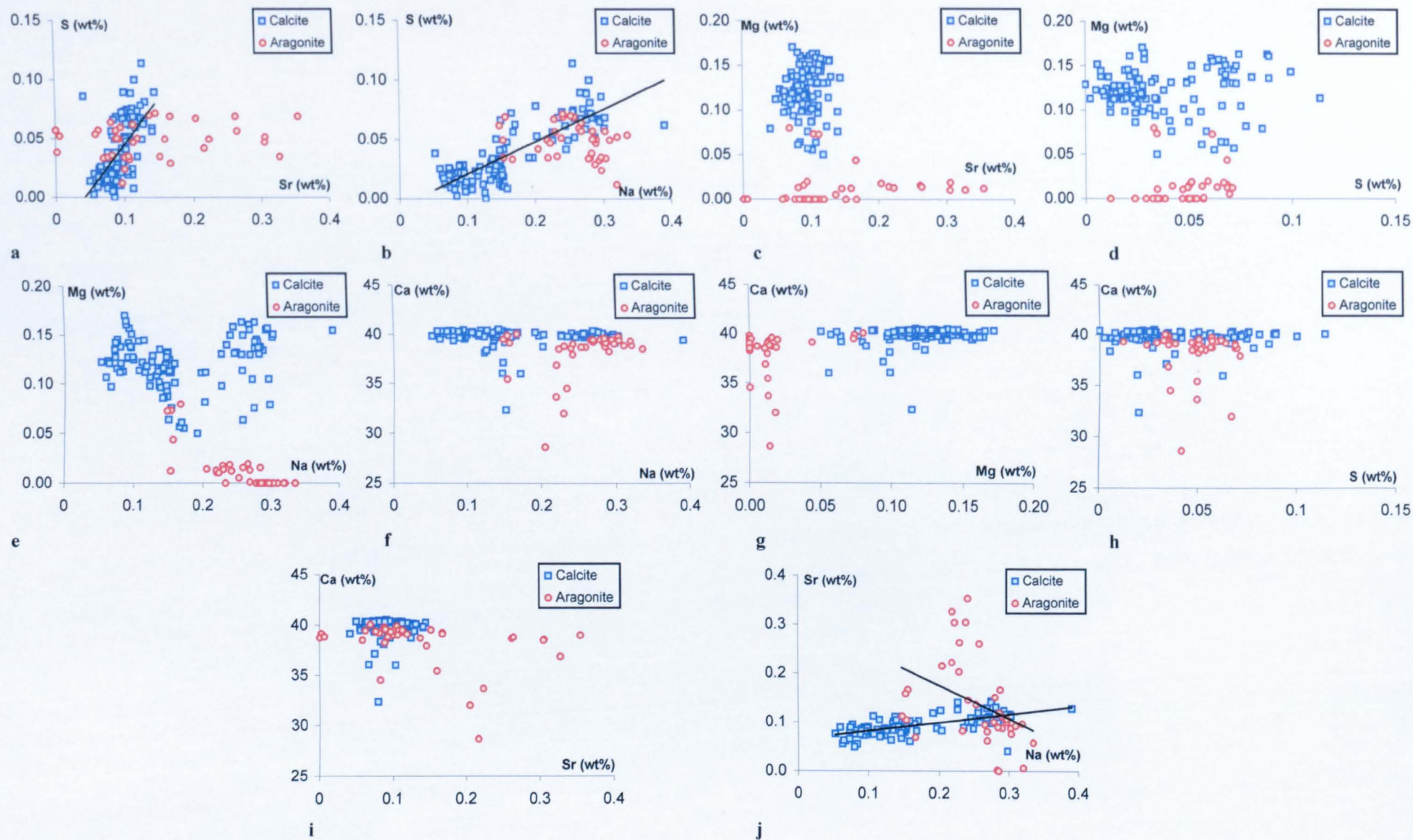


Figure 3.28 (a&b) Electron microprobe spot analyses of *Mytilus edulis*

Electron microprobe analyses were carried as described in Section 2.6.2. Elements displayed are above the limit of detection.

Figure 3.29 Scatterplots of element concentration in *Mytilus edulis*

*The concentration of minor elements in the calcite and aragonite layers of two specimens of *M. edulis* was analysed by electron microprobe as described in Section 2.6.2. The data from three sets of analyses from each specimen are plotted in order to determine if any relationships exist between elements present within the shell.*



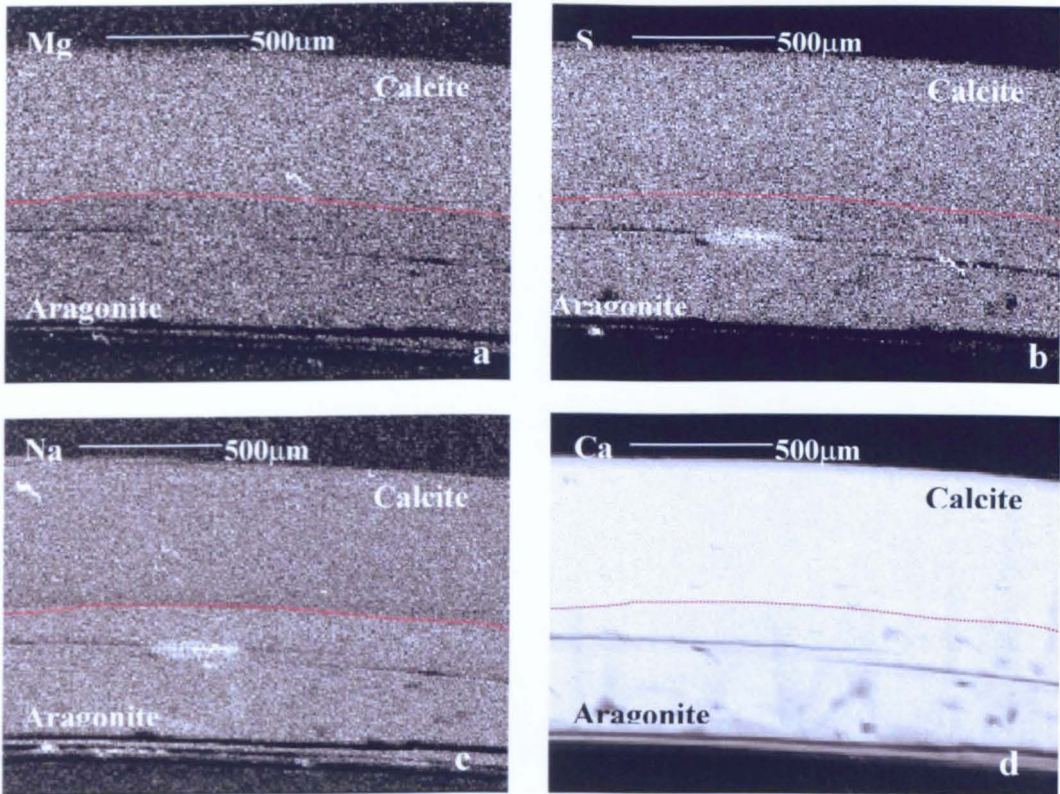


Figure 3.30 X-ray maps of element distribution in a specimen of *Mytilus edulis*

a. MgK α , b. SK α , c. NaK α , d. CaK α . A specimen of *M. edulis* was prepared for analysis as described in Section 2.6.1 and mapping was carried out as described in Section 2.6.4. For each map light grey areas indicate a greater element concentration while dark grey areas indicate lower element concentration. The boundary between the calcite and aragonite layers is marked by a red dashed line.

3.3.3.3 Cathodoluminescence Imaging and Spectroscopy

The optical CL image of *M. edulis* (Figure 3.31) shows a faint luminescence from the outer calcite layer but most of the layer is non-luminescent. The aragonite layer displays faint white/blue luminescence.

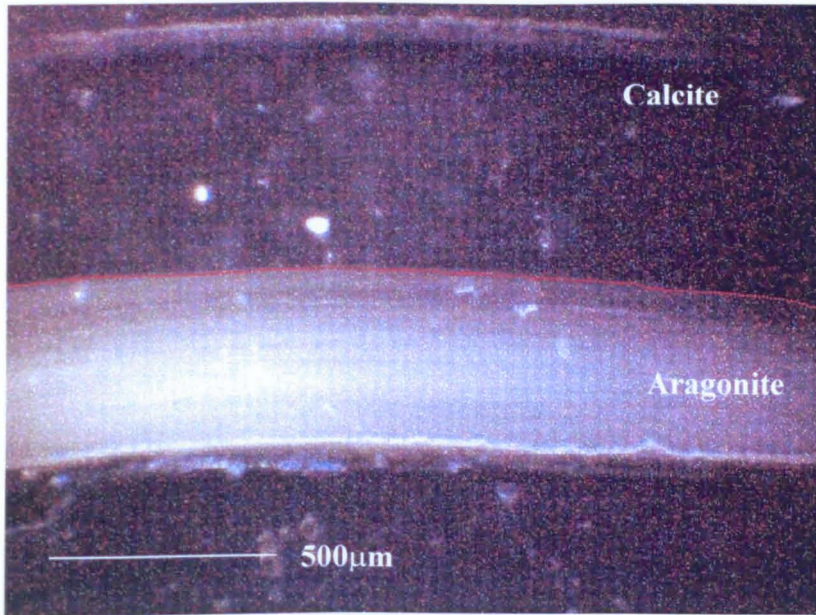


Figure 3.31 Cathodoluminescence image of a specimen of *Mytilus edulis*

A specimen of M. edulis was embedded in a resin block and prepared as described in Section 2.6.1. The image was captured as described in Section 2.6.5. The boundary between the calcite and aragonite layers is marked by a red dashed line.

In the hyperspectral map of *M. edulis* (Figure 3.32a) the calcite and aragonite layers have comparable peak wavelengths of emission but the intensity of luminescence differs both between the layers and within the aragonite layer (Figure 3.32b). A large proportion of the luminescence emitted from the specimen lies within the blue range of the visible spectrum (around 410 nm) (Figure 3.32b). In this case dark blue areas of the CL map (Figure 3.32a) do not result from beam damage to the sample.

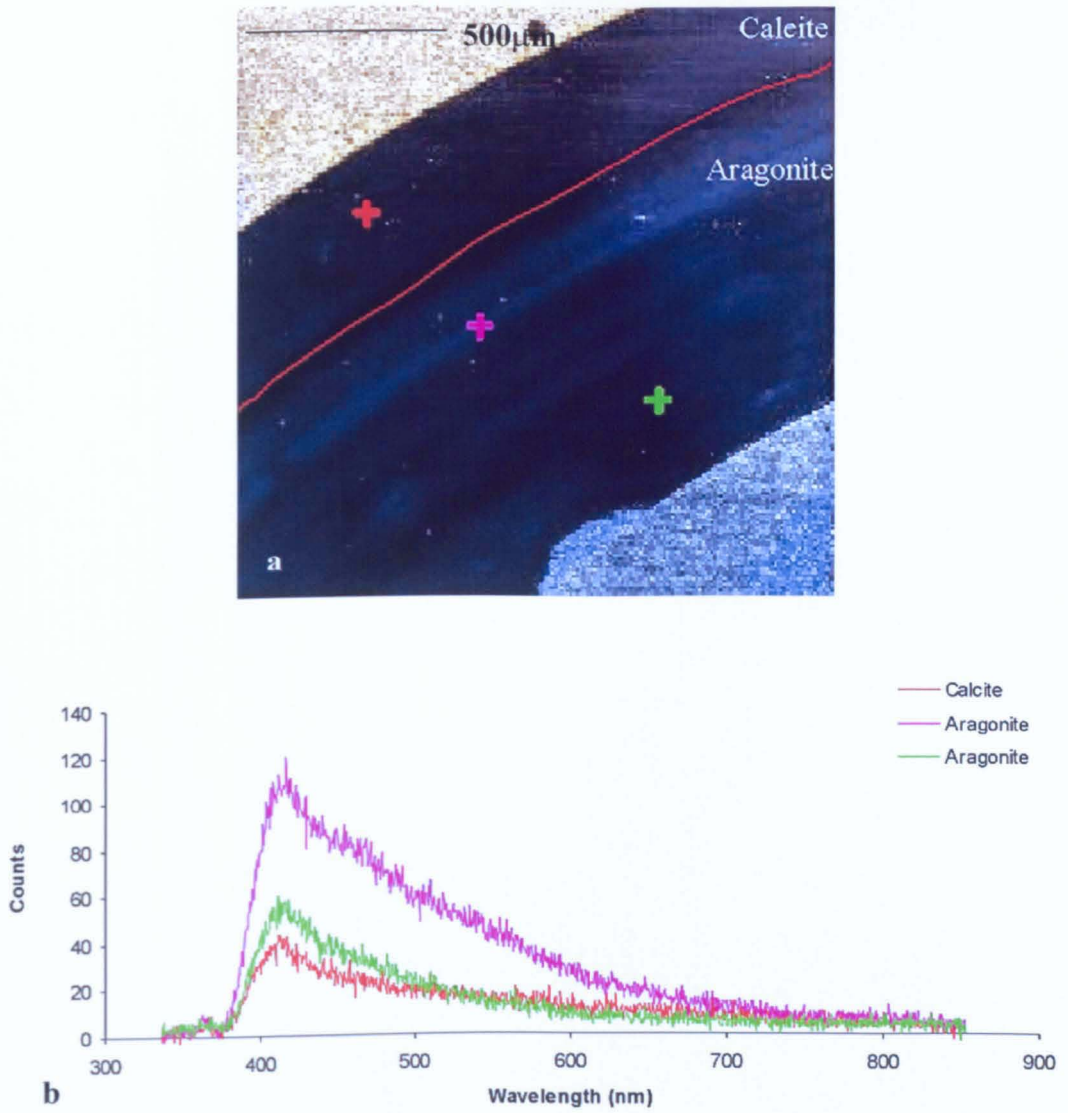


Figure 3.32 (a) Hyperspectral image showing the intensity and wavelength of CL emission from a specimen of *Mytilus edulis*, (b) CL emission spectrum acquired from *Mytilus edulis*

Cathodoluminescence spectroscopy was carried as described in Section 2.6.5. The image was produced using the software, CHIMP. The colour of the cross on the CL map corresponds to the same colour of line spectra. The division between the calcite and aragonite layers is marked by a red line. Units on the y axis of Figure 3.32b are arbitrary.

3.3.4 Avian eggshell (*Gallus gallus*) Ultrastructure and Minor Elements

3.3.4.1 Ultrastructure

The eggshell of the domestic fowl (*Gallus gallus*) consists of six regions; the inner and outer shell membranes which provide a surface for crystal nucleation, the mammillary caps, the palisade layer, the vertical crystal layer and an outer organic cuticle (Figure 3.33 and Figure 3.34).

Removal of the membrane (Section 2.2) reveals the mammillary caps (Figure 3.35), which are the first part of the shell to form. The most common mammillary cap structure found in the eggshell is presented in Figure 3.36 where the mammillary bodies are in close contact with each other and also the membrane, which leaves an imprint on the base of the mammillary caps (Solomon, 1991). Solomon (1991) described these mammillary caps and also identified the presence of two other types of mammillary body, termed Type A and Type B. Type A consists of conical shaped bodies that have minimal contact with the membrane while Type B consist of rounded structures that are in contact with the membrane (Figure 3.36).

As the mammillary caps grow they fuse and continued growth produces the palisade layer and the vertical crystal layer, which consists of columnar crystals aligned perpendicularly to the palisade layer. The organic cuticle, which covers the vertical crystal layer consists of an inner vesicle layer with vesicles which contain phosphorus and an outer non vesicular layer (Fraser, 1996, Dennis *et al.* 1996).

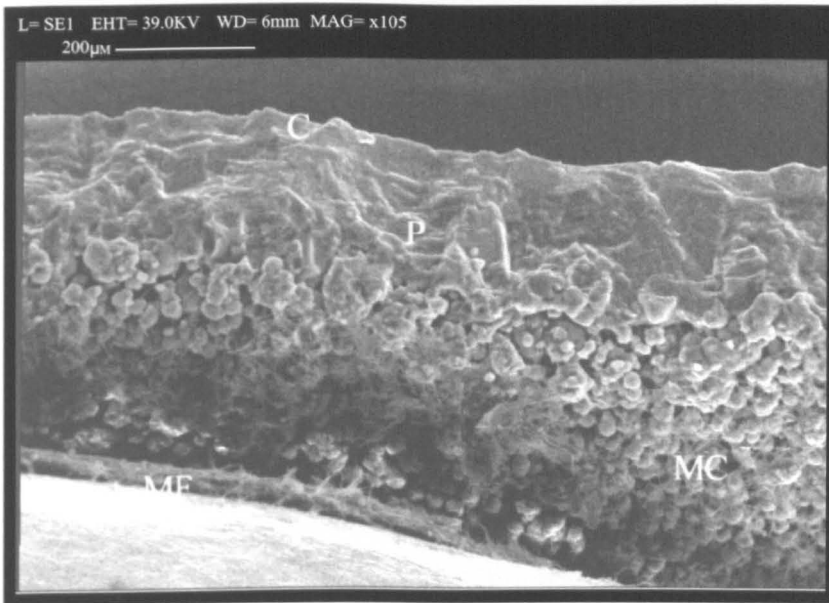


Figure 3.33 Secondary electron image of a section through an avian eggshell (*Gallus gallus*)

SEM image of a fractured section of a specimen of an eggshell. The section displays the membrane fibres (MF), the mammillary caps (MC), the palisade layer (P) and the cuticle(C).

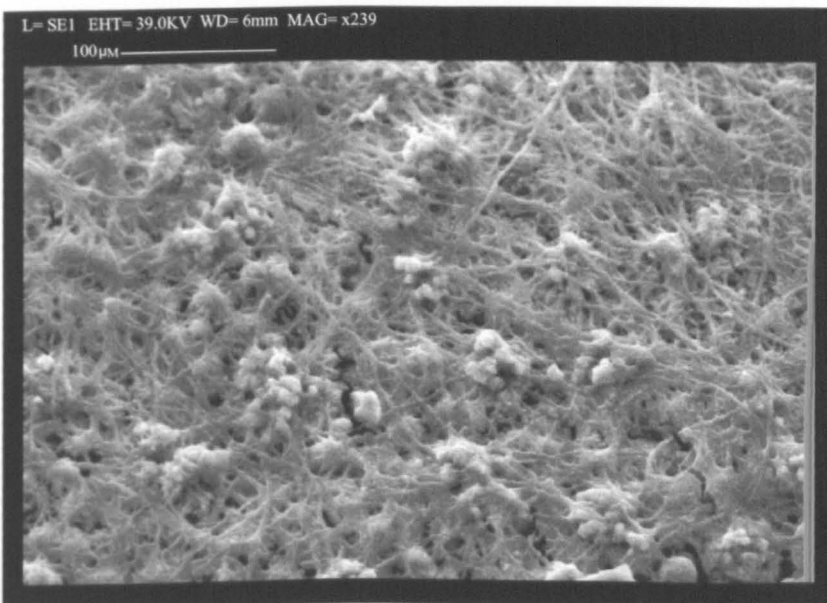


Figure 3.34 Secondary electron image of the membrane fibres covering the base of the mammillary caps in an avian eggshell (*Gallus gallus*)

SEM image of the inner surface of an eggshell.

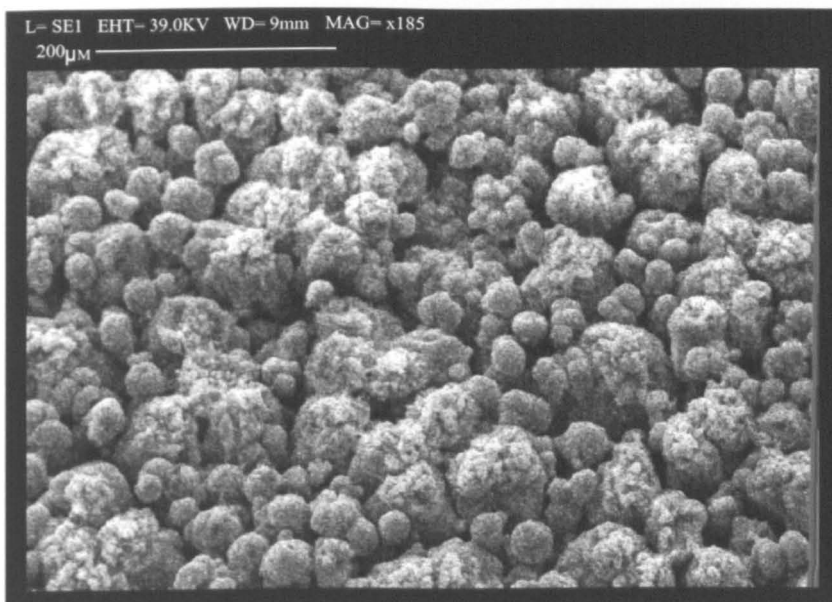


Figure 3.35 Secondary electron image of the mammillary caps in a specimen of an avian eggshell (*Gallus gallus*)

*SEM image of the mammillary caps at the inner surface of an avian eggshell (*Gallus gallus*) following the removal of membrane fibres.*

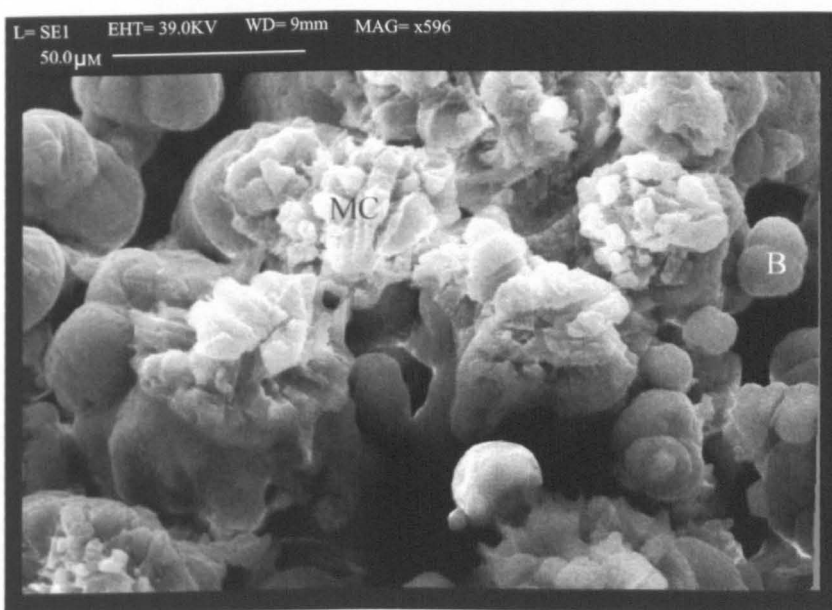


Figure 3.36 Secondary electron image of the mammillary caps displaying a normal growth pattern (MC) and Type B mammillary bodies (B)

*SEM image of the mammillary caps of an avian eggshell (*Gallus gallus*) following removal of the membrane fibres.*

3.3.4.2 Minor Element Composition-Electron Microprobe Analysis

Electron microprobe analyses were taken across the eggshell in a line perpendicular to the line of section (Figure 3.37). Magnesium, strontium, sodium, phosphorus and potassium are all above the limit of detection of the SX 50 electron microprobe. Sulphur is below the limit of detection and therefore will not be discussed. Results are summarised in Table 3.8.

Specimen	Mg Conc. Range (wt%)	Sr Conc. Range (wt%)	Na Conc. Range (wt%)	P Conc. Range (wt%)	K Conc. Range (wt%)	Figure No.
a	0.13-0.64	0-0.06	0.02-0.12	0.01-0.10	0.01-0.03	3.37a
b	0.09-0.59	0-0.03	n/a	0-0.12	0-0.03	3.37b

Table 3.8 Summary of electron microprobe results for *G. gallus* eggshell

The results displayed in Table 3.8 summarise the concentration range (i.e. the lowest concentration to the highest concentration) of Mg, Sr, Na, P and K in the eggshell of G. gallus

Figure 3.37a and b illustrate spot analyses of magnesium, sodium, phosphorus and potassium taken across two eggshell specimens. There is a high concentration of magnesium within the mammillary caps in both specimens. Magnesium concentrations abruptly decrease across the zone in which the mammillary caps fuse and then steadily increase through the shell towards the cuticle. Phosphorus and potassium concentrations gradually increase from the mammillary caps to the outer cuticle. Both phosphorus and potassium reach maximum concentration during termination of shell growth. Strontium displays a similar but more erratic pattern, gradually increasing towards the outer portion of the shell. Sodium concentration is at a maximum in the mammillary caps and gradually declines across the area in which the mammillary caps fuse. Unfortunately sodium analyses are not available for specimen b.

Scatter plots of element concentration are presented in Figure 3.38. Correlation coefficients are presented in Table 3.9. The graphs include four sets of spot analyses taken across two specimens of eggshell. From spot analysis (Figure 3.37) the distributions of some elements follow a similar trend. Magnesium positively correlates with phosphorus

(Figure 3.38a and Table 3.9). Within this plot there is a separate cluster of four data points that were obtained from the eggshell cuticle. Magnesium also displays a positive correlation with potassium (Figure 3.38i), while phosphorus and potassium also show a strong positive correlation (Figure 3.38e). Calcium displays a negative correlation with magnesium (Figures 3.38f and Table 3.9). Sodium displays a negative correlation with potassium (Table 3.9).

Variables	Correlation Coefficient	P-value
Mg/P	0.711	0.000
Sr/P	0.462	0.000
Mg/K	0.737	0.000
Ca/Sr	0.014	0.914
Ca/P	-0.280	0.026
P/Na	-0.292	0.020
Ca/Na	-0.181	0.156
Ca/K	-0.221	0.081
P/K	0.663	0.000
Ca/Mg	-0.430	0.000
Sr/K	0.480	0.000
Sr/Na	-0.242	0.056
Mg/Sr	0.599	0.000
Mg/Na	-0.215	0.090
Na/K	-0.572	0.000

Table 3.9. Pearson correlation coefficients with P-values for element concentration in the calcite eggshell of *G. gallus*

*Pearson correlation coefficients were calculated to determine the linear relationships between element concentrations in the calcite shell of *G. gallus*. Values close to 1 indicate a strong positive linear correlation.*

X-ray maps showing the distributions of a number of elements are illustrated in Figure 3.39. As shown by electron microprobe data, the highest concentration of magnesium is within the mammillary caps and the cuticle (Figure 3.39a). Although sulphur concentrations are below detection limits the sulphur X-ray map (Figure 3.39b) highlights

the sulphur rich organic membrane upon which the shell nucleates. Figure 3.39d displays the high concentration of phosphorus in the cuticle.

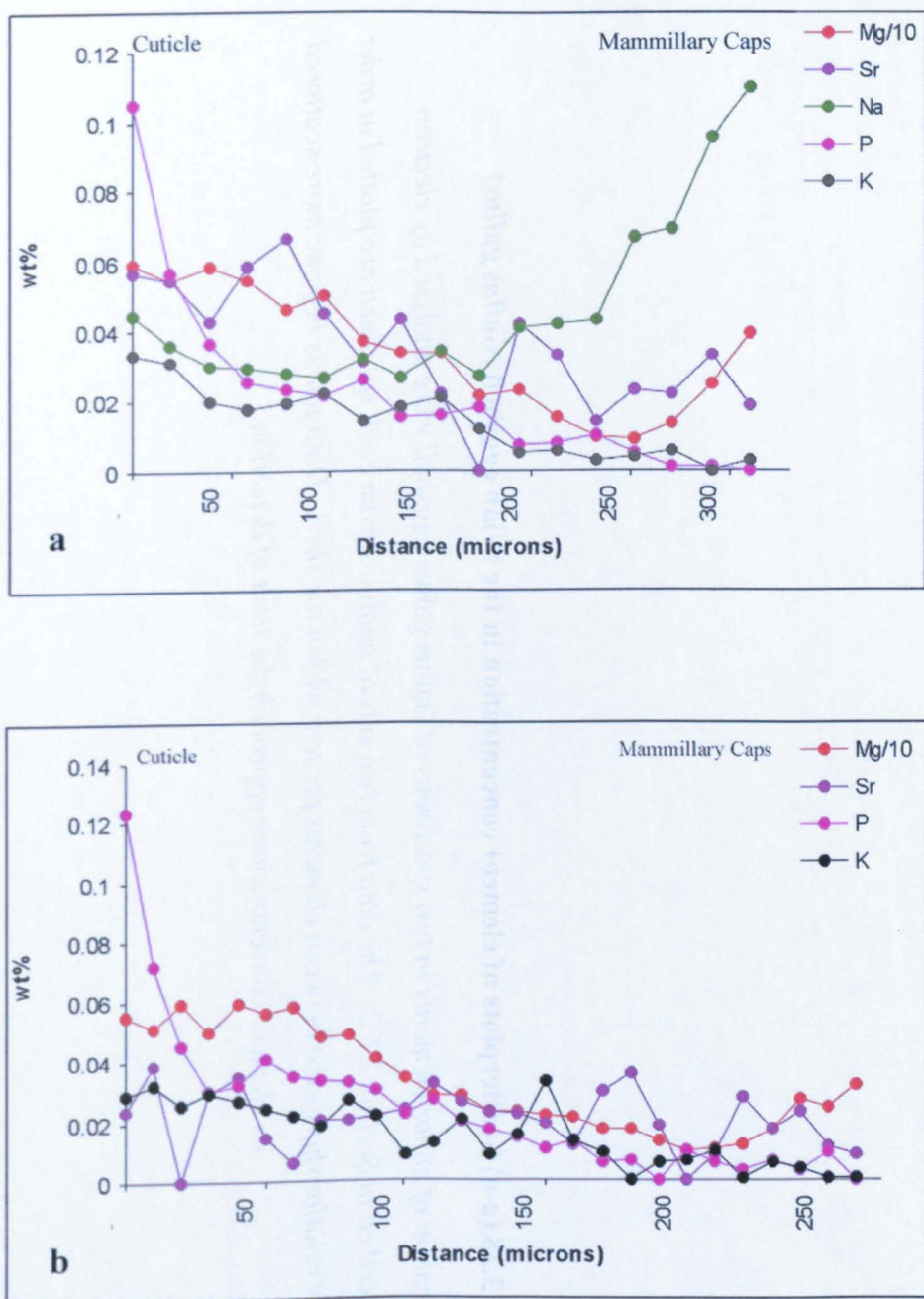
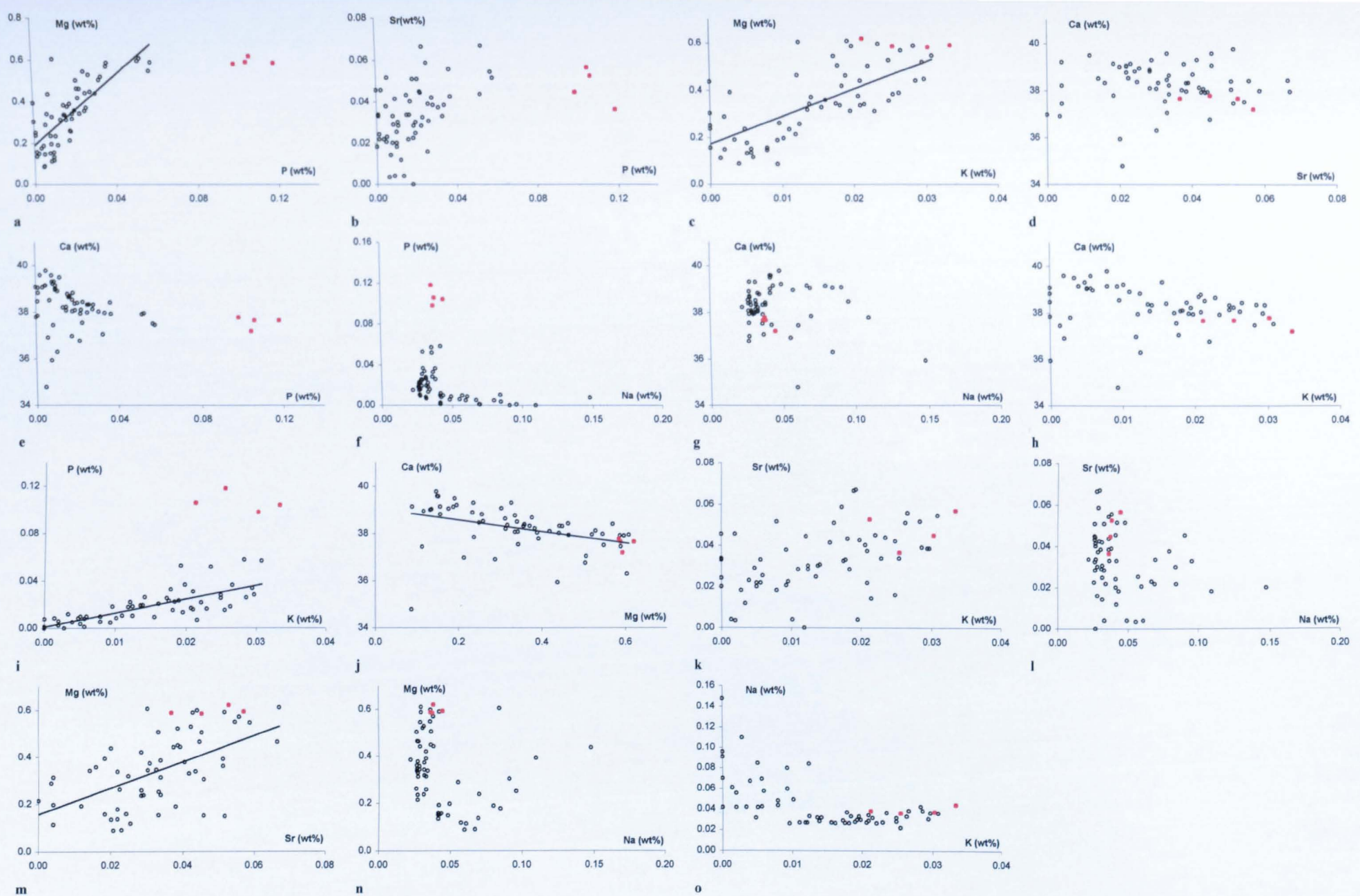


Figure 3.37 (a & b) Electron microprobe spot analyses across the avian eggshell

Specimens were prepared for electron microprobe analysis as described in Section 2.6.1. Electron microprobe analyses were carried out as described in Section 2.6.2.

Figure 3.38 (a-o) Scatterplots of element concentration in the avian eggshell (*Gallus gallus*)

*The concentration of minor elements in two specimens of *Gallus gallus* eggshell were analysed by electron microprobe as described in Section 2.6.2. The data from two sets of analyses from each specimen are plotted in order to determine if any relationships exist between elements present within the shell. Data points become more scattered as element concentrations approach the limit of detection.*



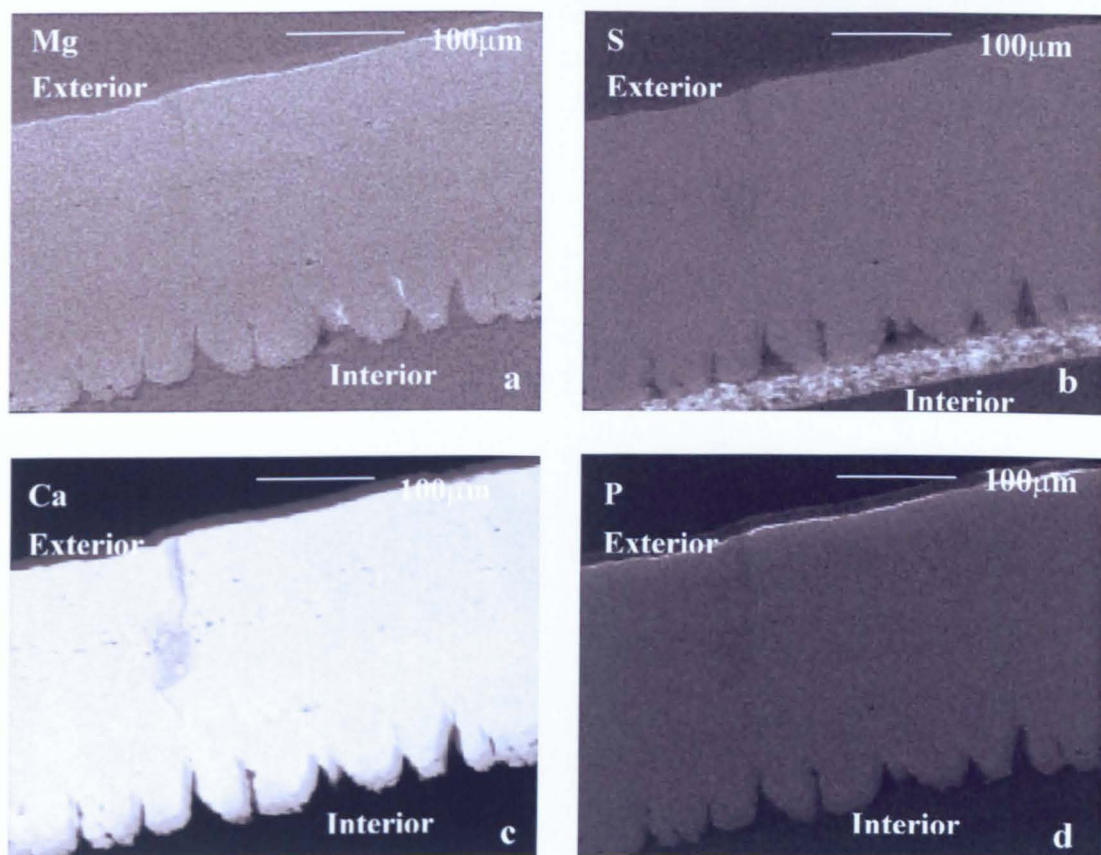


Figure 3.39 X-ray maps of element concentration in an avian eggshell (*Gallus gallus*)

a. MgK α , b. SK α , c. CaK α , d. PK α . A sample of an eggshell was prepared for analysis as described in Section 2.6.1 and mapping was carried out as described in Section 2.6.4. For each map, light grey areas indicate a greater element concentration while dark grey areas indicate lower element concentration.

3.3.4.3 Cathodoluminescence Imaging and Spectroscopy

The avian eggshell of *Gallus gallus* luminesces white in optical CL (Figure 3.40), but predominantly at blue wavelengths in the hyperspectral maps (Figure 3.41a), although there is also some emission within the ultraviolet range of the spectrum (less than 400nm) (Figure 3.41b).

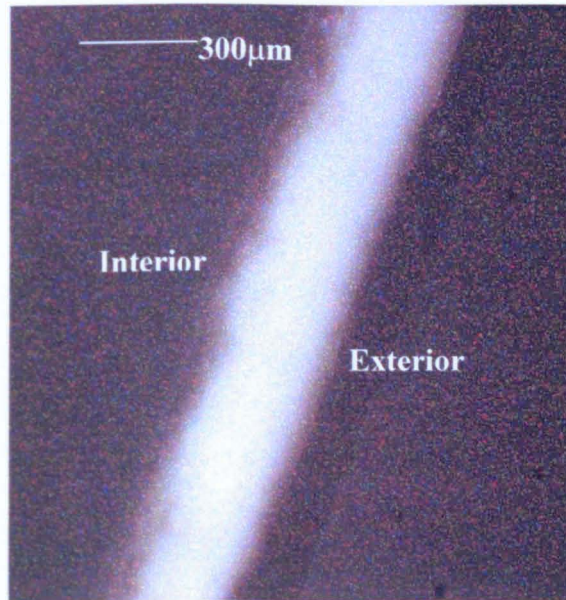
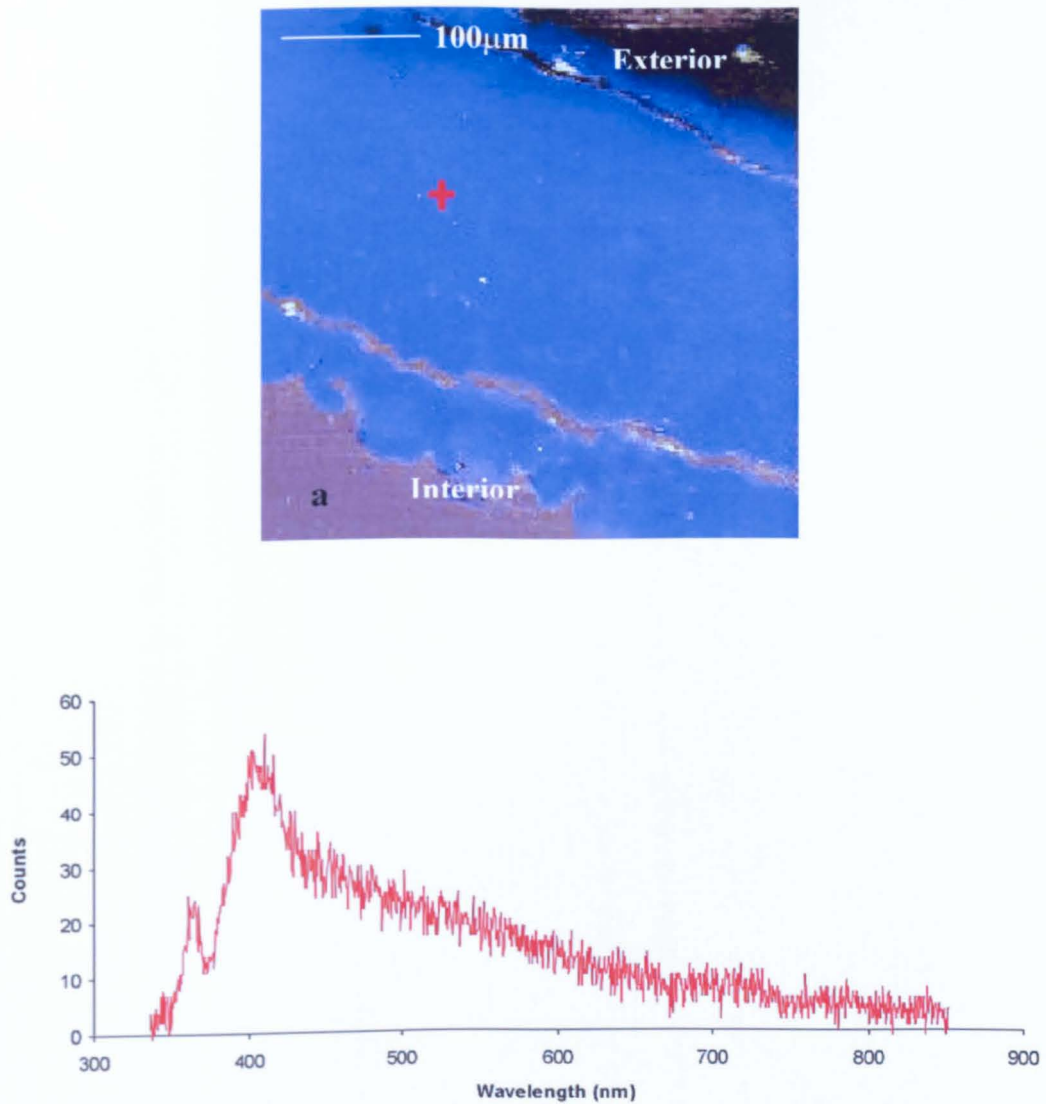


Figure 3.40 Optical CL image of a specimen of the avian eggshell (*Gallus gallus*)

*A specimen of an avian eggshell (*Gallus gallus*) was prepared as described in Section 2.6.1. The image was captured as described in Section 2.6.5.*



b

Figure 3.41 (a) Map of cathodoluminescence emission from a specimen of an eggshell (*Gallus gallus*), (b) Spectrum of luminescence emission from an eggshell (*Gallus gallus*)

Cathodoluminescence spectroscopy was carried as described in Section 2.6.6. The image was produced using the software, CHIMP. The red cross on the CL map corresponds to the red line spectra in Figure 3.41b. Units on the Y axis of Figure 3.41b are arbitrary.

3.4 Discussion

3.4.1 *Terebratulina retusa* and *Novocrania anomala*

As *T. retusa* and *N. anomala* were collected from the same location, they have experienced identical environmental conditions throughout ontogeny. The shell chemistry of each species can therefore be compared without having to consider possible effects of environmental variables. The shell of *T. retusa* is composed of low magnesium calcite, while the shell of *N. anomala* is high magnesium calcite, demonstrating that the main influences on the skeletal chemistry of these two species are biological rather than environmental.

The distribution of minor elements through the low magnesium calcite shell of *T. retusa* is distinctive. There is a significant difference in magnesium, calcium, sulphur, and strontium concentrations between the primary and secondary layers, with a higher concentration of magnesium, sulphur and strontium in the primary layer of the shell. The shell of *N. anomala* has a high organic matrix content (Section 4.3.1) and a greater concentration of minor elements than that of *T. retusa*, while electron microprobe analyses show that the distribution of elements across the primary and secondary layers is relatively invariant.

There have been a number of suggestions of the principal controls on the distribution of magnesium and other trace elements in calcium carbonate skeletons, including growth rate (Buening and Carlson, 1992) and temperature (Lowenstam, 1961, Dodd, 1967 and Lowenstam and Weiner, 1989). A number of studies have indicated that a high magnesium concentration in abiotic calcite is associated with rapid precipitation rates (Major and Wilber, 1991 and Burton and Walter, 1987). Auclair *et al.*, (2003) showed that the secondary layer of *Terebratalia transversa* is divided into two layers in terms of ultrastructure and isotopic composition. The variation in $\delta^{18}\text{O}$ between the two sections of the secondary layer is related to kinetic fractionation, as the growth rates of the primary and upper secondary layers, secreted by the marginal mantle are faster than that of the lower section of the secondary layer which is secreted by the posterior mantle (Auclair *et al.*, 2003 and Rosenberg *et al.*, 1988).

Curry (1982) found that the brachiopod *T. retusa* grows rapidly during the first three years of life and especially during the first three months, at the end of which it attains an average length of 2.75mm. The growth rate declines with age (Curry, 1982). Buening and Carlson (1992) found evidence that the trace element composition of the articulated brachiopods *T. unguicula* and *T. transversa* is influenced by changes in growth rate throughout ontogeny, where higher magnesium concentrations within the shell correlate to periods of faster growth. Variations in growth rate during ontogeny may therefore similarly influence the minor element composition of *T. retusa*.

A division between upper and lower sections of the secondary layer of *T. retusa* is evident both in thin section (Figures 3.4 and 3.5) and in chemical differences between the two sections (Figure 3.6b). If the primary and upper secondary layers are precipitated more rapidly than the lower secondary layer, as is the case for *T. transversa* (Auclair *et al.* 2003), then one would expect that the concentration of magnesium would be greater in the primary and upper secondary layers in comparison to the lower secondary layer.

If growth rate does exert a control over magnesium incorporation in calcite then it would be expected that this factor would influence the trace element composition of carbonate shells of other species. *Novocrania anomala* however, is a slow growing brachiopod with a high magnesium calcite shell (Ruggiero, 2001). This suggests that growth rate is not the sole factor which influences shell chemistry.

Rosenberg and Hughes (1991) propose that growth rate and composition of the shell of the bivalve *M. edulis* are a function of the metabolic activity of the mantle. They suggest that mantle metabolism is highest where the shell is chemically expensive to produce and that the growth rate of the shell varies according to both the relative metabolic rate of the mantle and the concentration of organic matrix and trace elements within the newly formed shell. In specimens of *M. edulis*, they determined that calcium rich, fast growing areas of the shell were underlain by mantle with a low metabolic activity while areas of the shell that are rich in organic matrix and trace element content and are slow growing and are underlain by mantle with a high metabolic activity. Rosenberg *et al.*, (1988) found evidence for a decline in both metabolic activity and growth rate with age in the brachiopod *T. transversa*. Rosenberg *et al.*, (1988) found that the metabolic activity of the marginal mantle, which forms the primary and upper secondary layer of *T. transversa* is higher than that of the posterior mantle, which forms the lower secondary layer. If the

metabolic activity of the mantle of *T. retusa* is similar to that of *T. transversa* then the marginal mantle, which produces the magnesium and sulphur-rich primary and upper secondary layers, may have a higher metabolic rate than the posterior mantle which produces the lower secondary layer. The decrease in trace element and matrix content may therefore be related to a decrease in metabolic activity throughout ontogeny. It should be recognised however that there are significant differences in the metabolism of bivalves and brachiopods and the extrapolation of theories from one system to another can be problematic.

N. anomala is a slow growing brachiopod with a high magnesium, organic rich calcite shell. If the trace element concentration and distribution through the shell of *N. anomala* reflects the metabolic activity of the mantle then the data presented in Section 3.3.2.2 suggests that the metabolic rate of the mantle is relatively stable throughout ontogeny as there is no significant difference in minor element concentration between the primary and secondary layers of the shell.

The data available on the metabolism of inarticulated brachiopods is limited and no information is available about the metabolism of *N. anomala*. Therefore the relationship between matrix/mineral ratios and metabolic rate can only be surmised. Hammen (1971) found that the inarticulated brachiopod *Lingula*, has a higher metabolic rate than the articulated brachiopods. This data concurs with the metabolic rate theory suggested by Palmer (1981) and Rosenberg *et al.*, (1991) as *Lingula* has an organic rich shell which would be metabolically expensive to produce.

Stanley *et al.*, (2002) found that simple organisms such as algae are passive in the uptake of magnesium from seawater and therefore have high magnesium calcite skeletons due to the high magnesium content of present day oceans. The high magnesium content of the calcite shell of *N. anomala* suggests that *N. anomala* does not have a physiological mechanism to exclude magnesium unlike those species which produce low magnesium calcite shells (Lowenstam and Weiner, 1989, Lorens and Bender, 1977 and Nurnberg *et al.*, 1996).

Sulphur is thought to be a reliable indicator of the distribution of organic matrix within calcium carbonate biominerals (Dauphin *et al.*, 2003a and 2003b). In the molluscs *Pinna* and *Pinctada*, sulphur is associated with the intercrystalline and intracrystalline organic matrix as sulphated mucopolysaccharides and the amino acids, methionine and cysteine

(Dauphin *et al.* 2003a). The correlation between magnesium and sulphur within the shell of *T. retusa* (Section 3.3.1.2) indicates that, in this case, magnesium may be associated with the organic matrix.

Maps of element concentration across the shell of *T. retusa* also highlight the relationship between magnesium and sulphur. The areas of high magnesium and sulphur content, which extend from the primary layer into the secondary layer are assumed to be extensions of the primary layer organic matrix crossing the boundary between the two layers. It is unlikely that these areas of high sulphur and magnesium concentration are associated with the mineral as no evidence has been found for extensions of the primary layer ultrastructure into the secondary layer. The high concentration of sulphur in the primary layer of *T. retusa* may be further due to a higher concentration of organic matrix in the primary layer in comparison to the secondary layer or a difference in the composition of the organic matrix between the two layers. If magnesium is associated with the organic matrix then this has implications for the biomineralisation mechanisms involved in the formation of the shell of *T. retusa*. The application of Mg/Ca ratios as palaeotemperature indicators in both the Brachiopoda and other taxa may also need to be considered since it is based on the assumption that Mg substitutes for Ca in the carbonate structure. These results suggest that, in some cases Mg is associated with the organic matrix and is not a true component of the carbonate structure.

Sulphate can also be accommodated within the calcite lattice as well as the organic matrix, while the negative relationship between calcium and minor elements such as magnesium can also be accounted for by the substitution of ions for Ca^{2+} in the lattice. As electron microprobe analysis does not distinguish between sources of ions it cannot be confirmed conclusively which phase the sulphur and other elements are associated with.

In *N. anomala*, sulphur does not correlate with the other elements indicating that the minor elements are concentrated in the crystal lattice rather than the organic matrix. The difference in peak position between XRD analyses of the low magnesium calcite shell of *T. retusa* and the high magnesium calcite shell of *N. anomala* indicate that the magnesium ions are encompassed within the calcite lattice of the *N. anomala* shell. It is also likely that strontium and sodium ions are also present within the lattice as they do not correlate with sulphur.

The concentration of minor elements in the shells of brachiopods may also be related to environmental conditions (Lee *et al.*, 2004 and Buening and Carlson, 1992). The data presented here indicates that the main trends may be related to physiological parameters. As environmental data are not available for this study, the influence of variations in environmental conditions on shell composition cannot be determined.

3.4.2 *Mytilus edulis*

The main factor determining chemical variations within the shell of *M. edulis* is the crystal structure of CaCO_3 . Mg^{2+} readily substitutes for Ca^{2+} in the calcite lattice, but not as easily within the aragonite lattice. The strontium ion however, is larger than Mg^{2+} and readily fits into the more open orthorhombic structure of the aragonite lattice. Differences in the concentrations of magnesium and strontium between the two layers can therefore to some extent be explained by contrasts in their crystal structure.

Sodium is present in relatively high concentration in both the calcite and aragonite layers. Electron microprobe data show that the concentration of sodium decreases across the calcite layer towards the boundary with aragonite. It is difficult however, to determine whether the sodium is present in the calcite-crystal lattice or associated with the organic matrix. Unlike Mg^{2+} and Sr^{2+} that can substitute for Ca^{2+} , sodium is monovalent and cannot so easily substitute for Ca^{2+} . Ions such as Na^+ may however sit in interstitial spaces and particularly within crystal lattice defects (Busenberg and Plummer, 1985).

Sulphur concentrations are low and are similar across the calcite and aragonite layers. As in the two brachiopods, sulphur may also be present in the calcite lattice as SO_4 . If Sr^{2+} is also present within the calcite crystal lattice then the number of crystal defects is likely to increase due to the larger ionic radius of strontium in comparison to the Ca^{2+} ion for which it substitutes. This may result in the incorporation of more Na^+ into the crystal defects, which may also account for the strong positive correlation between strontium and sodium. However following the work by Dauphin *et al.* (2003a), which determined that sulphur is associated with glycosaminoglycans within the organic matrix of molluscs, sulphur is likely to be associated with the organic matrix. It has also been confirmed that sulphated sugars are contained within the organic matrix of *M. edulis* (See Section 4.3.4). Both strontium and sodium positively correlate with sulphur in the calcite layer of the shell, therefore strontium and sodium may be associated with the organic matrix in the calcite

layer. The decrease in sodium from the outer periostracum through the calcite layer to the polymorph boundary suggests that there may be either a change in the structure of the calcite thus affecting sodium incorporation, or a decrease in the concentration of organic matrix.

There is some evidence for a correlation between strontium and sodium in the aragonite layer of the specimens in Section 3.3.3.2. There is also a variation in the concentration of sodium, sulphur, strontium and magnesium across the aragonite layer. Lorens and Bender (1980) found that both the Sr/Ca and Mg/Ca values of *M. edulis* aragonite increased linearly with increasing Sr/Ca and Mg/Ca in solution. While the Sr/Ca value of the calcite layer also increased linearly with increasing Sr/Ca in solution the Mg/Ca ratio of the calcite increased exponentially with Mg/Ca in solution (Lorens and Bender, 1980). As with the carbonate skeletons of other marine organisms however, the magnesium content of *M. edulis* is lower than that predicted from inorganic distribution coefficients, possibly because *M. edulis* has a physiological mechanism for exclusion of magnesium (Lorens and Bender, 1977).

As discussed in Section 3.4.1, Rosenberg and Hughes (1991) described an inverse relationship in the calcite layer of *M. edulis* between matrix/trace element rich shell and metabolic activity. From the analyses described in Section 3.3.3.2 this relationship cannot be confirmed, although a number of other authors have also found evidence to suggest that the metabolic activity of the mantle in certain bivalves influences the trace element composition and the concentration of organic matrix within the shell (Klein et. al, 1996).

3.4.3 Eggshell

The ionic composition of the uterine fluid may control the minor element composition of the eggshell. Electron microprobe analyses of the *G. gallus* eggshell (Figure 3.37) indicate that the concentration of magnesium is high in the mammillary caps and abruptly decreases towards the area of the shell within which the mammillary caps fuse. Furthermore, magnesium concentration gradually increases from the point at which the mammillary caps fuse towards the cuticle. The concentration of magnesium in the uterine fluid increases throughout the three phases of eggshell formation: initial (0.8mM), growth (4mM) and final phases (9mM) (Arad et al., 1989). In general, the magnesium concentration of the eggshell (Figure 3.37) follows the same pattern as variations in magnesium concentration

within the uterine fluid (i.e. magnesium concentration increases during the development of the eggshell). However, magnesium concentration within the mamillary caps is initially high. The discrepancy between the concentration of magnesium in the first formed part of the shell and the magnesium concentration within the uterine fluid may be a result of the time at which the first uterine fluid samples were extracted. Nys *et al.*, (1991, 1999) also present measurements of the ionic composition of the uterine fluid during the initial and final stages of eggshell formation. Sodium concentration in the uterine fluid is high during initial precipitation and decreases throughout the calcification process. This pattern is consistent with the distribution of sodium in the eggshell, which increases from the earliest formed part of the shell i.e. the mamillary caps to the outer shell cuticle (Figure 3.37). Potassium concentration in the uterine fluid increases during the final stages of shell formation, which corresponds with an increase in potassium through the palisade layer to the outer cuticle (Figure 3.37). Phosphorus concentration in the uterine fluid is also at its highest during the later stages of eggshell calcification, which is also consistent with the distribution of phosphorus in the eggshell (Figure 3.37).

Hincke and St. Maurice (1998) found that the addition of Mg^{2+} to calcite crystal growth solution accelerated the onset of calcite precipitation but inhibited the maximum rate of precipitation with respect to a control experiment. The addition of phosphate ions also resulted in the inhibition of the maximum precipitation rate. The influence of magnesium on calcite crystal morphology has also been reported (Meldrum and Hyde, 2001). Ions such as magnesium and phosphate may therefore have an active role in the formation of the eggshell and controlled changes in the ionic composition of the uterine fluid may therefore be a mechanism for controlling the onset of calcite precipitation, the precipitation rate and crystal morphology.

4 Organic Matrix Composition

4.1 Introduction

Biominerals are composite materials composed of a mineral phase with an organic matrix comprised of proteins, carbohydrates and lipids. The organic components control the nucleation, polymorph type and crystal morphology of the mineral (Lowenstam and Weiner, 1989, Simkiss and Wilbur, 1989). The matrix can be divided into two components: the intercrystalline organic matrix, which surrounds the crystals and the intracrystalline organic matrix which is present within the mineral itself and as such is resistant to strong chemical oxidation (Sykes *et al.*, 1995). The matrix can also be divided into insoluble and soluble fractions by the demineralisation of the biomineral with ethylene diamine tetra acetic acid (EDTA). The insoluble fraction differs in composition between species and in some instances is absent (Weiner *et al.*, 1983). These hydrophobic macromolecules provide a framework for crystal formation and as such are frequently referred to as "framework proteins". They exert control over crystal orientation and contribute to the final mechanical properties of the biomineral (Feng *et al.*, 2000a), while it has also been suggested that they may influence the mineral polymorph type (Matsushiro *et al.*, 2003). In contrast, the soluble matrix components are hydrophilic, contain a high proportion of acidic residues (Weiner *et al.*, 1983) and are commonly glycosylated (Hare, 1963, Weiner and Hood, 1975, and Weiner, 1979). The acidic nature of these macromolecules has led to the suggestion that they have a calcium-binding function and as such an important role in the mineralisation process (Weiner and Hood, 1975, Weiner and Traub, 1984 and Lowenstam and Weiner, 1989). A number of *in vitro* studies have confirmed that organic matrix macromolecules extracted from different biomineral systems exert control over crystal growth and morphology (Belcher *et al.*, 1996).

Organic matrices extracted from a range of biomineral systems have been characterised in relation to their protein composition and carbohydrate content (e.g. Cariolou and Morse, 1988, Hare, 1963, Panheleux *et al.* 2000, Kawaguchi and Watabe, 1993) and a number of comparative studies of matrix composition between species from the same phylum have been undertaken (e.g. Mitterer, 1978, Young, 1971 and Miyamoto, *et al.*, 2003) yet relatively few comparisons of species from different phyla (e.g. Dauphin, 2001) have been carried out.

The aim of this chapter is to compare the organic matrix composition of the four systems, including different phyla which produce different ultrastructures and two types of calcium carbonate polymorph; calcite and aragonite. This chapter describes the molecular weight, charge and amino acid composition of intercrystalline and intracrystalline proteins as well as the carbohydrate organic matrix component of the shells of *T. retusa*, *N. anomala*, *M. edulis* and *Gallus gallus*.

4.2 Previous Work

4.2.1 Organic Matrix Structure and Control of the Mineral Phase

The general model for the structure of the organic matrix comprises a framework of hydrophobic macromolecules i.e. the insoluble organic matrix, with hydrophilic macromolecules i.e. the soluble organic matrix anchored at sites on the framework surface. Weiner and Traub (1984) and Weiner *et al.*, (1983) proposed a model termed the template model, for the structure of organic matrix within the aragonite layer of mollusc shells. This model comprises a core layer of insoluble chitin and silk fibroin like protein covered on both sides by layers of soluble matrix. Certain layers that form the matrix framework appear to be absent in some mollusc species while the acidic soluble matrix components are widespread, which suggests that the soluble matrix components have a different role to the insoluble matrix proteins in the mineralisation process (Weiner *et al.*, 1983).

The template model requires that the arrangement of the aspartic acid residues in the soluble organic matrix match the crystallographic arrangement of Ca^{2+} in the lattice of aragonite (Weiner and Traub 1984). Weiner and Hood (1975) found a high concentration of glycine and aspartic acid in the soluble organic matrices of the molluscs, *Crassostrea virginica*, *Mercenaria mercenaria*, *Crassostrea irredecens* and *Nautilus pompilus*. The presence of proteins with a repeat $(\text{Asp-Y})_n$ sequence where the Y is glycine or serine was therefore inferred. If this repeat sequence is present in β -pleated sheet formation then there is a correlation between the carboxylate groups of the aspartic acid residues and the crystallographic arrangement of Ca^{2+} in the calcite and aragonite lattices (Weiner and Hood, 1975 and Weiner and Traub, 1984). However, this model does not explain the selective mineralisation of calcite and aragonite in the mollusc shell, as the distances between calcium ions in the (001) face of calcite are similar to the distances between calcium ions in the (001) face of aragonite (Mann, 1988, 2001). The correlation between

crystal lattice stereochemistry i.e. the arrangement of CO_3^{2-} anions around the Ca^{2+} ions as well as the location of the Ca^{2+} ions, and the molecular arrangement of the organic matrix may therefore exert control over the mineral phase and the polymorph that it nucleates (Mann, 2001).

4.2.2 Insoluble matrix composition

The dissolution of calcium carbonate biominerals with the calcium chelator Ethylene diamine tetra acetic acid (EDTA) results in two fractions of organic matrix, an EDTA insoluble fraction and an EDTA soluble fraction. The concentration of insoluble organic matrix varies significantly between species and in some instances the insoluble organic matrix is entirely absent which suggests that it has a different role in the mineralisation process than the soluble organic matrix (Weiner *et al.*, 1983). The insoluble matrix proteins provide a framework upon which the soluble matrix fraction is anchored, and upon which mineralisation takes place. It has also been suggested that the main purpose of the insoluble matrix may be to influence the mechanical properties of the biomineral and may not have a major role in the mineralisation process itself (Lowenstam and Weiner, 1989, Feng *et al.*, 2000a).

A high concentration of glycine within the organic matrix fraction is a common characteristic of the insoluble fraction of the organic matrix of calcium carbonate biominerals such as the shells of molluscs, brachiopods and bryozoans (Weiner *et al.*, 1983). In mollusc shells, a group of fibrous framework proteins have been identified with a high concentration of both glycine and alanine (Miyashita *et al.*, 2000, Kawaguchi and Watabe, 1993, Weiner *et al.*, 1983 and Hare, 1963). Sudo *et al.*, (1997) extracted two proteins, MSI 60 and MSI 31 from the shell of *Pinctada fucata*. Both proteins are thought to be framework proteins as they show no evidence of N-glycosylation or carbonic anhydrase activity both of which are features associated with the soluble acidic matrix proteins (Section 4.2.4). Lustrin A, a protein identified as a component of the shell matrix of the mollusc *Haliotis refuescens* has a combination of multifunctional structures which indicates that it serves a number of functions as well as being a structural framework protein (Shen *et al.*, 1997). Lustrin A is homologous with other organic matrix proteins including the protein group, frustulins, which are associated with diatom cell walls (Shen *et al.*, 1997). Data on the composition of the insoluble organic matrix of brachiopods is limited. Joep (1965) found that the exoskeletons of articulated brachiopods are enriched in glycine while the shell of the inarticulated brachiopod, *Crania* is also enriched in glycine

but to a lesser extent than the articulated brachiopods. Cusack *et al.*, (2000) also found that the shells of the articulated brachiopod *T. retusa* and the inarticulated brachiopod *N. anomala* both had a high glycine content. In *T. retusa* the ventral valve is enriched in glycine but depleted in alanine with respect to the dorsal valve. It is suggested that the difference in amino acid composition is the result of the presence of the loop in the dorsal valve of the *T. retusa* shell (Cusack *et al.*, 2000). In *N. anomala* the amino acid composition of the dorsal and ventral valves are quite different due to the differences in ultrastructure between the two valves.

4.2.3 Soluble matrix composition

Soluble matrix proteins extracted from both calcium carbonate biominerals and calcium phosphate biominerals such as bone and dentine, contain a high concentration of acidic amino acids (Lowenstam and Weiner, 1989. Mitterer, 1978. Mann, 2001 and Veis and Perry, 1967). These negatively charged macromolecules are thought to have a calcium binding function (Weiner, 1979, Wheeler *et al.*, 1981 and Weiner and Hood, 1975). The effect of the soluble matrix on crystal growth and morphology is thought to differ depending on whether the macromolecules are fixed to a framework in which case they act as a nucleating surface for crystals, or if they are free in solution where they have been found to act as inhibitors of nucleation (Lowenstam and Weiner, 1989 and Wheeler *et al.*, 1981). However, Weiss *et al.*, (2000) have identified the soluble protein Perlucin from the shell of *Haliotis laevigata*, which when in solution enhances rather than inhibits calcite nucleation. Soluble matrix proteins extracted from the exoskeletons of bivalve molluscs not only influence the crystal morphology but also exert control over the polymorph type (Belcher *et al.*, 1996 and Falini *et al.*, 1996). The roles of the soluble and insoluble organic matrices in polymorph control are not fully understood however, and evidence has also been found for the precipitation of aragonite in vitro with the addition of a water insoluble protein complex extracted from the pearls and nacreous shell layers of specimens of the oyster, *Pinctada fucata* (Matsushiro *et al.*, 2003). Control over polymorph type may therefore be the result of a complex interaction of both soluble and insoluble organic matrices and minor elements (e.g. magnesium) with the mineral precipitate (See Section 3.2.1).

Some proteins extracted from the shells of molluscs have carbonic anhydrase activity. Miyamoto *et al.* (1996) isolated a soluble organic matrix protein, Nacrein from the nacreous layer of the pearl oyster *Pinctada fucata* and from the shell of the gastropod

Turbo marmoratus (Miyamoto *et al.*, 2003), while Kono *et al.* (1999) cloned a soluble matrix protein, N66 from the shell of *Pinctada fucata*. All three proteins have carbonic anhydrase domains, which are thought to be involved in the calcification process. Miyamoto *et al.* (1996) and Shimomura *et al.* (2002) suggest that the nacreins are involved in the calcification process during the conversion of respiratory CO_2 to HCO_3^- in the presence of H_2O . Carbonic anhydrase activity increases the formation rate of calcium carbonate *in vitro* (Shimomura *et al.*, 2002). The faster the rate of formation of HCO_3^- , the faster the rate of precipitation of calcium carbonate (Shimomura *et al.*, 2002).

A large proportion of the soluble organic matrix proteins that have been extracted from the shells of marine invertebrates and from eggshells are glycosylated (Cusack *et al.*, 2000, Collins *et al.*, 1991 & Ameye *et al.*, 2001). Cusack *et al.*, (2000) identified two glycoproteins of 40KDa and 62KDa molecular weight in the soluble organic matrix of *T. retusa* and a 60KDa glycoprotein in the organic matrix of *N. anomala*. Two glycoproteins with molecular weights of 67KDa and 62KDa have also been isolated from the prismatic layer of the oyster *Crassostrea virginica* (Kawaguchi and Watabe, 1993), while Pinnes *et al.*, (1995) identified the glycoprotein osteopontin in the eggshell of the domestic fowl. The common occurrence of glycoproteins in calcium carbonate biominerals suggests that the carbohydrate groups may be involved in shell formation possibly via their negatively charged sulphate and carboxylic acid groups.

Proteoglycans such as mammillan, a keratan sulphate proteoglycan (Nys *et al.*, 1999), ovoglycan, a dermatan sulphate proteoglycan (Fernandez *et al.*, 2001) and glycosaminoglycans such as chondroitin-4-sulphate and dermatan sulphate have been identified in the eggshell of the domestic fowl (Carrino *et al.*, 1997 and Nys *et al.*, 1999). Glycosaminoglycans, and the extent to which they are sulphated, exert control over the morphology and number of calcite crystals grown *in vitro* (Arias *et al.*, 2002). The addition of dermatan sulphate exerts control over the morphology of calcite crystals nucleated both *in vitro* (Arias *et al.* 2002) and on eggshell mammillae (Fernandez *et al.*, 2004) resulting in crystals with a columnar morphology. Kawaguchi and Watabe (1993) found evidence to suggest that glycosaminoglycans contained within the soluble organic matrix of the oyster *Crassostrea virginica* surrounded the surfaces of the calcite crystals of the shell and were also in close contact with glycosaminoglycans contained within the insoluble organic matrix component. The presence of glycosaminoglycans such as chondroitin sulphate and keratan sulphate in the shells of the molluscs *Pinna nobilis* and *Pinctada margaritifera* has also been highlighted (Dauphin *et al.*, 2003a and Dauphin *et*

al., 2003b). Analysis of the interprismatic walls of both *Pinna* and *Pinctada* by X-ray absorption near-edge structure spectroscopy (XANES) revealed the presence of a high concentration of sulphate (indicative of the presence of sulphated sugars) within the organic matrices. The role of these sulphated sugars in the biomineralisation process has also been supported by *in vitro* studies of the interaction of organic matrix macromolecules with calcium carbonate crystals (Kitano and Hood, 1965, Addadi *et al.*, 1987 and Wu *et al.*, 1994).

4.3 Results

4.3.1 Concentration and Distribution of Organic Matrix

The concentration of organic material in the shells of *T. retusa*, *N. anomala*, *M. edulis* *Gallus gallus* was determined by Loss on Ignition (LOI) as described in Section 2.7.1. The results presented in Table 4.1 are an average of three sets of analyses.

Biomaterial	% Organic Content (range)	% Organic Content (average)
<i>T. retusa</i> Ventral Valve	2.34-2.68	2.48
<i>T. retusa</i> Dorsal Valve	2.36-3.11	2.62
<i>N. anomala</i> Dorsal Valve	4.46-5.76	5.05
<i>M. edulis</i> calcite	1.58-1.69	1.64
<i>M. edulis</i> aragonite	3.19-3.23	3.21
Avian Eggshell	2.25-5.21	3.73

Table 4.1 Loss on Ignition Results

The organic content of the shells of T. retusa, N. anomala, M. edulis and G. gallus was determined using Loss on Ignition (Section 2.7.1). The results presented are the range and mean values of three sets of analyses.

The backscattered electron signal increases with the mean atomic number the density of the material being analysed. As such, electron backscatter imaging can be used to highlight differences of atomic number of a sample. Biomaterials are organic/inorganic

composites therefore electron backscatter imaging should highlight the difference in atomic number between areas with a high organic content (low mean atomic number) and areas with a high mineral content (high mean atomic number).

Figure 4.1 presents backscattered electron images of the shells of *T. retusa*, *N. anomala*, *M. edulis* and *Gallus gallus* within which the lighter areas have the greater mean atomic number.

The backscatter image of *T. retusa* (Figure 4.1a) shows that the primary layer has a greater mean atomic number than the secondary layer. If spatial variations in the proportion of backscattered electrons does reflect the relative proportions of mineral and organic matrix then it is possible to determine the distribution of organic material in each system as follows: the secondary layer of *T. retusa* has a higher organic content than the primary layer of the shell. In *N. anomala* the central section of the secondary layer contains a higher concentration of organic matrix than the outer and inner portions of the shell. The aragonite layer of *M. edulis* has a higher organic content than the calcite layer of the shell. However, alternating bands of high/low density material are apparent in the outer portion of the calcite layer. In *G. gallus* the concentration of organic matrix is high in the mammillary caps but decreases across the zone where the mammillary caps fuse. The organic content increases in the outer portion of the eggshell.

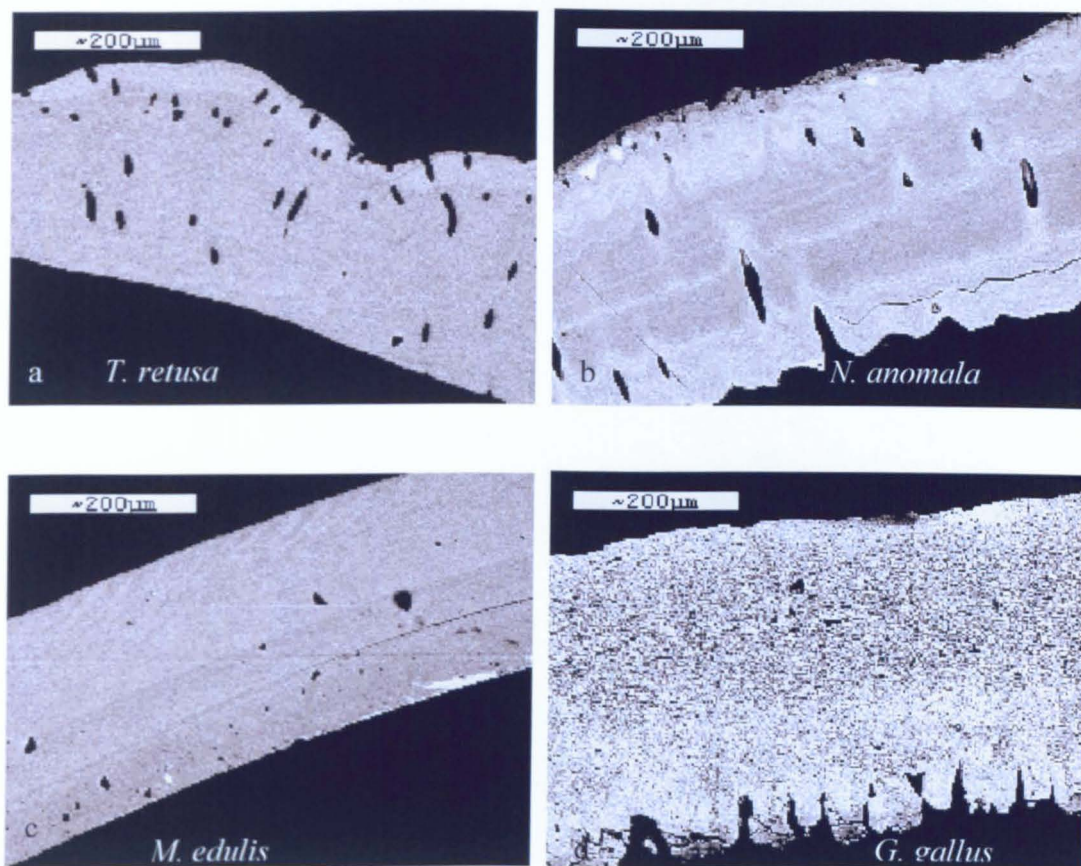


Figure 4.1 Backscattered electron images of *T. retusa*, *N. anomala*, *M. edulis* and the *G. gallus*

Backscattered electron images were produced as described in Section 2.7.2. White/light grey areas are composed of material with a higher mean atomic number than areas that are dark grey such as organic matrix. (a) *T. retusa*, (b) *N. anomala*, (c) *M. edulis* and (d) *G. gallus*

4.3.2 Molecular Weight of Intercrystalline and Intracrystalline Proteins

The intercrystalline and intracrystalline organic matrix fractions of *T. retusa*, *N. anomala* and *M. edulis* were extracted as described in Section 2.8.1 and Section 2.8.2 respectively. For *G. gallus* only the intracrystalline fraction was extracted by incubation of the sample in EDTA (Section 2.8.2), as the extraction of the intercrystalline proteins by incubation of the sample in GnHCl (Section 2.8.1) affects the intracrystalline protein extract and the final resolution of the proteins by SDS PAGE. The proteins from both the intercrystalline and intracrystalline fractions were separated by SDS PAGE (Section 2.8.4) and visualised using the staining techniques described in Section 2.8.6 and Section 2.8.7. Sample volumes and gel loadings are presented in Appendix C.

Three proteins of 47, 38 and 15kDa from the intercrystalline protein fraction of *T. retusa* and a 38kDa protein from the intracrystalline fraction were separated by SDS PAGE (Figure 4.2).

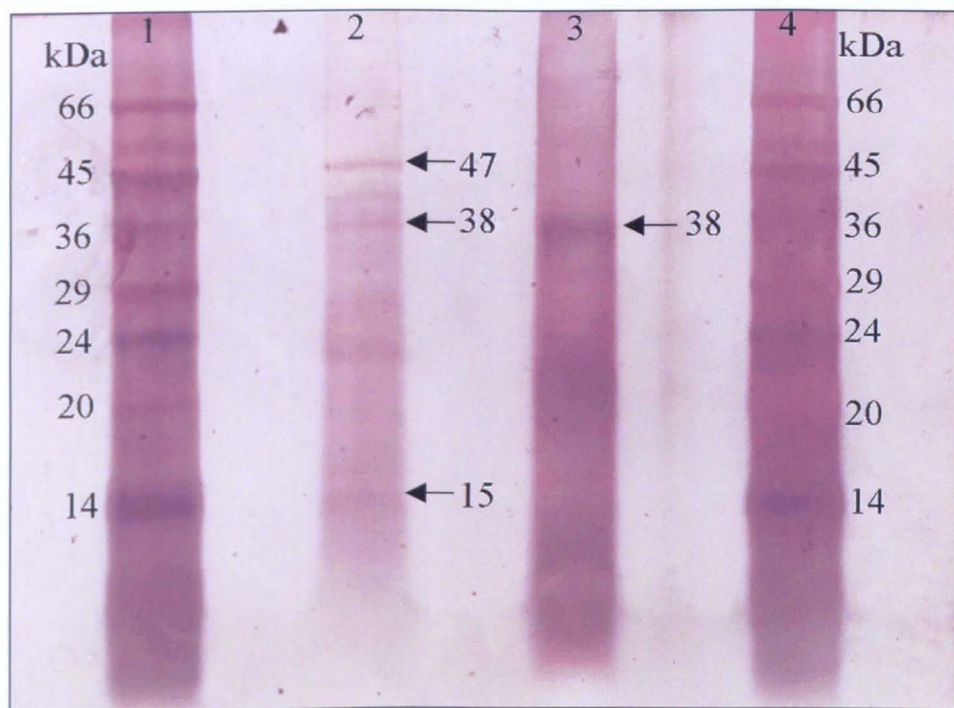


Figure 4.2 Silver stained, 15% polyacrylamide gel of the intercrystalline and intracrystalline protein fractions of *T. retusa*

Intercrystalline and intracrystalline protein extracts of T. retusa were prepared as described in Section 2.8. The proteins were electrophoresed on a Biorad™ minigel system at 60V. Lane 1 Mid range protein standards (Section 2.8.4). Lane 2 Soluble intercrystalline protein extract. Lane 3 Soluble intracrystalline protein extract. Lanes 4 Mid range protein standards (Section 2.8.4).

Proteins with molecular weight of 63kDa and 58kDa are present in both the intercrystalline and intracrystalline extracts of *N. anomala* (Figure 4.3). Three proteins with apparent molecular weights of 43kDa, 35kDa and 13kDa are also present in the intracrystalline protein extract.

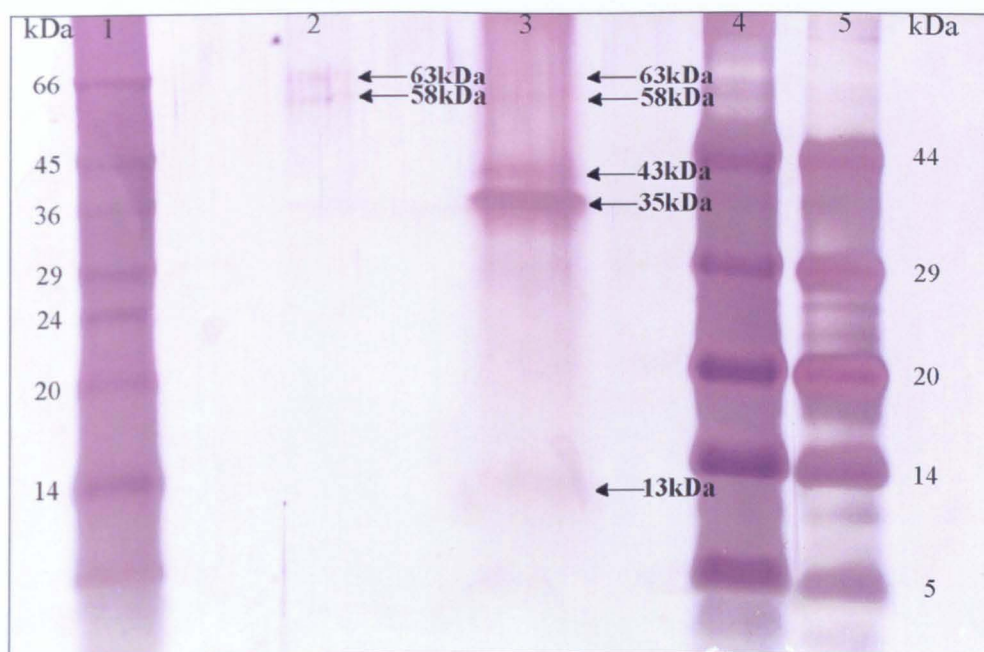


Figure 4.3 Silver stained, 15% polyacrylamide gel of the intercrystalline and intracrystalline protein fractions extracted from *N. anomala*

Intercrystalline and intracrystalline protein extracts of N. anomala were prepared as described in Section 2.8. The proteins were electrophoresed on a Biorad™ minigel system at 60V. Lane 1 Mid range molecular weight protein standards (Section 2.8.4). Lane 2 Soluble intercrystalline protein extract. Lane 3 Soluble intracrystalline protein extract. Lanes 4 and 5 Prestained low range protein standards (Section 2.8.4).

A number of proteins with molecular weights ranging between 26kDa to 81kDa are present in the intercrystalline extract of *M. edulis* (Figure 4.4). Two proteins of 35kDa and 26kDa are present in both the intercrystalline and intracrystalline protein fractions. It is difficult to resolve other protein bands in the intracrystalline extract due to the smear of material in the gel.

Extrapallial fluid was extracted from samples of *M. edulis* as described in Section 2.2. The fluid extract was washed with Milli QTM and concentrated through a Microcon 10kDa filter as described in Section 2.2. Proteins in the resultant fluid sample were separated by SDS PAGE and the proteins fixed and visualised by incubation in Coomassie Brilliant Blue as described in Section 2.8.5. The extrapallial fluid of *M. edulis* contains two proteins with molecular weights of 33kDa and 30kDa (Figure 4.5).

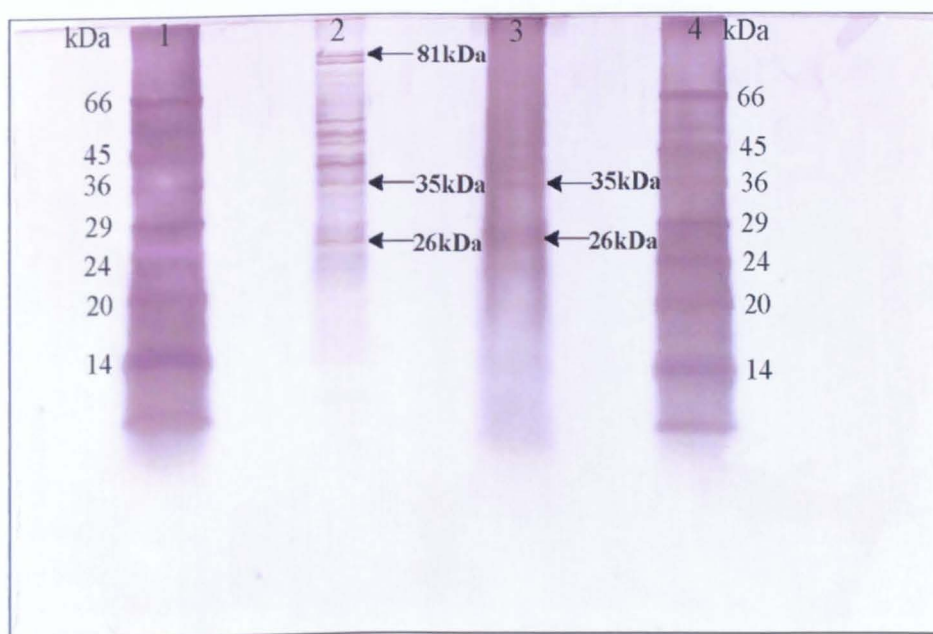


Figure 4.4 Silver stained, 15% polyacrylamide gel of the intercrystalline and intracrystalline protein fractions of *M. edulis*

Intercrystalline and intracrystalline protein extracts of M. edulis were prepared as described in Section 2.8. The proteins were electrophoresed on a BioradTM minigel system at 60V. Lane 1 Mid range molecular weight protein standards (Section 2.8.4). Lane 2 Soluble intercrystalline protein extract. Lane 3 Soluble intracrystalline protein extract. Lanes 4 Mid range protein standards (Section 2.8.4).

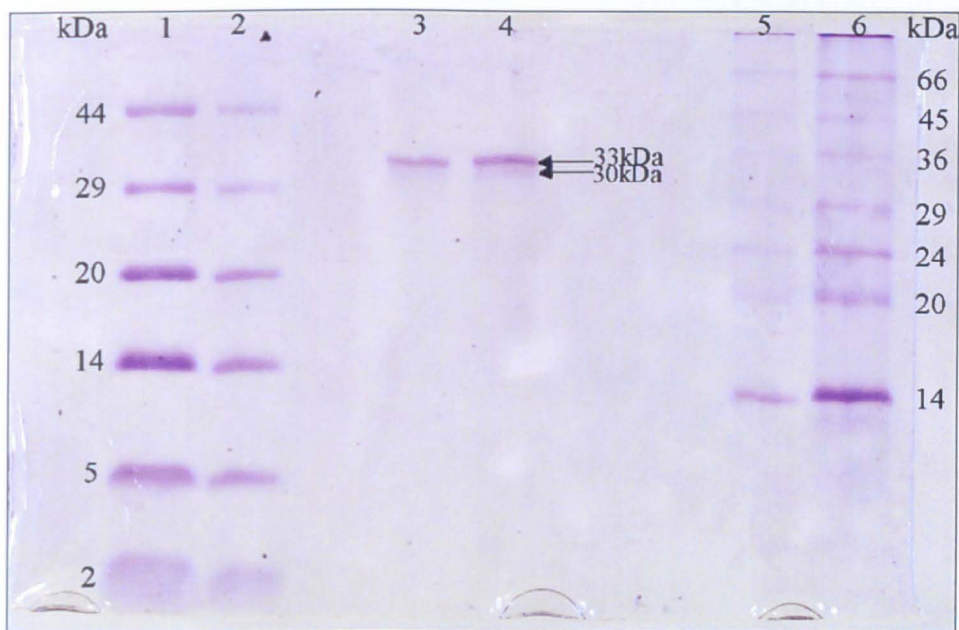


Figure 4.5 Coomassie Blue stained, 20% polyacrylamide gel of protein within the extrapallial fluid of *M. edulis*

Extrapallial fluid extracted from specimens of *M. edulis* was prepared as described in Section 2.2. The extract was electrophoresed on a BioradTM minigel system at 60V. Lane 1 and 2 Prestained low range molecular weight protein standards (Section 2.8.4). Lane 3 and 4 Extrapallial fluid extract from *M. edulis*. Lane 5 and 6 Mid range protein standards (Section 2.8.4).

Only the intracrystalline protein fraction was extracted from the avian eggshell as extraction of the intercrystalline organic matrix by incubation of the powdered mineral sample in GnHCL affects the intracrystalline matrix and the resolution of the proteins by gel electrophoresis. The intracrystalline organic matrix of the avian eggshell contains a number of proteins with molecular weights ranging from 16kDa upto 70kDa (Figure 4.6).

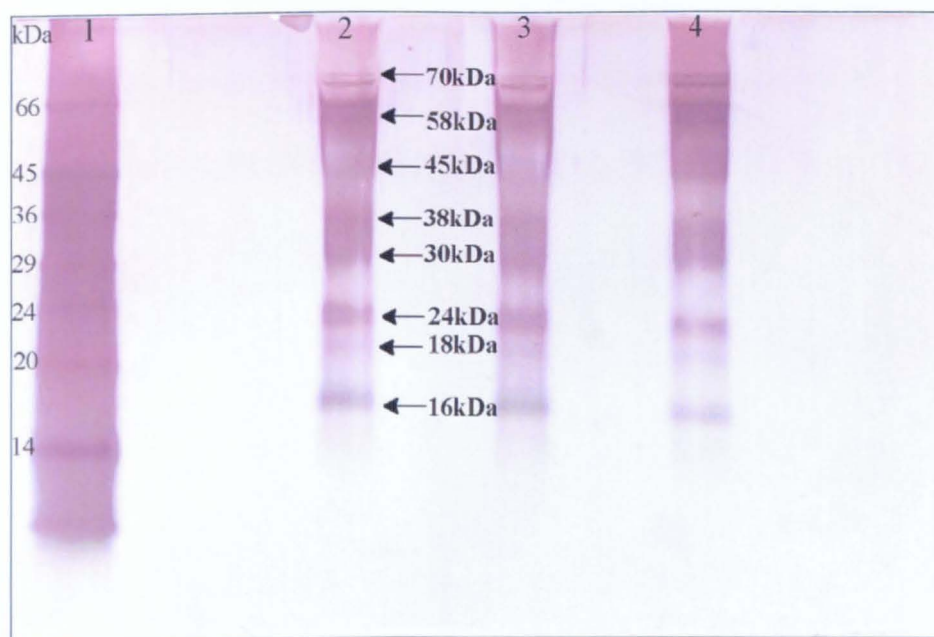


Figure 4.6 Silver stained, 15% polyacrylamide gel of eggshell (*Gallus gallus*) intracrystalline protein

Intracrystalline proteins extracted from the avian eggshell were prepared as described in Section 2.8. The proteins were electrophoresed on a BioradTM minigel system at 60V. Lane 1 Mid range molecular weight protein standards (Section 2.8.4). Lane 2, 3 and 4 Soluble intracrystalline protein extract.

4.3.3 Protein Charge

The intracrystalline proteins extracted from the shells of *T. retusa*, *N. anomala*, *M. edulis* (calcite and aragonite) and *G. gallus* were fractionated on the basis of their charge by isoelectric focusing (Section 2.8.8). The proteins were then visualised by incubation of the gel in Coomassie Brilliant Blue Stain. The isoelectric points of the intracrystalline proteins extracted from *T. retusa*, *N. anomala*, *M. edulis* and the avian eggshell range between approximately 3.5-7 indicating that they are acidic (Figure 4.7).

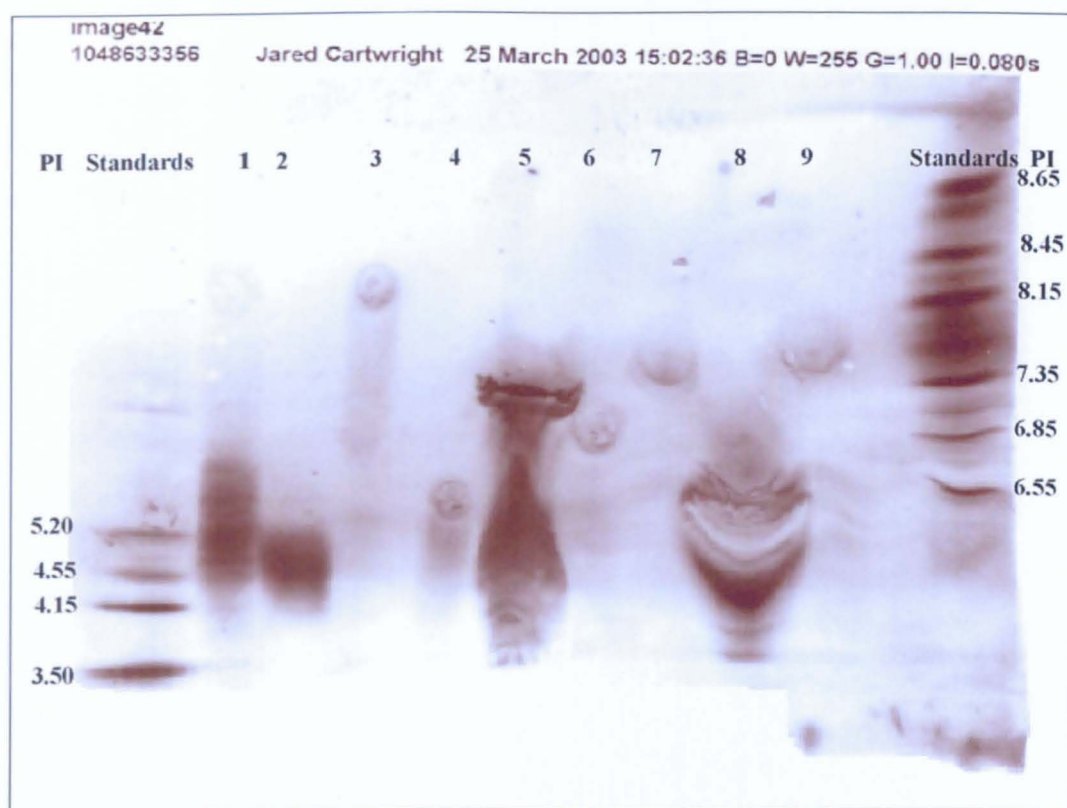


Figure 4.7 Intracrystalline proteins separated by isoelectric focusing

Intracrystalline proteins extracted from *T. retusa*, *N. anomala*, *M. edulis* (calcite and aragonite) and *G. gallus* were prepared as described in Section 2.8. Low PI standard proteins (Section 2.8.5) are to the left of lane 1. High PI standard proteins (Section 2.8.5) are to the right of Lane 9. Lane 1 and 2=*M. edulis* aragonite intracrystalline proteins, Lane 3 and 4=*M. edulis* calcite intracrystalline proteins, Lane 5= *G. gallus* intracrystalline proteins, Lane 6=Total mussel proteins (i.e. calcite and aragonite), Lane 7= *T. retusa* intracrystalline proteins, Lane 8 and 9=*N. anomala* intracrystalline proteins. Protein samples were loaded at different positions within each lane.

4.3.4 Organic Sulphate

The location of sulphur in the shells of *T. retusa*, *N. anomala*, *M. edulis* and *G. gallus* cannot be distinguished by electron microprobe analysis alone as this technique does not determine the phase that is analysed. In order to determine if organic sulphate is associated with the intercrystalline and intracrystalline organic matrix of *T. retusa*, *N. anomala*, *M. edulis* and *G. gallus* proteins were fractionated by SDS PAGE (Section 2.8.4) and stained with Acridine Orange in accordance with the technique described by Dauphin *et al.* (2003a), (Section 2.8.7).

Proteins extracted from the intercrystalline and intracrystalline organic matrix fractions of *T. retusa* stain in Coomassie Brilliant Blue and silver stain (Figure 4.2). These protein bands are not discernable when stained with Acridine Orange (Figure 4.8). Only larger matrix molecules extracted from the intercrystalline material stain faintly in Acridine Orange, while the intracrystalline extract of *T. retusa* appears as a smear of material in the gel.

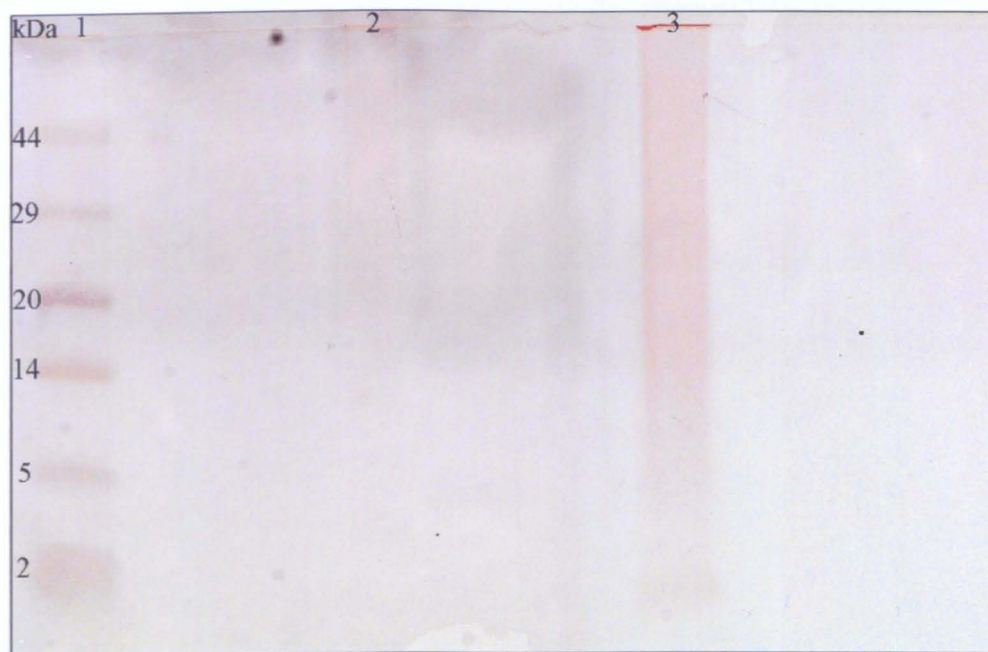


Figure 4.8 Acridine Orange stained, 15% polyacrylamide gel of *T. retusa* intercrystalline and intracrystalline protein fractions

Intercrystalline and intracrystalline proteins from T. retusa were prepared as described in Section 2.8. The proteins were electrophoresed on a BioradTM minigel system at 60V and visualised by staining with Acridine Orange (Dauphin et al., 2003). Lane 1 Prestained low molecular weight protein standards (See Section 2.8.4). Lane 2 Soluble intercrystalline protein extract. Lane 3 Soluble intracrystalline protein extract.

When stained with Coomassie Brilliant Blue and silver stain a number of proteins extracted from the intercrystalline and intracrystalline organic matrix fractions of *N. anomala* are apparent within the gel (Figure 4.3). When stained with Acridine Orange however only a smear of material larger than 44kDa is visualised (Figure 4.9).

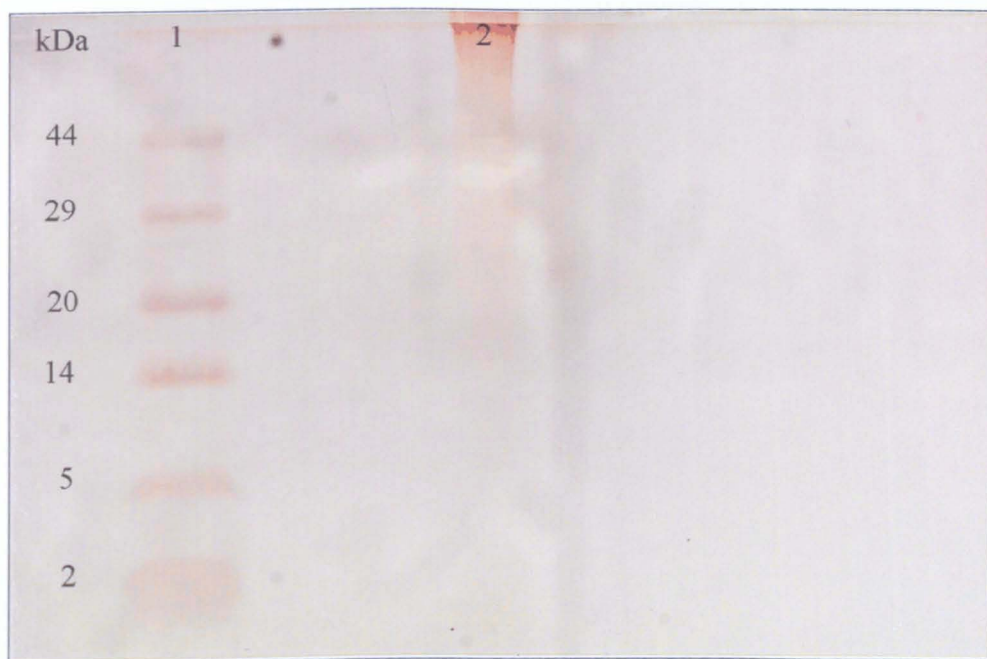


Figure 4.9 Acridine Orange stained, 15% polyacrylamide gel of *N. anomala* intracrystalline protein fraction

The intracrystalline protein extract of N. anomala was prepared as described in Section 2.8. The proteins were electrophoresed on a BioradTM minigel system at 60V (Section 2.8.4) and visualised by staining with Acridine Orange (Dauphin et al., 2003). Lane 1 Prestained low molecular weight protein standards (See Section 2.8.4). Lane 2 Soluble intracrystalline proteins.

When separated by gel electrophoresis and the gel stained with Coomassie Brilliant Blue and silver stain the intracrystalline extract of *M. edulis* appears as a smear in the gel. However, some proteins are discernable (Figure 4.4). When stained with Acridine Orange the intracrystalline material again appears as a smear in the gel while low molecular weight material, less than 14 kDa is heavily stained (Figure 4.10).

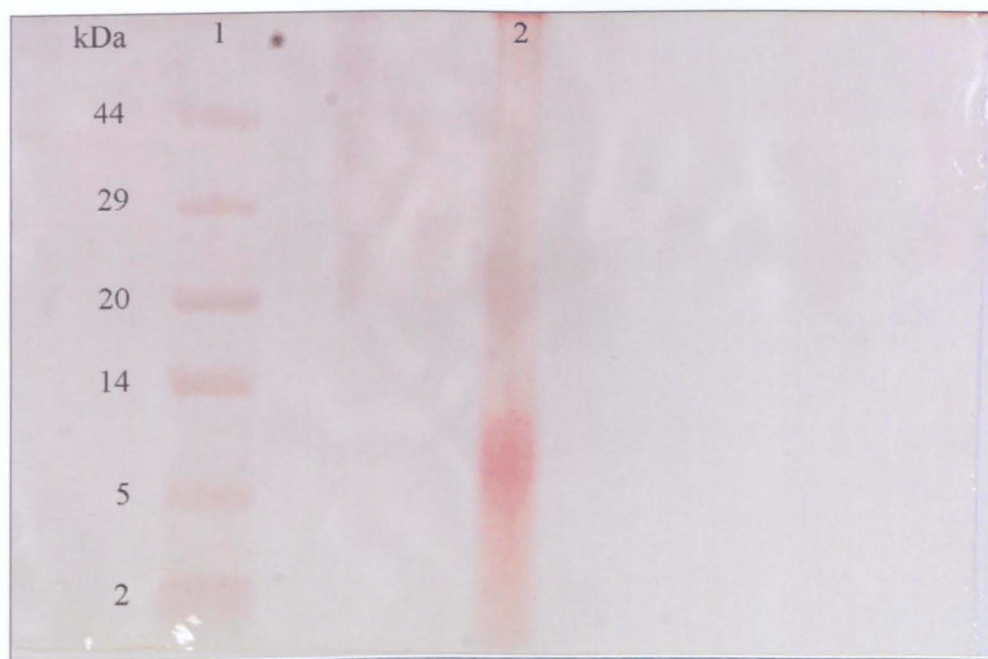


Figure 4.10 Acridine orange stained, 10% polyacrylamide gel of *M. edulis* intracrystalline fraction

The intracrystalline protein extract of *M. edulis* was prepared as described in Section 2.8. The proteins were electrophoresed on a BioradTM minigel system at 60V (Section 2.8.4) and visualised by staining with Acridine Orange (Duaphin et al., 2003). Lane 1 Prestained low molecular weight protein standards (See Section 2.8.4). Lane 2 Soluble intracrystalline protein extract.

A number of proteins extracted from the intracrystalline organic matrix of the eggshell of *G. gallus* are visualised in Coomassie Brilliant Blue and silver stain (Figure 4.6). However, when stained with Acridine Orange the intracrystalline appears as a smear in the gel (Figure 4.11).

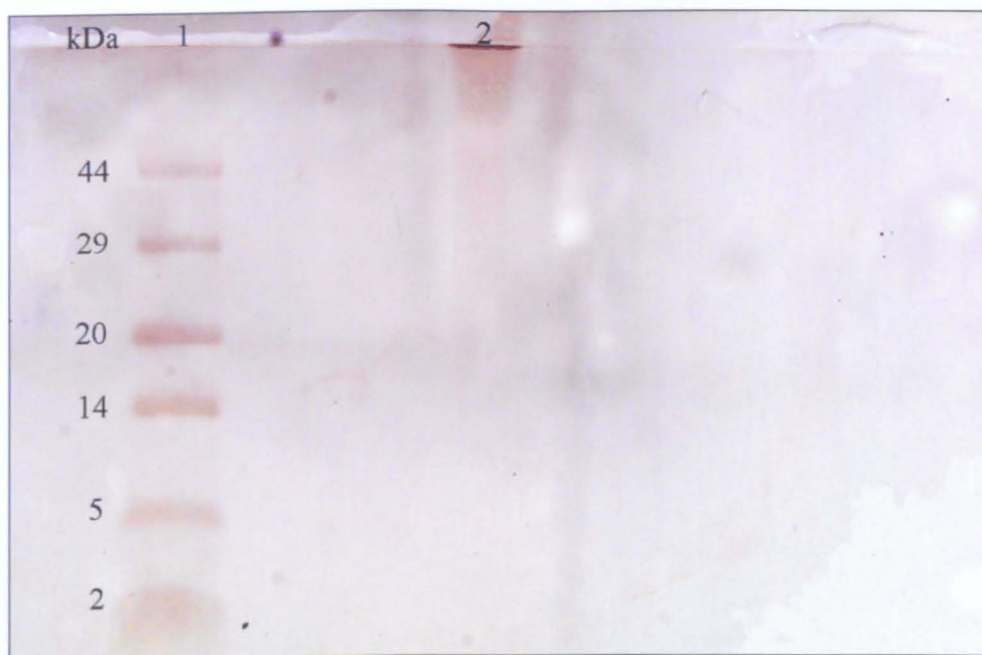


Figure 4.11 Acridine orange stained, 15% polyacrylamide gel of *G. gallus* eggshell intracrystalline protein fraction

The intracrystalline protein extract of the avian eggshell was prepared as described in Section 2.8. The proteins were electrophoresed on a Biorad™ minigel system at 60V and visualised by staining with Acridine Orange. Lane 1 Prestained low molecular weight protein standards (See Section 2.8.4). Lane 2 Soluble intracrystalline protein extract.

4.3.5 Distribution of Amino Acids in *T. retusa*, *N. anomala*, *M. edulis* and *G. gallus*

The distribution of amino acids between the intercrystalline and intracrystalline protein fractions of *T. retusa*, *N. anomala*, *M. edulis* and *G. gallus* was determined by amino acid analysis. Samples were manually hydrolysed (Section 2.9.1) and analysed using an Applied Biosystems 420-H analyser (Section 2.9.2). Figure 4.12 displays the concentration of amino acids in the total, intercrystalline and intracrystalline protein fractions. Intact valves were cleaned and rinsed using sodium hypochlorite (1% v/v) as described in Section 2.2. Cleaned valves were powdered using a ceramic mortar and pestle (Section 2.9.1). The total concentration of amino acids was extracted by dissolving the powder in an aqueous solution of HCL (2N). The solution was transferred to hydrolysis tubes and dried under vacuum. The tubes were placed in vials containing 500µl HCl (6N), purged with argon, sealed and heated at 165°C for one hour (Section 2.9.1). Treatment of shell powder with sodium hypochlorite (1%v/v) (Section 2.9.1) destroyed the intercrystalline amino acids therefore only intracrystalline amino acids were extracted upon dissolution of the sodium hypochlorite-treated shell powder (Section 2.9.1). The concentration of intercrystalline amino acids was the difference between the total and intracrystalline amino acid concentration.

Considering the concentration of amino acids in each of the systems in turn, for *T. retusa* the overall concentration of amino acids is greater in the ventral valve, while the concentration of amino acids is slightly higher in the intercrystalline fraction in relation to the intracrystalline fractions in both valves. In the dorsal valve of *N. anomala* there is an even distribution of amino acids between the intercrystalline and intracrystalline protein fractions. The concentration of amino acids is greater in the left valve of *M. edulis*, while the concentration of amino acids is greater in the intercrystalline protein fraction in relation to the intracrystalline protein fraction in both valves. In *G. gallus* the distribution of amino acids is highest in the intracrystalline protein fraction.

Between the four systems the dorsal valve of *N. anomala* has the lowest total concentration of amino acids, while *G. gallus* has the highest total concentration. The dorsal valve of *N. anomala* has the lowest concentration of intercrystalline amino acids, while *M. edulis* has the highest concentration of intercrystalline amino acids. The right valve of *M. edulis* has

the lowest concentration of intracrystalline amino acids, while *G. gallus* has the highest concentration of intracrystalline amino acids (Figure 4.12).

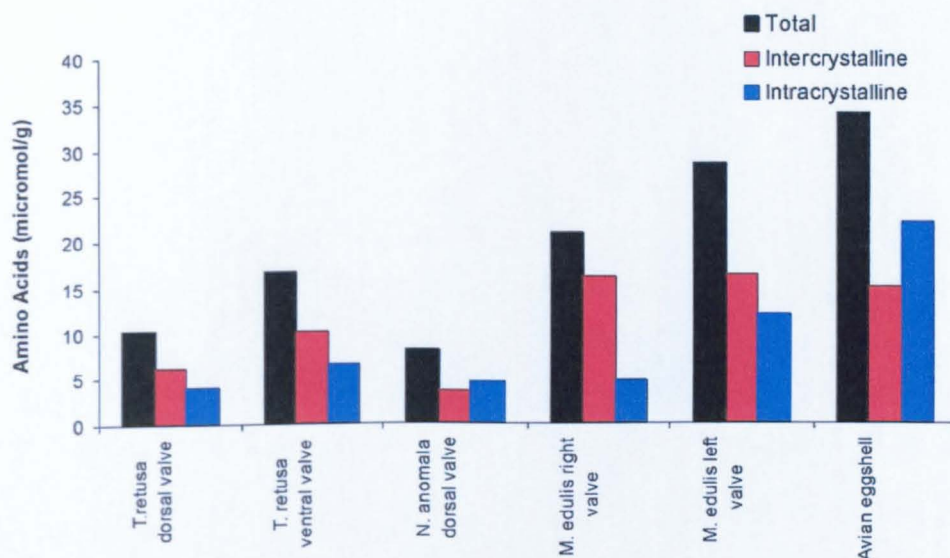


Figure 4.12 Distribution of amino acids in *T. retusa*, *N. anomala*, *M. edulis* and an avian eggshell (*Gallus gallus*)

Powdered shell samples were incubated in an aqueous solution of sodium hypochlorite (1% v/v) as described in Section 2.9.1. Total, inter and intracrystalline amino acids were extracted (Section 2.9.1) and the amino acid concentration determined (Sections 2.9.2 and 2.9.3).

One-letter codes for amino acids are presented in Table 4.2. The relative abundances of amino acids (displayed as amino acids per hundred residues) in the total, intercrystalline and intracrystalline protein fractions of *T. retusa*, *N. anomala*, *M. edulis* and *G. gallus* are presented in Tables 4.3-4.8, and Figures 4.1-4.15. In all cases, the total protein and intercrystalline protein extracts have a high glycine content. The intracrystalline fractions of *T. retusa*, *N. anomala* and *M. edulis* are also glycine rich. The total protein fraction of *T. retusa* also has a relatively high content of asparagine/aspartic acid, arginine, alanine and valine. The total protein fraction of the dorsal valve of *N. anomala* has a high concentration of asparagine/aspartic acid, alanine and proline. The total protein composition of both valves of *M. edulis* includes a high alanine and lysine content. The total protein fraction of the eggshell is enriched in alanine and lysine. However, overall the amino acid composition is more balanced than in the marine biominerals.

The intercrystalline fraction of *T. retusa* has a similar composition to the total protein fraction and is enriched in asparagine/aspartic acid, valine and alanine. The intercrystalline fraction of *N. anomala* is enriched in proline, alanine and asparagine/aspartic acid. The intercrystalline protein fraction of *M. edulis* has a similar composition to the total protein fraction and is enriched in alanine and lysine, while the intercrystalline fraction of the eggshell is proline rich.

The intracrystalline protein fraction of both valves of *T. retusa* is rich in glycine and valine, while the dorsal valve protein fraction is also enriched in proline. The intracrystalline protein fraction extracted from the dorsal valve of *N. anomala* is enriched in glycine, asparagine/aspartic acid and serine. The intracrystalline protein from the right valve of *M. edulis* is enriched in proline, threonine, glycine and serine, while the left valve is enriched in glycine, proline and alanine. The intracrystalline protein fraction of *G. gallus* is enriched in serine, histidine, tyrosine, threonine and isoleucine.

Amino Acid	One Letter Code
Aspartic Acid	D
Asparagine	N
Glutamic Acid	E
Glutamine	Q
Serine	S
Glycine	G
Histidine	H
Arginine	R
Threonine	T
Alanine	A
Proline	P
Tyrosine	Y
Valine	V
Methionine	M
Cysteine	C
Isoleucine	I
Leucine	L
Phenylalanine	F
Tryptophan	K

Table 4.2 One letter codes for amino acids

	D	E	S	G	H	R	T	A	P	Y	V	M	C	I	L	F	K
<i>T. retusa</i> dorsal valve	1437.7	349.4	263.0	6471.5	91.5	739.0	471.6	1010.1	1197.9	737.7	1307.6	0.0	210.1	393.0	302.7	143.4	155.4
<i>T. retusa</i> ventral valve	1021.2	433.9	494.6	7408.2	264.3	1090.9	581.3	975.6	239.9	1059.3	1679.9	0.0	174.0	388.6	352.9	179.2	255.5
<i>N. anomala</i> dorsal valve	1047.6	231.5	574.4	1904.5	260.0	392.7	500.7	638.3	738.3	136.9	495.0	0.0	120.4	326.7	391.1	147.3	178.3
<i>M.edulis</i> right valve	1595.1	527.6	1497.9	10784.9	162.2	1274.1	1098.4	5719.2	670.7	1024.4	1722.4	0.0	139.0	932.9	2457.8	725.4	911.4
<i>M.edulis</i> left valve	1877.9	982.8	2499.8	14333.5	138.4	2468.2	1372.8	7182.2	175.8	1456.1	2112.2	937.9	379.9	1177.9	3451.1	941.8	1069.1
<i>Gallus gallus</i>	1387.5	3878.2	3923.6	9225.6	2810.3	3790.8	3794.0	5611.5	5126.9	1077.3	4540.5	1935.4	370.1	2054.8	3406.8	947.1	1657.9

Table 4.3. Absolute amino acid composition (pmol) of the total protein fractions of *T. retusa* , *N. anomala* , *M. edulis* , and *G. gallus*

	D	E	S	G	H	R	T	A	P	Y	V	M	C	I	L	F	K
<i>T. retusa</i> dorsal valve	9.41	2.29	1.72	42.35	0.60	4.84	3.09	6.61	7.84	4.83	8.56	0.00	1.38	2.57	1.98	0.94	1.02
<i>T. retusa</i> ventral valve	6.15	2.61	2.98	44.63	1.59	6.57	3.50	5.88	1.45	6.38	10.12	0.00	1.05	2.34	2.13	1.08	1.54
<i>N. anomala</i> dorsal valve	12.96	2.86	7.11	23.56	3.22	4.86	6.19	7.90	9.13	1.69	6.12	0.00	1.49	4.04	4.84	1.82	2.21
<i>M.edulis</i> right valve	5.11	1.69	4.79	34.52	0.52	4.08	3.52	18.31	2.15	3.28	5.51	0.00	0.44	2.99	7.87	2.32	2.92
<i>M.edulis</i> left valve	4.41	2.31	5.87	33.68	0.33	5.80	3.23	16.88	0.41	3.42	4.96	2.20	0.89	2.77	8.11	2.21	2.51
<i>Gallus gallus</i>	2.50	6.98	7.07	16.62	5.06	6.83	6.83	10.11	9.23	1.94	8.18	3.49	0.67	3.70	6.14	1.71	2.99

Table 4.4. Amino acid composition of the total protein fraction of *T. retusa* , *N. anomala* , *M. edulis* and *G. gallus*

Values are presented as number of amino acids per 100 amino acids

Total amino acids (per 100 residues)	<i>T. retusa</i> dorsal valve	<i>T. retusa</i> ventral valve	<i>N. anomala</i> dorsal valve	<i>M.edulis</i> right valve	<i>M.edulis</i> left valve	Eggshell (<i>Gallus gallus</i>)
ACID:BASE RATIO	2.00	1.08	2.24	0.97	0.81	0.97

	D	E	S	G	H	R	T	A	P	Y	V	M	C	I	L	F	K
<i>T. retusa</i> dorsal valve	1264.4	261.9	141.8	5058.9	91.5	571.7	268.3	698.3	421.5	673.9	916.6	0.0	181.9	282.9	176.1	125.6	120.0
<i>T. retusa</i> ventral valve	723.7	269.3	303.7	4998.5	202.1	644.7	246.3	522.8	-146.2	701.7	901.3	0.0	119.0	192.0	136.7	127.8	181.6
<i>N. anomala</i> dorsal valve	336.4	68.2	-37.2	875.9	106.0	251.2	152.6	311.9	484.7	73.0	221.7	0.0	92.8	188.8	190.6	87.4	102.4
<i>M. edulis</i> right valve	1496.3	463.8	891.6	10199.9	124.8	1197.4	426.0	5459.8	-756.9	956.5	1544.6	0.0	131.3	814.1	2204.0	642.2	782.0
<i>M. edulis</i> left valve	1228.0	654.8	1516.4	10883.3	55.4	2167.8	845.0	5721.6	-1644.2	1280.0	1599.2	937.9	337.8	831.0	2676.9	745.7	733.8
<i>Gallus gallus</i>	693.3	2717.7	2851.9	6405.3	1941.6	2051.9	1316.0	2655.0	4702.3	754.2	2190.0	1915.3	269.3	1157.2	262.2	545.3	1106.4

Table 4.5. Absolute amino acid composition (pmol) of the intercrystalline protein fractions of *T. retusa* , *N. anomala* , *M. edulis* and *G. gallus*

	D	E	S	G	H	R	T	A	P	Y	V	M	C	I	L	F	K
<i>T. retusa</i> dorsal valve	11.23	2.33	1.26	44.95	0.81	5.08	2.38	6.20	3.75	5.99	8.14	0.00	1.62	2.51	1.57	1.12	1.07
<i>T. retusa</i> ventral valve	7.15	2.66	3.00	49.37	2.00	6.37	2.43	5.16	0.00	6.93	8.90	0.00	1.18	1.90	1.35	1.26	1.79
<i>N. anomala</i> dorsal valve	9.59	1.94	0.00	24.98	3.02	7.16	4.35	8.89	13.82	2.08	6.32	0.00	2.65	5.38	5.44	2.49	2.92
<i>M. edulis</i> right valve	5.63	1.75	3.36	38.38	0.47	4.51	1.60	20.55	0.00	3.60	5.81	0.00	0.49	3.06	8.29	2.42	2.94
<i>M. edulis</i> left valve	4.02	2.14	4.96	35.60	0.18	7.09	2.76	18.72	0.00	4.19	5.23	3.07	1.10	2.72	8.76	2.44	2.40
<i>Gallus gallus</i>	2.07	8.10	8.50	19.10	5.79	6.12	3.92	7.92	14.02	2.25	6.53	5.71	0.80	3.45	0.78	1.63	3.30

Table 4.6. Amino acid composition of the intercrystalline protein fraction of *T. retusa* , *N. anomala* , *M. edulis* and *G. gallus*

Values are presented as number of amino acids per 100 residues

Total amino acids (per 100 residues)	<i>T. retusa</i> dorsal valve	<i>T. retusa</i> ventral valve	<i>N. anomala</i> dorsal valve	<i>M. edulis</i> right valve	<i>M. edulis</i> left valve	Eggshell (<i>Gallus gallus</i>)
ACID:BASE RATIO	2.21	1.20	1.14	0.99	0.65	1.08

	D	E	S	G	H	R	T	A	P	Y	V	M	C	I	L	F	K
<i>T. retusa</i> dorsal valve	173.3	87.5	121.2	1412.5	0.0	167.3	203.4	311.8	776.4	63.7	391.0	0.0	28.3	110.1	126.5	17.7	35.4
<i>T. retusa</i> ventral valve	297.5	164.5	190.9	2409.7	62.2	446.1	335.0	452.8	386.1	357.6	778.6	0.0	55.0	196.6	216.2	51.4	73.9
<i>N. anomala</i> dorsal valve	711.3	163.3	611.6	1028.6	153.9	141.5	348.1	326.5	253.6	63.9	273.3	0.0	27.6	137.9	200.5	59.9	75.9
<i>M.edulis</i> right valve	98.8	63.7	606.3	585.0	37.4	76.7	672.4	259.4	1427.5	67.9	177.8	0.0	7.7	118.8	253.8	83.2	129.3
<i>M.edulis</i> left valve	649.9	328.0	983.4	3450.2	83.0	300.5	527.8	1460.7	1820.0	176.1	513.0	0.0	42.1	346.9	774.1	196.1	335.3
<i>Gallus gallus</i>	694.1	1160.5	1071.7	2820.3	868.7	1738.9	2478.0	2956.5	424.6	323.1	2350.4	20.0	100.8	897.7	3144.6	401.8	551.5

Table 4.7. Absolute amino acid composition of the intracrystalline protein fractions of *T. retusa* , *N. anomala* , *M. edulis* , and *G. gallus*

	D	E	S	G	H	R	T	A	P	Y	V	M	C	I	L	F	K
<i>T. retusa</i> dorsal valve	4.30	2.17	3.01	35.08	0.00	4.15	5.05	7.74	19.28	1.58	9.71	0.00	0.70	2.74	3.14	0.44	0.88
<i>T. retusa</i> ventral valve	4.60	2.54	2.95	37.22	0.96	6.89	5.17	6.99	5.96	5.52	12.03	0.00	0.85	3.04	3.34	0.79	1.14
<i>N. anomala</i> dorsal valve	15.54	3.57	13.36	22.47	3.36	3.09	7.61	7.13	5.54	1.40	5.97	0.00	0.60	3.01	4.38	1.31	1.66
<i>M.edulis</i> right valve	2.12	1.37	12.99	12.54	0.80	1.64	14.41	5.56	30.60	1.45	3.81	0.00	0.16	2.55	5.44	1.78	2.77
<i>M.edulis</i> left valve	5.42	2.74	8.20	28.78	0.69	2.51	4.40	12.18	15.18	1.47	4.28	0.00	0.35	2.89	6.46	1.64	2.80
<i>Gallus gallus</i>	3.15	5.27	4.87	12.82	3.95	7.90	11.26	13.44	1.93	1.47	10.68	0.09	0.46	4.08	14.29	1.83	2.51

Table 4.8. Amino acid composition of the intracrystalline protein fraction of *T. retusa* , *N. anomala* , *M. edulis* and *G. gallus*

Values are presented as number of amino acids per 100 residues

Total amino acids (per 100 residues)	<i>T. retusa</i> dorsal valve	<i>T. retusa</i> ventral valve	<i>N. anomala</i> dorsal valve	<i>M.edulis</i> right valve	<i>M.edulis</i> left valve	Eggshell (<i>Gallus gallus</i>)
ACID:BASE RATIO	1.29	0.89	4.02	0.79	1.54	0.81

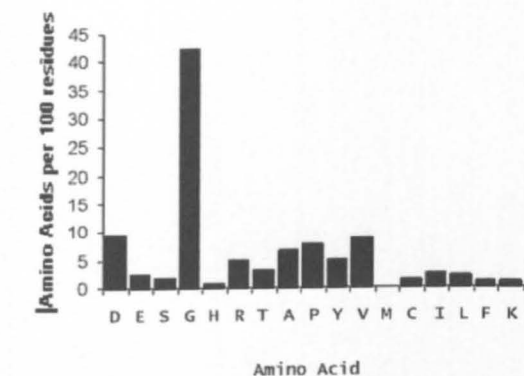
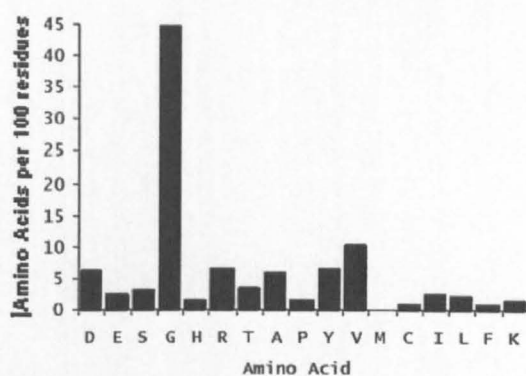
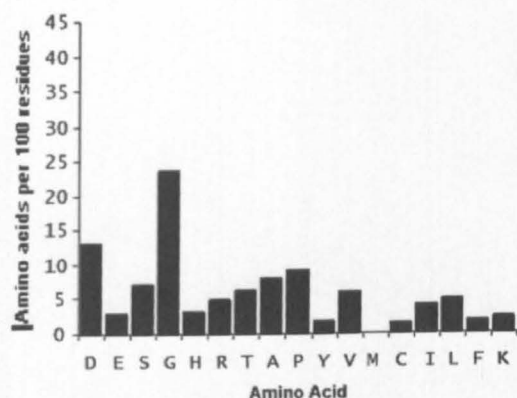
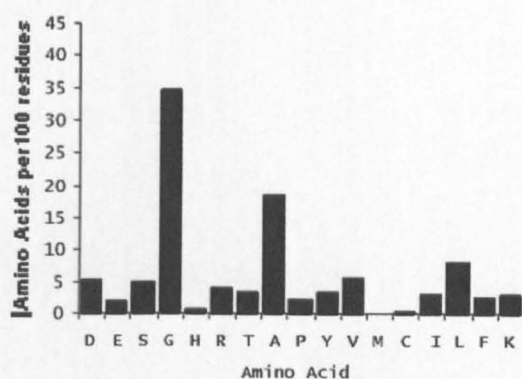
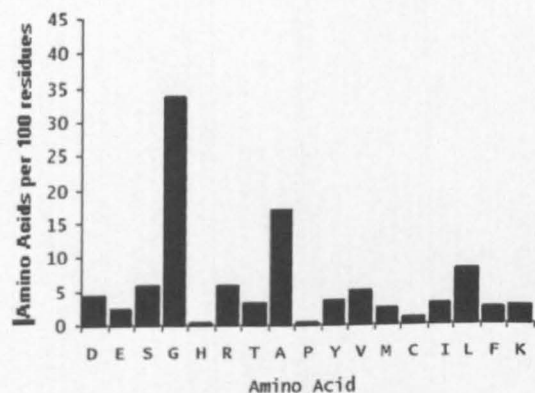
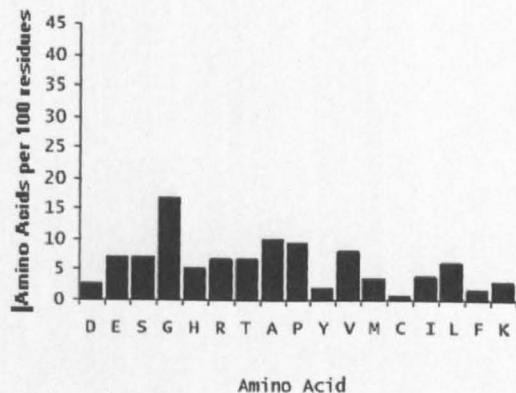
(a) *T. retusa* dorsal valve(b) *T. retusa* ventral valve(c) *N. anomala* dorsal valve(d) *M. edulis* right valve(e) *M. edulis* left valve(f) Eggshell (*Gallus gallus*)

Figure 4.13 Amino acid composition of the total protein fraction of *T. retusa*, *N. anomala*, *M. edulis* and *G. gallus*

Samples were prepared and hydrolysed as described in Section 2.9.1. The total amino acid composition was determined as described in Section 2.9.2. Values are presented as amino acids per 100 residues using the one-letter codes for amino acids (Table 4.2).

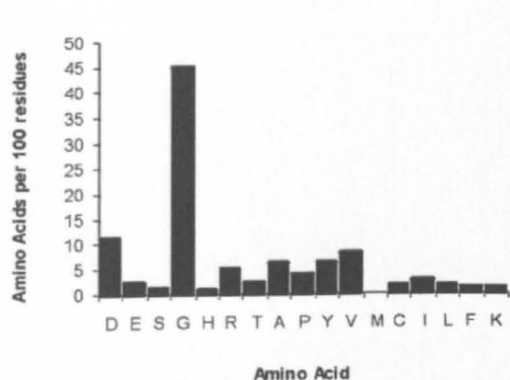
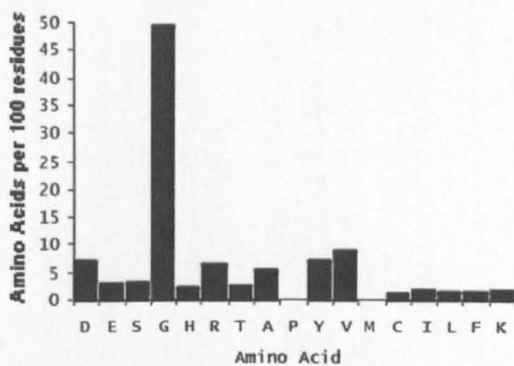
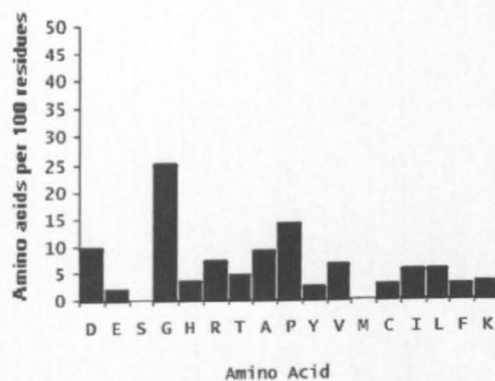
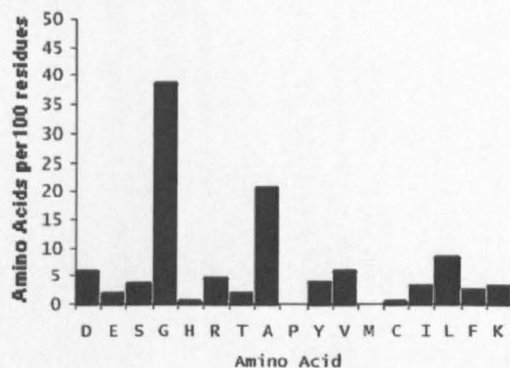
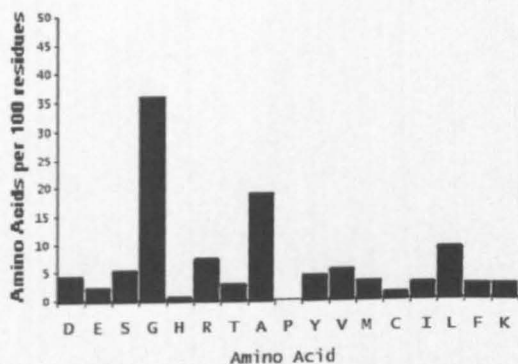
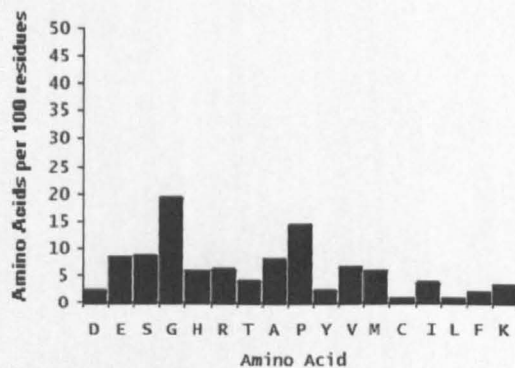
(a) *T. retusa* dorsal valve(b) *T. retusa* ventral valve(c) *N. anomala* dorsal valve(d) *M. edulis* right valve(e) *M. edulis* left valve(f) Eggshell (*Gallus gallus*)

Figure 4.14 Amino acid composition of the intercrystalline protein fraction of *T. retusa*, *N. anomala*, *M. edulis* and *G. gallus*

Samples were prepared and hydrolysed as described in Section 2.9.1. The intercrystalline amino acid composition was estimated from the concentration of amino acids destroyed by incubation in sodium hypochlorite. Values are presented as amino acids per 100 residues using the one letter codes for amino acids (Table 4.2).

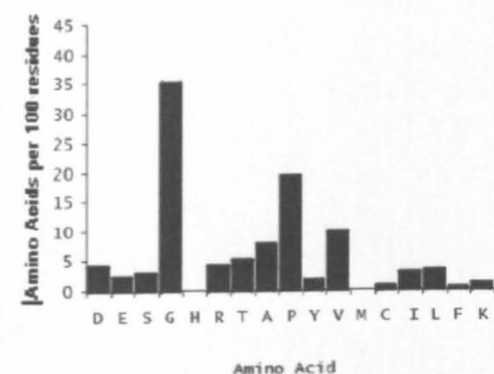
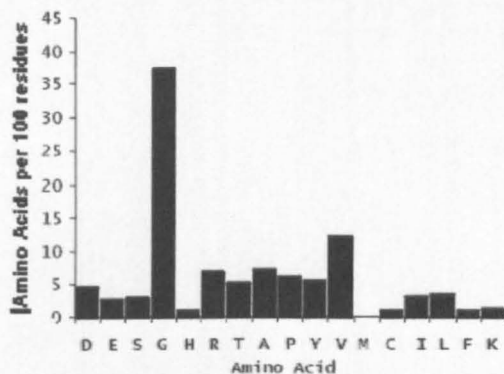
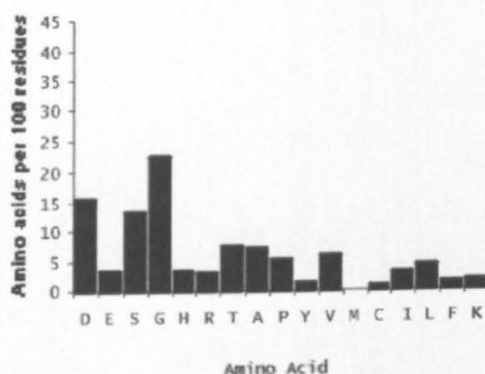
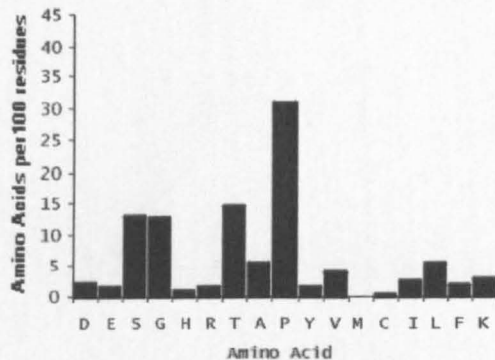
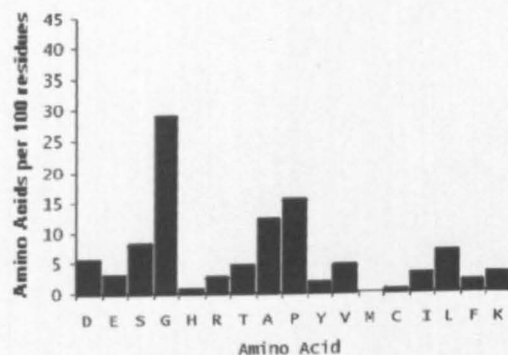
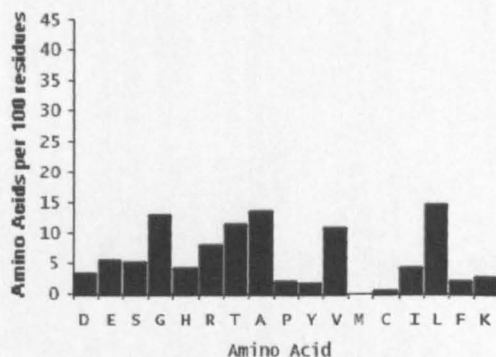
(a) *T. retusa* dorsal valve(b) *T. retusa* ventral valve(c) *N. anomala* dorsal valve(d) *M. edulis* right valve(e) *M. edulis* left valve(f) Eggshell (*Gallus gallus*)

Figure 4.15 Amino acid composition of the intracrystalline fraction of *T. retusa*, *N. anomala*, *M. edulis* and *G. gallus*

Samples were prepared and the intercrystalline matrix fraction destroyed as described in Section 2.9.1. Samples were hydrolysed as described in Section 2.9.1. The intracrystalline amino acid composition was determined as described in Section 2.9.2. Values are presented as amino acids per 100 residues using the one letter code for amino acids (Table 4.2)

4.3.6 N-Terminal Sequencing

Intracrystalline proteins extracted from the shells of *T. retusa* and *N. anomala* were transferred to a Problott Membrane using a Biorad Mini Transblot Electrophoretic Transfer Cell as described in Section 2.10.1. N-terminal sequencing of the most abundant protein (38kDa) from the organic matrix of *T. retusa* and the 35kDa protein from the matrix of *N. anomala* was undertaken as described in Section 2.10.2. The 38kDa protein of *T. retusa* could not be sequenced as the N-terminal of the protein was blocked preventing the Edman Degradation Chemistry. The N-terminal sequence of the 35kDa protein of *N. anomala* is shown below:

5 10 15

V/L H/Y I K K E Q E Q ? Y/Q I P D F G P

4.3.7 Calcite Growth in the Presence of Intracrystalline Proteins

Calcite crystals were grown in vitro according to the Kitano protocol (Kitano, 1962), (Section 2.11.1). A control experiment was carried out in which the crystals were allowed to develop over 24, 48 and 72 hours in the absence of additives. As the intracrystalline protein extracts are buffered by sodium phosphate buffer the effect of buffer on the development of the crystals was assessed by the addition of 2 μ L of sodium phosphate buffer to the crystal growth solution.

The method for analysis of crystal size was modified from Roque *et al.*, (2004). Images of the coverslips on which the crystals were grown were taken using an SEM. The magnification for each image was kept constant, therefore the area of each coverslip covered by the image was consistent. The number of crystals and the area of each crystal within the whole image were assessed using the computer software Scion Image. Histograms of crystal number and size were produced using the statistical package SPSS.

Crystals grown in solution without additives were calcite. Crystals grown in the presence of sodium phosphate buffer were also calcite, but were malformed and often present in clusters (Figure 4.18b). As a result all intracrystalline protein extracts were washed thoroughly with Milli QTM through microcon filters to remove the sodium phosphate buffer.

Figure 4.16 presents histograms of the number and size of crystals which developed over 24, 48 and 72 hours both with and without the addition of sodium phosphate buffer. The highest total number of crystals (N) was formed after 48 hours, however the overall difference between N for 24 and 48 hours was relatively small. In each experiment the sodium phosphate buffer had an inhibitory effect on calcite crystal growth.

Crystals that were grown with the addition of intracrystalline proteins were left to develop over 24 and 48 hours. Figure 4.17 presents histograms of the number and size of crystals grown in the presence of intracrystalline extracts of *T. retusa*, *N. anomala*, *M. edulis* and the eggshell over 24 hours. The concentration of protein added to each crystal growth experiment is presented in Table 2.4 (Chapter 2, Section 2.11.2). The addition of *T. retusa* intracrystalline organic matrix extract does not appear to have an inhibitory effect on calcite growth at a concentration of 1.6ng/ml. *N. anomala* and *M. edulis* intracrystalline extracts, and to some extent *M. edulis* extrapallial fluids had an inhibitory effect on calcite growth. It should be noted that the concentration of protein in the intracrystalline extracts that were added to the calcite growth solution varied due to the small concentration of protein that was available and therefore these results are preliminary.

Figure 4.18 displays representative examples of crystal morphology. Crystals that developed over 48 hours in the solution without additives commonly displayed a rhombohedral habit with well defined crystal faces (Figure 4.18a), while secondary crystal growth is also common. Crystals grown in the presence of *T. retusa* intracrystalline organic matrix extract for 48 hours show pitted surfaces and evidence of clustering (Figure 4.18c). With the addition of intracrystalline organic matrix extract from *N. anomala* the calcite crystals displayed evidence of a layered structure with the secondary growth of small rhombohedral calcite crystals on the surface of the crystal (Figure 4.18d and e). The addition of intracrystalline organic matrix extracted from the shell of *M. edulis* to the saturated calcium carbonate solution resulted in the formation of globular shaped precipitates (Figure 4.18f). Crystals grown with the addition of *M. edulis* extrapallial fluid display rounded edges and there is also evidence of crystal clustering and secondary crystal growth (Figure 4.18g). With the addition of eggshell intracrystalline organic matrix the crystals display a layered structure with pitted surfaces (Figure 4.18g and h). X-ray diffraction analysis confirmed that crystals that were grown in the presence of intracrystalline extracts of *T. retusa*, *N. anomala*, and the eggshell and extrapallial fluid extracted from *M. edulis* are composed of calcite. However, XRD analysis indicates that

the crystals grown in the presence of *M. edulis* intracrystalline organic matrix extract are amorphous (Figure 4.19).

Figure 4.16 Histograms of Crystal Number vs. Crystal Size for calcite growth *in vitro*

Calcite crystals were grown on coverslips according to the Kitano Protocol (Section 2.11.1). Coverslips were removed from the saturated calcium carbonate solution after 24, 48 and 72 hours. Sodium phosphate buffer was added to samples d, e and f at the start of crystallisation. (a) 24 hours, (b) 48 hours, (c) 72 hours, (d) 24 hours with buffer, (e) 48 hours with buffer and (f) 72 hours with buffer. SEM images of the coverslip were acquired (at a constant magnification) and the number of crystals and the area of the image that each crystal covered analysed using the computer software Scion Image. Histograms were produced using the statistical package SPSS.

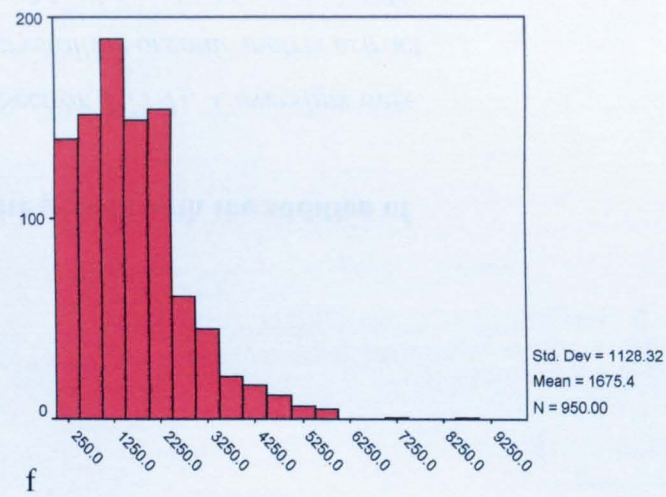
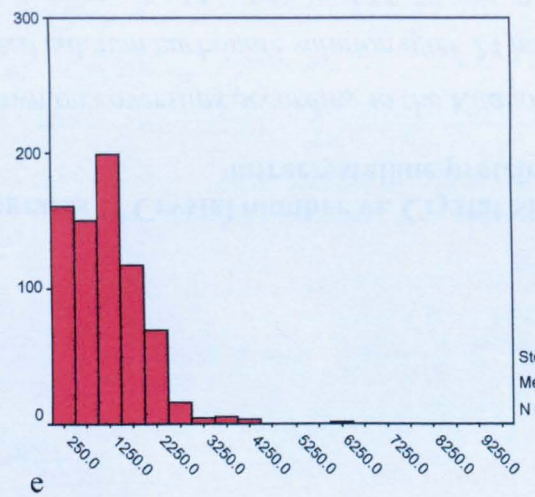
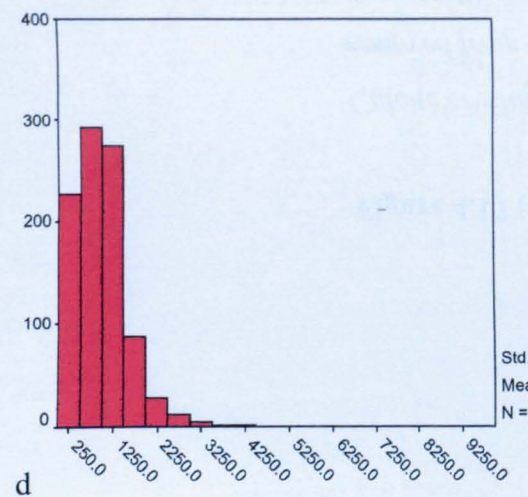
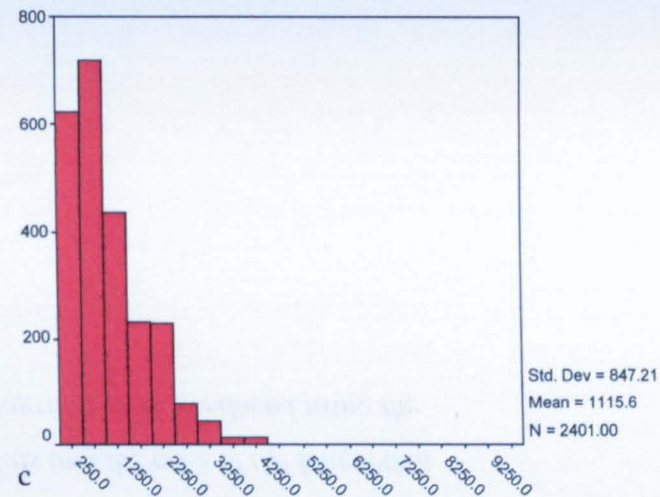
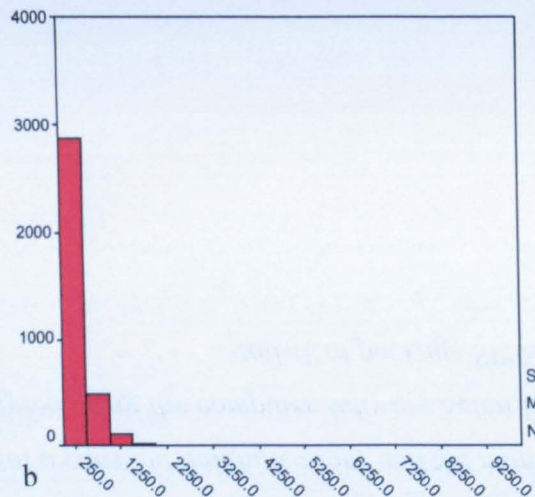
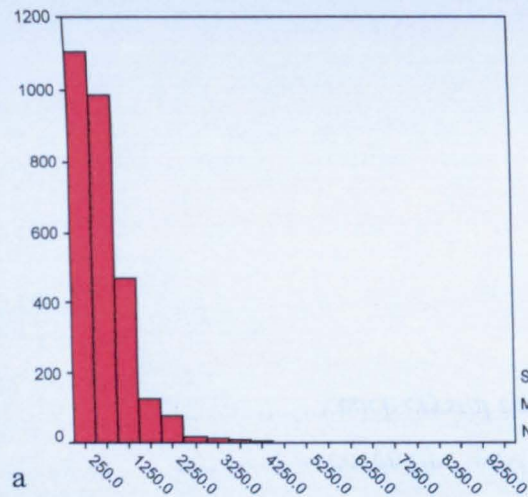


Figure 4.17 (a-d) Histograms of Crystal number vs. Crystal Size for calcite growth with the addition of intracrystalline proteins

Calcite crystals were grown on coverslips according to the Kitano Protocol (Section 2.11.1). Coverslips were removed from the saturated calcium carbonate solution after 24 hours. Intracrystalline organic matrix extract from (a) T. retusa, (b) N. anomala, (c) M. edulis and (d) Extrapallial fluid from M. edulis. SEM images of the coverslips were acquired (at a constant magnification) and the number of crystals and the area of the image that each crystal covered analysed using the computer software Scion Image. Histograms were produced using the statistical package SPSS.

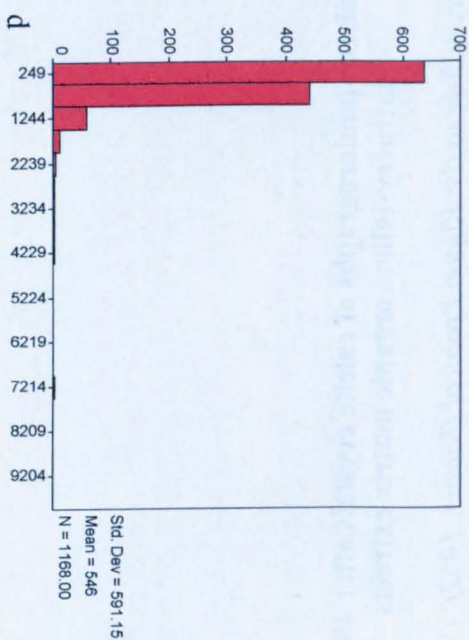
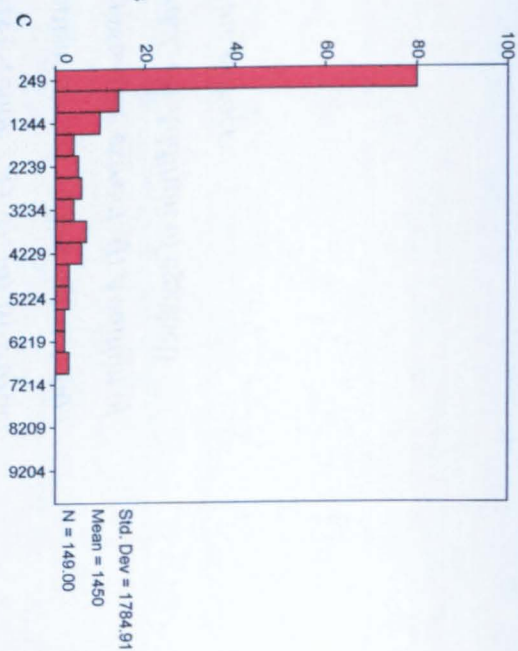
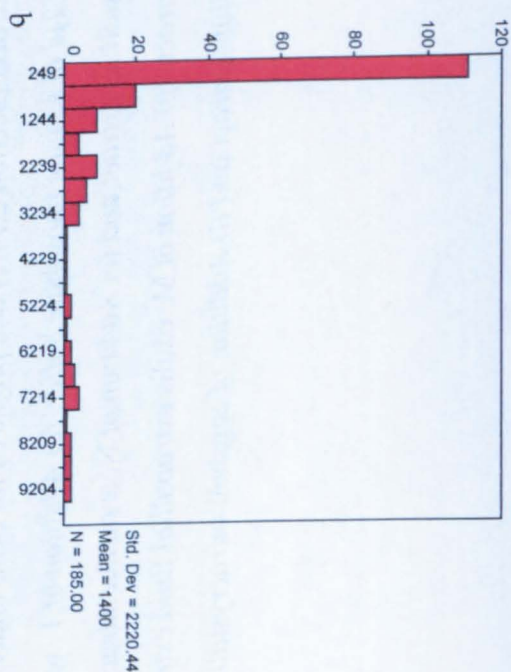
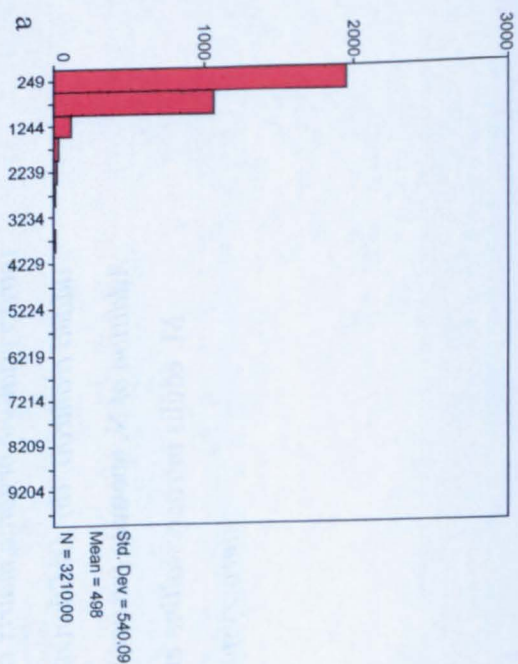
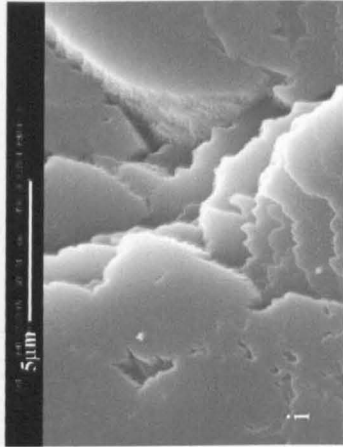
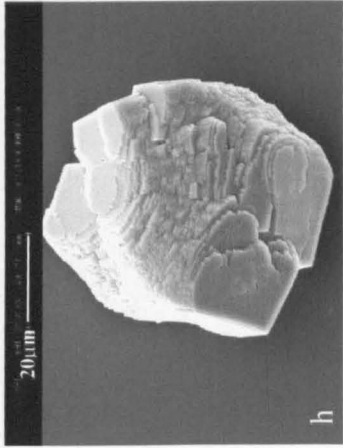
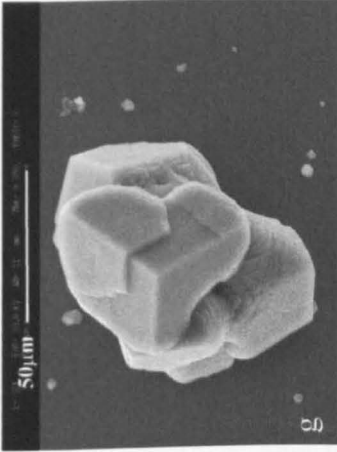
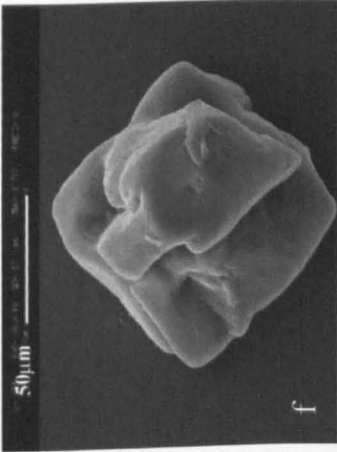
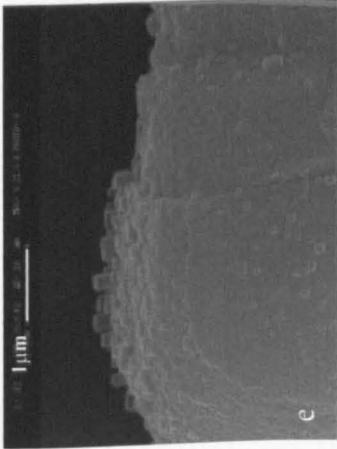
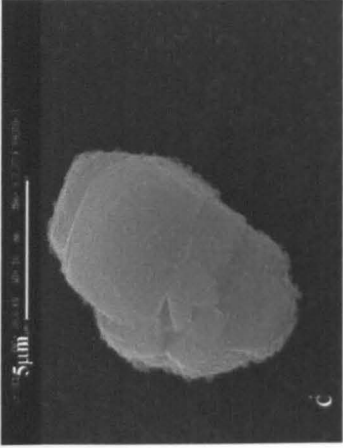
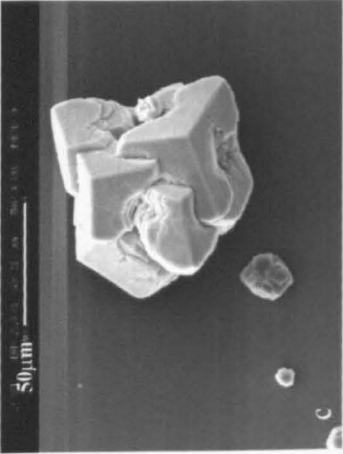
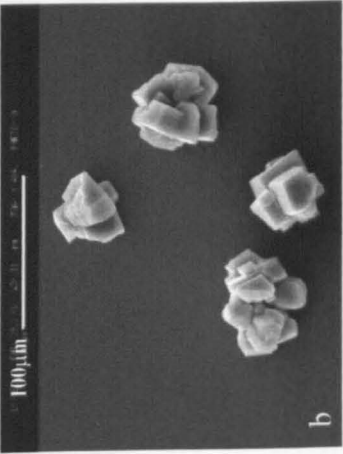
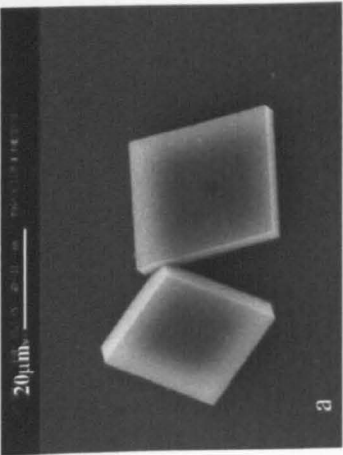


Figure 4.18 (a-i) Scanning electron micrographs of calcite crystals after 48 hours growth with addition of intracrystalline organic matrix extracts

Calcite crystals were grown according to the Kitano Protocol (Kitano, 1962), (Section 2.11.1) with the addition of intracrystalline organic matrix extracts (Section 2.11.2) and prepared for SEM analysis (Section 2.11.2). (a) No extract added (control), (b) Addition of 2 μ l of sodium phosphate buffer, (c) Addition of T. retusa intracrystalline extract, (d) Addition of N. anomala intracrystalline extract and (e) Addition of N. anomala intracrystalline extract, (f) Addition of M. edulis intracrystalline extract, (g) Addition of M. edulis extrapallial fluid extract, (h) Addition of eggshell intracrystalline extract and (i) Addition of eggshell intracrystalline extract.



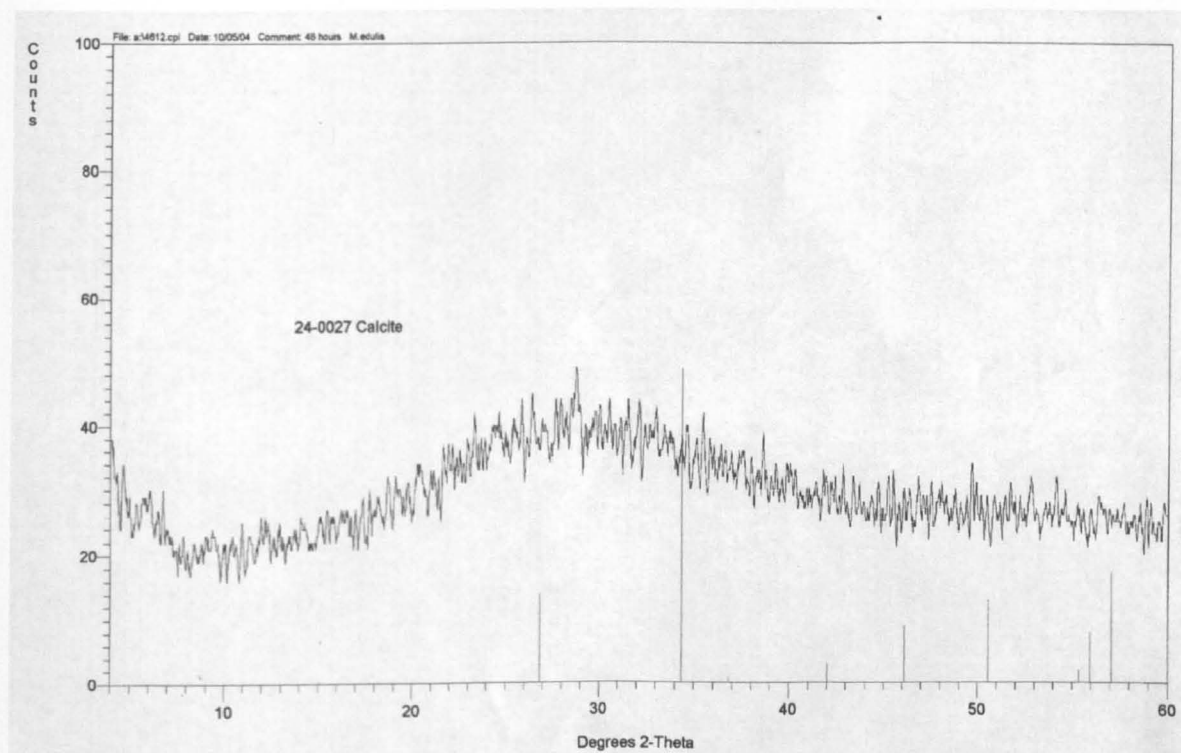


Figure 4.19 X-ray Diffraction pattern from crystals grown in the presence of *M. edulis* intracrystalline proteins

*Crystals were grown on coverslips according to the Kitano Protocol (Kitano, 1962) (Section 2.11.1). Intracrystalline protein extracted from *M. edulis* shell (Section 2.8.2) was added to the saturated calcium carbonate solution. Coverslips were removed from the saturated calcium carbonate solution after 48 hours. XRD analysis was carried out using a Phillips PW 1050/35 X-ray diffractometer (Section 2.3).*

4.4 Discussion

4.4.1 Intercrystalline and intracrystalline organic matrix composition

By comparing the composition of organic matrix from these four different carbonate biominerals, we can to some extent, determine if there are any common principles that underlie the biomineralisation process. The characterisation of the organic matrix composition and the crystal ultrastructure of biominerals from different species may also shed light on the relationship between the organic matrix composition and crystal morphology. This study has characterised proteins extracted from the shells of *T. retusa*, *N. anomala*, *M. edulis* and *G. gallus* in relation to their molecular weight and charge and the overall amino acid composition of the total, intercrystalline and intracrystalline organic matrix extracts. The relationship between the organic matrix and sulphate has also been investigated as it is recognised that sulphated polysaccharides within the matrix may also have a role in the mineralisation process (Dauphin, 2003, Miyashita *et al.*, 2000 and Yang *et al.*, 2003).

4.4.1.1 Comparison of the intercrystalline and intracrystalline organic matrix of *T. retusa*, *N. anomala*, *M. edulis* and the avian eggshell (*G. gallus*)

The intercrystalline and intracrystalline organic matrix extracts of *T. retusa*, *N. anomala*, *M. edulis* and *G. gallus* contain proteins of relatively low molecular weight.

The intercrystalline and intracrystalline protein fractions of *T. retusa* contain a protein with a molecular weight of 38kDa, which stains in silver nitrate. A less abundant protein with a molecular weight of 47kDa has also been identified in the intercrystalline protein fraction. A more abundant 39kDa protein and a 45kDa protein were identified from the intracrystalline organic matrix by Laing (1999), while Cusack *et al.*, (2000) identified a relatively abundant 40kDa protein in the intracrystalline protein fraction of *T. retusa*. The 39kDa protein described by Laing and the 40kDa protein described by Cusack *et al.*, (2000) are likely to be the same protein as the 38kDa protein that has been identified in this study.

The intracrystalline organic matrix of *N. anomala* contains a relatively abundant 35kDa protein. Two proteins with molecular weights of 63kDa and 58kDa were identified in both the intercrystalline and intracrystalline protein fractions. The 35kDa protein identified in

the intracrystalline protein fraction was not seen in the intercrystalline protein fraction. Brown (1998) identified a 44kDa protein and a less abundant 60kDa protein in the intracrystalline fraction of *N. anomala*, while Cusack *et al.*, (2000) identified a main protein of 40kDa from the intracrystalline fraction. Again this is likely to be the same protein as the 35kDa protein described here and the difference in estimated molecular weight is due to errors in estimating protein molecular weight from polyacrylamide gels (Section 4.3.2). The 63kDa and 58kDa proteins described here may also be related to the 60kDa protein described by Brown (1998). The difference in resolution of the proteins may be related to the difference in acrylamide content of the polyacrylamide gels used for the protein separation (i.e. 15% polyacrylamide gels were used for protein separation in this study). As the 35kDa protein is present only in the intracrystalline fraction this suggests that it has a different function in the mineralisation process in relation to the 63kDa and 58kDa proteins, which are present in both the intercrystalline and intracrystalline fractions.

Two proteins of 35kDa and 26kDa are present in both the intercrystalline and intracrystalline protein fractions of *M. edulis*. The intercrystalline protein fraction contains a number of proteins with molecular weights ranging up to 81kDa. A number of matrix proteins have been isolated from the shells of bivalve molluscs. Lustrin A, a framework protein with a molecular weight of 65kDa, has been identified in the shell of the marine gastropod *Haliotis rufescens* (Shen *et al.*, 1997), while Samata *et al.*, (1999) isolated a family of matrix proteins, N16 (16kDa) from the nacreous layer of the oyster, *Pinctada fucata*. Soluble mollusc shell matrix proteins include nacrein with a molecular weight of 60kDa (Miyashita *et al.*, 1996), and perlucin (17kDa) and perlustrin (13kDa) extracted from the shell of *Haliotis laevigata*.

The intracrystalline extract from the avian eggshell (*Gallus gallus*) contains proteins with a wide molecular weight range. A number of eggshell organic matrix proteins have been identified. Ovalbumin (Hincke, 1995), lysozyme and ovotransferrin (Gautron *et al.* 1997) occur at organic nucleation sites on the eggshell membrane. Proteins that have been extracted and characterised from the domestic fowl eggshell include Ovocleidin-17 (Hincke *et al.*, 1995), which has a molecular weight of 17kDa, Ovalbumin (45kDa) (Hincke, 1995), lysozyme (15kDa) (Gautron *et al.*, 1997), ovocalyxin-32 (32kDa) (Gautron *et al.*, 2001), ovotransferrin (80kDa) (Gautron *et al.*, 1997). The larger molecule ovocleidin-116 (Mann *et al.*, 2002) is present in two forms, a core protein without attached

glycosaminoglycans, which has a molecular weight of 116-120kDa and as a proteoglycan with a molecular weight of 180-200kDa.

The total amino acid extracts of *T. retusa*, *N. anomala*, *M. edulis* and *G. gallus* are all enriched in glycine. The total protein extract of the brachiopods *T. retusa* and *N. anomala* are enriched in asparagine/aspartic acid. The eggshell has the lowest asparagines/aspartic acid content of the four systems but has a higher concentration of glutamine/glutamic acid. The total protein extract of *M. edulis* differs from the protein extract from the two brachiopods in that it is enriched in both alanine and leucine. The total extract of *T. retusa* and the avian eggshell are both enriched in valine, while the protein extract from *N. anomala* and the avian eggshell are both enriched in proline.

The intercrystalline extract of *T. retusa*, *N. anomala*, *M. edulis* and *G. gallus* are all glycine rich. As for the total protein extracts, the avian eggshell has the lowest concentration of glycine of the four systems and has a higher concentration of glutamine/glutamic acid. *T. retusa* and *N. anomala* are enriched in asparagine/aspartic acid, while *N. anomala* and *M. edulis* are both enriched in leucine.

Fibrous proteins that are rich in glycine and alanine have been identified as a major component of the EDTA insoluble organic matrix of molluscs (Miyashita *et al.*, 2000). Weiner and Traub (1980) suggest that these fibrous proteins provide the organic matrix framework core as proposed in the template model for molluscan organic matrix. Sudo *et al.*, (1997) isolated two framework proteins from the shell of *Pinctada fucata*. Protein MSI 60 is enriched glycine and alanine while protein (MSI 31) is rich in glycine and glutamic acid. The intercrystalline fraction of *M. edulis* is also slightly more enriched in alanine than the intracrystalline fraction which may be explained by the presence of glycine-alanine rich framework proteins. Hare (1963) described a high glycine, alanine and aspartic acid content from the organic matrix of *Mytilus californianus*. The overall amino acid composition and the ratio of acidic to basic residues extracted from *M. californianus* also differed between the calcite and aragonite layers. The difference in amino acid composition between the left and right valves of *M. edulis* may therefore be explained by differences in the ratio of calcite:aragonite between the two valves.

The intracrystalline protein fraction of *T. retusa*, *N. anomala*, *M. edulis* and *G. gallus* are all glycine rich. The intracrystalline fraction of *N. anomala* is asparagine/aspartic acid rich, while *G. gallus* is glutamine/glutamic acid rich. *N. anomala* and *M. edulis* contain

high concentrations of serine, while *M. edulis* contains a high concentration of proline. The avian eggshell is enriched in threonine and leucine.

EDTA-soluble organic matrices extracted from a variety of invertebrate skeletons have a high content of acidic amino acids, in particular aspartic acid (Section 4.2.4). As discussed in Section 4.2.4 aspartic acid residues may have a calcium binding function and may therefore have an important role in skeletal formation. The template model described by Weiner and Hood (1975) suggests that the presence of proteins in β -sheet conformation with repeat sequences of the type $(\text{Asp-Y})_n$ where Y is commonly glycine or serine results in a repetitive negative charge and as such may determine the arrangement of Ca^{2+} ions on the matrix surface. Acidic proteins with calcium binding properties have also been extracted from the organic matrix of the eggshell of the domestic fowl. Cortivo *et al* (1982) identified a low molecular weight protein with calcium binding property that was related to the aspartic acid and glutamic acid residues.

The amino acid composition of *T. retusa*, *N. anomala*, *M. edulis* and the eggshell show some similarities e.g. all are enriched in glycine. However, there are also differences in composition i.e. the marine systems all have a relatively high asparagine/aspartic acid content while the eggshell is enriched in glutamic acid. In all cases the proteins are acidic as confirmed by isoelectric focusing (Section 4.3.3). There are similarities in amino acid composition between species from the same phylum i.e. *T. retusa* and *N. anomala*. However, there are also similarities between the brachiopods and the bivalve mollusc, *M. edulis*. The similarities in amino acid composition between *N. anomala* and *M. edulis* are of particular interest due to the similarity in crystal ultrastructure. *N. anomala* produces calcite semi-nacre while *M. edulis* produces a layer of aragonite nacre. Similarities in amino acid composition may therefore be indicative of matrix proteins with similar functions in the development of the mineral ultrastructure.

Weiner and Traub (1984) proposed the template model for the composition of molluscan organic matrix in which the core of the organic matrix layers are composed of a silk-fibroin-like protein which is covered on both surfaces by layers of soluble matrix components with calcium-binding properties. The amino acid data presented here suggests that the intercrystalline organic matrix extracted from *M. edulis* is slightly more enriched in glycine than the intracrystalline organic matrix fraction. Weiner and Hood (1975) found that the soluble organic matrix of the molluscs *Crassostrea virginica*, *Mercenaria mercenaria*, *Crassostrea irredescens* and *Nautilus pompilius* were enriched in glycine and

aspartic acid. However, the concentration of alanine is lower than that reported in this study and by Hare (1963) for *M. californianus*. The high glycine content of *T. retusa* and *N. anomala* is in common with the high glycine content identified in the shells of other brachiopod species (Walton, 1992) and suggests that proteins with repeat sequences containing glycine may also be components of the organic matrix in these biomineral systems. However, little information is available on the amino acid sequences of proteins extracted from the organic matrices of brachiopods. Brown (1998) determined the N-terminal sequence of a 44kDa protein from the shell of *N. anomala*, which has been confirmed by this study (Section 4.3.6).

4.4.2 Organic Matrix Carbohydrate

When separated by SDS-PAGE, intracrystalline proteins extracted from the organic matrix stain in Coomassie Brilliant Blue and silver stain (Section 4.3.2). However, these protein bands do not stain in Acridine Orange (Section 4.3.4). Dauphin *et al.*, (2003a) suggest that the Acridine Orange staining technique is sensitive to acidic sulphated sugars such as chondroitin sulphate, which stains easily with acridine orange, while proteins such as bovine serum albumin do not stain with Acridine Orange.

The intracrystalline extracts from the *T. retusa*, *N. anomala*, *M. edulis* and *G. gallus* all stain in Acridine Orange indicating the presence of acidic sulphated sugars. The sulphated acidic sugar, chondroitin sulphate is associated with the soluble organic matrices of the bivalve molluscs *Pinna* and *Pinctada* (Dauphin *et al.*, 2003a and Dauphin, 2003). Glycosaminoglycans such as dermatan sulphate and chondroitin sulphate have also been identified in the organic matrix of the eggshell (Nys *et al.*, 1999 and Arias *et al.*, 1992), while Arias *et al.*, (2002) presented evidence of the effect of glycosaminoglycan concentration on the nucleation and morphology of calcite crystals *in vitro*. The presence of acidic sulphated sugars in the soluble organic matrices extracted from *T. retusa*, *N. anomala*, *M. edulis* and *G. gallus* suggests that these macromolecules may have an important role in biomineralisation which is not yet completely understood.

Electron microprobe analysis of minor elements does not determine the phase in which the element is present. EPMA of the minor element concentration of *T. retusa* (Section 3.3.1.2) indicates that sulphur displays a positive covariation with magnesium, strontium and sodium. The intercrystalline and intracrystalline organic matrix of *T. retusa* and the intracrystalline organic matrix extracts of *N. anomala*, *M. edulis* and the avian eggshell all

stain in Acridine Orange indicating the presence of acidic sugars with associated sulphate (SO_4), (Dauphin *et al.*, 2003a). This suggests that a proportion of the sulphur analysed by electron microprobe may be associated with the organic matrix. The correlation between sulphur and magnesium, strontium and sodium suggests that some of these elements may be associated with the organic phase as well as the mineral phase. In the case of *N. anomala* minor element analyses indicate that sulphur does not correlate with other elements suggesting that, in *N. anomala* the minor elements are not associated with the organic matrix. Sulphur correlates with strontium and sodium in the calcite layer of *M. edulis* but does not correlate with magnesium. The differences in correlation between sulphur and other minor elements between the four biominerals may be the result of differences in the composition and structure of the organic matrix macromolecules. The exact location of these ions within the biomineral cannot be confirmed however, and more work is needed to establish if minor elements are associated with the mineral or organic phase in these biomineral systems.

4.4.3 Influence of intracrystalline proteins on crystal growth

Organic matrix proteins extracted from biomineral systems have been found to influence the nucleation, morphology and polymorph of calcium carbonate crystals *in vitro* (Wheeler *et al.*, 1988, Weiss *et al.*, 2000, Gautron *et al.*, 1996, Belcher *et al.*, 1996 and Falini *et al.*, 1996).

In this case the addition of intracrystalline extract from *N. anomala* and *M. edulis* to a saturated calcium carbonate solution inhibited the growth of calcite *in vitro*. The addition of intracrystalline extract from *T. retusa* did not inhibit calcite growth. Laing (1998) found that as the concentration of *T. retusa* protein extract added to the calcite crystal growth solution increased the number of calcite crystals formed decreased. In this case the concentration of *T. retusa* protein added to the crystal growth solution was low in comparison to the concentration of protein in extracts of *N. anomala*, *M. edulis* and *M. edulis* extrapallial fluid. At higher concentrations the addition of *T. retusa* soluble organic matrix may inhibit calcite formation.

The addition of soluble organic matrix proteins from molluscs also induces crystal nucleation (Roque *et al.*, 2004 and Weiss *et al.*, 2000). The addition of *M. edulis* acidic organic matrix proteins induced the nucleation of calcite and vaterite crystals *in vitro* (Roque *et al.*, 2004). In this case the product of the addition of *M. edulis* soluble matrix

proteins to a calcium carbonate growth solution was amorphous. It should be noted however that the difference in results between *in vitro* crystallisation experiments might in part be due to the different methods used for calcium carbonate crystallisation *in vitro*.

The addition of intracrystalline organic matrix from each system and extrapallial fluid from *M. edulis* also influenced crystal morphology (Figure 4.18). The morphology of crystals grown in the presence of protein extracts from each system varied. In the presence of *T. retusa* intracrystalline protein, crystals were present as clusters and displayed pitted surfaces. The addition of protein extracted from *N. anomala* produced small crystals that displayed secondary growth on the surface. With the addition of *M. edulis* organic matrix the crystals were amorphous while the extrapallial fluid extract produced crystal clusters. The addition of eggshell intracrystalline proteins produced smaller crystals with a layered structure. Due to the low quantity of protein available these experiments are preliminary and should be replicated to confirm the results.

Chapter 5 Discussion and Further Work

5.1 Aims of the Study

This study aimed to consider the extent to which calcium carbonate biominerals that are distinct in appearance are of similar composition. The minor element and organic matrix composition, in particular the protein component of the shells, of three marine invertebrates and an avian eggshell have been characterised in order to compare their components. The biomineral systems include an articulated brachiopod *Terebratulina retusa*, an inarticulated brachiopod *Novocrania anomala*, and the bivalve mollusc *Mytilus edulis*, and a fourth outlying system, the eggshell of the domestic fowl, *Gallus gallus*. Together they comprise a range of ultrastructures and two types of calcium carbonate polymorph: calcite and aragonite. *G. gallus* is formed under very different environmental conditions than the marine biominerals.

The following chapter summarises the main findings of this study and discusses the biomineral components and mineralisation processes involved in the formation of each system. For detailed results and discussion on individual topics the reader is referred to the appropriate chapter. Chapter 3 outlines the distribution of minor elements within the context of the ultrastructure and polymorph type of the mineral phase. Chapter 4 details the molecular weight, charge and amino acid composition of intercrystalline and intracrystalline proteins extracted from the four systems. The carbohydrate content of the organic matrix and its role in the biomineralisation process is also discussed in Chapter 4.

5.2 The Four Biomineral Systems

The brachiopods, *T. retusa* and *N. anomala* were collected from the same location at a depth of 200m in the Firth of Lorne off the coast of Oban, NW Scotland. Specimens of *T. retusa* and *N. anomala* have developed under the same environmental conditions i.e. water temperature and salinity, throughout ontogeny. The bivalve *M. edulis* although also taken from a marine environment is likely to have been subjected to different environmental conditions to the two brachiopods as it is found in shallower water in which there are greater fluctuations in temperature and salinity. In contrast to the

marine systems the eggshell is formed rapidly i.e. approximately 3g of calcite is deposited within 24 hours, in a controlled constant temperature environment.

5.2.1 Mineral Ultrastructure and Polymorph Type

The shell of *T. retusa* consists of an outer primary layer composed of acicular calcite with a thicker underlying secondary layer of calcite fibres (Figure 3.1). The shell of *N. anomala* also comprises two layers; a thin primary layer of acicular calcite and a secondary layer composed of calcite semi-nacre (Figure 3.12). *Mytilus edulis* shell is composed of two calcium carbonate polymorphs, calcite and aragonite. The outer layer of the shell is prismatic calcite while the inner layer is composed of aragonite nacre (Figure 3.23). The calcite eggshell of the domestic fowl comprises six regions (Figure 3.33). The inner shell is lined with an organic membrane upon which initial crystal nucleation takes place forming the mammillary caps. The mammillary caps eventually fuse and are overlain by the palisade layer and the vertical crystal layer, which comprises calcite columns aligned perpendicular to the palisade layer. The outer cuticle is composed of organic material and hydroxyapatite crystals (Dennis *et al.*, 1996).

5.3 Minor Element Concentration and Distribution in Relation to Mineral Ultrastructure

In Chapter 3, the distribution of the minor elements, magnesium, sulphur, sodium, strontium and in some instances, phosphorus is discussed in context of the mineral ultrastructure. Any relationships between crystal ultrastructure and minor element composition can therefore be determined.

Mg/Ca ratio in the shells of marine invertebrates has mainly been of interest due to its potential as a palaeoseawater thermometer (Watannabe *et al.*, 2000, Lear *et al.*, 2002, Lear *et al.*, 2000). Analysis of shell chemistry may also provide clues as to the processes involved in biomineralisation (Lowenstam and Weiner, 1989). In the four systems discussed here, magnesium is present at different concentrations and displays a variety of distribution patterns. *T. retusa* and *N. anomala* were collected from the same location, yet *T. retusa* produces a low magnesium calcite shell, (Section 3.3.1.2) while *N. anomala* produces a high magnesium calcite shell, (Section 3.3.2.2). This suggests that differences in magnesium concentration between the two brachiopods reflect

biological rather than environmental factors. In the shell of *T. retusa*, the greatest concentration of magnesium is found in the primary layer and decreases across the primary/secondary layer boundary (Figure 3.6). Within the secondary layer there is also a decrease in magnesium concentration from the outer to the inner part of the secondary layer (Figure 3.6b). In *N. anomala*, magnesium concentrations across both the primary and secondary layers of the shell are relatively invariant and there is no significant difference in overall magnesium concentrations between the primary and secondary layers (Figure 3.17 and Table 3.4). The patterns of magnesium distribution in *T. retusa* and *N. anomala* therefore show that ultrastructure is not the main determinant of variations in shell chemistry in these brachiopods. In *M. edulis*, concentrations of magnesium in each layer are determined by the calcium carbonate polymorph present. Owing to similarities in ionic size and charge, Mg^{2+} can substitute for Ca^{2+} in the calcite lattice. However, it substitutes less readily for Ca^{2+} in the more open orthorhombic lattice of aragonite. Therefore, magnesium concentration is consistently higher in the calcite than aragonite layer of *M. edulis*. There is variation in magnesium distribution within the calcite layer of *M. edulis* and the distribution pattern can vary between individuals (Figure 3.29). Magnesium concentration in the eggshell changes as the ultrastructure changes. The eggshell displays a high concentration of magnesium in the mammillary caps, which are formed at the start of lay but decreases across the zone in which the mammillary caps fuse and then increases gradually through the palisade layer and vertical crystal layer to the cuticle. However the abrupt change from the palisade layer to the vertical crystal layer is not apparent in magnesium concentration, which changes gradually from the inner to the outer shell surface.

It has been suggested that incorporation of Mg^{2+} into calcite is related to growth rate (Major and Wilber, 1991, Burton and Walter, 1987). At slow growth rates the mineral system has time to equilibrate and thus discriminate against ions such as Mg^{2+} . In contrast fast growth rates result in a higher rate of substitution of Mg^{2+} for Ca^{2+} . The results of this study suggest that, although this may apply to some biotic systems (Buenning and Carlson, 1992), it does not apply to others. The primary layer of *T. retusa* is formed quickly and has a higher concentration of magnesium than the secondary layer. The overall concentration of magnesium decreases from the primary layer through the secondary layer to the inner surface of the *T. retusa* shell in correspondence with a decline in growth rate throughout ontogeny (Curry, 1982). This supports the suggestion that growth rate influences the concentration and distribution of

magnesium. If a physical process such as precipitation rate is the principal influence on the concentration of magnesium in calcite it might be expected that it would influence magnesium concentration in all calcite biomineral systems. However, *N. anomala* is a slow growing brachiopod with a shell composed of high magnesium calcite (Ruggiero, 2001). While the bivalve *M. edulis* secretes its shell faster than the brachiopod *T. retusa* it has a lower concentration of magnesium in the calcite layer of the shell than that found within the shell of *T. retusa*. In the case of the eggshell, growth rate may have an influence on the uptake of magnesium but further work is required to determine the precipitation rate of the calcite during various stages of eggshell formation.

Temperature may also exert a control over the Mg/Ca and Sr/Ca values of calcium carbonate (Rosenthal *et al.*, 1997, Lea *et al.*, 1999, Beck *et al.*, 1992). There is an exponential relationship between seawater temperature and the concentration of magnesium in the skeletons of marine invertebrates including benthic foraminifera (Rosenthal *et al.*, 1997, Nurnberg *et al.*, 1997 and Lea *et al.*, 1999), while an exponential relationship has also been found in some species of recent articulated brachiopod (Lowenstam, 1961, Lowenstam and Weiner, 1989). The relationship between strontium concentration and seawater temperature in the shells of articulated and inarticulated brachiopods differed. In articulated brachiopods strontium is positively correlated with temperature, whereas the shells of inarticulated brachiopods (Craniidae) show a negative correlation (Lowenstam and Weiner, 1989). A negative correlation between Sr/Ca and temperature is also found in aragonite coral skeletons (Beck *et al.*, 1992).

Samples of *T. retusa* and *N. anomala* studied here grew in the same environment but have significantly different concentrations of magnesium within their shells. Therefore, temperature cannot be the main control on magnesium incorporation into the calcite shells of these brachiopods. Temperature is also not the primary control on magnesium incorporation in the avian eggshell. The eggshell is formed in a constant temperature environment yet has a range of Mg concentrations. Even though results of this study demonstrate temperature is not the principal control on magnesium incorporation in the four systems studied, the role of temperature in determining the uptake of magnesium into marine calcite biominerals cannot be dismissed. Finer resolution analyses combined with detailed environmental data would be needed to determine if there is an underlying correlation between temperature and magnesium/strontium concentration.

Spatial variations in minor and trace element concentration of the shell of *M. edulis* have been related to spatial variation in metabolic activity of the mantle (Rosenberg *et al.* 1991). Areas of the shell that are rich in minor elements and organic matrix are metabolically expensive to produce and are therefore linked to the areas of the mantle that have a high metabolic activity (Rosenberg *et al.*, 1991). Although this hypothesis cannot be confirmed by results of this study, the impact of metabolic activity on shell chemistry should not be ignored. The marginal mantle of *T. transversa*, which produces the primary and upper secondary layers of the shell, has a higher metabolic activity than the posterior mantle which produces the lower secondary layer (Rosenberg *et al.* 1988 and Auclair *et al.* 2003). If these variations in mantle metabolic activity are also present in *T. retusa* then areas of the shell that are relatively rich in minor elements i.e. the primary and upper secondary layers are secreted by mantle with a high metabolic activity. Differences in the physiology and biomineralisation mechanisms of molluscs and brachiopods make it difficult to make comparisons between the two phyla. More work is required on the metabolism of brachiopods and its role in determining shell composition and development.

If extant marine invertebrates are passive in relation to the uptake of elements from seawater, it would be expected that they will produce high magnesium calcite skeletons reflecting present high marine Mg/Ca values (Stanley *et al.*, 2002 and Hardie, 1996). Stanley *et al.*, (2002) suggest that this is indeed the case for simple organisms such as algae in which the composition of the biomineral appears to change with variations in solution composition. Therefore, modern marine invertebrates that produce low magnesium calcite skeletons such as *M. edulis* must employ physiological mechanisms for the exclusion of magnesium (Lorens and Bender, 1977 and Nurnberg *et al.* 1996). However, the brachiopod *N. anomala* produces a high magnesium calcite skeleton. Lowenstam and Weiner (1989) found that the trace element content of the shells of inarticulated brachiopods (Craniidae) is in equilibrium with the seawater. As this is not the case for the trace element content of articulated brachiopod shells it suggests that inarticulated brachiopods such as *N. anomala* do not have the same physiological mechanisms in place to exclude magnesium from their tissues.

Variations in chemistry across the shell of *G. gallus* (Section 3.3.4.2) may simply be related to changes in the composition of the uterine fluid from which the shell precipitates. The pattern of magnesium, sodium, potassium and phosphorus

concentration throughout the eggshell appears to correlate with the concentration of these elements in the uterine fluid as reported by Arad *et al.*, (1989) and Nys *et al.*, (1991 and 1999), (Section 3.4.3).

The influence of magnesium ions on the morphology of carbonate crystals (Meldrum and Hyde, 2001 and Loste *et al.*, 2003), and the effect of magnesium on calcite precipitation rate have been established (Hincke and St. Maurice, 1998). Hincke and St. Maurice (1998) found that the addition of magnesium to a calcium carbonate crystal growth solution accelerated the onset of calcite precipitation but inhibited the maximum rate of precipitation with respect to the control experiment. The addition of phosphate ions also inhibited the maximum rate of calcite precipitation. If the chemical composition of the eggshell is related to the composition of the uterine fluid then changes in ionic composition of the uterine fluid during lay may be a fundamental mechanism for controlling calcite precipitation rates and crystal morphologies of *G. gallus* shells.

There are good correlations between the concentrations of certain chemical elements within the four systems. In *T. retusa* and the calcite layer of *M. edulis*, strontium displays a positive correlation with sodium (Figure 3.8 and Figure 3.30). Determining the location of Na^+ within the calcite lattice is difficult as sodium is monovalent and therefore not expected to substitute for Ca^{2+} . It is possible that Na^+ sits in interstitial spaces in the lattice. If this is the case, the substitution of the larger Sr^{2+} ion for Ca^{2+} in the calcite lattice may result in lattice defects due to the differences in ionic size into which Na^+ can be accommodated. In the calcite layer of *M. edulis*, strontium and sodium both correlate positively with sulphur, while magnesium, strontium and sodium display a positive correlation with sulphur in the shell of *T. retusa*. If sulphur is associated with the organic matrix, as has been found in molluscs such as *Pinna* and *Pinctada* (Dauphin *et al.*, 2003a), then the correlation between sulphur and other elements suggests that these elements are also associated with the organic matrix in both *T. retusa* and *M. edulis* (Section 3.4.1 and Section 3.4.2).

There are no good correlations between elements in the shell of *N. anomala* (Figure 3.18). As sulphur does not correlate with any of the other elements this suggests that elements are not associated with the organic matrix and are accommodated within the lattice. The difference in lattice structure of high magnesium calcite and low

magnesium calcite may also explain some differences in element concentration between *N. anomala* and *T. retusa*. However, the principal differences in element concentration between the two brachiopods probably relate to differences in physiology (Section 3.4.1).

5.4 Minor Element Distribution in Relation to the Distribution of Organic Matrix

Sulphur is a good measure of the distribution of organic matrix within calcium carbonate biominerals (Dauphin *et al.*, 2003a, Lorens and Bender, 1980). In the shell of *T. retusa*, sodium, strontium and magnesium all correlate positively with sulphur, while in the calcite layer of *M. edulis* sodium and strontium positively correlate with sulphur. However, this trend is not evident in the high Mg-calcite shell of *N. anomala*.

Sulphur is present in the shells of the molluscs *Pinna* and *Pinctada* predominantly as sulphate associated with the organic matrices (Dauphin *et al.*, 2003a). Lorens and Bender (1980) and Vander Putten *et al.*, (2000) suggest that sulphur may be associated with the organic matrix of *M. edulis*. Organic matrices extracted from *T. retusa*, *N. anomala*, *M. edulis* and *G. gallus* all stain with Acridine Orange, which indicates the presence of acidic sulphated sugars (Dauphin *et al.*, 2003a). In each system sulphur is associated with the organic component of the shell (Section 4.3.4), therefore correlation between sulphur and other elements may indicate that these elements are also associated with the organic matrix.

Magnesium and sodium may be present in the aragonite skeleton as MgSO_4 and NaSO_4^- and are not associated with the organic matrix in significant concentrations (Mitsuguchi *et al.*, 2001). The association of magnesium and sodium with SO_4 in the mineral phase in the shells of *T. retusa* and *M. edulis* cannot be dismissed.

5.5 Organic Matrix Composition

The organic matrix of *T. retusa*, *N. anomala*, *M. edulis* and the avian eggshell, all contain small, acidic proteins as confirmed by gel electrophoresis (Section 4.3.2) and isoelectric focusing (Figure 4.7). The presence of acidic proteins in the soluble organic matrix is a common factor in calcium carbonate biominerals. These acidic proteins may

have a calcium-binding function in the biomineralisation process (Weiner *et al.* 1983, Weiner and Hood, 1975, Weiner and Traub, 1984). The role of these acidic matrix components in controlling the nucleation, morphology and crystal structure of the mineral has also been confirmed by *in vitro* studies (Albeck *et al.*, 1993, Belcher *et al.* 1996, Greenfield and Crenshaw, 1989, Falini *et al.* 1996, Feng *et al.* 2000). The soluble organic matrix of the marine invertebrates *T. retusa*, *N. anomala* and *M. edulis* are all acidic as confirmed by isoelectric focusing (Section 4.3.3), while the organic matrix of the marine invertebrates is enriched in aspartic acid with respect to the eggshell which has a higher content of glutamic acid. Even though the organic matrix macromolecules display some similarities i.e. they are all acidic, they show some differences in terms of their overall amino acid composition. The three marine invertebrates are enriched in aspartic acid with respect to the eggshell which has a higher concentration of glutamic acid while *M. edulis* is enriched in alanine with respect to the other three systems. However, all four systems have a high glycine content. Fernandez *et al.*, (2004) noted that there are insufficient similarities between the amino acid sequences of eggshells and seashells to indicate that they have common mechanisms for regulating crystal growth.

The carbohydrate component of the organic matrix may also have an important role in biomineralisation. The organic matrix of *T. retusa*, *N. anomala*, *M. edulis* and *G. gallus* all contain sulphated sugars (Section 4.3.4). Glycosaminoglycans have also been found in the organic matrices of the molluscs, *Pinna* and *Pinctada* (Dauphin *et al.* 2003a) and the avian eggshell (Nys *et al.*, 1999). The common occurrence of sulphated sugars such as chondroitin sulphate and dermatan sulphate in the organic matrices of calcium carbonate biominerals suggests that these macromolecules may be involved in the biomineralisation process.

5.6 Calcium Carbonate Biomineralisation in Disparate Systems- Common Mechanisms?

The four calcium carbonate biomineral systems differ in appearance, ultrastructure and in some cases crystal structure i.e. *M. edulis*. The minor element composition of the shells of *T. retusa*, *N. anomala*, *M. edulis* and *G. gallus* do not clearly correspond with differences in ultrastructure. Contrasts in minor element composition between the two brachiopods are possibly to be related to differences in physiology. In particular, the fact that *T. retusa* has a low magnesium calcite shell while *N. anomala* has a high

magnesium calcite shell suggests that *N. anomala* lacks the ability to exclude magnesium from its tissues, a physiological mechanism that is prevalent in organisms which secrete low magnesium calcite skeletons in present day aragonite seas. In *M. edulis* crystal structure is the principal determinant of the distribution of minor elements. Metabolic processes and fluctuations in environmental conditions (i.e. temperature and salinity) may also influence the chemical composition of the shell (Rosenberg and Hughes, 1991 and Vander Putten *et al.*, 2000). The incorporation of minor elements into the shell of *G. gallus* is similar to that of *N. anomala* in being related to the passive uptake of elements from the mineralising medium. However in the case of *G. gallus*, the ionic composition of the uterine fluid is regulated, which suggests that ions such as Mg^{2+} and P^+ may have an active role in the growth and development of the shell. It is also possible that elements such as magnesium are associated with the organic matrix in some biomineral system, for example *T. retusa* and *M. edulis*. Differences in the structure and composition of the matrix macromolecules may therefore be reflected in the association of these elements with sulphur (i.e. sulphated macromolecules in the organic matrix). In conclusion, the results of this study suggest that there may be similarities between some calcium carbonate biomineral systems such as metabolic influence on shell chemistry and the ability to control the ionic composition of the mineralising medium, but there is not an underlying mechanism that controls the inorganic shell chemistry in all four systems.

The proteins extracted from the shells of *T. retusa*, *N. anomala*, *M. edulis* and *G. gallus* are small (Section 4.3.2) and all are acidic (Section 4.3.3). The amino acid compositions of the four systems display similarities and differences (e.g. all have a high glycine content), while the eggshell differs from the shells of *T. retusa*, *N. anomala* and *M. edulis* in that glutamic acid is present in higher concentration than aspartic acid.

All four systems contain sulphated sugars (Section 4.3.4). Arias and Fernandez (2003) and Dauphin *et al.*, (2003) also recognised a common occurrence of sulphated macromolecules (proteoglycans) in the eggshell and marine invertebrate shells, which suggests that these macromolecules may have an important role in the formation of calcium carbonate biominerals.

The organic components of the shells of *T. retusa*, *N. anomala*, *M. edulis* and *G. gallus* display some superficial biochemical similarities which suggest that there are common

underlying mechanisms involved in the interaction of the organic matrix with the biomineral, however in detail the protein profiles from each system are ultimately different.

5.7 Suggestions for Further Work


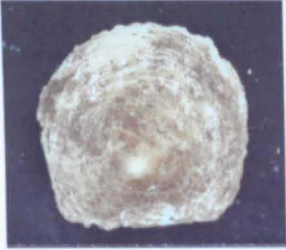


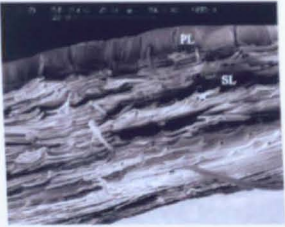
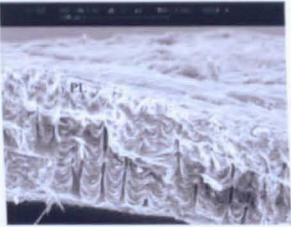

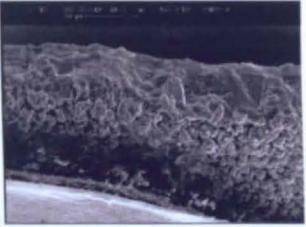
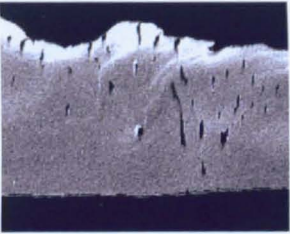
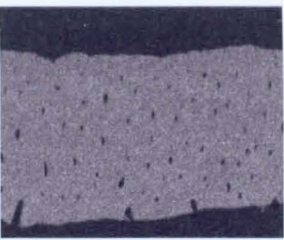
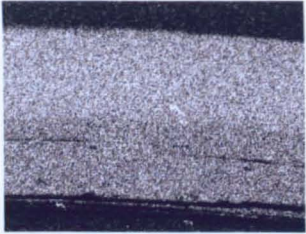
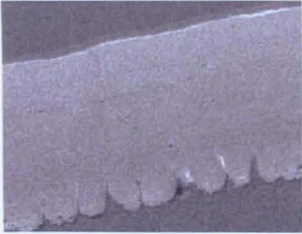
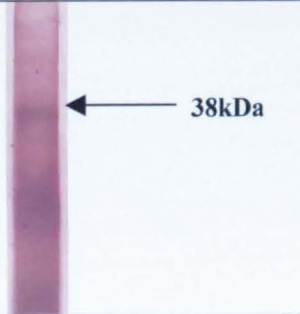
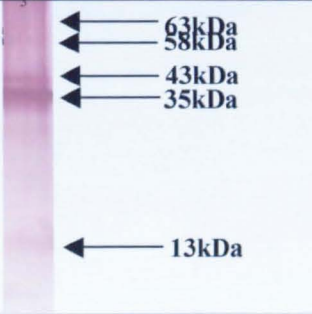
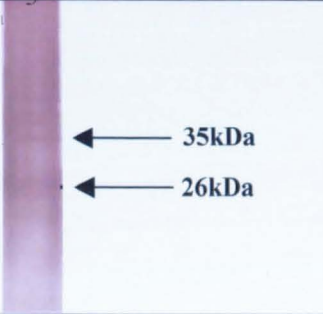
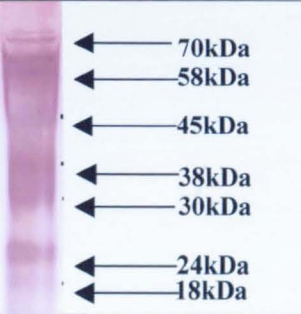
Future work on the minor and trace element composition of these four systems should aim to determine whether individual elements are coordinated with the organic matrix or are present within the mineral lattice. Detailed analyses of the shell crystal structure using Electron Backscatter Diffraction (EBSD) together with high-resolution chemical maps produced by Scanning X-ray Microscopy (XANES) may shed light on this problem. In the case of the marine systems trace element data might also be correlated with environmental conditions e.g. temperature and salinity in order to determine the effect of environmental variations on the uptake of elements into the shells. Electron microprobe analyses of the *G. gallus* eggshell indicate that variations in the minor and trace element composition of the shell may be related to changes in uterine fluid composition. Detailed work should therefore be undertaken to establish if shell chemistry is primarily a function of the composition of the uterine fluid.

Cathodoluminescence spectroscopy is a new technique for the study of biominerals. Further development of this method could provide a powerful tool for the analysis of carbonate biomineral composition. In particular, correlation of the wavelengths of luminescence emitted in relation to the distribution of elements within a system would provide a method for detailed chemical analysis.

Little work has been undertaken on the amino sequence of proteins within the organic matrix of brachiopods. This has hindered attempts to determine whether these proteins display homology with other biomineralisation proteins. An attempt should be made therefore to determine the amino acid sequences of these proteins. This may also be of use in evolutionary studies.

Detailed crystal growth experiments with the addition of proteins extracted from the four systems should be undertaken with the addition of different protein concentrations.

Figure 5.1 Summary Diagram

	<i>Terebratulina retusa</i>	<i>Novocrania anomala</i>	<i>Mytilus edulis</i>	<i>Gallus gallus</i>	Characteristics
Common Mechanisms?					Four calcium carbonate biominerals. Different in appearance, ultrastructure and crystal structure- common chemical and biochemical characteristics?
Ultrastructure					Variety of Ultrastructures
Minor Elements (Mg)					No characteristics common to all systems. Different element distributions
Intracrystalline Proteins					Some characteristics common to all systems. Small acidic proteins. All contain sulphated sugars

References

- Addadi, L., Moradian, J., Shay, E., Maroudas, N.G. & Weiner, S. 1987 A chemical model for the cooperation of sulfates and carboxylates in calcite crystal nucleation: relevance to biomineralization. *Proceedings of the National Academy of Science USA* **84**, 2372-2736
- Aizenberg, J., Lambert, G., Weiner, S. & Addadi, L. 2002 Factors involved in the formation of amorphous and crystalline calcium carbonate: A study of an Ascidian skeleton. *Journal of the American Chemical Society* **124** (1), 32-39
- Ameye, L., De Becker, G., Killan, C., Wilt, F., Kemps, R., Kuypers, S. & Dubois P. 2001 Proteins and saccharides of the sea urchin organic matrix of mineralization: Characterization and localization in the spine skeleton. *Journal of Structural Biology* **134**, 56-66
- Arad, Z., Eylath, U., Ginsburg, M., Eyal-Giladi, H. 1989 Changes in uterine fluid composition and acid-base status during shell formation in the chicken. *American Journal of Physiology* **257**, R732-737.
- Arias, J.L., Carrino, D.A., Fernandez, M.S., Rodriguez, J.P., Dennis, J.E. & Caplan, A.I. 1992 Partial biochemical and immunochemical characterization of avian eggshell extracellular matrices. *Archives of Biochemistry and Biophysics* **298**, 293-302
- Arias, J.L., Jure, C., Wiff, J.P., Fernandez, M.S., Fuenzalida, V. & Arias, J.L. 2002 Effect of sulfate content of biomacromolecules on the crystallization of calcium carbonate. *Materials Research Society Symposium Proceedings* **711**, 243-248
- Auclair, A-C., Joachimski, M.M. & Lecuyer, C. 2003 Deciphering kinetic, metabolic and environmental controls on stable isotope fractionations between seawater and the shell of *Terebratalia transversa* (Brachiopoda). *Chemical Geology* **202**, 59-78
- Barbin, V., Ramseyer, K., Debenay, J.P., Schein, E., Roux, M. & Decrouez, D. 1991 Cathodoluminescence of recent biogenic carbonates: an environmental and ontogenetic fingerprint. *Geological Magazine* **128**, 19-26

- Barbin, V. 1992 Fluctuation in shell composition in *Nautilus* (Cephalopoda, Mollusca): evidence from cathodoluminescence. *Lethaia* **25** (4), 391-400
- Barbin, V., Brand, U., Hewitt, R.A. & Ramseyer, K. 1995a Similarity in cephalopod shell biogeochemistry since carboniferous: Evidence from cathodoluminescence. *Geobios* **28**, 701-710
- Barbin, V. & Gaspard D. 1995b Cathodoluminescence of recent articulate brachiopod shells. Implications for growth stages and diagenesis evolution. *Geobios* **18**, 39-45
- Belcher, A.M., Wu, X.H., Christensen, R.J., Hansma, P.K., Stucky, G.D. & Morse, D.E. 1996 Control of crystal phase switching and orientation by soluble mollusc-shell proteins. *Nature* **381**, 56-58
- Bengtson, S. 1994 The advent of animal skeletons. In *Early Life on Earth, Nobel Symposium 84* (ed. Bengtson, S.) Columbia University Press, New York pp 421-425
- Beniash, E., Aizenberg, J., Addadi, L. & Weiner, S. 1997 Amorphous calcium carbonate transforms into calcite during sea urchin larval spicule growth. *Proceedings of the Royal Society of London* **264B**, 478-491
- Blackwelder, P.L., Weiss, R.E. & Wilbur, K.M. 1976 Effects of calcium, strontium and magnesium on the coccolithophorid *Cricosphaera* (*Hymenomonas*) *carterae*. I. Calcification. *Marine Biology* **34**, 11-16
- Brown, K.E. 1998 Biomineralisation of the calcitic-shelled, inarticulated brachiopod, *Neocrania anomala*. Unpublished PhD Thesis, University of Glasgow
- Budd, D.A., Hammes, U & Ward, W.B. 2000 Cathodoluminescence in calcite cements: New insights on Pb and Zn sensitising, Mn activation, and Fe quenching at low trace element concentrations. *Journal of Sedimentary Research* **70** (1), 217-226
- Buening, N. & Carlson, S.J. 1992 Geochemical investigation of growth in selected recent articulate brachiopods. *Lethaia* **25**, 331-345
- Burton, E.A. & Walter, L.M. 1987 Relative precipitation rates of aragonite and Mg calcite from seawater: Temperature or carbonate ion control? *Geology* **15**, 111-114

Busenberg, E. & Plummer, L.N. 1985 Kinetic and thermodynamic factors controlling the distribution of SO_4^{2-} and Na^+ in calcites and selected aragonites. *Geochimica et Cosmochimica Acta* **49**, 713-725

Cariolou, M.A. & Morse, D.E. 1988 Purification and characterisation of calcium-binding conchiolin shell peptides from the mollusc, *Haliotis rufescens*, as a function of development. *Journal of Comparative Physiology B* **157**, 717-729

Carpenter, S.J. & Lohmann, K.C. 1992 Sr/Mg ratios of modern marine calcite: Empirical indicators of ocean chemistry and precipitation rate. *Geochimica et Cosmochimica Acta* **56**, 1837-1849

Carrino, D.A., Rodriguez, J.P. & Caplan A.I. 1997 Dermatan sulfate proteoglycans from the mineralized matrix of the avian eggshell. *Connective Tissue Research* **36** (3), 175-193

Collins, M.J., Muyzer, G., Curry, G.B., Sandberg, P. & Westbroek, P. 1991 Macromolecules in brachiopod shells: characterization and diagenesis. *Lethaia* **24**, 387-397

Cortivo, R., Castellani, I., Martelli, M., Michellotto, G. & Abatangelo, G. 1982 Chemical characterization of the hen eggshell matrix: isolation of an alkali-resistant peptide. *Journal of Chromatography* **237**, 127-135

Crenshaw, M.A. 1972 The inorganic composition of molluscan extrapallial fluid. *Biological Bulletin* **143**, 505-512

Curry, G.B. 1982 Ecology and population structure of the recent brachiopod *Terebratulina* from Scotland. *Palaeontology* **25**, 227-246

Cusack, M., Curry, G.B., Clegg, H. & Abbott, H. 1992 An intracrystalline chromoprotein from red brachiopod shells: Implications for the process of biomineralisation. *Comparative Biochemistry and Physiology B* **102**, 93-95

Cusack, M., Laing, J.H., Brown, K. & Walton, D. 2000 Amino acids and proteins of calcitic brachiopod shells. *Trends in Comparative Biochemistry and Physiology* **6**, 47-56

Cusack, M. & Fraser, A.C. 2002 Eggshell membrane removal for subsequent extraction of intermineral and intramineral proteins. *Crystal Growth and Design* **2** (6), 529-532

- Cusack, M., Fraser, A.C. & Stachel, T. 2003 Magnesium and phosphorus distribution in the avian eggshell. *Comparative Biochemistry and Physiology B* **134**, 63-69
- de Leeuw, H.H. 2002 Molecular dynamics simulations of the growth inhibiting effect of Fe^{2+} , Mg^{2+} , Cd^{2+} and Sr^{2+} on calcite crystal growth. *Journal of Physical Chemistry B* **106**, 5241-5249
- Dauphin, Y. 2001 Comparative studies of skeletal soluble matrices from some Scleractinian corals and Molluscs. *International Journal of Biological Macromolecules* **28**, 293-304
- Dauphin, Y. 2003 Soluble organic matrices of the calcitic prismatic shell layers of two pteriomorphid bivalves. *The Journal of Biological Chemistry* **278** (17), 15168-15177
- Dauphin, Y., Cuif, J.P., Doucet, J., Salome, M., Susini, J. & Williams C.T. 2003a In situ chemical speciation of sulfur in calcitic biominerals and the simple prism concept. *Journal of Structural Biology* **142**, 272-280
- Dauphin, Y., Cuif, J.P., Doucet, J., Salome, M., Susini, J. & Williams, C.T. 2003b In situ mapping of the growth lines in the calcitic prismatic layers of mollusc shells using X-ray absorption near-edge structure (XANES) spectroscopy at the sulphur K-edge. *Marine Biology* **142**, 299-304
- Davis, K.J., Dove, P.M & De Yoreo, J.J. 2000 The role of Mg^{2+} as an impurity in calcite growth. *Science* **290**, 1134-1137
- Dennis, J.E., Xiao, S.Q., Agarwal, M., Fink, D.J., Heuer, A.H. & Caplan, A.I. 1996 Microstructure of the matrix and mineral components of eggshells from white Leghorn chickens (*Gallus gallus*). *Journal of Morphology* **228**, 287-306
- Dickson, J.A.D. 2002 Fossil echinoderms as monitor of the Mg/Ca of Phanerozoic oceans. *Science* **298**, 1222-1224
- Dodd, J.R. 1965 Environmental control of strontium and magnesium in *Mytilus*. *Geochimica et Cosmochimica Acta* **29**, 385-398

Dodd, J.R. 1967 Magnesium and strontium in calcareous skeletons: A review. *Journal of Palaeontology* **41** (6), 1313-1329

Eggins, S., Deckker, P.D. & Marshall, J. 2003 Mg/Ca variation in planktonic foraminifera tests: implications for reconstructing palaeo-seawater temperature and habitat migration. *Earth and Planetary Science Letters* **212**, 291-306

Elderfield, H., Bertram, C.J. & Eraz, J. 1996 A biomineralization model for the incorporation of trace elements into foraminiferal calcium carbonate. *Earth and Planetary Science Letters* **142**, 409-423

Elderfield, H. & Ganssen, G. 2000 Past temperature and $\delta^{18}\text{O}$ of surface ocean waters inferred from foraminiferal Mg/Ca ratios. *Nature* **405**, 442-445

Falini, G., Albeck, S., Weiner, S. & Addadi, L. 1996 Control of aragonite or calcite polymorphism by mollusc shell macromolecules. *Science* **271**, 67-69

Feng, Q.L., Cui, F.Z., Pu, G., Wang, R.Z. & Li, H.D. 2000a Crystal orientation, toughening mechanisms and a mimic of nacre. *Materials Science and Engineering* **11**, 19-25

Feng, Q.L., Pu, G., Pei, Y., Cui, F.Z., Li, H.D. & Kim, T.N. 2000b Polymorph and morphology of calcium carbonate crystals induced by proteins extracted from mollusk shell. *Journal of Crystal Growth* **216**, 459-465

Fernandez, M.S., Moya, A., Lopez, L. & Arias, J.L. 2001 Secretion pattern, ultrastructural localization and function of extracellular matrix molecules involved in eggshell formation. *Matrix Biology* **19**, 793-803

Fernandez, M.S., Passalacqua, K., Arias, J.I. & Arias, J.L. 2004 Partial biomimetic reconstitution of avian eggshell formation. *Journal of Structural Biology* **148**, 1-10

Fraser, A.C. 1996 Environmental and physiological factors influencing the eggshell of the domestic fowl. Unpublished PhD Thesis. University of Glasgow, pp 199

Friedman, G.M. 1993 Discussion of cathodoluminescence of recent biogenic carbonates: an environmental and ontogenetic fingerprint. *Geological Magazine* **130** (2), 269-270

- Gauron, J. 1994 Mineralisation de la coquille de l'oeuf dans l'uterus: Mise en evidence du role de la matiere organique. PhD Thesis.
- Gautron, J., Bain, M., Solomon, S. & Nys, Y. 1996 Soluble matrix of hen's eggshell extracts changes *in vitro* the rate of calcium carbonate precipitation and crystal morphology. *British Poultry Science* **37**, 853-866
- Gautron, J., Hincke, M.T., Dominguez-Vera, J., Garcia-Ruiz, J.M. & Nys, Y. 1997 Ovotransferrin and lysozyme are constituents of the hen eggshell matrix. In *Proceedings of the European Poultry Meat and Egg Quality Symposium* (eds. Kijoski, J. et al. Pikul, J., Poznan. pp. 172-181
- Gautron, J., Hincke, M. T., Mann, K., Panheleux, M., Bain, M., McKee, M.D. Solomon, S. E. & Nys Y. 2001 Ovocalyxin-32, a novel chicken eggshell matrix protein. *The Journal of Biological Chemistry* **276** (42), 39243-39252
- Given, R.K. & Wilkinson, B.H. 1985 Kinetic control of morphology. Composition, and mineralogy of abiotic sedimentary carbonates. *Journal of Sedimentary Petrology* **55** (1), 109-119
- Greenfield, E.M., Wilson, D.C. & Crenshaw, M.A. 1984 Ionotropic nucleation of calcium carbonate by molluscan matrix. *American Zoologist* **24**, 925-932
- Habermann, D. 2002 Quantitative cathodoluminescence (CL) spectroscopy of minerals: possibilities and limitations. *Mineralogy and Petrology* **76**, 247-259
- Habermann, D., Neuser, R.D. & Richter, D.K. 1998 Low limit of Mn^{2+} -activated cathodoluminescence of calcite: state of the art. *Sedimentary Geology* **116**, 13-24
- Habermann, D., Meijer, J., Richter, D.K., Rolfs, C. and Stephan, A. 1999 Micro-PIXE and quantitative cathodoluminescence spectroscopy: Combined high resolution trace element analyses in minerals. *Nuclear Instruments and Methods in Physics Research B* **150**, 470-477
- Hames, B.D. & Rickwood, D. 1990 *Gel electrophoresis of proteins: A practical approach*. Oxford University Press.

- Hammen, C.S. 1971 Metabolism of brachiopods and bivalve molluscs. *Acta del Simposio Internacional de Zoofilogenia, Salamanca*, 471-478
- Hardie, L.A. 1996 Secular variation in seawater chemistry: An explanation for the coupled secular variation in the mineralogies of marine limestones and potash evaporates over the past 600m.y. *Geology* **24** (3), 279-283
- Hare, P.E. 1963 Amino acids in the proteins from aragonite and calcite in the shells of *Mytilus californianus*. *Science* **139**, 216-217
- Hincke, M.T. 1995 Ovalbumin is a component of the chicken eggshell matrix. *Connective Tissue Research* **31**, 227-233
- Hincke, M.T., Tsang, C.P.W., Courtney, M., Hill, V. & Narbaitz, R. 1995 Purification and immunochemistry of a soluble matrix protein of the chicken eggshell (Ovocleidin-17). *Calcified Tissue International* **56**, 578-583
- Hincke, M. T. & St. Maurice, M. 1998 Phosphorylation-dependant modulation of calcium carbonate precipitation by chicken eggshell matrix proteins. In *Chemistry and Biology of Mineralized Tissues. American Academy of Orthopaedic Surgeons, Proceedings of the Sixth International Conference* (eds. Goldberg, M., Boskey, A. & Robinson, C.)
- Hockett, D., Ingram, P. & LeFurgey A. 1997 Strontium and manganese uptake in the barnacle shell: Electron probe microanalysis imaging to attain fine temporal resolution of biomineralization activity. *Marine Environmental Research* **43** (3), 131-143
- Joep, M. 1965 Composition of brachiopod shell. *Treatise on Invertebrate Palaeontology Part H*. (ed. Moore, R. C.) H156
- Kawaguchi, T. & Watabe, N. 1993 The organic matrices of the shell of the American oyster *Crassostrea virginica* Gmelin. *Journal of Experimental Marine Biology and Ecology* **170**, 11-28
- Kitamura, M. 2002 Controlling factor of polymorphism in crystallisation process. *Journal of Crystal Growth* **237-239**, 2205-2214

Kitano, Y. 1962 Behaviour of various inorganic ions in the process of calcium carbonate separation from bicarbonate separation from bicarbonate solution. *Bulletin of the Chemical society of Japan* **35** (12), 1973-1980

Kitano, Y. & Hood, D. W. 1965 The influence of organic material on the polymorphic crystallization of calcium carbonate. *Geochimica et Cosmochimica Acta* **39**, 29-41

Klein, R. T., Lohmann, K. C. & Thayer, C. W. 1996 Sr/Ca and $^{13}\text{C}/^{12}\text{C}$ ratios in skeletal calcite of *Mytilus trossulus*: Covariation with metabolic rate, salinity, and carbon isotopic composition of seawater. *Geochimica et Cosmochimica Acta* **60** (21), 4207-4221

Knoll, A. H. 2003 Biomineralization and evolutionary history. In *Biomineralization, Reviews in Mineralogy and Geochemistry Volume 54* (eds. Dove, P. M., De Yoreo, J. J. and Weiner, S.)

Kono, M. Hayashi, N. & Samata, T. 2000 Molecular mechanism of the nacreous layer formation in *Pinctada maxima*. *Biochemical and Biophysical Research Communications* **269**, 213-218

Laing, J. H. 1999 Intracrystalline macromolecules from the shell of the articulated brachiopod, *Terebratulina retusa* (Linnaeus). Unpublished PhD Thesis, University of Derby

Lea, D., Mashiotto, T.A. & Spero, H. J. 1999 Controls on magnesium and strontium uptake in planktonic foraminifera determined by live culturing. *Geochimica et Cosmochimica Acta* **63** (16), 2369-2379

Lear, C. H., Elderfield, H. & Wilson, P. A. 2000 Cenozoic deep-sea temperatures and global ice volumes from Mg/Ca in benthic foraminiferal calcite. *Science* **287**, 269-272

Lear, C. H., Rosenthal, Y. and Slowey, N. 2002 Benthic foraminiferal Mg/Ca-palaeothermometry: A revised core-top calibration. *Geochimica et Cosmochimica Acta* **19**, 3375-3387

Lee, X., Hu, R., Brand, U., Zhou, H., Liu, X., Yuan, H., Yan, C. & Cheng, H. 2004 Ontogenetic trace element distribution in brachiopod shells: an indicator of original seawater chemistry. *Chemical Geology* **209**, 49-65

- Levi, Y., Albeck, S., Brack, A., Weiner, S. & Addadi, L. 1998 Control over aragonite crystal nucleation and growth: An in vitro study of biomineralization. *European Journal of Chemistry* **4** (3), 389-396
- Levi-Kalishman, Y., Falini, G., Addadi, L. & Weiner, S. 2001 Structure of the nacreous organic matrix of a bivalve mollusk shell examined in the hydrated state using cryo-TEM. *Journal of Structural Biology* **135**, 8-17
- Lorens, R. B. & Bender, M. L. 1977 Physiological exclusion of magnesium from *Mytilus edulis* calcite. *Nature* **269**, 793-794
- Lorens, R. B. & Bender, M. L. 1980 The impact of solution chemistry on *Mytilus edulis* calcite and aragonite. *Geochimica et Cosmochimica Acta* **44**, 1265-1278
- Lorens, R. B. 1981 Sr, Cd, Mn and Co distribution coefficients in calcite as a function of calcite precipitation rate. *Geochimica et Cosmochimica Acta* **45**, 553-561
- Loste, E., Wilson, R. M., Seshadri, R. & Meldrum, F. C. The role of magnesium in stabilising amorphous calcium carbonate and controlling calcite morphologies. *Journal of Crystal Growth* **254**, 206-218
- Lowenstam, H. A. 1961 Mineralogy, O^{18}/O^{16} ratios, and strontium and magnesium contents of recent and fossil brachiopods and their bearing on the history of the oceans. *The Journal of Geology* **69** (3), 241-260
- Lowenstam, H. A. & Weiner, S. 1989 *On Biomineralization*. New York, Oxford University Press
- Magdams, U. and Gies, H. 2004 Single crystal structure analysis of sea urchin spine calcites: Systematic investigations of the Ca/Mg distribution as a function of habitat of the sea urchin and the sample location in the spine. *European Journal of Mineralogy* **16**, 261-268
- Major, R. P. and Wilber R. J. 1991 Crystal habit, geochemistry, and cathodoluminescence of magnesian calcite marine cements from the lower slope of Little Bahama Bank. *Geological Society of America Bulletin* **103**, 461-471

- Mann, K., Hincke, M.T. & Nys, Y. 2002 Isolation of ovocleidin-116 from chicken eggshells, correction of its amino acid sequence and identification of disulfide bonds and glycosylated Asn. *Matrix Biology* **21**, 383-387
- Mann, S. 1988 Molecular recognition in biomineralization. *Nature* **332**, 119-124
- Mann, S. 1990 Crystal engineering: the natural way *New Scientist*, 42-47
- Mann, S. 2001 *Biomineralization: Principles and concepts in bioinorganic materials chemistry*. Oxford University Press
- Mann, K., Hincke, M. T. & Nys, Y. 2002 Isolation of ovocleidin-116 from chicken eggshells, correction of its amino acid sequence and identification of disulfide bonds and glycosylated Asn. *Matrix Biology* **21**, 383-387
- Marin, F., Smith, M., Isa, Y., Muyzer, G. & Westbroek, P. 1996 Skeletal matrices, muci, and the origin of invertebrate calcification. *Proceedings of the National Academy of Sciences USA* **93**, 1554-1559
- Marin, F., Corstjen, P., de Gaulejac, B., de Vrind-de Jong, E. & Westbroek, P. 2000 Mucins and molluscan calcification. *The Journal of Biological Chemistry* **275** (27), 20667-2075
- Marshall, D. J. 1988 Cathodoluminescence of geological materials. Unwin Hyman Inc. pp 146
- Martin, P. A., Lea, D. W., Rosenthal, Y., Shackleton, N. J., Sarnthein, M. & Papenfuss T. 2002 Quaternary deep sea temperature histories derived from benthic foraminiferal Mg/Ca. *Earth and Planetary Science Letters* **198**, 193-209
- Mason, R. A. & Mariano, A. N. 1990 Cathodoluminescence activation in manganese bearing and rare-earth bearing synthetic calcites. *Chemical Geology* **88**, 191-206
- Matsushiro, A., Miyashita, T., Miyamoto, H., Morimoto, K., Tonomura, B., Tanaka, A. & Sata, K. 2003 Presence of protein complex is a prerequisite for aragonite crystallization in the nacreous layer. *Marine Biotechnology* **5**, 37-44

- Meldrum, F. C. & Hyde, S. T. 2001 Morphological influence of magnesium and organic additives on the precipitation of calcite. *Journal of Crystal Growth* **231**, 544-558
- Mii, H-S. & Grossman, E. L. 1994 Late Pennsylvanian seasonality reflected in the ^{18}O and elemental composition of a brachiopod shell. *Geology* **22**, 661-664
- Mitterer, R. M. 1978 Amino acid composition and metal binding capability of the skeletal protein of corals. *Bulletin of Marine Science* **28** (1), 173-180
- Miyamoto, H., Miyashita, T., Okushima, M., Nakano, S., Morita, T. & Matsushiro, A. 1996 A carbonic anhydrase from the nacreous layer in oyster pearls. *Proceedings of the National Academy of Science* **93**, 9657-9660
- Miyamoto, H., Yano, M. & Miyashita, T. 2003 Similarities in the structure of nacrein, the shell-matrix protein, in a bivalve and a gastropod. *Journal of Molluscan Studies* **69**, 87-89
- Miyashita, T., Takagi, R., Okushima, M., Miyamoto, H., Nishikawa and Matsushiro, A. 2000 Complementary DNA cloning and characterization of Pearlin, a new class of matrix protein in the nacreous layer of oyster pearls. *Marine Biotechnology* **2**, 409-418
- Mucci, A. & Morse, J. W. 1983 The incorporation of Mg^{2+} and Sr^{2+} into calcite overgrowths: Influences of growth rate and solution composition. *Geochimica et Cosmochimica Acta* **47**, 217-233
- Nurnberg, D., Bijma, J. & Hemleben, C. 1996 Assessing the reliability of magnesium in foraminiferal calcite as a proxy for water mass temperatures. *Geochimica et Cosmochimica Acta* **60** (5), 803-814
- Nys, Y., Zawadzki, J., Gautron, J. & Mills, A. D. 1991 Whitening of brown-shelled eggs: Mineral composition of uterine fluid and rate of protoporphyrin deposition. *Poultry Science* **70**, 1236-1245
- Nys, Y., Hincke, M. T., Arias, J. L., Garcia-Ruiz, J. M. & Solomon, S. 1999 Avian eggshell mineralization. *Poultry and Avian Biology Reviews* **10** (3), 143-166
- Palmer, A. R. 1981 Do carbonate skeletons limit the rate of body growth? *Nature* **292**, 150-152

- Panheleux, M., Nys, Y., Williams, J., Gautron, J., Boldicke, T. & Hincke, M. T. 2000 Extraction and quantification by ELISA of eggshell organic matrix proteins (Ovocleidin-17, Ovalbumin, Ovotransferrin) in shell from young and old hens. *Poultry Science* **79**, 580-588
- Parkinson, D., Curry, G.B., Cusack, M. & Fallick, A.E. *in press* Shell structure patterns of oxygen and carbon stable isotopes in modern brachiopod shells. *Chemical Geology*
- Pierson, B. J. 1981 The control of cathodoluminescence in dolomite y iron and manganese. *Sedimentology* **28**, 01-610
- Pinnes, M., Knopov, V. & Bar, A. 1995 Involvement of osteopontin in eggshell formation in the laying chicken. *Matrix biology* **14**, 765-771
- Popp, B. N., Podosek, F. A., Brannon, J. C., Anderson, T. F & Pier, J. 1986 $^{87}\text{Sr}/^{86}\text{Sr}$ ratios in Permo-Carboniferous sea water from the analyses of well-preserved brachiopods. *Geochimica et Cosmochimica Acta* **50**, 1321-1328
- Rathburn, A. E. & De Deckker, P. 1997 Magnesium and strontium compositions of recent benthic foraminifera from the Coral Sea, Australia and Prydz Bay, Antarctica. *Marine Micropalaeontology* **32**, 231-248
- Reichert, G.-J., Jorissen, F., Anschutz, P. & Mason, P. R. D. 2003 Single foraminiferal test chemistry records the marine environment. *Geology* **31**, 355-358
- Richter, D. K. & Zinkernagel, U. 1981 Zur anwendung der kathodolumineszenz in der karbonatpetrographie. *Geologische Rundschau* **70**, 1276-1302
- Roque, J., Molera, J., Vendrall-Saz, M. & Salvado, N. 2004 Crystal size distributions of induced calcium carbonate crystals in polyaspartic acid and *Mytilus edulis* acidic organic proteins aqueous solutions. *Journal of Crystal Growth* **262**, 543-553
- Rosenberg, G. D., Hughes, W. W. & Tkachuck, R. D. 1988 Intermediary metabolism and shell growth in the brachiopod *Terebratalia transversa*. *Lethaia*, **21**, 219-230

Rosenberg, G. D. 1990 The "Vital Effect" on skeletal trace element content as exemplified by magnesium. In *Skeletal Biomineralization: Patterns, Processes and Evolutionary Trends Volume 1* (ed. Carter, J. G.) Van Nostrand Reinhold

Rosenberg, G. D. & Hughes, W. W. 1991 A metabolic model for the determination of shell composition in the bivalve mollusc, *Mytilus edulis*. *Lethaia* **24**, 83-96

Rosenthal, Y., Boyle, E. A. & Slowey, N. 1997 Temperature control on the incorporation of magnesium, strontium, fluorine, and cadmium into benthic foraminiferal shells from Little Bahama Bank: Prospects for thermocline palaeoceanography. *Geochimica et Cosmochimica Acta* **61** (17), 3633-3643

Ruggiero, E.T. 2001 Brachiopods of the Isca submarine cave: observations during ten years. In: *Brachiopods Past and Present* (eds Brunton, C.H.C., Cocks, L.R.M. & Long, S.L.) Taylor and Francis. 441pp

Samata, T., Hayashi, N., Kono, M., Hasegawa, K., Horita, C. & Akera, S. 1999 A new matrix protein family related to the nacreous layer formation of *Pinctada fucata*. *FEBS Letters* **462**, 225-229

Samtleben, C., Munnecke, A., Bickert, T. & Patzold, J. 2001 Shell succession, assemblage and species dependant effects on the C/O-isotopic composition of brachiopods-examples from the Silurian of Gotland. *Chemical Geology* **175**, 61-107

Schagger, H. & Von Jagow, G 1987 Tricine-sodium dodecyl sulphate polyacrylamide gel electrophoresis for the separation of proteins in the range from 1 to 100kDa. *Analytical Biochemistry* **166** (2), 368-379

Shen, X., Belcher, A., Hansma, P. K., Stucky, G. D. & Morse, D. E. 1997 Molecular cloning and characterization of Lustrin A, a matrix protein from shell and pearl nacre of *Haliotis rufescens*. *The Journal of Biological Chemistry* **272**, 32472-32481

Shimomura, N., Ohkubo, N. & Ichikawa, K. 2002 Control of the production amount and polymorphism of calcium carbonate by biomimetic mineralization. *Chemistry Letters* 902-903

- Simkiss, K. 1989 Biomineralisation in the context of geological time. *Transactions of the Royal Society of Edinburgh* **80**, 193-199
- Simkiss, K & Wilbur, K. M. 1989 *Biomineralization: Cell Biology and Mineral Deposition*. Academic Press Inc.
- Solomon, S. E. 1991 *Egg and Eggshell Quality*. Wolfe Publishing LTD, London, England. pp149
- Sommer, S. E. 1972 Cathodoluminescence of carbonates, 2. Geological applications. *Chemical Geology* **9**, 275-284
- Stanley, S. M. Ries, J. B & Hardie, L. A. 2002 Low-magnesium carbonate produced by coralline algae in seawater of Late Cretaceous composition. *Proceedings of the National Academy of Sciences* **99** (24), 15323-15326
- Stecher III, H. A., Krantz D. E., Lord III, C. J., Luther III, G. W & Bock, K. W. 1996 Profiles of strontium and barium in *Mercenaria mercenaria* and *Spisula solidissima* shells. *Geochimica et Cosmochimica Acta* **60** (18), 3445-3456
- Stoll, H.M., Rosenthal, Y. & Fallowski, P. 2002 Climate proxies from Sr/Ca of coccolith calcite: Calibrations from continuous culture of *Emiliania huxleyi*. *Geochimica et Cosmochimica Acta* **66** (6), 927-936
- Sudo, S., Fujikawa, T., Nagakura, T., Ohkubo, T., Sakaguchi, K., Tanaka, M. & Nakashima, K. 1997 Structures of mollusc shell framework proteins. *Nature* **387**, 563-564
- Sykes, G. A., Collins, M. J. & Walton, D. I. 1995 The significance of a geochemically isolated intracrystalline organic fraction within biominerals. *Organic Geochemistry* **23**, 1059-1065
- Thompson, J. B., Palocz, G. T., Kindt, J. H., Michenfelder, M., Smith, B. L., Stucky, G., Morse, D. E. & Hansma, P. K. 2000 Direct observation of the transition from calcite to aragonite growth as induced by abalone shell proteins. *Biophysical Journal* **79**, 3307-3312
- Towe, K. M. 1970 Oxygen-collagen priority and the early metazoan fossil record. *Proceedings of the National Academy of Sciences* **64** (4), 781-788

- Vander Putten, E., Dehairs, F., Keppens, E. & Baeyens, W. 2000 High resolution distribution of trace elements in the calcite shell layer of modern *Mytilus edulis*: Environmental and biological controls. *Geochimica et Cosmochimica Acta* **64** (6), 997-1011
- Veis, A. & Perry, A. 1967 The phosphoprotein of the dentin matrix. *Biochemistry* **6**, 2409-2416
- Watabe, N. 1988 Shell Structure. In: *The Mollusca. Volume 11. Form and Function*. (eds. Trueman, E. R. & Clarke, M. R.) Academic Press Inc.
- Walton, D.I. 1992 Biogeochemistry of brachiopod intracrystalline proteins and amino acids. PhD Thesis, University of Glasgow ppl-237
- Watanabe, T., Winter, A. & Oba, T. 2001 Seasonal changes in sea surface temperature and salinity during the Little Ice Age in the Caribbean Sea deduced from Mg/Ca and O-18/O-16 ratios in corals. *Marine Geology* **173** (1-4), 21-35
- Weber, J.N. 1973 Incorporation of strontium into reef coral skeletal carbonate. *Geochimica et Cosmochimica Acta* **37**, 2173-2190
- Weedon, J. M. & Taylor, P. D. 1995 Calcitic nacreous ultrastructures in bryozoans: Implications for comparative biomineralization of Lophophorates and Molluscs. *Biological Bulletin* **188**, 281-292
- Weiner, S. 1979 Aspartic acid-rich proteins: Major components of the soluble matrix of mollusk shells. *Calcified Tissue International* **29**, 163-167
- Weiner, S. 1984 Organization of organic matrix components in mineralized tissues. *American Zoologist* **24**, 945-951
- Weiner, S. & Hood, L. 1975 Soluble protein of the organic matrix of mollusk shells: A potential template for shell formation. *Science* **190**, 987-988
- Weiner, S., Traub, W. & Lowenstam, H. A. 1983 Organic matrix in calcified exoskeletons. In: *Biomineralization and Biological Metal Accumulation* (eds. Westbrook, P. & de Jong, E. W.) Reidel Publishing Company, Holland. 205-224

- Weiner, S. & Traub, W. 1984 Macromolecules in mollusc shells and their functions in biomineralization. *Philosophical Transactions of the Royal Society of London B* **304**, 425-434
- Weiss, I. M., Tuross, N., Addadi, L. & Weiner, S. 2002 Mollusc larval shell formation: Amorphous calcium carbonate is a precursor phase for aragonite. *Journal of Experimental Zoology* **293**, 478-491
- Westbroek, P. & Marin, F. 1998 A marriage of bone and nacre. *Nature* **392**, 861-862
- Wheeler, A. P. & Sikes, C. S. Regulation of carbonate calcification by organic matrix. *American Zoologist* **24**, 933-944
- Wheeler, A. P., George, L. W. & Evans, C. A. 1981 Control of calcium carbonate nucleation and crystal growth by soluble matrix of oyster shell. *Science* **212**, 1397-1398
- Wheeler, A. P., Rusenko, K. W., Swift, D. M. & Sikes, C. S. 1988 Regulation of in vitro and in vivo CaCO_3 crystallization by fractions of oyster shell organic matrix. *Marine Biology* **98**, 71-80
- Wilbur, K. M. & Bernhardt, A. M. 1984 Effects of amino acids, magnesium, and molluscan extrapallial fluid on crystallisation of calcium carbonate: *In vitro* experiments. *Biological Bulletin* **166**, 251-259
- Williams, A. 1968 Evolution of the shell structure of articulate brachiopods. *Special Papers in Palaeontology* **2**, 1-55
- Williams, A. & Wright, A. D. 1970 Shell structure of the Craniacea and other calcareous inarticulate Brachiopoda. *Special Papers in Palaeontology* **7**, 1-51
- Williams, A., Carlson, S.J., Brunton, C.H.C., Holmer, L.E. & Popov, L. 1996 A supra-ordinal classification of the Brachiopoda. *Philosophical Transactions of the Royal Society of London B* **351**, 1171-1193
- Wu, T-M., Rodriguez, J. P., Fink, D. J., Carrino, D. A., Blackwell, J., Caplan, A. & Heuer, A. H. 1994 Crystallization studies on avian eggshell membranes: Implications for the molecular factors controlling eggshell formation. *Matrix Biology* **14**, 507-513

Yang, L., Zhang, X., Liao, Z., Guo, Y., Hu, Z. & Cao, Y. 2003 Interfacial molecular recognition between polysaccharides and calcium carbonate during crystallization. *Journal of Inorganic Biochemistry* **97**, 377-383

Young, S. D. 1971 Organic material from Scleractinian coral skeletons-I. Variation in composition between several species. *Comparative Biochemistry and Physiology* **40B**, 113-120

Zaremba, C. A., Belcher, A. M., Fritz, M., Li, Y., Mann, S., Hansma, P. K., Morse, D. E., Speck, J. S. & Stucky, G. D. 1996 Critical transitions in the biofabrication of abalone shells and flat pearls. *Chem. Mater.* **8**, 679-690

Appendix A

Materials

Item	Supplier
Milli Q TM water	Millipore
Guanidine hydrochloride	Sigma
Tris buffer	Sigma
Benzamidine-HCl	Sigma
N-ethylmaleimide	Sigma
Phenyl methyl sulphonyl fluoride	Sigma
Sodium Phosphate	Sigma
Ethylene diamine tetra acetic acid (EDTA)	Sigma
Minitan TM Tangential Flow Ultrafiltration System	Millipore
Centriprep TM Concentrators	Millipore
Microcon TM Concentrators	Millipore
Acrylamide/bisacrylamide (40% solution)	Sigma
Ammonium persulphate (APS)	Sigma
Tetramethylethane (TEMED)	Sigma
Sodium dodecyl sulphate (SDS)	Sigma
Glycerol	Sigma
β-Mercaptoethanol	Sigma
Bromophenol Blue	Sigma
Unstained Proteins of known molecular weight	Sigma
Full range proteins of known molecular weight	Amersham Life Science
Low Molecular weight protein standards	GibcoBRL Life Technologies
Coomassie Brilliant Blue	Sigma
Methanol	BDH
Acetic Acid	Fisher
Dithiothreitol	Sigma
Silver nitrate	Sigma
Sodium Ten Decahydrate	BDH
Formaldehyde	Sigma
Acridine Orange	Sigma
Hydrochloric Acid (Amino acid analysis)	Applied Biosystems
K ₃ EDTA	Applied Biosystems
Polyvinylidene fluoride (Problott) Membrane	Applied Biosystems
CAPS buffer	Sigma
Ethanol	BDH
Calcium carbonate	Sigma
Carbon dioxide	BOC

Appendix B Microprobe Analyses expressed as carbonates

Terebratulina retusa

Sample 1

Point	P ₂ (CO ₃) ₂	Si(CO ₃) ₂	Si(CO ₃) ₂	Mg(CO ₃)	Ca(CO ₃)	Mn(CO ₃)	Fe(CO ₃)	Sr(CO ₃)	Na ₂ (CO ₃)	K ₂ (CO ₃)	Total
1	0.212	0.024	1.466	5.347	91.782	0.000	0.013	0.253	0.751	0.000	99.848
2	0.270	0.026	1.413	4.053	90.900	0.000	0.000	0.244	0.809	0.039	97.754
3	0.176	0.014	1.267	3.450	84.695	0.011	0.000	0.203	0.800	0.016	90.632
4	0.205	0.028	0.907	1.399	96.020	0.000	0.000	0.162	0.589	0.009	99.319
5	0.181	0.019	0.877	1.044	97.609	0.008	0.000	0.178	0.538	0.003	100.457
6	0.199	0.027	0.906	0.976	97.026	0.013	0.051	0.142	0.538	0.018	99.896
7	0.222	0.073	1.072	1.467	96.142	0.012	0.000	0.146	0.605	0.032	99.771
8	0.293	0.018	0.949	2.576	95.152	0.000	0.000	0.193	0.650	0.010	99.841
9	0.128	0.000	0.641	0.671	96.914	0.000	0.015	0.173	0.495	0.016	99.053
10	0.018	0.020	0.756	0.546	96.857	0.039	0.000	0.209	0.614	0.022	99.081
11	0.029	0.033	0.752	0.640	96.824	0.000	0.005	0.223	0.606	0.020	99.132
12	0.070	0.026	0.727	0.518	96.985	0.000	0.000	0.130	0.602	0.001	99.059
13	0.128	0.003	0.773	0.641	96.502	0.000	0.009	0.206	0.589	0.016	98.867
14	0.053	0.022	0.757	0.736	96.972	0.000	0.000	0.202	0.595	0.000	99.337
15	0.070	0.013	0.884	0.876	96.063	0.000	0.038	0.218	0.659	0.012	98.833
16	0.053	0.008	0.744	0.758	96.975	0.000	0.011	0.205	0.626	0.001	99.381
17	0.093	0.044	0.757	0.749	96.309	0.018	0.000	0.190	0.637	0.004	98.801
18	0.000	0.000	0.921	0.693	96.935	0.040	0.000	0.194	0.645	0.004	99.432
19	0.193	2.393	0.913	0.549	79.070	0.000	0.044	0.152	0.497	0.003	83.814
20	0.041	0.087	0.868	0.740	95.679	0.000	0.000	0.224	0.628	0.009	98.276
21	0.134	0.022	0.922	0.683	96.088	0.000	0.000	0.206	0.702	0.029	98.786
22	0.064	0.010	1.136	0.753	95.241	0.013	0.000	0.256	0.680	0.000	98.153
23	0.111	0.020	1.327	0.919	95.405	0.000	0.000	0.239	0.723	0.019	98.763
24	0.082	0.018	1.292	0.963	95.367	0.001	0.000	0.248	0.750	0.018	98.739
25	0.053	0.222	1.573	1.186	95.007	0.016	0.012	0.272	0.713	0.034	99.088
26	0.059	0.036	1.443	3.112	93.205	0.000	0.000	0.268	0.760	0.013	98.896

punctae

1	0.246	0.022	1.319	2.353	90.649	0.019	0.026	0.177	0.550	0.008	95.369
2	0.199	0.039	1.307	1.923	95.677	0.000	0.033	0.202	0.623	0.006	100.009
3	0.094	0.015	1.247	1.119	93.861	0.000	0.007	0.190	0.604	0.025	97.162
4	0.199	0.000	1.052	1.657	95.951	0.019	0.017	0.190	0.523	0.013	99.621
5	0.416	0.000	1.313	2.593	94.423	0.065	0.056	0.205	0.650	0.008	99.729
6	0.375	0.016	1.054	2.547	94.880	0.015	0.000	0.183	0.606	0.025	99.701
7	0.211	0.043	0.708	0.724	97.003	0.029	0.000	0.165	0.596	0.001	99.480
8	0.111	0.023	0.902	0.736	96.570	0.000	0.001	0.228	0.507	0.000	99.078
9	0.129	0.017	0.716	0.748	97.299	0.000	0.000	0.195	0.588	0.015	99.707
10	0.076	0.053	0.691	0.625	96.662	0.010	0.000	0.199	0.652	0.018	98.986
11	0.000	0.051	0.736	0.590	97.680	0.019	0.024	0.195	0.506	0.000	99.801
12	0.088	0.055	0.608	0.559	96.938	0.042	0.000	0.162	0.545	0.000	98.997
13	0.076	0.033	0.733	0.735	96.816	0.048	0.024	0.208	0.660	0.006	99.339
14	0.041	0.000	0.811	0.865	96.796	0.000	0.000	0.166	0.668	0.009	99.356
15	0.000	0.038	0.889	0.750	96.601	0.016	0.003	0.198	0.655	0.000	99.150
16	0.012	0.028	0.899	1.012	95.900	0.007	0.007	0.207	0.711	0.016	98.799
17	0.058	0.050	1.109	1.046	96.230	0.028	0.003	0.195	0.744	0.014	99.477
18	0.357	0.031	1.082	1.561	95.874	0.045	0.000	0.217	0.724	0.000	99.891
19	0.064	0.042	0.980	1.001	96.830	0.034	0.021	0.187	0.584	0.015	99.758
20	0.100	0.020	0.825	1.160	96.711	0.010	0.045	0.196	0.645	0.007	99.719
21	0.000	0.032	0.836	0.918	96.629	0.073	0.008	0.157	0.589	0.023	99.265
22	0.000	0.161	0.903	0.972	94.817	0.057	0.008	0.200	0.604	0.004	97.726
23	0.105	0.000	1.169	1.096	95.488	0.000	0.047	0.208	0.784	0.020	98.917
24	0.093	0.029	0.877	0.873	81.138	0.000	0.000	0.161	0.586	0.010	83.767

Point	P ₂ (CO ₃) _x	Si(CO ₃) ₂	Si(CO ₃) ₂	Mg(CO ₃)	Ca(CO ₃)	Mn(CO ₃)	Fe(CO ₃)	Sr(CO ₃)	Na ₂ (CO ₃)	K ₂ (CO ₃)	Total
1	0.223	0.021	0.863	1.109	96.406	0.016	0.024	0.169	0.532	0.019	99.382
2	0.105	0.475	1.024	0.835	91.896	0.000	0.222	0.164	0.568	0.004	95.293
3	0.105	0.003	0.949	0.771	96.280	0.021	0.035	0.173	0.539	0.004	98.880
4	0.187	0.000	0.981	0.854	95.024	0.000	0.064	0.121	0.545	0.013	97.789
5	0.117	0.014	1.216	1.464	89.562	0.005	0.059	0.176	0.716	0.034	93.363
6	0.205	0.006	1.744	2.511	93.273	0.023	0.084	0.205	0.872	0.016	98.939
7	0.194	0.057	1.598	3.130	93.325	0.067	0.063	0.234	0.843	0.029	99.540
8	0.165	0.027	1.528	3.766	92.551	0.024	0.018	0.282	0.952	0.015	99.328
9	0.047	0.018	1.755	4.404	91.172	0.042	0.024	0.288	1.002	0.024	98.776
10	0.136	0.088	0.539	1.857	32.343	0.000	0.000	0.121	0.292	0.015	35.391
11	0.304	0.018	1.003	1.310	93.837	0.042	0.021	0.113	0.564	0.032	97.244
12	0.047	0.012	0.713	0.714	88.993	0.001	0.020	0.144	0.576	0.015	91.235
13	0.135	0.081	0.936	0.823	96.514	0.029	0.005	0.163	0.542	0.001	99.229
14	0.211	0.050	1.016	0.719	94.195	0.024	0.040	0.148	0.530	0.006	96.939
15	0.082	0.000	1.035	0.725	93.708	0.002	0.099	0.144	0.590	0.008	96.393
16	0.082	0.024	0.899	0.658	90.195	0.000	0.034	0.130	0.653	0.002	92.677
17	0.105	0.031	0.865	0.655	96.165	0.000	0.011	0.169	0.618	0.010	98.629
18	0.105	0.018	0.862	0.604	96.119	0.004	0.020	0.188	0.576	0.012	98.508
19	0.146	0.023	1.140	0.697	96.339	0.000	0.000	0.169	0.670	0.019	99.203
20	0.064	0.149	0.253	0.199	28.667	0.029	0.026	0.060	0.159	0.001	29.607
21	0.213	3.659	0.670	0.659	51.390	0.019	0.120	0.072	0.425	0.008	57.235
22	0.094	0.743	0.978	0.630	93.200	0.000	0.002	0.119	0.585	0.002	96.353
23	0.059	0.124	1.049	0.661	95.908	0.000	0.000	0.208	0.588	0.018	98.615
24	0.082	0.016	1.163	0.764	95.865	0.069	0.007	0.184	0.672	0.004	98.826
25	0.094	0.061	1.102	0.887	95.564	0.000	0.000	0.218	0.686	0.000	98.612
26	0.047	0.040	0.729	0.641	97.356	0.025	0.000	0.186	0.633	0.003	99.660
27	0.018	0.012	0.803	0.673	95.823	0.007	0.037	0.206	0.685	0.014	98.278
28	0.047	0.005	0.920	0.595	96.619	0.000	0.000	0.199	0.645	0.000	99.030
29	0.082	0.050	1.425	0.962	94.872	0.035	0.032	0.179	0.750	0.000	98.387
30	0.058	0.024	0.546	0.419	96.877	0.000	0.000	0.174	0.547	0.002	98.647
31	0.023	0.000	0.620	0.476	96.315	0.037	0.000	0.193	0.570	0.000	98.234
32	0.105	0.063	0.798	0.491	96.859	0.033	0.027	0.157	0.529	0.000	99.062
33	0.023	0.055	0.845	0.510	95.800	0.000	0.003	0.168	0.583	0.000	97.987
34	0.047	0.063	0.878	0.620	96.115	0.000	0.000	0.152	0.631	0.000	98.506
35	0.070	0.077	1.110	0.758	94.491	0.000	0.004	0.219	0.630	0.018	97.377

Sample 2

1	0.029	0.073	1.438	1.944	93.875	0.000	0.000	0.284	0.813	0.020	98.476
2	0.000	0.048	1.076	1.307	95.087	0.060	0.000	0.266	0.740	0.030	98.614
3	0.041	0.041	0.848	0.886	95.092	0.080	0.000	0.233	0.703	0.000	97.924
4	0.000	0.025	0.799	0.777	96.646	0.000	0.000	0.230	0.698	0.009	99.184
5	0.076	0.037	0.944	0.919	95.690	0.000	0.000	0.221	0.744	0.005	98.636
6	0.105	0.009	0.824	0.874	95.978	0.030	0.000	0.230	0.717	0.021	98.788
7	0.075	0.055	1.031	0.984	95.851	0.000	0.060	0.228	0.708	0.001	98.993
8	0.041	0.061	1.014	0.920	96.217	0.002	0.010	0.220	0.741	0.012	99.238
9	0.151	0.000	0.980	1.111	95.610	0.000	0.011	0.214	0.681	0.028	98.786
10	0.047	0.133	0.165	0.153	18.160	0.031	0.000	0.000	0.100	0.022	18.811
11	0.029	0.045	0.762	0.832	95.751	0.000	0.001	0.200	0.705	0.001	98.326
12	0.000	0.066	0.828	0.861	95.795	0.019	0.000	0.185	0.973	0.027	98.754
13	0.058	0.062	0.667	0.773	96.573	0.000	0.003	0.243	0.675	0.019	99.073
14	0.017	0.062	0.889	0.810	96.308	0.006	0.000	0.212	0.702	0.002	99.008
15	0.023	0.052	0.872	0.839	96.234	0.020	0.000	0.185	0.709	0.000	98.934
16	0.087	0.044	0.927	0.734	96.863	0.020	0.010	0.213	0.638	0.020	99.556
17	0.093	0.000	0.823	0.832	97.390	0.041	0.000	0.174	0.672	0.008	100.033
18	0.035	0.088	0.713	0.767	97.152	0.002	0.020	0.215	0.610	0.007	99.609
19	0.134	0.009	0.869	0.699	97.211	0.031	0.005	0.175	0.754	0.014	99.901
20	0.110	0.019	0.933	0.747	97.362	0.000	0.010	0.187	0.732	0.002	100.102
21	0.163	0.063	0.861	0.841	97.385	0.025	0.014	0.182	0.670	0.029	100.233
22	0.256	0.040	0.650	0.662	98.235	0.071	0.000	0.207	0.570	0.000	100.691

punctae
punctae

punctae

Point	P ₂ (CO ₃) ₂	Si(CO ₃) ₂	Si(CO ₃) ₂	Mg(CO ₃)	Ca(CO ₃)	Mn(CO ₃)	Fe(CO ₃)	Sr(CO ₃)	Na ₂ (CO ₃)	K ₂ (CO ₃)	Total
1	0.064	0.047	1.748	2.880	94.848	0.022	0.000	0.286	0.876	0.014	100.785
2	0.000	0.074	1.703	3.016	94.792	0.004	0.000	0.320	0.863	0.025	100.797
3	0.006	0.107	1.237	1.388	96.622	0.000	0.003	0.235	0.773	0.008	100.379
4	0.029	0.051	1.059	1.114	96.727	0.016	0.010	0.257	0.754	0.007	100.024
5	0.070	0.074	0.820	1.104	97.429	0.017	0.007	0.230	0.710	0.000	100.461
6	0.151	0.035	1.005	1.119	96.843	0.000	0.000	0.205	0.680	0.015	100.053
7	0.122	0.071	0.845	0.955	96.993	0.081	0.026	0.218	0.704	0.016	100.031
8	0.012	0.036	0.742	0.928	96.790	0.035	0.000	0.225	0.713	0.020	99.501
9	0.000	0.047	0.881	0.864	97.299	0.067	0.007	0.205	0.692	0.006	100.068
10	0.035	0.041	0.725	1.012	97.075	0.000	0.000	0.235	0.815	0.030	99.968
11	0.052	0.016	0.865	0.920	96.506	0.071	0.014	0.226	0.714	0.005	99.389
12	0.047	0.019	0.783	0.920	97.464	0.000	0.000	0.239	0.693	0.002	100.167
13	0.029	0.026	0.902	0.910	97.368	0.048	0.000	0.226	0.672	0.007	100.188
14	0.052	0.002	0.659	0.720	97.152	0.038	0.000	0.216	0.636	0.000	99.475
15	0.105	0.049	0.667	0.728	97.305	0.012	0.000	0.204	0.561	0.002	99.633
16	0.198	0.064	0.910	0.711	97.401	0.093	0.000	0.185	0.529	0.024	100.115
17	0.064	0.032	0.729	0.663	97.738	0.000	0.000	0.179	0.634	0.000	100.039
18	0.087	0.073	0.716	0.722	96.547	0.024	0.000	0.201	0.639	0.004	99.013
19	0.076	0.022	0.672	0.839	97.931	0.000	0.000	0.223	0.675	0.001	100.439
20	0.058	0.041	0.804	0.728	97.623	0.041	0.000	0.221	0.628	0.018	100.162
21	0.146	0.069	0.684	0.722	97.405	0.000	0.150	0.176	0.611	0.000	99.963
22	0.087	0.079	0.743	0.766	97.600	0.000	0.000	0.194	0.671	0.018	100.158
23	0.116	0.049	0.745	0.897	96.968	0.035	0.013	0.127	0.576	0.000	99.526
24	0.280	0.060	0.751	1.464	93.426	0.000	0.025	0.158	0.614	0.000	96.778

1	0.041	0.077	1.529	2.605	95.478	0.065	0.000	0.245	0.749	0.032	100.821
2	0.029	0.068	1.602	1.869	96.662	0.071	0.004	0.259	0.744	0.034	101.342
3	0.134	0.045	1.027	0.975	96.486	0.024	0.007	0.233	0.741	0.022	99.694
4	0.157	0.027	0.878	0.878	96.879	0.000	0.000	0.232	0.676	0.005	99.732
5	0.058	0.046	0.709	0.970	96.745	0.000	0.024	0.269	0.732	0.010	99.563
6	0.047	0.053	1.151	1.241	96.155	0.000	0.000	0.275	0.792	0.009	99.723
7	0.087	0.055	0.882	1.035	96.474	0.000	0.000	0.231	0.767	0.022	99.553
8	0.000	0.070	0.903	1.135	97.083	0.000	0.000	0.264	0.725	0.025	100.205
9	0.087	0.000	0.866	1.008	96.428	0.013	0.000	0.254	0.755	0.022	99.433
10	0.006	0.057	0.696	0.921	97.206	0.016	0.000	0.225	0.647	0.000	99.774
11	0.017	0.060	0.854	1.069	96.465	0.000	0.000	0.246	0.759	0.000	99.470
12	0.052	0.053	0.705	1.002	96.889	0.023	0.023	0.215	0.727	0.000	99.689
13	0.052	0.020	0.742	0.900	96.665	0.031	0.000	0.218	0.700	0.000	99.328
14	0.151	0.058	0.726	1.209	96.816	0.000	0.012	0.170	0.696	0.000	99.838
15	0.058	0.022	0.486	0.623	97.937	0.013	0.000	0.187	0.581	0.000	99.907
16	0.064	0.060	0.577	0.513	97.519	0.004	0.013	0.149	0.597	0.000	99.496
17	0.017	0.044	0.671	0.449	98.150	0.069	0.035	0.156	0.545	0.000	100.136
18	0.122	0.038	0.721	0.466	97.419	0.030	0.048	0.209	0.591	0.017	99.661
19	0.151	0.028	0.725	0.527	97.893	0.000	0.000	0.146	0.515	0.003	99.988
20	0.070	0.072	0.589	0.568	97.596	0.052	0.000	0.207	0.620	0.036	99.810
21	0.064	0.110	0.511	0.501	97.531	0.118	0.007	0.191	0.573	0.000	99.606
22	0.186	0.048	0.638	0.584	98.163	0.000	0.000	0.191	0.536	0.005	100.351
23	0.128	0.023	0.590	0.668	98.007	0.031	0.000	0.188	0.611	0.003	100.249

1	0.094	0.068	1.636	3.869	93.705	0.023	0.026	0.293	0.862	0.041	100.617
2	0.012	0.023	1.559	3.021	95.790	0.018	0.045	0.303	0.832	0.031	101.634
3	0.099	0.050	1.389	2.279	95.619	0.010	0.008	0.289	0.822	0.016	100.581
4	0.070	0.065	1.156	1.502	95.592	0.000	0.004	0.256	0.791	0.032	99.468
5	0.093	0.046	1.205	1.102	95.904	0.006	0.030	0.256	0.777	0.007	99.426
6	0.087	0.043	0.998	1.106	96.305	0.025	0.011	0.277	0.740	0.000	99.592
7	0.012	0.067	0.977	0.994	95.822	0.083	0.000	0.199	0.715	0.015	98.884
8	0.035	0.049	0.923	0.901	96.366	0.100	0.000	0.180	0.657	0.003	99.214
9	0.058	0.005	0.804	0.865	96.374	0.000	0.038	0.191	0.648	0.010	98.993

Point	P ₂ (CO ₃) ₂	Si(CO ₃) ₂	Si(CO ₃) ₂	Mg(CO ₃)	Ca(CO ₃)	Mn(CO ₃)	Fe(CO ₃)	Sr(CO ₃)	Na ₂ (CO ₃)	K ₂ (CO ₃)	Total
10	0.122	0.006	0.623	0.827	96.765	0.045	0.000	0.194	0.595	0.000	99.177
11	0.058	0.031	0.932	0.830	97.013	0.057	0.000	0.210	0.690	0.003	99.824
12	0.000	0.052	0.841	0.725	96.359	0.007	0.005	0.202	0.683	0.000	98.874
13	0.064	0.000	0.887	0.865	93.802	0.004	0.025	0.186	0.730	0.016	96.579
14	0.047	0.019	0.854	0.731	97.077	0.008	0.000	0.222	0.638	0.017	99.613
15	0.041	0.029	0.738	0.640	97.132	0.000	0.000	0.166	0.626	0.000	99.372
16	0.099	0.061	0.854	0.712	96.724	0.000	0.000	0.190	0.704	0.012	99.356
17	0.093	0.011	0.866	0.763	97.109	0.053	0.000	0.172	0.633	0.000	99.700
18	0.140	0.009	1.064	0.740	96.963	0.012	0.000	0.197	0.716	0.000	99.841
19	0.082	0.060	0.899	0.626	97.197	0.000	0.012	0.204	0.681	0.009	99.770
20	0.070	0.052	0.651	0.658	96.748	0.000	0.047	0.186	0.625	0.001	99.038
21	0.035	0.045	0.647	0.577	96.979	0.013	0.002	0.130	0.617	0.006	99.051
22	0.140	0.088	0.685	0.716	91.229	0.018	0.015	0.193	0.690	0.008	93.782
23	0.029	1.008	0.372	0.298	44.520	0.000	0.000	0.101	0.318	0.000	46.646
24	0.134	0.068	0.660	0.603	94.843	0.013	0.000	0.186	0.636	0.000	97.143
25	0.052	0.055	0.726	0.854	95.812	0.004	0.018	0.206	0.620	0.013	98.360
26	0.006	0.041	0.734	0.665	96.490	0.005	0.038	0.209	0.565	0.012	98.765

Sample 3

1	1.438	0.026	1.668	2.647	93.827	n/a	0.000	0.272	0.755	0.025	100.658
2	1.384	0.066	1.790	3.546	92.976	n/a	0.000	0.326	0.838	0.017	100.943
3	1.501	0.011	1.542	2.519	94.281	n/a	0.004	0.290	0.813	0.011	100.972
4	1.590	0.012	1.105	1.097	95.137	n/a	0.000	0.240	0.733	0.022	99.936
5	1.574	0.000	1.062	0.872	96.025	n/a	0.000	0.192	0.687	0.002	100.414
6	1.487	0.005	0.914	0.848	95.214	n/a	0.006	0.213	0.615	0.000	99.302
7	1.450	0.000	0.977	0.811	96.419	n/a	0.000	0.154	0.619	0.000	100.430
8	1.455	0.004	0.935	0.821	95.236	n/a	0.000	0.207	0.643	0.026	99.327
9	1.471	0.033	1.178	1.030	95.276	n/a	0.000	0.231	0.675	0.022	99.916
10	1.612	0.017	1.066	0.784	95.991	n/a	0.000	0.175	0.589	0.021	100.255
11	1.567	0.024	1.169	0.829	95.547	n/a	0.000	0.203	0.584	0.000	99.923
12	1.599	0.000	1.098	0.892	95.656	n/a	0.000	0.176	0.677	0.011	100.109
13	1.522	0.006	1.107	0.893	95.682	n/a	0.030	0.227	0.722	0.012	100.201
14	1.655	0.011	0.836	0.864	96.478	n/a	0.009	0.153	0.660	0.043	100.709
15	1.488	0.076	0.795	0.642	96.101	n/a	0.000	0.200	0.647	0.000	99.949
16	1.590	0.028	0.766	0.498	95.818	n/a	0.000	0.212	0.604	0.001	99.517
17	1.608	0.012	0.703	0.578	96.549	n/a	0.034	0.194	0.592	0.000	100.270
18	1.527	0.017	0.633	0.538	96.070	n/a	0.000	0.194	0.632	0.001	99.612
19	1.620	0.011	0.782	0.603	96.791	n/a	0.000	0.172	0.607	0.003	100.589
20	1.599	0.001	0.958	0.634	95.859	n/a	0.000	0.190	0.571	0.005	99.817
21	1.636	0.000	0.863	0.745	95.327	n/a	0.020	0.161	0.631	0.003	99.386
22	1.771	0.073	0.837	0.740	96.250	n/a	0.000	0.193	0.576	0.008	100.448
23	1.732	0.071	0.885	1.474	95.267	n/a	0.006	0.158	0.612	0.021	100.226

1	1.431	0.072	1.461	2.144	93.916	n/a	0.000	0.255	0.686	0.035	100.000
2	1.468	0.051	1.498	2.429	93.598	n/a	0.000	0.274	0.764	0.039	100.121
3	1.567	0.000	1.361	1.578	93.424	n/a	0.024	0.244	0.767	0.000	98.965
4	1.592	0.000	1.037	0.909	94.824	n/a	0.000	0.202	0.705	0.005	99.274
5	1.478	0.006	1.010	0.811	94.912	n/a	0.001	0.228	0.669	0.014	99.129
6	1.486	0.069	0.901	0.710	95.241	n/a	0.030	0.183	0.594	0.000	99.214
7	1.569	0.042	0.911	0.886	95.720	n/a	0.021	0.176	0.633	0.007	99.965
8	1.277	0.060	0.670	0.753	76.035	n/a	0.030	0.159	0.521	0.028	79.533
9	1.495	0.017	1.105	0.899	94.803	n/a	0.000	0.237	0.624	0.007	99.187
10	1.661	0.024	1.008	0.723	95.120	n/a	0.000	0.174	0.638	0.014	99.362
11	1.522	0.050	0.958	0.840	95.542	n/a	0.000	0.219	0.675	0.000	99.806
12	1.543	0.025	0.984	0.794	95.212	n/a	0.000	0.147	0.685	0.022	99.412
13	1.555	0.017	0.961	0.631	95.623	n/a	0.016	0.223	0.693	0.005	99.724
14	1.446	0.029	0.791	0.639	95.542	n/a	0.015	0.208	0.702	0.005	99.377
15	1.515	0.055	0.801	0.594	95.966	n/a	0.000	0.214	0.662	0.023	99.830

Point	P ₂ (CO ₃) ₂	Si(CO ₃) ₂	S(CO ₃) ₂	Mg(CO ₃)	Ca(CO ₃)	Mn(CO ₃)	Fe(CO ₃)	Sr(CO ₃)	Na ₂ (CO ₃)	K ₂ (CO ₃)	Total
16	1.500	0.017	0.781	0.667	96.162	n/a	0.006	0.181	0.663	0.020	99.997
17	1.493	0.077	0.818	0.659	95.567	n/a	0.000	0.210	0.624	0.000	99.448
18	1.597	0.000	0.769	0.592	95.665	n/a	0.044	0.184	0.602	0.008	99.461
19	1.568	0.031	0.876	0.663	96.185	n/a	0.000	0.204	0.643	0.015	100.185
20	1.572	0.003	0.907	0.720	96.241	n/a	0.000	0.179	0.660	0.034	100.316
21	1.481	0.074	0.746	0.696	95.528	n/a	0.000	0.163	0.637	0.000	99.325
22	1.717	0.020	0.783	0.817	96.718	n/a	0.007	0.193	0.612	0.005	100.872
23	1.707	0.027	0.861	1.647	95.011	n/a	0.000	0.163	0.663	0.005	100.084

1	1.383	0.085	1.504	1.701	93.668	n/a	0.000	0.280	0.719	0.000	99.340
2	1.482	0.000	1.015	1.053	95.726	n/a	0.000	0.239	0.721	0.011	100.247
3	1.566	0.019	1.173	0.940	95.419	n/a	0.015	0.191	0.713	0.021	100.057
4	1.427	0.005	0.816	0.836	94.854	n/a	0.021	0.232	0.691	0.000	98.882
5	1.457	0.024	1.057	0.938	94.666	n/a	0.000	0.206	0.742	0.015	99.105
6	1.572	0.056	1.060	0.967	94.219	n/a	0.000	0.231	0.747	0.014	98.866
7	1.522	0.059	1.090	1.064	94.989	n/a	0.000	0.209	0.720	0.004	99.657
8	1.512	0.028	1.040	1.205	94.284	n/a	0.000	0.209	0.699	0.009	98.986
9	1.471	0.050	1.125	1.321	94.247	n/a	0.000	0.199	0.717	0.000	99.130
10	1.437	0.014	1.000	1.310	94.030	n/a	0.000	0.241	0.761	0.010	98.803
11	1.066	0.018	0.608	0.915	67.638	n/a	0.013	0.171	0.549	0.014	70.992
12	1.494	0.042	0.842	0.822	94.722	n/a	0.000	0.194	0.655	0.026	98.797
13	1.493	0.008	0.779	0.812	94.685	n/a	0.000	0.171	0.694	0.008	98.650
14	1.567	0.019	0.765	0.715	95.560	n/a	0.036	0.215	0.605	0.000	99.482
15	1.517	0.030	0.705	0.786	94.987	n/a	0.000	0.213	0.648	0.006	98.892
16	1.511	0.011	0.664	0.718	95.198	n/a	0.000	0.155	0.610	0.000	98.867
17	1.550	0.038	0.828	0.631	95.791	n/a	0.038	0.184	0.587	0.000	99.647
18	1.526	0.014	0.875	0.723	94.856	n/a	0.022	0.196	0.627	0.003	98.842
19	1.640	0.045	0.773	0.745	95.512	n/a	0.002	0.157	0.632	0.000	99.506
20	1.561	0.036	0.670	0.663	96.228	n/a	0.025	0.225	0.564	0.013	99.985
21	1.568	0.057	0.810	0.700	95.319	n/a	0.028	0.193	0.595	0.000	99.270
22	1.670	0.014	0.811	1.395	93.599	n/a	0.000	0.184	0.622	0.000	98.295

1	1.452	0.024	1.439	1.708	94.762	n/a	0.006	0.259	0.693	0.031	100.374
2	1.519	0.000	1.261	1.145	95.400	n/a	0.000	0.252	0.693	0.016	100.286
3	1.461	0.051	1.050	0.913	95.134	n/a	0.031	0.229	0.683	0.000	99.552
4	1.546	0.010	0.926	0.820	95.374	n/a	0.029	0.225	0.723	0.021	99.674
5	1.474	0.008	0.967	0.810	94.812	n/a	0.000	0.167	0.699	0.016	98.953
6	1.594	0.018	0.928	0.877	95.675	n/a	0.000	0.188	0.681	0.004	99.965
7	1.582	0.008	1.148	0.977	95.049	n/a	0.028	0.268	0.729	0.019	99.808
8	1.429	0.036	0.944	1.077	94.516	n/a	0.000	0.203	0.634	0.002	98.841
9	1.479	0.024	1.082	1.012	95.002	n/a	0.000	0.219	0.681	0.020	99.519
10	1.484	0.023	1.001	0.889	95.772	n/a	0.000	0.247	0.671	0.000	100.087
11	1.573	0.034	0.987	1.045	95.418	n/a	0.000	0.211	0.675	0.000	99.943
12	1.465	0.014	0.957	1.036	94.821	n/a	0.000	0.220	0.679	0.001	99.193
13	1.640	0.036	0.829	0.969	96.298	n/a	0.000	0.196	0.648	0.007	100.623
14	1.502	0.014	0.816	0.665	96.492	n/a	0.000	0.179	0.580	0.011	100.259
15	1.569	0.056	0.763	0.597	96.060	n/a	0.009	0.166	0.563	0.000	99.783
16	1.622	0.000	0.589	0.542	95.806	n/a	0.024	0.187	0.552	0.024	99.346
17	1.580	0.017	0.727	0.627	95.694	n/a	0.000	0.211	0.594	0.000	99.450
18	1.547	0.012	0.826	0.624	95.352	n/a	0.000	0.178	0.620	0.027	99.186
19	1.802	0.040	1.111	1.085	95.267	n/a	0.009	0.172	0.647	0.009	100.142
20	1.564	0.027	0.755	0.598	96.153	n/a	0.025	0.170	0.565	0.000	99.857
21	1.524	0.013	0.648	0.476	96.815	n/a	0.000	0.178	0.577	0.007	100.238
22	1.503	0.000	0.761	0.676	96.039	n/a	0.000	0.161	0.611	0.009	99.760

Novocrania anomala

Sample 1

1	0.822	0.143	1.357	7.279	80.668	0.088	0.026	0.381	0.934	0.031	91.729
---	-------	-------	-------	-------	--------	-------	-------	-------	-------	-------	--------

Point	P ₂ (CO ₃) ₅	Si(CO ₃) ₂	S(CO ₃) ₂	Mg(CO ₃)	Ca(CO ₃)	Mn(CO ₃)	Fe(CO ₃)	Sr(CO ₃)	Na ₂ (CO ₃)	K ₂ (CO ₃)	Total
2	1.340	0.062	1.331	9.600	86.473	0.044	0.028	0.364	1.206	0.049	100.497
3	0.639	0.000	1.471	9.017	88.942	0.024	0.019	0.369	1.111	0.030	101.622
4	0.396	0.050	1.424	8.231	86.657	0.062	0.064	0.329	1.064	0.035	98.312
5	0.219	0.060	1.212	6.607	79.811	0.037	0.009	0.314	1.029	0.024	89.322
6	0.237	0.025	1.290	8.439	88.092	0.060	0.000	0.371	1.310	0.044	99.868
7	0.313	0.058	1.365	8.545	88.303	0.008	0.000	0.339	1.228	0.046	100.205
8	0.384	0.003	1.448	8.702	88.927	0.054	0.067	0.318	1.086	0.024	101.013
9	0.349	0.057	1.437	8.616	87.671	0.000	0.069	0.390	1.103	0.039	99.731
10	0.468	0.077	1.584	8.555	87.056	0.000	0.025	0.399	1.098	0.015	99.277
11	0.302	0.034	1.654	8.023	90.120	0.080	0.030	0.336	0.879	0.052	101.510
12	0.408	0.127	1.726	8.523	87.756	0.000	0.000	0.392	1.020	0.029	99.981
13	0.343	0.125	1.725	7.793	87.831	0.065	0.000	0.381	0.948	0.027	99.238
14	0.260	0.021	1.600	8.619	88.985	0.025	0.033	0.403	0.978	0.022	100.946
15	0.408	0.053	1.836	8.183	90.423	0.064	0.026	0.310	0.882	0.022	102.207
16	0.367	0.090	1.671	7.726	86.095	0.033	0.016	0.407	0.818	0.032	97.255
17	0.278	0.072	1.665	8.148	90.065	0.050	0.052	0.367	0.719	0.027	101.443
18	0.118	0.061	1.721	8.669	89.522	0.040	0.000	0.335	0.841	0.035	101.342
19	0.189	0.008	1.690	8.544	89.895	0.183	0.020	0.334	0.802	0.019	101.684
20	0.213	0.048	1.592	8.308	83.490	0.087	0.016	0.437	0.950	0.038	95.179
21	0.201	0.049	1.683	7.952	90.412	0.063	0.000	0.351	0.951	0.038	101.700
22	0.207	0.042	1.687	8.598	89.622	0.079	0.002	0.352	0.892	0.038	101.519
23	0.207	0.064	1.989	8.635	90.669	0.152	0.033	0.348	0.836	0.038	102.971
24	0.166	0.040	1.833	8.433	90.132	0.000	0.039	0.331	0.710	0.050	101.734
25	0.047	0.059	1.796	8.688	90.085	0.113	0.000	0.332	0.797	0.021	101.938
26	0.219	0.042	1.793	8.829	89.463	0.133	0.004	0.365	0.837	0.030	101.715
27	0.165	0.044	1.656	7.865	90.566	0.083	0.000	0.342	0.848	0.017	101.586
28	0.320	0.293	1.445	7.851	84.065	0.048	0.013	0.351	0.763	0.047	95.196
29	0.308	0.208	2.098	7.786	84.709	0.018	0.044	0.370	0.700	0.022	96.263
30	0.337	0.068	1.537	8.472	89.670	0.108	0.028	0.337	0.823	0.025	101.405
31	0.195	0.007	1.613	8.856	89.088	0.104	0.035	0.328	0.794	0.029	101.049
32	0.343	0.018	1.431	7.517	85.644	0.016	0.060	0.310	0.758	0.030	96.127
33	0.267	0.000	1.308	9.057	86.537	0.051	0.000	0.410	0.689	0.014	98.333
34	0.201	0.043	1.466	8.849	88.952	0.010	0.007	0.389	0.840	0.014	100.771
35	0.397	0.063	1.565	9.207	88.475	0.050	0.000	0.419	0.876	0.038	101.090
36	0.195	0.000	1.574	8.973	89.139	0.060	0.034	0.331	0.746	0.029	101.081
37	0.586	0.036	1.332	8.536	88.460	0.015	0.000	0.360	0.561	0.027	99.913
38	0.847	0.450	1.284	7.708	81.425	0.065	0.041	0.327	0.421	0.037	92.605
1	1.343	0.185	1.460	6.533	74.956	0.039	0.038	0.326	0.973	0.049	85.902
2	0.792	0.053	1.566	8.055	90.338	0.001	0.037	0.350	0.884	0.049	102.125
3	0.468	0.036	1.299	9.088	88.451	0.000	0.028	0.338	1.168	0.031	100.907
4	0.350	0.000	1.367	9.048	86.557	0.015	0.066	0.338	1.283	0.028	99.052
5	0.273	0.000	1.321	8.795	87.933	0.038	0.028	0.380	1.099	0.035	99.902
6	0.278	0.019	1.286	8.234	87.385	0.000	0.015	0.308	1.258	0.055	98.838
7	0.296	0.006	1.232	7.740	84.248	0.000	0.000	0.339	1.264	0.031	95.156
8	0.332	0.026	1.289	8.504	87.313	0.063	0.047	0.317	1.228	0.031	99.150
9	0.261	0.005	1.342	8.572	86.986	0.063	0.034	0.343	1.295	0.035	98.936
10	0.248	0.000	1.264	8.142	87.788	0.000	0.048	0.318	1.155	0.052	99.015
11	0.326	0.037	1.463	8.114	87.898	0.086	0.026	0.327	1.234	0.031	99.542
12	0.373	0.011	1.321	8.682	86.779	0.000	0.026	0.361	1.260	0.018	98.831
13	0.433	0.044	1.479	8.243	88.067	0.033	0.013	0.348	1.009	0.051	99.720
14	0.373	0.050	1.744	8.674	89.736	0.064	0.030	0.355	0.814	0.048	101.888
15	0.474	0.005	1.740	8.552	90.026	0.111	0.054	0.320	0.791	0.020	102.093
16	0.148	0.036	1.757	8.239	89.390	0.023	0.000	0.392	0.770	0.011	100.766
17	0.207	0.120	1.775	7.291	84.896	0.068	0.001	0.345	0.653	0.008	95.364
18	0.154	0.000	1.947	8.895	89.168	0.006	0.000	0.369	0.725	0.024	101.288

Point	P ₂ (CO ₃) ₂	Si(CO ₃) ₂	S(CO ₃) ₂	Mg(CO ₃)	Ca(CO ₃)	Mn(CO ₃)	Fe(CO ₃)	Sr(CO ₃)	Na ₂ (CO ₃)	K ₂ (CO ₃)	Total
1	0.914	0.056	1.127	9.352	83.051	0.098	0.012	0.393	1.266	0.058	96.327
2	0.326	0.031	1.112	8.421	81.242	0.040	0.000	0.364	1.210	0.034	92.780
3	0.285	0.010	1.074	7.999	79.579	0.000	0.025	0.330	1.058	0.022	90.382
4	0.414	0.046	1.302	8.290	78.941	0.000	0.000	0.408	0.997	0.042	90.440
5	0.496	0.058	1.374	9.279	85.898	0.002	0.056	0.335	1.244	0.030	98.772
6	0.262	0.006	1.286	8.431	84.873	0.002	0.032	0.368	1.069	0.022	96.351
7	0.337	0.042	1.466	8.466	88.335	0.000	0.043	0.298	1.091	0.064	100.142
8	0.278	0.039	1.366	7.597	84.893	0.051	0.058	0.347	1.102	0.047	95.778
9	0.283	0.011	1.353	7.887	83.740	0.021	0.010	0.371	1.133	0.042	94.851
10	0.350	0.017	1.480	8.510	88.507	0.016	0.051	0.335	1.192	0.027	100.485
11	0.219	0.024	1.400	8.005	84.089	0.017	0.023	0.327	0.890	0.038	95.032
12	0.314	0.005	1.208	7.608	83.745	0.000	0.024	0.368	1.177	0.048	94.497
13	0.255	0.031	1.090	7.856	87.031	0.010	0.012	0.346	1.261	0.046	97.938
14	0.207	0.047	1.036	8.013	85.136	0.000	0.031	0.371	1.223	0.031	96.095
15	0.202	0.033	1.192	8.207	82.256	0.019	0.011	0.370	1.213	0.021	93.524
16	0.380	0.000	1.167	8.498	84.993	0.055	0.026	0.326	1.186	0.003	96.634
17	0.225	0.000	1.251	8.533	80.814	0.028	0.046	0.312	1.160	0.019	92.388
18	0.285	0.024	1.280	8.378	80.633	0.000	0.016	0.364	1.102	0.039	92.121
19	0.279	0.028	1.296	8.330	88.318	0.045	0.059	0.304	1.095	0.038	99.792
20	0.225	0.033	1.245	7.799	86.261	0.015	0.055	0.326	1.176	0.022	97.157
21	0.391	0.030	1.225	8.175	84.580	0.000	0.033	0.302	1.135	0.005	95.876
22	0.225	0.026	1.443	8.566	85.748	0.000	0.012	0.393	1.022	0.015	97.450
23	0.325	0.018	1.528	7.400	88.758	0.004	0.038	0.321	1.030	0.043	99.465
24	0.415	0.069	1.304	8.120	85.002	0.062	0.032	0.385	1.139	0.032	96.560
25	0.332	0.009	1.405	8.250	84.923	0.000	0.019	0.355	1.086	0.026	96.405
26	0.249	0.035	1.548	8.336	89.119	0.028	0.000	0.342	0.979	0.036	100.672
27	0.337	0.034	1.797	7.910	88.239	0.023	0.024	0.331	0.775	0.028	99.498
28	0.361	0.037	1.848	8.022	89.928	0.006	0.028	0.352	0.901	0.022	101.505

Sample 2

1	0.496	0.197	1.623	7.779	84.408	0.000	0.000	0.391	0.927	0.042	95.863
2	0.403	0.023	1.110	9.768	87.192	0.054	0.041	0.407	1.138	0.031	100.167
3	0.319	0.034	1.552	8.413	89.718	0.008	0.027	0.308	0.939	0.047	101.365
4	0.325	0.061	1.444	8.188	85.957	0.000	0.032	0.292	1.038	0.036	97.373
5	0.266	0.023	1.364	7.937	82.340	0.027	0.029	0.311	1.076	0.045	93.418
6	0.225	0.007	1.355	8.345	87.500	0.000	0.037	0.329	1.061	0.015	98.874
7	0.290	0.057	1.469	8.659	87.522	0.000	0.035	0.363	1.211	0.032	99.638
8	0.189	0.016	1.239	8.601	86.898	0.000	0.000	0.404	1.153	0.024	98.524
9	0.172	0.047	1.348	8.916	87.279	0.041	0.000	0.375	1.261	0.033	99.472
10	0.272	0.075	1.363	8.032	88.834	0.015	0.059	0.336	1.058	0.024	100.068
11	0.195	0.042	1.193	7.772	80.415	0.000	0.044	0.370	1.118	0.024	91.173
12	0.207	0.041	1.156	9.123	86.147	0.070	0.061	0.344	1.261	0.030	98.440
13	0.414	0.026	1.458	8.755	87.782	0.042	0.036	0.388	1.037	0.017	99.955
14	0.325	0.042	1.389	8.913	87.612	0.036	0.035	0.351	1.118	0.018	99.839
15	0.284	0.028	1.558	8.821	88.156	0.046	0.080	0.338	1.154	0.039	100.504
16	0.278	0.021	1.624	8.411	86.293	0.034	0.000	0.383	0.789	0.020	97.853
17	0.219	0.021	1.503	8.905	89.223	0.131	0.000	0.368	0.882	0.023	101.275
18	0.124	0.048	1.748	8.403	88.091	0.028	0.000	0.375	0.804	0.011	99.632
19	0.112	0.000	1.811	8.676	89.673	0.018	0.019	0.355	0.850	0.020	101.534
20	0.171	0.036	1.844	8.238	90.347	0.062	0.011	0.354	0.727	0.045	101.835
21	0.142	0.032	1.852	8.241	90.148	0.085	0.011	0.360	0.863	0.024	101.758
22	0.154	0.003	1.578	8.915	88.029	0.000	0.000	0.379	0.760	0.020	99.838
23	0.284	0.537	1.515	7.823	85.817	0.065	0.023	0.346	0.619	0.015	97.044
1	2.201	0.070	1.321	7.595	89.021	n/a	0.000	0.372	0.901	n/a	101.109
2	1.770	0.024	1.237	8.056	93.221	n/a	0.000	0.453	0.809	n/a	105.117
3	1.680	0.020	1.251	7.950	93.194	n/a	0.000	0.410	0.934	n/a	105.029

Point	P ₂ (CO ₃) ₂	Si(CO ₃) ₂	S(CO ₃) ₂	Mg(CO ₃)	Ca(CO ₃)	Mn(CO ₃)	Fe(CO ₃)	Sr(CO ₃)	Na ₂ (CO ₃)	K ₂ (CO ₃)	Total
4	1.717	0.040	0.929	7.995	88.804	n/a	0.060	0.385	1.315	n/a	100.860
5	1.804	0.081	0.933	8.469	90.008	n/a	0.040	0.455	1.283	n/a	102.618
6	1.762	0.035	1.052	8.869	89.388	n/a	0.000	0.386	1.091	n/a	102.197
7	1.706	0.048	1.146	8.237	94.105	n/a	0.000	0.371	0.919	n/a	106.161
8	1.866	0.076	1.000	8.250	91.764	n/a	0.032	0.374	1.119	n/a	104.107
9	1.756	0.000	1.220	8.230	91.241	n/a	0.051	0.425	1.032	n/a	103.530
10	1.796	0.045	1.008	8.479	91.686	n/a	0.004	0.398	1.040	n/a	104.058
11	1.742	0.002	1.257	8.341	93.112	n/a	0.044	0.406	0.720	n/a	105.218
12	1.652	0.047	1.055	8.786	92.003	n/a	0.028	0.412	1.098	n/a	104.669
13	1.622	0.027	1.287	7.874	93.448	n/a	0.057	0.413	0.869	n/a	105.184
14	1.722	0.043	1.170	7.674	90.914	n/a	0.069	0.382	0.951	n/a	102.543
15	1.500	0.669	1.380	8.036	87.609	n/a	0.797	0.449	0.725	n/a	100.716
16	1.763	0.053	1.339	8.483	90.607	n/a	0.067	0.390	0.852	n/a	103.164
17	1.883	0.062	1.083	8.062	91.577	n/a	0.033	0.419	0.774	n/a	103.474

Sample 3

1	1.666	0.059	1.040	7.638	90.968	n/a	0.039	0.415	1.131	n/a	102.956
2	1.813	0.042	1.090	8.508	89.681	n/a	0.004	0.393	1.095	n/a	102.626
3	1.781	0.073	1.103	8.802	90.490	n/a	0.026	0.436	1.014	n/a	103.725
4	1.686	0.022	0.981	9.309	88.574	n/a	0.011	0.340	1.028	n/a	101.951
5	1.818	0.076	1.012	8.186	90.475	n/a	0.042	0.358	1.082	n/a	103.049
6	1.948	0.105	1.048	8.276	89.946	n/a	0.004	0.407	1.136	n/a	102.870
7	2.013	0.022	1.090	8.249	90.763	n/a	0.066	0.412	0.916	n/a	103.531
8	1.643	0.007	1.107	8.600	91.186	n/a	0.000	0.404	1.026	n/a	103.973
9	1.689	0.053	1.207	8.026	91.896	n/a	0.023	0.410	0.901	n/a	104.205
10	1.850	0.069	1.125	7.961	90.345	n/a	0.068	0.391	0.937	n/a	102.746
11	1.722	0.079	1.040	8.876	89.409	n/a	0.021	0.412	1.025	n/a	102.584
12	1.722	0.059	1.221	7.752	90.395	n/a	0.015	0.389	0.855	n/a	102.408
13	1.531	0.018	1.238	7.852	90.849	n/a	0.036	0.420	0.965	n/a	102.909
14	1.571	0.019	1.286	7.987	88.710	n/a	0.038	0.453	0.794	n/a	100.858
15	1.645	0.043	1.342	8.599	90.298	n/a	0.055	0.407	0.950	n/a	103.339
16	1.714	0.013	1.387	8.797	89.940	n/a	0.055	0.429	0.849	n/a	103.184
17	1.708	0.036	1.342	8.396	90.685	n/a	0.055	0.399	0.693	n/a	103.314
18	1.605	0.060	1.207	8.062	91.000	n/a	0.032	0.388	0.744	n/a	103.098
19	1.630	0.050	1.055	8.016	90.955	n/a	0.040	0.407	0.925	n/a	103.078
20	1.851	0.063	1.389	7.910	88.775	n/a	0.014	0.414	0.922	n/a	101.338

Mytilus edulis

Sample 1

1	0.111	0.050	0.268	0.326	97.761	0.006	0.000	0.170	0.561	0.007	99.260
2	0.093	0.054	0.301	0.340	99.479	0.000	0.000	0.157	0.454	0.000	100.878
3	0.215	0.007	0.268	0.209	91.549	0.022	0.026	0.126	0.376	0.006	92.804
4	0.093	0.000	0.301	0.204	98.861	0.020	0.037	0.158	0.361	0.000	100.035
5	0.093	0.026	0.202	0.246	100.160	0.029	0.000	0.159	0.438	0.000	101.353
6	0.105	0.054	0.189	0.250	99.535	0.070	0.036	0.138	0.431	0.000	100.808
7	0.064	0.033	0.181	0.361	99.449	0.017	0.000	0.139	0.483	0.020	100.747
8	0.134	0.012	0.136	0.383	93.294	0.000	0.066	0.141	0.530	0.005	94.701
9	0.000	0.052	0.260	0.483	99.474	0.040	0.000	0.165	0.454	0.007	100.935
10	0.157	0.057	0.140	0.482	99.974	0.000	0.000	0.139	0.423	0.000	101.372
11	0.093	0.030	0.128	0.466	99.763	0.001	0.029	0.120	0.412	0.010	101.052
12	0.041	0.009	0.165	0.308	99.807	0.011	0.000	0.132	0.358	0.000	100.831
13	0.052	0.000	0.189	0.442	98.790	0.008	0.007	0.103	0.365	0.000	99.956
14	0.122	0.067	0.231	0.340	99.214	0.000	0.080	0.113	0.371	0.018	100.556
15	0.047	0.053	0.132	0.473	99.382	0.022	0.000	0.154	0.444	0.011	100.718
16	0.058	0.020	0.078	0.524	99.481	0.005	0.009	0.171	0.453	0.004	100.803
17	0.134	0.068	0.087	0.496	99.714	0.096	0.010	0.151	0.462	0.008	101.226
18	0.076	0.009	0.156	0.400	100.230	0.000	0.041	0.103	0.398	0.000	101.413
19	0.105	0.046	0.062	0.422	100.398	0.000	0.000	0.160	0.442	0.000	101.635
20	0.000	0.034	0.103	0.515	99.840	0.008	0.000	0.122	0.397	0.001	101.020

Point	P ₂ (CO ₃) ₃	Si(CO ₃) ₂	S(CO ₃) ₂	Mg(CO ₃)	Ca(CO ₃)	Mn(CO ₃)	Fe(CO ₃)	Sr(CO ₃)	Na ₂ (CO ₃)	K ₂ (CO ₃)	Total
21	0.023	0.026	0.169	0.473	100.258	0.012	0.017	0.119	0.357	0.003	101.457
22	0.163	0.036	0.185	0.451	100.274	0.041	0.009	0.096	0.308	0.000	101.563
23	0.087	0.028	0.218	0.407	99.965	0.000	0.000	0.114	0.290	0.000	101.109
24	0.000	0.027	0.169	0.365	100.903	0.022	0.008	0.124	0.344	0.000	101.962
25	0.093	0.017	0.132	0.361	100.187	0.012	0.000	0.132	0.286	0.000	101.220
26	0.105	0.047	0.128	0.328	100.665	0.040	0.050	0.182	0.301	0.000	101.846
27	0.029	0.037	0.128	0.325	100.111	0.000	0.004	0.141	0.330	0.000	101.105
28	0.052	0.000	0.078	0.310	100.325	0.028	0.000	0.091	0.315	0.003	101.202
29	0.058	0.033	0.070	0.436	101.186	0.027	0.010	0.156	0.341	0.000	102.317
30	0.070	0.060	0.049	0.336	100.298	0.018	0.000	0.136	0.269	0.000	101.236
31	0.029	0.027	0.041	0.425	100.241	0.061	0.000	0.071	0.267	0.000	101.162
32	0.122	0.010	0.095	0.374	99.808	0.000	0.007	0.128	0.274	0.016	100.834
33	0.111	0.023	0.210	0.444	100.089	0.048	0.000	0.132	0.258	0.009	101.324
34	0.087	0.017	0.309	0.522	92.354	0.022	0.050	0.129	0.255	0.000	93.745
35	0.047	0.034	0.305	0.688	100.520	0.000	0.000	0.135	0.240	0.001	101.970
36	0.116	0.046	0.235	0.384	100.269	0.000	0.038	0.131	0.228	0.011	101.458
37	0.064	0.019	0.140	0.377	100.815	0.000	0.001	0.157	0.285	0.000	101.858
38	0.070	0.013	0.111	0.288	100.751	0.013	0.004	0.142	0.259	0.000	101.651
39	0.047	0.008	0.103	0.319	100.305	0.000	0.000	0.115	0.262	0.020	101.179
40	0.017	0.026	0.128	0.369	100.849	0.000	0.003	0.135	0.259	0.000	101.786
41	0.000	0.018	0.161	0.464	100.567	0.000	0.000	0.133	0.278	0.003	101.624
42	0.006	0.000	0.119	0.423	98.883	0.060	0.055	0.106	0.216	0.000	99.868
43	0.099	0.024	0.454	1.102	99.034	0.088	0.001	0.131	0.201	0.010	101.144
44	0.105	0.007	0.598	0.887	99.052	0.000	0.003	0.153	0.129	0.000	100.934
45	0.111	0.045	0.144	0.004	97.931	0.002	0.000	0.213	1.003	0.021	99.474
46	0.146	0.038	0.285	0.003	97.091	0.000	0.000	0.254	1.072	0.005	98.894

1	0.186	0.055	0.371	0.284	96.744	0.000	0.000	0.210	0.933	0.000	98.783
2	0.093	0.012	0.297	0.192	89.941	0.000	0.020	0.174	0.792	0.000	91.521
3	0.128	0.037	0.313	0.223	97.811	0.000	0.009	0.143	0.695	0.006	99.365
4	0.122	0.045	0.078	0.263	89.132	0.066	0.009	0.147	0.677	0.001	90.540
5	0.134	0.039	0.132	0.341	98.369	0.001	0.014	0.166	0.630	0.000	99.826
6	0.047	0.000	0.181	0.341	95.186	0.012	0.011	0.147	0.569	0.000	96.494
7	0.023	0.000	0.149	0.354	99.332	0.000	0.000	0.171	0.630	0.000	100.659
8	0.041	0.046	0.161	0.325	92.764	0.000	0.031	0.127	0.683	0.000	94.178
9	0.099	0.000	0.128	0.405	96.698	0.000	0.033	0.161	0.624	0.000	98.148
10	0.152	0.017	0.140	0.390	99.729	0.000	0.028	0.164	0.626	0.003	101.249
11	0.047	0.000	0.161	0.394	99.359	0.000	0.007	0.158	0.649	0.000	100.775
12	0.064	0.000	0.058	0.414	99.215	0.116	0.009	0.139	0.684	0.000	100.699
13	0.146	0.017	0.095	0.343	89.266	0.000	0.027	0.149	0.663	0.001	90.707
14	0.082	0.017	0.120	0.460	99.256	0.000	0.016	0.143	0.692	0.000	100.786
15	0.198	0.028	0.091	0.410	99.119	0.000	0.000	0.188	0.670	0.000	100.704
16	0.082	0.046	0.049	0.432	99.217	0.043	0.002	0.159	0.701	0.018	100.749
17	0.047	0.014	0.050	0.413	99.466	0.076	0.000	0.157	0.713	0.000	100.936
18	0.116	0.031	0.115	0.335	99.184	0.024	0.007	0.188	0.639	0.000	100.639
19	0.064	0.025	0.091	0.342	90.055	0.000	0.000	0.113	0.679	0.000	91.369
20	0.000	0.039	0.070	0.359	86.320	0.054	0.000	0.152	0.683	0.000	87.677
21	0.087	0.018	0.058	0.371	99.333	0.000	0.025	0.122	0.570	0.005	100.589
22	0.041	0.026	0.091	0.503	99.515	0.023	0.029	0.177	0.534	0.005	100.944
23	0.017	0.023	0.066	0.434	99.798	0.008	0.000	0.152	0.461	0.008	100.967
24	0.111	0.007	0.087	0.439	99.747	0.000	0.027	0.134	0.423	0.000	100.975
25	0.082	0.001	0.054	0.477	98.706	0.027	0.066	0.125	0.446	0.021	100.005
26	0.093	0.029	0.029	0.525	99.133	0.053	0.009	0.143	0.451	0.015	100.480
27	0.000	0.000	0.136	0.546	99.015	0.000	0.000	0.150	0.436	0.005	100.288
28	0.012	0.034	0.107	0.493	99.561	0.070	0.033	0.123	0.430	0.003	100.866
29	0.017	0.020	0.062	0.392	100.000	0.000	0.000	0.139	0.387	0.014	101.031
30	0.058	0.000	0.012	0.391	99.169	0.017	0.031	0.093	0.389	0.000	100.160
31	0.111	0.020	0.078	0.442	99.103	0.013	0.025	0.143	0.423	0.000	100.358

Point	P ₂ (CO ₃) ₅	Si(CO ₃) ₂	S(CO ₃) ₂	Mg(CO ₃)	Ca(CO ₃)	Mn(CO ₃)	Fe(CO ₃)	Sr(CO ₃)	Na ₂ (CO ₃)	K ₂ (CO ₃)	Total
32	0.099	0.037	0.045	0.403	99.668	0.000	0.010	0.132	0.349	0.000	100.743
33	0.087	0.000	0.103	0.421	99.588	0.006	0.000	0.139	0.376	0.003	100.723
34	0.058	0.018	0.103	0.558	98.961	0.006	0.007	0.145	0.417	0.000	100.273
35	0.041	0.000	0.037	0.479	98.243	0.000	0.050	0.127	0.375	0.000	99.352
36	0.111	0.019	0.058	0.338	100.066	0.012	0.032	0.104	0.310	0.008	101.058
37	0.000	0.002	0.095	0.429	98.662	0.000	0.038	0.094	0.292	0.007	99.619
38	0.058	0.041	0.181	0.425	99.507	0.043	0.007	0.128	0.245	0.000	100.635
39	0.123	0.049	0.326	0.152	97.688	0.002	0.000	0.282	0.724	0.000	99.346
40	0.018	0.008	0.326	0.054	96.634	0.030	0.033	0.441	1.191	0.021	98.756
41	0.018	0.000	0.331	0.018	96.642	0.052	0.116	0.231	1.165	0.018	98.591
42	0.053	0.026	0.165	0.037	92.121	0.043	0.045	0.551	1.013	0.001	94.055
43	0.099	0.010	0.339	0.057	78.285	0.000	0.017	0.320	1.021	0.003	80.151
44	0.093	0.000	0.199	0.049	71.560	0.027	0.042	0.364	0.946	0.000	73.280
45	0.018	0.000	0.318	0.062	79.932	0.000	0.050	0.344	1.056	0.014	81.794
46	0.111	0.008	0.244	0.065	96.350	0.000	0.019	0.515	1.102	0.000	98.414
47	0.134	0.153	0.235	0.043	88.510	0.043	0.029	0.269	0.709	0.004	90.129
1	0.198	0.005	0.537	0.265	96.848	0.039	0.000	0.218	0.942	0.000	99.052
2	0.093	0.002	0.430	0.208	98.503	0.103	0.000	0.194	0.955	0.000	100.488
3	0.093	0.017	0.380	0.224	98.429	0.000	0.000	0.223	1.027	0.007	100.400
4	0.058	0.056	0.343	0.326	97.973	0.062	0.024	0.185	0.984	0.000	100.011
5	0.163	0.000	0.215	0.369	98.808	0.000	0.004	0.181	0.938	0.000	100.678
6	0.064	0.008	0.252	0.360	98.749	0.000	0.000	0.145	0.962	0.010	100.550
7	0.158	0.043	0.128	0.347	97.596	0.028	0.034	0.213	1.020	0.000	99.567
8	0.070	0.047	0.194	0.369	98.262	0.000	0.015	0.137	0.958	0.000	100.052
9	0.076	0.014	0.194	0.393	98.516	0.065	0.000	0.135	0.955	0.000	100.348
10	0.029	0.060	0.194	0.360	98.459	0.017	0.000	0.172	0.880	0.000	100.171
11	0.233	0.055	0.203	0.371	99.333	0.000	0.000	0.190	0.883	0.009	101.277
12	0.140	0.000	0.149	0.369	98.730	0.000	0.000	0.190	0.915	0.000	100.493
13	0.105	0.023	0.103	0.398	99.023	0.039	0.052	0.193	0.816	0.007	100.759
14	0.070	0.020	0.202	0.367	98.738	0.000	0.000	0.209	0.873	0.000	100.479
15	0.070	0.019	0.128	0.370	98.648	0.001	0.000	0.150	0.769	0.000	100.155
16	0.111	0.035	0.231	0.369	98.791	0.007	0.000	0.167	0.786	0.008	100.505
17	0.076	0.026	0.248	0.376	98.482	0.000	0.013	0.205	0.762	0.000	100.188
18	0.140	0.054	0.273	0.343	98.747	0.000	0.000	0.146	0.776	0.014	100.493
19	0.076	0.000	0.157	0.391	99.013	0.010	0.000	0.140	0.818	0.007	100.612
20	0.047	0.083	0.078	0.359	99.369	0.000	0.000	0.145	0.763	0.001	100.845
21	0.058	0.000	0.145	0.375	98.997	0.000	0.000	0.178	0.761	0.000	100.514
22	0.070	0.030	0.132	0.383	99.094	0.046	0.000	0.175	0.699	0.000	100.629
23	0.111	0.000	0.182	0.399	98.659	0.034	0.000	0.209	0.704	0.012	100.310
24	0.187	0.069	0.153	0.384	99.245	0.005	0.007	0.149	0.684	0.000	100.883
25	0.146	0.003	0.140	0.438	99.485	0.078	0.000	0.175	0.650	0.014	101.129
26	0.204	0.000	0.124	0.447	99.841	0.001	0.027	0.124	0.592	0.025	101.385
27	0.088	0.041	0.211	0.548	99.317	0.000	0.026	0.141	0.583	0.000	100.955
28	0.210	0.039	0.161	0.469	99.838	0.000	0.021	0.171	0.576	0.000	101.485
29	0.076	0.000	0.211	0.493	99.528	0.001	0.004	0.156	0.566	0.000	101.035
30	0.093	0.037	0.116	0.560	99.530	0.000	0.033	0.154	0.501	0.000	101.024
31	0.169	0.030	0.186	0.518	99.210	0.012	0.021	0.130	0.472	0.000	100.748
32	0.058	0.051	0.128	0.434	99.547	0.000	0.005	0.167	0.405	0.000	100.795
33	0.012	0.053	0.128	0.540	99.867	0.025	0.011	0.165	0.430	0.006	101.237
34	0.023	0.047	0.153	0.568	100.079	0.014	0.000	0.148	0.491	0.008	101.531
35	0.239	0.000	0.145	0.476	99.619	0.000	0.056	0.131	0.441	0.005	101.112
36	0.035	0.004	0.194	0.462	99.755	0.000	0.001	0.139	0.455	0.000	101.045
37	0.187	0.026	0.169	0.562	99.399	0.010	0.000	0.111	0.442	0.010	100.916
38	0.099	0.066	0.116	0.537	99.319	0.070	0.041	0.130	0.385	0.000	100.763
39	0.087	0.000	0.153	0.650	99.210	0.080	0.047	0.117	0.317	0.001	100.662
40	0.070	0.020	0.235	0.596	99.325	0.081	0.000	0.176	0.292	0.000	100.795
41	0.029	0.006	0.318	0.452	99.470	0.000	0.000	0.151	0.270	0.000	100.696

Point	P ₂ (CO ₃) ₂	Si(CO ₃) ₂	S(CO ₃) ₂	Mg(CO ₃)	Ca(CO ₃)	Mn(CO ₃)	Fe(CO ₃)	Sr(CO ₃)	Na ₂ (CO ₃)	K ₂ (CO ₃)	Total
42	0.105	0.035	0.211	0.015	96.815	0.008	0.027	0.210	1.124	0.000	98.550
43	0.000	0.000	0.194	0.068	94.973	0.000	0.049	0.417	1.012	0.023	96.736
44	0.064	0.042	0.170	0.001	82.681	0.002	0.035	0.202	1.117	0.000	84.314
45	0.018	0.000	0.165	0.009	75.058	0.000	0.039	0.181	1.012	0.000	76.482
46	0.012	0.000	0.207	0.014	73.740	0.000	0.010	0.157	1.025	0.009	75.174
47	0.023	0.004	0.161	0.037	68.905	0.072	0.023	0.171	0.977	0.000	70.373
48	0.053	0.029	0.174	0.000	65.402	0.022	0.012	0.158	0.981	0.002	66.833
49	0.053	0.016	0.228	0.087	68.057	0.000	0.047	0.165	1.000	0.009	69.662
50	0.058	0.000	0.244	0.026	66.059	0.007	0.032	0.214	0.942	0.003	67.585
51	0.064	0.009	0.203	0.044	65.959	0.000	0.002	0.413	1.021	0.011	67.726
52	0.082	0.000	0.253	0.055	64.655	0.054	0.033	0.205	0.979	0.000	66.316
53	0.000	0.000	0.236	0.003	62.601	0.006	0.000	0.134	0.997	0.000	63.977
54	0.000	0.018	0.145	0.070	59.284	0.000	0.044	0.243	0.910	0.000	60.714
55	0.041	0.049	0.137	0.075	61.961	0.000	0.003	0.315	0.938	0.005	63.524
56	0.023	0.000	0.195	0.051	61.892	0.000	0.000	0.268	0.916	0.013	63.358
57	0.023	0.046	0.232	0.054	61.500	0.000	0.003	0.207	0.952	0.000	63.017
58	0.088	0.007	0.191	0.080	59.131	0.029	0.029	0.250	0.895	0.000	60.700
59	0.041	0.034	0.170	0.059	62.343	0.000	0.002	0.295	0.934	0.000	63.878
60	0.041	0.001	0.137	0.066	58.254	0.004	0.001	0.235	0.913	0.000	59.652
61	0.041	0.000	0.128	0.037	61.046	0.008	0.011	0.336	0.952	0.006	62.565
62	0.000	0.030	0.265	0.084	61.416	0.000	0.000	0.267	0.947	0.002	63.011
63	0.059	0.002	0.087	0.145	63.506	0.007	0.000	0.363	0.994	0.000	65.163
64	0.082	0.022	0.178	0.104	79.211	0.039	0.017	0.549	1.002	0.007	81.211
65	0.023	0.005	0.157	0.091	75.098	0.000	0.039	0.259	0.954	0.023	76.649
66	0.012	0.007	0.174	0.064	81.919	0.000	0.010	0.242	1.084	0.000	83.512
67	0.023	0.019	0.323	0.077	97.360	0.000	0.046	0.357	0.996	0.019	99.220

1	0.012	0.046	0.342	0.198	99.636	0.010	0.002	0.163	0.766	0.000	101.175
2	0.064	0.019	0.165	0.174	100.433	0.016	0.025	0.201	0.885	0.009	101.991
3	0.041	0.000	0.223	0.196	84.949	0.000	0.000	0.140	0.767	0.025	86.341
4	0.140	0.029	0.268	0.213	100.367	0.016	0.000	0.138	0.778	0.009	101.958
5	0.029	0.003	0.198	0.264	100.525	0.025	0.009	0.163	0.712	0.010	101.938
6	0.105	0.004	0.194	0.304	100.747	0.035	0.014	0.173	0.686	0.002	102.264
7	0.035	0.029	0.239	0.301	100.660	0.000	0.000	0.172	0.663	0.001	102.100
8	0.052	0.020	0.227	0.352	100.323	0.046	0.013	0.174	0.733	0.022	101.962
9	0.070	0.029	0.115	0.387	99.374	0.030	0.000	0.142	0.699	0.000	100.846
10	0.070	0.044	0.161	0.470	100.125	0.049	0.009	0.151	0.638	0.000	101.717
11	0.099	0.000	0.087	0.388	98.901	0.000	0.066	0.143	0.709	0.007	100.400
12	0.029	0.020	0.103	0.399	99.852	0.000	0.022	0.176	0.647	0.000	101.248
13	0.105	0.000	0.095	0.394	80.815	0.000	0.000	0.134	0.700	0.005	82.248
14	0.035	0.074	0.115	0.299	100.670	0.000	0.000	0.140	0.653	0.007	101.993
15	0.117	1.303	0.153	0.457	99.239	0.000	0.162	0.136	0.689	0.022	102.278
16	0.035	0.020	0.041	0.420	99.220	0.060	0.065	0.103	0.733	0.000	100.697
17	0.076	0.006	0.132	0.443	99.948	0.000	0.014	0.143	0.683	0.025	101.470
18	0.058	0.076	0.115	0.377	100.132	0.000	0.014	0.107	0.612	0.000	101.491
19	0.000	0.034	0.074	0.393	100.365	0.000	0.036	0.141	0.622	0.000	101.665
20	0.081	0.045	0.132	0.416	100.853	0.144	0.027	0.131	0.675	0.000	102.504
21	0.076	0.021	0.132	0.404	101.180	0.076	0.037	0.153	0.660	0.000	102.739
22	0.064	0.012	0.000	0.448	100.911	0.008	0.017	0.144	0.589	0.000	102.193
23	0.076	0.000	0.025	0.426	95.771	0.005	0.000	0.140	0.582	0.000	97.025
24	0.099	0.017	0.111	0.425	100.022	0.096	0.034	0.142	0.519	0.012	101.477
25	0.145	0.022	0.070	0.395	100.573	0.007	0.000	0.126	0.497	0.000	101.835
26	0.064	0.000	0.128	0.411	100.912	0.006	0.000	0.124	0.549	0.000	102.194
27	0.058	0.000	0.111	0.389	100.053	0.033	0.000	0.118	0.538	0.000	101.300
28	0.000	0.000	0.037	0.500	100.404	0.030	0.027	0.190	0.495	0.014	101.697
29	0.087	0.034	0.066	0.443	100.475	0.000	0.002	0.148	0.456	0.000	101.711
30	0.000	0.000	0.103	0.480	101.027	0.029	0.000	0.137	0.441	0.000	102.217
31	0.116	0.020	0.136	0.571	100.563	0.000	0.028	0.138	0.416	0.007	101.995

Point	P ₂ (CO ₃) ₂	Si(CO ₃) ₂	S(CO ₃) ₂	Mg(CO ₃)	Ca(CO ₃)	Mn(CO ₃)	Fe(CO ₃)	Sr(CO ₃)	Na ₂ (CO ₃)	K ₂ (CO ₃)	Total
32	0.076	0.025	0.132	0.592	100.616	0.000	0.023	0.126	0.409	0.000	101.999
33	0.041	0.020	0.099	0.505	100.879	0.099	0.017	0.160	0.357	0.000	102.177
34	0.035	0.000	0.091	0.371	85.348	0.000	0.000	0.144	0.350	0.000	86.339
35	0.046	0.015	0.066	0.389	100.782	0.047	0.048	0.084	0.369	0.009	101.855
36	0.093	0.038	0.095	0.442	100.797	0.004	0.000	0.138	0.339	0.001	101.947
37	0.128	0.059	0.082	0.421	100.741	0.043	0.003	0.105	0.300	0.000	101.882
38	0.029	0.023	0.115	0.494	100.818	0.000	0.000	0.150	0.344	0.006	101.979
39	0.157	0.034	0.124	0.469	100.699	0.076	0.012	0.110	0.338	0.000	102.019
40	0.128	0.020	0.120	0.371	100.709	0.000	0.070	0.150	0.277	0.013	101.858
41	0.128	0.077	0.293	0.253	98.627	0.077	0.000	0.190	0.685	0.004	100.334
42	0.099	0.028	0.326	0.043	97.425	0.019	0.002	0.597	1.115	0.004	99.658
43	0.023	0.021	0.338	0.042	94.749	0.000	0.000	0.246	1.113	0.012	96.544
44	0.000	0.026	0.285	0.051	74.092	0.033	0.039	0.339	1.003	0.000	75.868
45	0.035	0.033	0.190	0.002	73.458	0.000	0.017	0.329	1.028	0.008	75.100
46	0.099	0.012	0.169	0.034	69.352	0.031	0.041	0.386	0.959	0.000	71.083
47	0.041	0.023	0.165	0.048	71.198	0.000	0.019	0.366	1.035	0.010	72.905
48	0.076	0.000	0.235	0.044	84.135	0.014	0.000	0.376	1.010	0.018	85.908
49	0.140	0.055	0.223	0.036	96.137	0.000	0.000	0.514	1.029	0.000	98.134
50	0.023	0.008	0.268	0.048	96.876	0.001	0.000	0.445	1.061	0.020	98.750

1	0.117	0.009	0.208	0.207	98.116	0.000	0.000	0.225	0.698	0.000	99.580
2	0.134	0.021	0.248	0.247	98.581	0.000	0.000	0.172	0.725	0.000	100.128
3	0.064	0.019	0.214	0.248	97.857	0.033	0.000	0.157	0.782	0.000	99.374
4	0.093	0.034	0.227	0.218	97.947	0.016	0.000	0.152	0.843	0.001	99.531
5	0.064	0.005	0.379	0.298	98.035	0.047	0.000	0.139	0.797	0.000	99.764
6	0.139	0.002	0.202	0.230	98.283	0.048	0.000	0.194	0.732	0.000	99.830
7	0.000	0.042	0.157	0.296	98.397	0.000	0.045	0.186	0.816	0.016	99.955
8	0.012	0.016	0.179	0.300	85.350	0.000	0.032	0.179	0.817	0.020	86.905
9	0.087	0.015	0.197	0.334	98.611	0.000	0.007	0.192	0.741	0.007	100.191
10	0.110	0.059	0.193	0.419	98.651	0.018	0.000	0.183	0.636	0.000	100.269
11	0.070	0.022	0.210	0.478	98.790	0.107	0.002	0.170	0.624	0.018	100.491
12	0.070	0.056	0.198	0.454	98.788	0.000	0.015	0.161	0.624	0.001	100.367
13	0.117	0.011	0.153	0.468	99.442	0.000	0.030	0.170	0.654	0.000	101.045
14	0.198	0.022	0.120	0.420	99.442	0.069	0.011	0.177	0.590	0.030	101.079
15	0.023	0.000	0.215	0.402	98.782	0.089	0.007	0.131	0.616	0.001	100.266
16	0.041	0.025	0.070	0.391	99.480	0.022	0.000	0.144	0.643	0.000	100.816
17	0.093	0.058	0.095	0.379	99.756	0.000	0.000	0.134	0.579	0.007	101.101
18	0.111	0.005	0.103	0.434	99.262	0.049	0.026	0.163	0.600	0.005	100.758
19	0.023	0.032	0.107	0.500	98.804	0.060	0.064	0.155	0.596	0.019	100.360
20	0.128	0.055	0.177	0.523	100.030	0.010	0.025	0.146	0.589	0.010	101.693
21	0.087	0.000	0.099	0.460	99.253	0.008	0.017	0.178	0.528	0.000	100.630
22	0.087	0.028	0.161	0.550	99.050	0.037	0.000	0.141	0.496	0.016	100.566
23	0.093	0.023	0.091	0.452	99.188	0.049	0.000	0.148	0.491	0.014	100.549
24	0.017	0.027	0.049	0.431	99.259	0.008	0.007	0.132	0.483	0.018	100.431
25	0.087	0.045	0.140	0.482	99.073	0.029	0.000	0.148	0.511	0.000	100.515
26	0.076	0.025	0.025	0.552	99.599	0.045	0.012	0.139	0.557	0.000	101.030
27	0.087	0.056	0.107	0.429	98.607	0.000	0.021	0.106	0.487	0.010	99.910
28	0.064	0.000	0.066	0.439	99.349	0.000	0.030	0.152	0.468	0.000	100.568
29	0.047	0.000	0.140	0.530	100.079	0.005	0.004	0.152	0.439	0.000	101.396
30	0.105	0.051	0.041	0.506	99.834	0.000	0.000	0.129	0.446	0.000	101.112
31	0.070	0.042	0.132	0.541	100.036	0.071	0.000	0.139	0.409	0.014	101.454
32	0.064	0.005	0.116	0.579	100.016	0.018	0.012	0.141	0.401	0.012	101.364
33	0.070	0.057	0.095	0.443	100.743	0.011	0.000	0.086	0.291	0.000	101.796
34	0.128	0.018	0.087	0.397	100.144	0.010	0.050	0.104	0.284	0.008	101.230
35	0.064	0.027	0.371	0.560	100.738	0.070	0.011	0.101	0.226	0.003	102.171
36	0.099	0.013	0.273	0.040	96.389	0.007	0.056	0.466	0.955	0.010	98.308
37	0.140	0.034	0.294	0.063	89.222	0.000	0.043	0.322	1.016	0.015	91.149
38	0.029	0.000	0.302	0.030	87.194	0.041	0.035	0.296	1.142	0.016	89.085

Point	P ₂ (CO ₃) ₂	Si(CO ₃) ₂	S(CO ₃) ₂	Mg(CO ₃) ₂	Ca(CO ₃) ₂	Mn(CO ₃) ₂	Fe(CO ₃) ₂	Sr(CO ₃) ₂	Na ₂ (CO ₃) ₂	K ₂ (CO ₃) ₂	Total
39	0.105	0.000	0.231	0.031	76.452	0.075	0.020	0.209	1.110	0.000	78.233
40	0.053	0.047	0.227	0.106	70.025	0.002	0.019	0.339	0.954	0.005	71.777
41	0.029	0.000	0.290	0.034	73.170	0.018	0.016	0.310	1.077	0.015	74.959
42	0.012	0.034	0.248	0.056	69.303	0.006	0.031	0.396	0.993	0.026	71.105
43	0.088	0.075	0.191	0.068	80.741	0.000	0.025	0.378	1.037	0.000	82.603
44	0.041	0.035	0.227	0.067	97.234	0.034	0.071	0.317	1.019	0.010	99.055
45	0.134	0.011	0.232	0.087	96.447	0.013	0.003	0.473	1.088	0.010	98.498
46	0.163	0.038	0.248	0.057	96.565	0.000	0.000	0.472	1.036	0.017	98.596

Sample 2

1	1.328	0.098	0.408	0.275	97.743	0.002	0.000	0.070	1.373	0.023	101.320
2	1.187	0.083	0.323	0.222	99.229	0.000	0.051	0.183	1.190	0.000	102.468
3	1.140	0.095	0.359	0.364	100.710	0.009	0.000	0.189	1.252	0.017	104.135
4	1.194	0.031	0.246	0.467	98.200	0.018	0.016	0.182	1.328	0.000	101.682
5	1.110	0.064	0.540	0.395	100.232	0.000	0.000	0.215	1.184	0.001	103.741
6	1.152	0.036	0.424	0.473	100.483	0.000	0.014	0.244	1.269	0.001	104.096
7	1.159	0.024	0.282	0.514	99.508	0.000	0.000	0.197	1.392	0.001	103.077
8	1.145	0.033	0.343	0.506	99.949	0.016	0.007	0.172	1.285	0.024	103.480
9	1.150	0.076	0.319	0.541	99.435	0.000	0.033	0.210	1.350	0.000	103.114
10	1.150	0.033	0.420	0.567	100.224	0.000	0.061	0.186	1.274	0.007	103.922
11	1.124	0.033	0.424	0.558	100.188	0.027	0.051	0.169	1.234	0.004	103.812
12	1.114	0.049	0.355	0.567	99.074	0.000	0.036	0.176	1.186	0.025	102.582
13	1.152	0.094	0.246	0.521	99.590	0.022	0.076	0.169	1.192	0.016	103.078
14	1.120	0.125	0.307	0.541	98.473	0.011	0.000	0.218	1.239	0.015	102.049
15	1.150	0.068	0.291	0.551	99.262	0.008	0.052	0.184	1.129	0.023	102.718
16	1.188	0.052	0.234	0.459	99.818	0.000	0.007	0.146	1.147	0.028	103.079
17	1.151	0.045	0.234	0.454	99.740	0.000	0.000	0.213	1.045	0.000	102.882
18	1.175	0.049	0.165	0.387	99.540	0.000	0.000	0.148	0.909	0.000	102.373
19	1.229	0.021	0.165	0.255	99.609	0.000	0.011	0.177	0.711	0.010	102.188
20	1.162	0.003	0.113	0.000	97.419	0.000	0.038	0.169	1.370	0.009	100.283
21	1.145	0.044	0.165	0.000	98.713	0.023	0.000	0.256	1.292	0.000	101.638
22	1.162	0.076	0.222	0.000	98.092	0.000	0.018	0.191	1.333	0.007	101.101
23	1.078	0.098	0.270	0.000	99.349	0.051	0.023	0.148	1.396	0.000	102.413
24	1.081	0.067	0.161	0.000	98.519	0.000	0.013	0.170	1.283	0.020	101.314
25	1.135	0.019	0.282	0.068	98.359	0.009	0.025	0.160	1.224	0.000	101.281
26	1.126	0.006	0.303	0.045	97.942	0.000	0.027	0.137	1.238	0.015	100.839
27	0.469	0.468	0.491	0.048	29.805	0.000	0.137	0.123	0.599	0.063	32.203
28	0.691	0.067	0.194	0.002	64.150	0.044	0.000	0.131	0.884	0.009	66.172
29	1.075	0.007	0.238	0.000	95.532	0.000	0.063	0.149	1.337	0.006	98.407
30	1.095	0.090	0.235	0.000	96.952	0.000	0.072	0.156	1.428	0.010	100.038
31	1.147	0.013	0.182	0.000	97.761	0.000	0.000	0.004	1.303	0.000	100.410
32	1.114	0.081	0.271	0.000	96.764	0.000	0.024	0.001	1.312	0.009	99.576
33	1.084	0.065	0.247	0.000	97.012	0.029	0.051	0.011	1.478	0.006	99.983

Avian Eggshell (*Gallus gallus*)

Sample 1

1	2.059	0.129	0.099	2.056	92.938	0.028	0.026	0.096	0.206	0.118	97.755
2	1.125	0.086	0.112	1.901	93.691	0.039	0.000	0.092	0.167	0.109	97.322
3	0.724	0.010	0.066	2.037	94.733	0.010	0.031	0.072	0.137	0.070	97.890
4	0.496	0.007	0.070	1.891	94.874	0.000	0.000	0.099	0.134	0.061	97.632
5	0.454	0.050	0.058	1.604	95.972	0.019	0.000	0.112	0.128	0.067	98.464
6	0.423	0.654	0.033	1.744	91.813	0.029	0.091	0.076	0.122	0.078	95.063
7	0.513	0.104	0.120	1.288	95.708	0.000	0.000	0.052	0.147	0.050	97.982
8	0.297	0.150	0.091	1.168	95.091	0.000	0.000	0.073	0.122	0.064	97.056
9	0.309	0.029	0.091	1.167	96.820	0.000	0.000	0.037	0.158	0.074	98.685
10	0.350	0.458	0.062	0.742	92.336	0.028	0.029	0.000	0.124	0.042	94.171
11	0.140	1.333	0.124	0.808	79.329	0.000	0.048	0.071	0.190	0.018	82.061
12	0.157	0.017	0.033	0.525	98.844	0.000	0.015	0.056	0.195	0.020	99.862
13	0.204	1.408	0.409	0.332	82.930	0.029	0.013	0.024	0.201	0.010	85.560
14	0.099	0.000	0.078	0.307	97.744	0.025	0.000	0.039	0.310	0.014	98.616

Point	P ₂ (CO ₃) ₅	Si(CO ₃) ₂	S(CO ₃) ₂	Mg(CO ₃)	Ca(CO ₃)	Mn(CO ₃)	Fe(CO ₃)	Sr(CO ₃)	Na ₂ (CO ₃)	K ₂ (CO ₃)	Total
15	0.023	0.075	0.082	0.470	97.500	0.000	0.000	0.037	0.320	0.020	98.527
16	0.017	0.011	0.062	0.868	96.042	0.000	0.000	0.056	0.442	0.000	97.498
17	0.000	0.154	0.128	1.363	94.384	0.000	0.000	0.031	0.506	0.010	96.576
1	1.940	0.031	0.062	2.026	94.387	0.000	0.053	0.076	0.173	0.107	98.855
2	1.039	0.027	0.074	2.112	94.802	0.006	0.000	0.113	0.137	0.068	98.378
3	0.665	0.046	0.079	1.804	94.831	0.039	0.000	0.065	0.142	0.104	97.775
4	0.181	0.167	0.137	0.687	37.032	0.024	0.021	0.049	0.054	0.031	38.383
5	0.431	0.029	0.074	1.609	94.754	0.023	0.000	0.075	0.124	0.043	97.162
6	0.356	0.045	0.165	1.352	95.016	0.036	0.000	0.086	0.153	0.093	97.302
7	0.403	0.043	0.116	1.245	95.873	0.000	0.000	0.086	0.122	0.057	97.945
8	0.380	0.072	0.128	1.189	95.100	0.005	0.027	0.051	0.131	0.049	97.132
9	0.321	0.014	0.058	1.083	96.492	0.040	0.000	0.057	0.126	0.081	98.272
10	0.262	0.033	0.087	1.087	95.419	0.040	0.015	0.007	0.153	0.069	97.172
11	0.362	0.387	0.045	0.893	96.944	0.000	0.000	0.048	0.153	0.044	98.876
12	0.192	0.129	0.041	0.541	97.747	0.068	0.000	0.031	0.201	0.028	98.978
13	0.192	0.052	0.004	0.404	97.283	0.006	0.023	0.043	0.265	0.021	98.293
14	0.093	1.707	0.186	0.301	86.860	0.000	0.134	0.035	0.276	0.033	89.625
15	0.093	0.020	0.103	0.652	97.722	0.019	0.000	0.064	0.369	0.033	99.075
16	0.017	0.056	0.033	0.824	94.514	0.021	0.022	0.057	0.323	0.000	95.867
17	0.152	0.074	0.562	1.515	89.738	0.005	0.003	0.034	0.682	0.000	92.765
1	2.331	0.121	0.133	2.040	94.097	0.042	0.001	0.062	0.168	0.090	99.085
2	1.021	0.034	0.045	2.071	94.703	0.000	0.025	0.074	0.168	0.083	98.224
3	0.718	0.049	0.000	1.974	95.941	0.000	0.024	0.094	0.177	0.094	99.071
4	0.546	0.008	0.071	1.832	95.218	0.030	0.000	0.071	0.146	0.088	98.010
5	0.508	0.064	0.128	1.532	95.730	0.017	0.000	0.066	0.177	0.101	98.323
6	0.437	0.005	0.145	1.452	95.147	0.000	0.053	0.048	0.153	0.065	97.505
7	0.449	0.076	0.074	1.193	93.769	0.000	0.000	0.055	0.123	0.062	95.801
8	0.332	0.031	0.025	1.307	96.606	0.000	0.000	0.068	0.125	0.073	98.567
9	0.134	0.023	0.045	1.184	96.158	0.050	0.013	0.024	0.146	0.076	97.853
10	0.146	0.142	0.173	0.505	45.350	0.000	0.007	0.033	0.071	0.024	46.451
11	0.181	0.020	0.041	1.137	98.169	0.000	0.000	0.070	0.125	0.055	99.798
12	0.163	0.000	0.082	0.819	98.142	0.072	0.000	0.049	0.145	0.017	99.489
13	0.233	0.010	0.054	0.663	98.615	0.013	0.007	0.020	0.193	0.012	99.820
14	0.105	0.007	0.132	0.508	99.331	0.011	0.005	0.087	0.222	0.028	100.436
15	0.047	0.335	0.000	0.517	98.860	0.000	0.004	0.077	0.192	0.007	100.039
16	0.070	0.101	0.116	0.612	97.531	0.000	0.033	0.037	0.391	0.018	98.909
1	2.092	0.034	0.129	2.152	94.089	0.027	0.000	0.089	0.177	0.075	98.864
2	1.144	0.054	0.149	2.044	93.556	0.000	0.000	0.087	0.196	0.100	97.330
3	0.339	0.044	0.153	1.030	50.267	0.000	0.000	0.074	0.082	0.032	52.021
4	0.646	4.047	0.004	1.751	92.520	0.005	0.000	0.056	0.170	0.063	99.262
5	0.555	0.031	0.095	1.554	95.704	0.056	0.007	0.065	0.168	0.105	98.340
6	0.607	0.029	0.108	1.528	94.975	0.011	0.000	0.063	0.133	0.074	97.528
7	0.297	0.038	0.091	1.332	95.461	0.008	0.014	0.057	0.102	0.090	97.490
8	0.498	0.026	0.091	1.237	95.688	0.041	0.000	0.027	0.130	0.088	97.826
9	0.378	0.023	0.070	1.101	95.810	0.000	0.000	0.042	0.147	0.048	97.619
10	0.356	0.065	0.112	0.904	96.224	0.019	0.000	0.038	0.120	0.034	97.872
11	0.210	0.010	0.074	0.812	97.132	0.018	0.000	0.048	0.124	0.039	98.467
12	0.169	0.067	0.021	0.681	97.914	0.006	0.007	0.007	0.227	0.036	99.135
13	0.192	0.089	0.107	0.461	97.428	0.000	0.022	0.034	0.192	0.018	98.543
14	0.169	0.250	0.124	0.391	93.504	0.000	0.061	0.007	0.281	0.005	94.792
15	0.023	0.212	0.103	0.543	96.947	0.000	0.037	0.041	0.192	0.000	98.098
16	0.117	0.577	0.095	1.000	92.173	0.000	0.019	0.006	0.256	0.007	94.250
17	0.000	0.000	0.041	1.053	97.580	0.010	0.000	0.077	0.420	0.000	99.181

Point	P ₂ (CO ₃) ₅	Si(CO ₃) ₂	S(CO ₃) ₂	Mg(CO ₃)	Ca(CO ₃)	Mn(CO ₃)	Fe(CO ₃)	Sr(CO ₃)	Na ₂ (CO ₃)	K ₂ (CO ₃)	Total
Sample 2											
1	2.428	0.080	0.083	1.931	98.308	0.000	0.000	0.040	n/a	0.102	102.972
2	1.414	0.164	0.100	1.778	96.257	0.000	0.031	0.066	n/a	0.115	99.925
3	0.902	0.030	0.157	2.056	95.431	0.000	0.000	0.000	n/a	0.090	98.666
4	0.603	0.005	0.087	1.738	96.480	0.074	0.000	0.050	n/a	0.104	99.141
5	0.639	0.048	0.174	2.055	95.710	0.038	0.000	0.059	n/a	0.096	98.819
6	0.803	0.043	0.104	1.946	95.950	0.000	0.035	0.025	n/a	0.087	98.993
7	0.686	0.076	0.021	2.007	94.888	0.095	0.029	0.010	n/a	0.076	97.888
8	0.668	0.045	0.120	1.677	95.491	0.056	0.000	0.035	n/a	0.066	98.158
9	0.656	0.089	0.128	1.695	95.112	0.051	0.000	0.035	n/a	0.095	97.861
10	0.603	0.077	0.149	1.421	95.117	0.026	0.000	0.037	n/a	0.077	97.507
11	0.439	0.109	0.161	1.192	96.389	0.100	0.025	0.040	n/a	0.030	98.485
12	0.533	0.090	0.132	0.995	96.136	0.018	0.036	0.054	n/a	0.044	98.038
13	0.392	0.080	0.174	0.989	95.096	0.038	0.010	0.044	n/a	0.073	96.896
14	0.334	0.019	0.108	0.793	96.006	0.000	0.000	0.039	n/a	0.030	97.329
15	0.287	0.038	0.062	0.795	96.932	0.000	0.002	0.038	n/a	0.054	98.208
16	0.207	5.897	0.075	0.746	94.514	0.031	0.096	0.032	n/a	0.117	101.715
17	0.258	0.051	0.046	0.736	97.607	0.000	0.014	0.020	n/a	0.047	98.779
18	0.123	0.019	0.087	0.592	98.899	0.038	0.000	0.050	n/a	0.032	99.840
19	0.129	0.047	0.041	0.599	98.674	0.115	0.017	0.060	n/a	0.000	99.682
20	0.006	0.065	0.091	0.457	97.979	0.015	0.048	0.031	n/a	0.020	98.712
21	0.199	0.051	0.087	0.341	97.541	0.021	0.025	0.000	n/a	0.023	98.288
22	0.123	0.047	0.079	0.368	98.053	0.121	0.028	0.015	n/a	0.036	98.870
23	0.059	0.000	0.079	0.414	99.148	0.000	0.043	0.047	n/a	0.002	99.792
24	0.135	0.000	0.012	0.597	98.615	0.000	0.000	0.029	n/a	0.022	99.410
25	0.064	0.061	0.037	0.946	97.430	0.059	0.012	0.039	n/a	0.014	98.662
26	0.181	0.097	0.079	0.843	89.923	0.010	0.019	0.019	n/a	0.002	91.173
27	0.000	0.026	0.025	1.109	98.199	0.087	0.055	0.014	n/a	0.002	99.517
1	6.385	0.115	0.385	2.615	91.260	0.000	0.033	0.010	n/a	0.120	100.923
2	2.251	0.038	0.087	1.765	97.320	0.000	0.047	0.004	n/a	0.110	101.622
3	1.138	0.000	0.141	1.920	96.245	0.000	0.005	0.030	n/a	0.098	99.577
4	0.810	0.062	0.182	1.943	95.116	0.074	0.000	0.029	n/a	0.097	98.313
5	0.580	0.043	0.128	1.691	95.767	0.033	0.010	0.031	n/a	0.087	98.370
6	0.569	0.028	0.104	1.948	94.663	0.000	0.021	0.000	n/a	0.102	97.435
7	0.516	0.038	0.046	2.042	94.617	0.000	0.054	0.026	n/a	0.101	97.440
8	0.616	0.001	0.203	1.894	95.151	0.054	0.000	0.019	n/a	0.058	97.996
9	0.698	0.073	0.220	1.695	94.959	0.082	0.045	0.020	n/a	0.075	97.867
10	0.527	0.027	0.070	1.354	95.849	0.000	0.013	0.000	n/a	0.081	97.921
11	0.521	0.008	0.062	1.201	95.102	0.026	0.045	0.034	n/a	0.063	97.062
12	0.545	0.023	0.153	1.127	96.328	0.036	0.004	0.000	n/a	0.049	98.265
13	0.381	0.024	0.095	0.949	96.363	0.000	0.013	0.012	n/a	0.043	97.880
14	0.480	0.051	0.099	0.891	97.113	0.000	0.030	0.003	n/a	0.040	98.707
15	0.240	0.047	0.033	0.804	97.662	0.041	0.053	0.001	n/a	0.024	98.905
16	0.246	0.027	0.029	0.553	98.333	0.072	0.000	0.013	n/a	0.000	99.273
17	0.182	0.024	0.054	0.579	97.698	0.003	0.000	0.010	n/a	0.032	98.582
18	0.111	0.066	0.103	0.436	98.276	0.000	0.023	0.030	n/a	0.016	99.061
19	0.164	0.043	0.099	0.341	96.704	0.028	0.035	0.055	n/a	0.006	97.475
20	0.053	0.004	0.066	0.366	97.293	0.000	0.000	0.007	n/a	0.000	97.789
21	0.000	0.027	0.083	0.356	97.886	0.092	0.000	0.005	n/a	0.006	98.455
22	0.000	0.000	0.000	0.519	98.993	0.000	0.000	0.041	n/a	0.000	99.553
23	0.023	0.077	0.041	0.667	98.719	0.015	0.005	0.031	n/a	0.019	99.597
24	0.053	0.009	0.166	1.184	94.305	0.046	0.013	0.010	n/a	0.000	95.786
25	0.053	0.030	0.435	1.468	93.623	0.000	0.015	0.020	n/a	0.028	95.672

Microprobe Analyses expressed as elements

Terebratulina retusa

Sample 1

Point	P	Si	S	Mg	Ca	Mn	Fe	Sr	Na	K
1	0.011	0.005	0.309	1.542	36.756	0.000	0.006	0.150	0.163	0.000
2	0.014	0.005	0.298	1.169	36.403	0.000	0.000	0.145	0.175	0.011
3	0.009	0.003	0.267	0.995	33.918	0.005	0.000	0.120	0.174	0.005
4	0.010	0.005	0.191	0.403	38.453	0.000	0.000	0.096	0.128	0.003
5	0.009	0.004	0.185	0.301	39.089	0.004	0.000	0.106	0.117	0.001
6	0.010	0.005	0.191	0.281	38.856	0.006	0.025	0.084	0.117	0.005
7	0.011	0.014	0.226	0.423	38.502	0.006	0.000	0.087	0.131	0.009
8	0.015	0.003	0.200	0.743	38.105	0.000	0.000	0.115	0.141	0.003
9	0.007	0.000	0.135	0.193	38.811	0.000	0.007	0.103	0.107	0.005
10	0.001	0.004	0.159	0.157	38.788	0.019	0.000	0.124	0.133	0.006
11	0.001	0.006	0.159	0.185	38.775	0.000	0.002	0.132	0.131	0.006
12	0.004	0.005	0.153	0.149	38.839	0.000	0.000	0.077	0.131	0.000
13	0.007	0.001	0.163	0.185	38.646	0.000	0.004	0.122	0.128	0.005
14	0.003	0.004	0.160	0.212	38.834	0.000	0.000	0.120	0.129	0.000
15	0.004	0.002	0.186	0.253	38.470	0.000	0.018	0.129	0.143	0.003
16	0.003	0.002	0.157	0.219	38.835	0.000	0.005	0.122	0.136	0.000
17	0.005	0.008	0.160	0.216	38.569	0.009	0.000	0.113	0.138	0.001
18	0.000	0.000	0.194	0.200	38.819	0.019	0.000	0.115	0.140	0.001
19	0.010	0.454	0.193	0.158	31.665	0.000	0.021	0.090	0.108	0.001
20	0.002	0.016	0.183	0.213	38.316	0.000	0.000	0.133	0.136	0.003
21	0.007	0.004	0.194	0.197	38.480	0.000	0.000	0.122	0.152	0.008
22	0.003	0.002	0.240	0.217	38.141	0.006	0.000	0.152	0.148	0.000
23	0.006	0.004	0.280	0.265	38.207	0.000	0.000	0.142	0.157	0.005
24	0.004	0.003	0.272	0.278	38.191	0.000	0.000	0.147	0.163	0.005
25	0.003	0.042	0.332	0.342	38.047	0.008	0.006	0.161	0.155	0.010
26	0.003	0.007	0.304	0.897	37.326	0.000	0.000	0.159	0.165	0.004
	0.000	0.000	0.000	0.000	0.000	0.000	0.000	0.000	0.000	0.000
1	0.012	0.004	0.278	0.679	36.302	0.009	0.013	0.105	0.119	0.002
2	0.010	0.007	0.276	0.555	38.316	0.000	0.016	0.120	0.135	0.002
3	0.005	0.003	0.263	0.323	37.588	0.000	0.003	0.113	0.131	0.007
4	0.010	0.000	0.222	0.478	38.425	0.009	0.008	0.113	0.113	0.004
5	0.021	0.000	0.277	0.748	37.813	0.031	0.027	0.122	0.141	0.002
6	0.019	0.003	0.222	0.734	37.996	0.007	0.000	0.109	0.131	0.007
7	0.011	0.008	0.149	0.209	38.847	0.014	0.000	0.098	0.129	0.000
8	0.006	0.004	0.190	0.212	38.673	0.000	0.000	0.135	0.110	0.000
9	0.007	0.003	0.151	0.216	38.965	0.000	0.000	0.116	0.128	0.004
10	0.004	0.010	0.146	0.180	38.710	0.005	0.000	0.118	0.141	0.005
11	0.000	0.010	0.155	0.170	39.118	0.009	0.012	0.116	0.110	0.000
12	0.004	0.010	0.128	0.161	38.821	0.020	0.000	0.096	0.118	0.000
13	0.004	0.006	0.155	0.212	38.772	0.023	0.012	0.123	0.143	0.002
14	0.002	0.000	0.171	0.249	38.764	0.000	0.000	0.099	0.145	0.003
15	0.000	0.007	0.187	0.216	38.686	0.008	0.001	0.118	0.142	0.000
16	0.001	0.005	0.190	0.292	38.405	0.003	0.003	0.123	0.154	0.005
17	0.003	0.009	0.234	0.302	38.537	0.013	0.001	0.116	0.161	0.004
18	0.018	0.006	0.228	0.450	38.394	0.022	0.000	0.129	0.157	0.000
19	0.003	0.008	0.207	0.289	38.777	0.016	0.010	0.111	0.127	0.004
20	0.005	0.004	0.174	0.334	38.730	0.005	0.022	0.116	0.140	0.002
21	0.000	0.006	0.176	0.265	38.697	0.035	0.004	0.093	0.128	0.007
22	0.000	0.031	0.190	0.280	37.971	0.027	0.004	0.119	0.131	0.001
23	0.005	0.000	0.247	0.316	38.240	0.000	0.023	0.123	0.170	0.006
24	0.005	0.005	0.185	0.252	32.493	0.000	0.000	0.096	0.127	0.003

Point	P	Si	S	Mg	Ca	Mn	Fe	Sr	Na	K
1	0.011	0.004	0.182	0.320	38.608	0.008	0.012	0.100	0.115	0.005
2	0.005	0.090	0.216	0.241	36.801	0.000	0.107	0.097	0.123	0.001
3	0.005	0.001	0.200	0.222	38.557	0.010	0.017	0.103	0.117	0.001
4	0.009	0.000	0.207	0.246	38.054	0.000	0.031	0.072	0.118	0.004
5	0.006	0.003	0.256	0.422	35.867	0.002	0.028	0.104	0.155	0.010
6	0.010	0.001	0.368	0.724	37.353	0.011	0.040	0.122	0.189	0.005
7	0.010	0.011	0.337	0.903	37.374	0.032	0.030	0.139	0.183	0.008
8	0.008	0.005	0.322	1.086	37.064	0.011	0.009	0.167	0.207	0.004
9	0.002	0.003	0.370	1.270	36.511	0.020	0.012	0.171	0.217	0.007
10	0.007	0.017	0.114	0.535	12.952	0.000	0.000	0.072	0.063	0.004
11	0.015	0.003	0.212	0.378	37.579	0.020	0.010	0.067	0.122	0.009
12	0.002	0.002	0.150	0.206	35.639	0.000	0.010	0.085	0.125	0.004
13	0.007	0.015	0.197	0.237	38.651	0.014	0.002	0.097	0.118	0.000
14	0.011	0.009	0.214	0.207	37.722	0.011	0.019	0.088	0.115	0.002
15	0.004	0.000	0.218	0.209	37.527	0.001	0.048	0.085	0.128	0.002
16	0.004	0.005	0.190	0.190	36.120	0.000	0.016	0.077	0.142	0.001
17	0.005	0.006	0.182	0.189	38.511	0.000	0.005	0.100	0.134	0.003
18	0.005	0.003	0.182	0.174	38.493	0.002	0.010	0.112	0.125	0.003
19	0.007	0.004	0.240	0.201	38.581	0.000	0.000	0.100	0.145	0.005
20	0.003	0.028	0.053	0.057	11.480	0.014	0.013	0.036	0.034	0.000
21	0.011	0.694	0.141	0.190	20.580	0.009	0.058	0.043	0.092	0.002
22	0.005	0.141	0.206	0.182	37.324	0.000	0.001	0.071	0.127	0.001
23	0.003	0.024	0.221	0.191	38.408	0.000	0.000	0.123	0.128	0.005
24	0.004	0.003	0.245	0.220	38.391	0.033	0.003	0.109	0.146	0.001
25	0.005	0.012	0.232	0.256	38.270	0.000	0.000	0.129	0.149	0.000
26	0.002	0.008	0.154	0.185	38.988	0.012	0.000	0.110	0.137	0.001
27	0.001	0.002	0.169	0.194	38.374	0.003	0.018	0.122	0.149	0.004
28	0.002	0.001	0.194	0.172	38.693	0.000	0.000	0.118	0.140	0.000
29	0.004	0.009	0.300	0.277	37.993	0.017	0.015	0.106	0.163	0.000
30	0.003	0.005	0.115	0.121	38.796	0.000	0.000	0.103	0.119	0.001
31	0.001	0.000	0.131	0.137	38.571	0.018	0.000	0.115	0.124	0.000
32	0.005	0.012	0.168	0.142	38.789	0.016	0.013	0.093	0.115	0.000
33	0.001	0.010	0.178	0.147	38.365	0.000	0.001	0.100	0.126	0.000
34	0.002	0.012	0.185	0.179	38.491	0.000	0.000	0.090	0.137	0.000
35	0.004	0.015	0.234	0.219	37.841	0.000	0.002	0.130	0.137	0.005

Sample 2

1	0.001	0.014	0.303	0.561	37.594	0.000	0.000	0.169	0.176	0.006
2	0.000	0.009	0.227	0.377	38.079	0.029	0.000	0.158	0.161	0.008
3	0.002	0.008	0.179	0.255	38.081	0.038	0.000	0.138	0.152	0.000
4	0.000	0.005	0.168	0.224	38.704	0.000	0.000	0.137	0.151	0.003
5	0.004	0.007	0.199	0.265	38.321	0.000	0.000	0.131	0.161	0.001
6	0.005	0.002	0.174	0.252	38.436	0.014	0.000	0.137	0.156	0.006
7	0.004	0.010	0.217	0.284	38.385	0.000	0.029	0.135	0.154	0.000
8	0.002	0.012	0.214	0.265	38.532	0.001	0.005	0.131	0.161	0.003
9	0.008	0.000	0.207	0.320	38.289	0.000	0.005	0.127	0.148	0.008
10	0.002	0.025	0.035	0.044	7.272	0.015	0.000	0.000	0.022	0.006
11	0.001	0.009	0.161	0.240	38.345	0.000	0.000	0.119	0.153	0.000
12	0.000	0.013	0.175	0.248	38.363	0.009	0.000	0.110	0.211	0.008
13	0.003	0.012	0.141	0.223	38.674	0.000	0.001	0.144	0.146	0.005
14	0.001	0.012	0.187	0.234	38.568	0.003	0.000	0.126	0.152	0.001
15	0.001	0.010	0.184	0.242	38.539	0.010	0.000	0.110	0.154	0.000
16	0.004	0.008	0.195	0.212	38.791	0.010	0.005	0.126	0.138	0.006
17	0.005	0.000	0.174	0.240	39.002	0.020	0.000	0.103	0.146	0.002
18	0.002	0.017	0.150	0.221	38.906	0.001	0.010	0.128	0.132	0.002
19	0.007	0.002	0.183	0.202	38.930	0.015	0.002	0.104	0.164	0.004
20	0.006	0.004	0.197	0.215	38.990	0.000	0.005	0.111	0.159	0.001
21	0.008	0.012	0.182	0.243	39.000	0.012	0.007	0.108	0.145	0.008
22	0.013	0.008	0.137	0.191	39.340	0.034	0.000	0.123	0.124	0.000

Point	P	Si	S	Mg	Ca	Mn	Fe	Sr	Na	K
1	0.003	0.009	0.369	0.830	37.984	0.011	0.000	0.170	0.190	0.004
2	0.000	0.014	0.359	0.870	37.961	0.002	0.000	0.190	0.187	0.007
3	0.000	0.020	0.261	0.400	38.694	0.000	0.001	0.139	0.168	0.002
4	0.001	0.010	0.223	0.321	38.736	0.008	0.005	0.153	0.164	0.002
5	0.004	0.014	0.173	0.318	39.017	0.008	0.003	0.137	0.154	0.000
6	0.008	0.007	0.212	0.323	38.783	0.000	0.000	0.122	0.148	0.004
7	0.006	0.013	0.178	0.275	38.843	0.039	0.013	0.129	0.153	0.005
8	0.001	0.007	0.156	0.268	38.761	0.017	0.000	0.134	0.155	0.006
9	0.000	0.009	0.186	0.249	38.965	0.032	0.003	0.122	0.150	0.002
10	0.002	0.008	0.153	0.292	38.875	0.000	0.000	0.139	0.177	0.008
11	0.003	0.003	0.182	0.265	38.648	0.034	0.007	0.134	0.155	0.001
12	0.002	0.004	0.165	0.265	39.031	0.000	0.000	0.142	0.150	0.001
13	0.001	0.005	0.190	0.262	38.993	0.023	0.000	0.134	0.146	0.002
14	0.003	0.000	0.139	0.208	38.906	0.018	0.000	0.128	0.138	0.000
15	0.005	0.009	0.141	0.210	38.968	0.006	0.000	0.121	0.122	0.001
16	0.010	0.012	0.192	0.205	39.006	0.044	0.000	0.110	0.115	0.007
17	0.003	0.006	0.154	0.191	39.141	0.000	0.000	0.106	0.138	0.000
18	0.004	0.014	0.151	0.208	38.664	0.011	0.000	0.119	0.139	0.001
19	0.004	0.004	0.142	0.242	39.218	0.000	0.000	0.132	0.146	0.000
20	0.003	0.008	0.170	0.210	39.095	0.020	0.000	0.131	0.136	0.005
21	0.007	0.013	0.144	0.208	39.008	0.000	0.072	0.104	0.133	0.000
22	0.004	0.015	0.157	0.221	39.086	0.000	0.000	0.115	0.146	0.005
23	0.006	0.009	0.157	0.259	38.833	0.017	0.006	0.075	0.125	0.000
24	0.014	0.011	0.158	0.422	37.414	0.000	0.012	0.094	0.133	0.000
1	0.002	0.015	0.322	0.751	38.236	0.031	0.000	0.145	0.162	0.009
2	0.001	0.013	0.338	0.539	38.710	0.034	0.002	0.154	0.161	0.010
3	0.007	0.009	0.217	0.281	38.640	0.011	0.003	0.138	0.161	0.006
4	0.008	0.005	0.185	0.253	38.797	0.000	0.000	0.138	0.147	0.001
5	0.003	0.009	0.150	0.280	38.743	0.000	0.012	0.160	0.159	0.003
6	0.002	0.010	0.243	0.358	38.507	0.000	0.000	0.163	0.172	0.003
7	0.004	0.010	0.186	0.298	38.635	0.000	0.000	0.137	0.166	0.006
8	0.000	0.013	0.190	0.327	38.879	0.000	0.000	0.157	0.157	0.007
9	0.004	0.000	0.183	0.291	38.616	0.006	0.000	0.151	0.164	0.006
10	0.000	0.011	0.147	0.266	38.928	0.008	0.000	0.134	0.140	0.000
11	0.001	0.011	0.180	0.308	38.631	0.000	0.000	0.146	0.165	0.000
12	0.003	0.010	0.149	0.289	38.801	0.011	0.011	0.128	0.158	0.000
13	0.003	0.004	0.156	0.260	38.711	0.015	0.000	0.129	0.152	0.000
14	0.008	0.011	0.153	0.349	38.772	0.000	0.006	0.101	0.151	0.000
15	0.003	0.004	0.102	0.180	39.221	0.006	0.000	0.111	0.126	0.000
16	0.003	0.011	0.122	0.148	39.053	0.002	0.006	0.088	0.130	0.000
17	0.001	0.008	0.141	0.129	39.306	0.033	0.017	0.093	0.118	0.000
18	0.006	0.007	0.152	0.134	39.013	0.014	0.023	0.124	0.128	0.005
19	0.008	0.005	0.153	0.152	39.203	0.000	0.000	0.087	0.112	0.001
20	0.004	0.014	0.124	0.164	39.084	0.025	0.000	0.123	0.134	0.010
21	0.003	0.021	0.108	0.144	39.058	0.056	0.003	0.113	0.124	0.000
22	0.009	0.009	0.135	0.168	39.311	0.000	0.000	0.113	0.116	0.001
23	0.007	0.004	0.124	0.193	39.249	0.015	0.000	0.112	0.133	0.001
1	0.005	0.013	0.345	1.116	37.526	0.011	0.013	0.174	0.187	0.012
2	0.001	0.004	0.329	0.871	38.361	0.009	0.022	0.180	0.180	0.009
3	0.005	0.009	0.293	0.657	38.292	0.005	0.004	0.172	0.178	0.005
4	0.004	0.012	0.244	0.433	38.282	0.000	0.002	0.152	0.172	0.009
5	0.005	0.009	0.254	0.318	38.406	0.003	0.014	0.152	0.169	0.002
6	0.004	0.008	0.210	0.319	38.567	0.012	0.005	0.164	0.161	0.000
7	0.001	0.013	0.206	0.287	38.374	0.040	0.000	0.118	0.155	0.004
8	0.002	0.009	0.195	0.260	38.591	0.048	0.000	0.107	0.143	0.001
9	0.003	0.001	0.170	0.249	38.595	0.000	0.018	0.113	0.141	0.003

Point	P	Si	S	Mg	Ca	Mn	Fe	Sr	Na	K
10	0.006	0.001	0.131	0.238	38.751	0.022	0.000	0.115	0.129	0.000
11	0.003	0.006	0.197	0.239	38.851	0.027	0.000	0.125	0.150	0.001
12	0.000	0.010	0.177	0.209	38.589	0.003	0.002	0.120	0.148	0.000
13	0.003	0.000	0.187	0.249	37.565	0.002	0.012	0.110	0.158	0.005
14	0.002	0.004	0.180	0.211	38.876	0.004	0.000	0.132	0.138	0.005
15	0.002	0.005	0.156	0.185	38.898	0.000	0.000	0.099	0.136	0.000
16	0.005	0.012	0.180	0.205	38.735	0.000	0.000	0.113	0.153	0.003
17	0.005	0.002	0.183	0.220	38.889	0.025	0.000	0.102	0.137	0.000
18	0.007	0.002	0.224	0.213	38.831	0.006	0.000	0.117	0.155	0.000
19	0.004	0.011	0.190	0.181	38.924	0.000	0.006	0.121	0.148	0.003
20	0.004	0.010	0.137	0.190	38.744	0.000	0.023	0.110	0.136	0.000
21	0.002	0.009	0.136	0.166	38.837	0.006	0.001	0.077	0.134	0.002
22	0.007	0.017	0.144	0.206	36.534	0.009	0.007	0.115	0.150	0.002
23	0.001	0.191	0.078	0.086	17.829	0.000	0.000	0.060	0.069	0.000
24	0.007	0.013	0.139	0.174	37.982	0.006	0.000	0.110	0.138	0.000
25	0.003	0.010	0.153	0.246	38.370	0.002	0.009	0.122	0.134	0.004
26	0.000	0.008	0.155	0.192	38.641	0.002	0.018	0.124	0.123	0.003

Sample 3

1	0.073	0.005	0.352	0.763	37.575	N/A	0.000	0.161	0.164	0.007
2	0.070	0.013	0.377	1.023	37.234	N/A	0.000	0.193	0.182	0.005
3	0.076	0.002	0.325	0.726	37.757	N/A	0.002	0.172	0.176	0.003
4	0.081	0.002	0.233	0.316	38.099	N/A	0.000	0.142	0.159	0.006
5	0.080	0.000	0.224	0.251	38.455	N/A	0.000	0.114	0.149	0.001
6	0.076	0.001	0.193	0.245	38.130	N/A	0.003	0.126	0.133	0.000
7	0.074	0.000	0.206	0.234	38.613	N/A	0.000	0.091	0.134	0.000
8	0.074	0.001	0.197	0.237	38.139	N/A	0.000	0.123	0.139	0.007
9	0.075	0.006	0.248	0.297	38.155	N/A	0.000	0.137	0.146	0.006
10	0.082	0.003	0.225	0.226	38.441	N/A	0.000	0.104	0.128	0.006
11	0.080	0.005	0.247	0.239	38.264	N/A	0.000	0.120	0.127	0.000
12	0.081	0.000	0.232	0.257	38.307	N/A	0.000	0.104	0.147	0.003
13	0.077	0.001	0.233	0.258	38.318	N/A	0.014	0.135	0.157	0.003
14	0.084	0.002	0.176	0.249	38.636	N/A	0.004	0.091	0.143	0.012
15	0.076	0.014	0.168	0.185	38.485	N/A	0.000	0.119	0.140	0.000
16	0.081	0.005	0.162	0.144	38.372	N/A	0.000	0.126	0.131	0.000
17	0.082	0.002	0.148	0.167	38.665	N/A	0.016	0.115	0.128	0.000
18	0.078	0.003	0.133	0.155	38.473	N/A	0.000	0.115	0.137	0.000
19	0.082	0.002	0.165	0.174	38.762	N/A	0.000	0.102	0.132	0.001
20	0.081	0.000	0.202	0.183	38.388	N/A	0.000	0.113	0.124	0.001
21	0.083	0.000	0.182	0.215	38.175	N/A	0.010	0.096	0.137	0.001
22	0.090	0.014	0.177	0.213	38.545	N/A	0.000	0.115	0.125	0.002
23	0.088	0.013	0.187	0.425	38.151	N/A	0.003	0.094	0.133	0.006

1	0.073	0.014	0.308	0.618	37.610	N/A	0.000	0.151	0.149	0.010
2	0.075	0.010	0.316	0.700	37.483	N/A	0.000	0.163	0.166	0.011
3	0.080	0.000	0.287	0.455	37.413	N/A	0.012	0.145	0.166	0.000
4	0.081	0.000	0.219	0.262	37.974	N/A	0.000	0.120	0.153	0.001
5	0.075	0.001	0.213	0.234	38.009	N/A	0.000	0.135	0.145	0.004
6	0.075	0.013	0.190	0.205	38.141	N/A	0.014	0.109	0.129	0.000
7	0.080	0.008	0.192	0.255	38.333	N/A	0.010	0.104	0.137	0.002
8	0.065	0.011	0.141	0.217	30.450	N/A	0.014	0.094	0.113	0.008
9	0.076	0.003	0.233	0.259	37.966	N/A	0.000	0.141	0.135	0.002
10	0.084	0.005	0.213	0.208	38.093	N/A	0.000	0.103	0.138	0.004
11	0.077	0.009	0.202	0.242	38.262	N/A	0.000	0.130	0.146	0.000
12	0.078	0.005	0.208	0.229	38.129	N/A	0.000	0.087	0.149	0.006
13	0.079	0.003	0.203	0.182	38.294	N/A	0.008	0.132	0.150	0.001
14	0.073	0.005	0.167	0.184	38.262	N/A	0.007	0.123	0.152	0.001
15	0.077	0.010	0.169	0.171	38.431	N/A	0.000	0.127	0.144	0.007

Point	P	Si	S	Mg	Ca	Mn	Fe	Sr	Na	K
16	0.076	0.003	0.165	0.192	38.510	N/A	0.003	0.107	0.144	0.006
17	0.076	0.015	0.172	0.190	38.272	N/A	0.000	0.125	0.135	0.000
18	0.081	0.000	0.162	0.171	38.311	N/A	0.021	0.109	0.131	0.002
19	0.080	0.006	0.185	0.191	38.519	N/A	0.000	0.121	0.139	0.004
20	0.080	0.001	0.191	0.208	38.541	N/A	0.000	0.106	0.143	0.010
21	0.075	0.014	0.157	0.201	38.256	N/A	0.000	0.097	0.138	0.000
22	0.087	0.004	0.165	0.236	38.732	N/A	0.003	0.115	0.133	0.001
23	0.087	0.005	0.182	0.475	38.049	N/A	0.000	0.097	0.144	0.001
1	0.070	0.016	0.317	0.490	37.511	N/A	0.000	0.166	0.156	0.000
2	0.075	0.000	0.214	0.304	38.335	N/A	0.000	0.142	0.156	0.003
3	0.080	0.004	0.247	0.271	38.212	N/A	0.007	0.113	0.155	0.006
4	0.072	0.001	0.172	0.241	37.986	N/A	0.010	0.138	0.150	0.000
5	0.074	0.005	0.223	0.270	37.911	N/A	0.000	0.122	0.161	0.004
6	0.080	0.011	0.224	0.279	37.732	N/A	0.000	0.137	0.162	0.004
7	0.077	0.011	0.230	0.307	38.040	N/A	0.000	0.124	0.156	0.001
8	0.077	0.005	0.219	0.347	37.758	N/A	0.000	0.124	0.152	0.003
9	0.075	0.009	0.237	0.381	37.743	N/A	0.000	0.118	0.156	0.000
10	0.073	0.003	0.211	0.378	37.656	N/A	0.000	0.143	0.165	0.003
11	0.054	0.003	0.128	0.264	27.087	N/A	0.006	0.101	0.119	0.004
12	0.076	0.008	0.178	0.237	37.933	N/A	0.000	0.115	0.142	0.007
13	0.076	0.002	0.164	0.234	37.918	N/A	0.000	0.101	0.151	0.002
14	0.080	0.004	0.161	0.206	38.269	N/A	0.017	0.128	0.131	0.000
15	0.077	0.006	0.149	0.227	38.039	N/A	0.000	0.126	0.141	0.002
16	0.077	0.002	0.140	0.207	38.124	N/A	0.000	0.092	0.132	0.000
17	0.079	0.007	0.175	0.182	38.361	N/A	0.018	0.109	0.127	0.000
18	0.078	0.003	0.185	0.208	37.987	N/A	0.011	0.116	0.136	0.001
19	0.083	0.009	0.163	0.215	38.249	N/A	0.001	0.093	0.137	0.000
20	0.079	0.007	0.141	0.191	38.536	N/A	0.012	0.134	0.122	0.004
21	0.080	0.011	0.171	0.202	38.172	N/A	0.013	0.115	0.129	0.000
22	0.085	0.003	0.171	0.402	37.483	N/A	0.000	0.109	0.135	0.000
1	0.074	0.005	0.303	0.493	37.949	N/A	0.003	0.154	0.150	0.009
2	0.077	0.000	0.266	0.330	38.205	N/A	0.000	0.150	0.150	0.005
3	0.074	0.010	0.221	0.263	38.098	N/A	0.015	0.136	0.148	0.000
4	0.079	0.002	0.195	0.236	38.194	N/A	0.014	0.134	0.157	0.006
5	0.075	0.002	0.204	0.234	37.969	N/A	0.000	0.099	0.152	0.005
6	0.081	0.003	0.196	0.253	38.315	N/A	0.000	0.112	0.148	0.001
7	0.080	0.002	0.242	0.282	38.064	N/A	0.013	0.159	0.158	0.005
8	0.073	0.007	0.199	0.311	37.851	N/A	0.000	0.120	0.138	0.001
9	0.075	0.005	0.228	0.292	38.045	N/A	0.000	0.130	0.148	0.006
10	0.075	0.004	0.211	0.256	38.354	N/A	0.000	0.147	0.146	0.000
11	0.080	0.006	0.208	0.301	38.212	N/A	0.000	0.125	0.146	0.000
12	0.074	0.003	0.202	0.299	37.973	N/A	0.000	0.131	0.147	0.000
13	0.083	0.007	0.175	0.279	38.564	N/A	0.000	0.116	0.141	0.002
14	0.076	0.003	0.172	0.192	38.642	N/A	0.000	0.106	0.126	0.003
15	0.080	0.011	0.161	0.172	38.469	N/A	0.004	0.099	0.122	0.000
16	0.082	0.000	0.124	0.156	38.367	N/A	0.012	0.111	0.120	0.007
17	0.080	0.003	0.153	0.181	38.322	N/A	0.000	0.125	0.129	0.000
18	0.079	0.002	0.174	0.180	38.185	N/A	0.000	0.106	0.134	0.008
19	0.092	0.008	0.234	0.313	38.151	N/A	0.004	0.102	0.140	0.003
20	0.079	0.005	0.159	0.172	38.506	N/A	0.012	0.101	0.123	0.000
21	0.077	0.002	0.137	0.137	38.771	N/A	0.000	0.106	0.125	0.002
22	0.076	0.000	0.160	0.195	38.461	N/A	0.000	0.096	0.133	0.003

Point	P	Si	S	Mg	Ca	Mn	Fe	Sr	Na	K
<i>Novocrania anomala</i>										
Sample 1										
1	0.042	0.027	0.286	2.099	32.305	0.042	0.013	0.226	0.203	0.009
2	0.068	0.012	0.281	2.768	34.630	0.021	0.013	0.216	0.262	0.014
3	0.032	0.000	0.310	2.600	35.618	0.011	0.009	0.219	0.241	0.008
4	0.020	0.009	0.300	2.373	34.703	0.030	0.031	0.195	0.231	0.010
5	0.011	0.011	0.256	1.905	31.962	0.018	0.004	0.186	0.223	0.007
6	0.012	0.005	0.272	2.433	35.278	0.029	0.000	0.220	0.284	0.012
7	0.016	0.011	0.288	2.464	35.363	0.004	0.000	0.201	0.266	0.013
8	0.020	0.001	0.305	2.509	35.612	0.026	0.032	0.189	0.236	0.007
9	0.018	0.011	0.303	2.484	35.109	0.000	0.033	0.231	0.239	0.011
10	0.024	0.015	0.334	2.467	34.863	0.000	0.012	0.237	0.238	0.004
11	0.015	0.006	0.349	2.313	36.090	0.038	0.014	0.199	0.191	0.015
12	0.021	0.024	0.364	2.458	35.143	0.000	0.000	0.233	0.221	0.008
13	0.017	0.024	0.364	2.247	35.174	0.031	0.000	0.226	0.206	0.008
14	0.013	0.004	0.337	2.485	35.636	0.012	0.016	0.239	0.212	0.006
15	0.021	0.010	0.387	2.360	36.212	0.031	0.013	0.184	0.191	0.006
16	0.019	0.017	0.352	2.228	34.478	0.016	0.008	0.242	0.177	0.009
17	0.014	0.014	0.351	2.350	36.068	0.024	0.025	0.218	0.156	0.008
18	0.006	0.012	0.363	2.500	35.851	0.019	0.000	0.199	0.182	0.010
19	0.010	0.002	0.356	2.464	36.000	0.087	0.010	0.198	0.174	0.005
20	0.011	0.009	0.336	2.396	33.435	0.042	0.008	0.259	0.206	0.011
21	0.010	0.009	0.355	2.293	36.207	0.030	0.000	0.208	0.206	0.011
22	0.011	0.008	0.356	2.479	35.891	0.038	0.001	0.209	0.193	0.011
23	0.011	0.012	0.419	2.490	36.310	0.073	0.016	0.207	0.181	0.011
24	0.008	0.008	0.387	2.432	36.095	0.000	0.019	0.196	0.154	0.014
25	0.002	0.011	0.379	2.505	36.076	0.054	0.000	0.197	0.173	0.006
26	0.011	0.008	0.378	2.546	35.827	0.064	0.002	0.217	0.182	0.008
27	0.008	0.008	0.349	2.268	36.269	0.040	0.000	0.203	0.184	0.005
28	0.016	0.056	0.305	2.264	33.665	0.023	0.006	0.208	0.166	0.013
29	0.016	0.039	0.442	2.245	33.923	0.009	0.021	0.220	0.152	0.006
30	0.017	0.013	0.324	2.443	35.910	0.052	0.013	0.200	0.179	0.007
31	0.010	0.001	0.340	2.554	35.677	0.050	0.017	0.195	0.172	0.008
32	0.017	0.003	0.302	2.168	34.298	0.008	0.029	0.184	0.164	0.008
33	0.014	0.000	0.276	2.612	34.655	0.024	0.000	0.243	0.149	0.004
34	0.010	0.008	0.309	2.552	35.622	0.005	0.003	0.231	0.182	0.004
35	0.020	0.012	0.330	2.655	35.431	0.024	0.000	0.249	0.190	0.011
36	0.010	0.000	0.332	2.587	35.697	0.029	0.016	0.196	0.162	0.008
37	0.030	0.007	0.281	2.461	35.425	0.007	0.000	0.214	0.122	0.008
38	0.043	0.085	0.271	2.223	32.608	0.031	0.020	0.194	0.091	0.010
1	0.068	0.035	0.308	1.884	30.017	0.019	0.018	0.193	0.211	0.014
2	0.040	0.010	0.330	2.323	36.177	0.000	0.018	0.208	0.192	0.014
3	0.024	0.007	0.274	2.621	35.422	0.000	0.013	0.201	0.253	0.009
4	0.018	0.000	0.288	2.609	34.663	0.007	0.032	0.201	0.278	0.008
5	0.014	0.000	0.279	2.536	35.214	0.018	0.013	0.226	0.238	0.010
6	0.014	0.004	0.271	2.374	34.995	0.000	0.007	0.183	0.273	0.016
7	0.015	0.001	0.260	2.232	33.739	0.000	0.000	0.201	0.274	0.009
8	0.017	0.005	0.272	2.452	34.966	0.030	0.023	0.188	0.266	0.009
9	0.013	0.001	0.283	2.472	34.835	0.030	0.016	0.204	0.281	0.010
10	0.013	0.000	0.267	2.348	35.156	0.000	0.023	0.189	0.251	0.015
11	0.017	0.007	0.309	2.340	35.200	0.041	0.013	0.194	0.268	0.009
12	0.019	0.002	0.279	2.504	34.752	0.000	0.013	0.214	0.273	0.005
13	0.022	0.008	0.312	2.377	35.268	0.016	0.006	0.207	0.219	0.014
14	0.019	0.009	0.368	2.501	35.936	0.031	0.014	0.211	0.177	0.014
15	0.024	0.001	0.367	2.466	36.053	0.053	0.026	0.190	0.172	0.006
16	0.008	0.007	0.371	2.376	35.798	0.011	0.000	0.233	0.167	0.003
17	0.011	0.023	0.374	2.102	33.998	0.033	0.000	0.205	0.142	0.002
18	0.008	0.000	0.411	2.565	35.709	0.003	0.000	0.219	0.157	0.007

Point	P	Si	S	Mg	Ca	Mn	Fe	Sr	Na	K
1	0.046	0.011	0.238	2.697	33.259	0.047	0.006	0.233	0.275	0.016
2	0.017	0.006	0.234	2.428	32.535	0.019	0.000	0.216	0.262	0.010
3	0.014	0.002	0.226	2.307	31.869	0.000	0.012	0.196	0.230	0.006
4	0.021	0.009	0.275	2.390	31.613	0.000	0.000	0.242	0.216	0.012
5	0.025	0.011	0.290	2.676	34.399	0.001	0.027	0.199	0.270	0.008
6	0.013	0.001	0.271	2.431	33.989	0.001	0.015	0.218	0.232	0.006
7	0.017	0.008	0.309	2.441	35.375	0.000	0.021	0.177	0.237	0.018
8	0.014	0.007	0.288	2.191	33.997	0.024	0.028	0.206	0.239	0.013
9	0.014	0.002	0.285	2.274	33.535	0.010	0.005	0.220	0.246	0.012
10	0.018	0.003	0.312	2.454	35.444	0.008	0.025	0.199	0.259	0.008
11	0.011	0.005	0.295	2.308	33.675	0.008	0.011	0.194	0.193	0.011
12	0.016	0.001	0.255	2.194	33.537	0.000	0.012	0.218	0.255	0.014
13	0.013	0.006	0.230	2.265	34.853	0.005	0.006	0.205	0.274	0.013
14	0.011	0.009	0.218	2.311	34.094	0.000	0.015	0.220	0.265	0.009
15	0.010	0.006	0.251	2.367	32.941	0.009	0.005	0.220	0.263	0.006
16	0.019	0.000	0.246	2.450	34.037	0.026	0.013	0.193	0.257	0.001
17	0.011	0.000	0.264	2.461	32.363	0.013	0.022	0.185	0.252	0.005
18	0.014	0.005	0.270	2.416	32.291	0.000	0.008	0.216	0.239	0.011
19	0.014	0.005	0.273	2.402	35.369	0.022	0.028	0.180	0.238	0.011
20	0.011	0.006	0.263	2.249	34.545	0.007	0.027	0.193	0.255	0.006
21	0.020	0.006	0.258	2.357	33.872	0.000	0.016	0.179	0.246	0.001
22	0.011	0.005	0.304	2.470	34.339	0.000	0.006	0.233	0.222	0.004
23	0.017	0.003	0.322	2.134	35.545	0.002	0.018	0.191	0.223	0.012
24	0.021	0.013	0.275	2.341	34.041	0.030	0.015	0.229	0.247	0.009
25	0.017	0.002	0.296	2.379	34.009	0.000	0.009	0.211	0.236	0.007
26	0.013	0.007	0.326	2.404	35.689	0.013	0.000	0.203	0.212	0.010
27	0.017	0.006	0.379	2.281	35.337	0.011	0.012	0.196	0.168	0.008
28	0.018	0.007	0.390	2.313	36.013	0.003	0.013	0.209	0.195	0.006

Sample 2										
1	0.025	0.037	0.342	2.243	33.803	0.000	0.000	0.232	0.201	0.012
2	0.020	0.004	0.234	2.817	34.918	0.026	0.020	0.242	0.247	0.009
3	0.016	0.006	0.327	2.426	35.929	0.004	0.013	0.183	0.204	0.013
4	0.017	0.012	0.305	2.361	34.423	0.000	0.015	0.173	0.225	0.010
5	0.014	0.004	0.288	2.289	32.975	0.013	0.014	0.185	0.233	0.013
6	0.011	0.001	0.286	2.406	35.041	0.000	0.018	0.195	0.230	0.004
7	0.015	0.011	0.310	2.497	35.050	0.000	0.017	0.215	0.263	0.009
8	0.010	0.003	0.261	2.480	34.800	0.000	0.000	0.240	0.250	0.007
9	0.009	0.009	0.284	2.571	34.952	0.020	0.000	0.223	0.274	0.009
10	0.014	0.014	0.287	2.316	35.575	0.007	0.028	0.199	0.230	0.007
11	0.010	0.008	0.252	2.241	32.204	0.000	0.021	0.220	0.243	0.007
12	0.011	0.008	0.244	2.631	34.499	0.033	0.029	0.204	0.274	0.008
13	0.021	0.005	0.307	2.525	35.154	0.020	0.017	0.230	0.225	0.005
14	0.017	0.008	0.293	2.570	35.086	0.017	0.017	0.208	0.243	0.005
15	0.014	0.005	0.329	2.544	35.304	0.022	0.039	0.201	0.250	0.011
16	0.014	0.004	0.342	2.425	34.558	0.016	0.000	0.227	0.171	0.006
17	0.011	0.004	0.317	2.568	35.731	0.063	0.000	0.218	0.191	0.007
18	0.006	0.009	0.369	2.423	35.278	0.013	0.000	0.223	0.174	0.003
19	0.006	0.000	0.382	2.502	35.911	0.009	0.009	0.211	0.184	0.006
20	0.009	0.007	0.389	2.375	36.181	0.030	0.005	0.210	0.158	0.013
21	0.007	0.006	0.391	2.376	36.101	0.041	0.005	0.214	0.187	0.007
22	0.008	0.001	0.333	2.571	35.253	0.000	0.000	0.225	0.165	0.006
23	0.014	0.102	0.319	2.256	34.367	0.031	0.011	0.205	0.134	0.004

1	0.112	0.013	0.279	2.190	35.650	N/A	0.000	0.221	0.195	N/A
2	0.090	0.005	0.261	2.323	37.332	N/A	0.000	0.269	0.175	N/A
3	0.085	0.004	0.264	2.292	37.321	N/A	0.000	0.243	0.203	N/A
4	0.087	0.008	0.196	2.305	35.563	N/A	0.029	0.229	0.285	N/A

Point	P	Si	S	Mg	Ca	Mn	Fe	Sr	Na	K
5	0.092	0.015	0.197	2.442	36.045	N/A	0.019	0.270	0.278	N/A
6	0.090	0.007	0.222	2.557	35.797	N/A	0.000	0.229	0.237	N/A
7	0.087	0.009	0.242	2.375	37.686	N/A	0.000	0.220	0.199	N/A
8	0.095	0.014	0.211	2.379	36.749	N/A	0.015	0.222	0.243	N/A
9	0.089	0.000	0.257	2.373	36.539	N/A	0.025	0.252	0.224	N/A
10	0.091	0.009	0.213	2.445	36.717	N/A	0.002	0.236	0.226	N/A
11	0.088	0.000	0.265	2.405	37.288	N/A	0.021	0.241	0.156	N/A
12	0.084	0.009	0.222	2.534	36.844	N/A	0.013	0.245	0.238	N/A
13	0.082	0.005	0.271	2.271	37.423	N/A	0.027	0.245	0.189	N/A
14	0.087	0.008	0.247	2.213	36.408	N/A	0.033	0.227	0.206	N/A
15	0.076	0.127	0.291	2.317	35.085	N/A	0.384	0.267	0.157	N/A
16	0.090	0.010	0.282	2.446	36.285	N/A	0.032	0.231	0.185	N/A
17	0.096	0.012	0.228	2.325	36.674	N/A	0.016	0.249	0.168	N/A

Sample 3

1	0.085	0.011	0.219	2.202	36.430	N/A	0.019	0.246	0.245	N/A
2	0.092	0.008	0.230	2.453	35.914	N/A	0.002	0.233	0.238	N/A
3	0.090	0.014	0.233	2.538	36.238	N/A	0.013	0.259	0.220	N/A
4	0.086	0.004	0.207	2.684	35.471	N/A	0.005	0.202	0.223	N/A
5	0.092	0.014	0.213	2.360	36.232	N/A	0.020	0.212	0.235	N/A
6	0.099	0.020	0.221	2.386	36.020	N/A	0.002	0.242	0.246	N/A
7	0.102	0.004	0.230	2.379	36.348	N/A	0.032	0.245	0.199	N/A
8	0.083	0.001	0.233	2.480	36.517	N/A	0.000	0.240	0.223	N/A
9	0.086	0.010	0.255	2.314	36.801	N/A	0.011	0.243	0.195	N/A
10	0.094	0.013	0.237	2.296	36.180	N/A	0.033	0.232	0.203	N/A
11	0.087	0.015	0.219	2.559	35.805	N/A	0.010	0.245	0.222	N/A
12	0.087	0.011	0.257	2.235	36.200	N/A	0.007	0.231	0.185	N/A
13	0.078	0.003	0.261	2.264	36.382	N/A	0.017	0.249	0.209	N/A
14	0.080	0.004	0.271	2.303	35.526	N/A	0.018	0.269	0.172	N/A
15	0.084	0.008	0.283	2.480	36.161	N/A	0.027	0.242	0.206	N/A
16	0.087	0.002	0.292	2.537	36.018	N/A	0.027	0.255	0.184	N/A
17	0.087	0.007	0.283	2.421	36.316	N/A	0.027	0.237	0.150	N/A
18	0.082	0.011	0.255	2.325	36.443	N/A	0.015	0.230	0.161	N/A
19	0.083	0.009	0.222	2.311	36.425	N/A	0.019	0.242	0.201	N/A
20	0.094	0.012	0.293	2.281	35.552	N/A	0.007	0.246	0.200	N/A

Mytilus edulis

Sample1

1	0.006	0.009	0.057	0.094	39.150	0.003	0.000	0.101	0.122	0.002
2	0.005	0.010	0.063	0.098	39.838	0.000	0.000	0.093	0.098	0.000
3	0.011	0.001	0.057	0.060	36.662	0.011	0.013	0.075	0.082	0.002
4	0.005	0.000	0.063	0.059	39.591	0.010	0.018	0.094	0.078	0.000
5	0.005	0.005	0.043	0.071	40.111	0.014	0.000	0.094	0.095	0.000
6	0.005	0.010	0.040	0.072	39.861	0.033	0.017	0.082	0.093	0.000
7	0.003	0.006	0.038	0.104	39.826	0.008	0.000	0.083	0.105	0.006
8	0.007	0.002	0.029	0.110	37.361	0.000	0.032	0.084	0.115	0.001
9	0.000	0.010	0.055	0.139	39.836	0.019	0.000	0.098	0.098	0.002
10	0.008	0.011	0.030	0.139	40.036	0.000	0.000	0.083	0.092	0.000
11	0.005	0.006	0.027	0.134	39.952	0.000	0.014	0.071	0.089	0.003
12	0.002	0.002	0.035	0.089	39.970	0.005	0.000	0.078	0.078	0.000
13	0.003	0.000	0.040	0.127	39.562	0.004	0.003	0.061	0.079	0.000
14	0.006	0.013	0.049	0.098	39.732	0.000	0.039	0.067	0.080	0.005
15	0.002	0.010	0.028	0.136	39.799	0.011	0.000	0.091	0.096	0.003
16	0.003	0.004	0.016	0.151	39.839	0.002	0.004	0.101	0.098	0.001
17	0.007	0.013	0.018	0.143	39.932	0.046	0.005	0.090	0.100	0.002
18	0.004	0.002	0.033	0.115	40.139	0.000	0.020	0.061	0.086	0.000
19	0.005	0.009	0.013	0.122	40.206	0.000	0.000	0.095	0.096	0.000
20	0.000	0.006	0.022	0.149	39.983	0.004	0.000	0.072	0.086	0.000
21	0.001	0.005	0.036	0.136	40.150	0.006	0.008	0.071	0.077	0.001
22	0.008	0.007	0.039	0.130	40.157	0.020	0.004	0.057	0.067	0.000

Point	P	Si	S	Mg	Ca	Mn	Fe	Sr	Na	K
23	0.004	0.005	0.046	0.117	40.033	0.000	0.000	0.068	0.063	0.000
24	0.000	0.005	0.036	0.105	40.408	0.011	0.004	0.074	0.075	0.000
25	0.005	0.003	0.028	0.104	40.122	0.006	0.000	0.078	0.062	0.000
26	0.005	0.009	0.027	0.095	40.313	0.019	0.024	0.108	0.065	0.000
27	0.001	0.007	0.027	0.094	40.091	0.000	0.002	0.084	0.072	0.000
28	0.003	0.000	0.016	0.089	40.177	0.013	0.000	0.054	0.068	0.001
29	0.003	0.006	0.015	0.126	40.522	0.013	0.005	0.093	0.074	0.000
30	0.004	0.011	0.010	0.097	40.166	0.009	0.000	0.081	0.058	0.000
31	0.001	0.005	0.009	0.123	40.143	0.029	0.000	0.042	0.058	0.000
32	0.006	0.002	0.020	0.108	39.970	0.000	0.003	0.076	0.059	0.005
33	0.006	0.004	0.044	0.128	40.082	0.023	0.000	0.078	0.056	0.003
34	0.004	0.003	0.065	0.151	36.985	0.011	0.024	0.077	0.055	0.000
35	0.002	0.006	0.064	0.198	40.255	0.000	0.000	0.080	0.052	0.000
36	0.006	0.009	0.050	0.111	40.155	0.000	0.018	0.078	0.049	0.003
37	0.003	0.004	0.030	0.109	40.373	0.000	0.000	0.093	0.062	0.000
38	0.004	0.002	0.023	0.083	40.348	0.006	0.002	0.084	0.056	0.000
39	0.002	0.002	0.022	0.092	40.169	0.000	0.000	0.068	0.057	0.006
40	0.001	0.005	0.027	0.106	40.387	0.000	0.001	0.080	0.056	0.000
41	0.000	0.003	0.034	0.134	40.274	0.000	0.000	0.079	0.060	0.001
42	0.000	0.000	0.025	0.122	39.599	0.029	0.027	0.063	0.047	0.000
43	0.005	0.005	0.096	0.318	39.660	0.042	0.000	0.078	0.044	0.003
44	0.005	0.001	0.126	0.256	39.667	0.000	0.001	0.091	0.028	0.000
45	0.006	0.009	0.030	0.001	39.218	0.001	0.000	0.126	0.218	0.006
46	0.007	0.007	0.060	0.001	38.882	0.000	0.000	0.151	0.233	0.001
1	0.009	0.010	0.078	0.082	38.743	0.000	0.000	0.125	0.202	0.000
2	0.005	0.002	0.063	0.055	36.018	0.000	0.010	0.103	0.172	0.000
3	0.007	0.007	0.066	0.064	39.170	0.000	0.004	0.085	0.151	0.002
4	0.006	0.009	0.016	0.076	35.695	0.032	0.004	0.087	0.147	0.000
5	0.007	0.007	0.028	0.098	39.394	0.000	0.007	0.099	0.137	0.000
6	0.002	0.000	0.038	0.098	38.119	0.006	0.005	0.087	0.123	0.000
7	0.001	0.000	0.031	0.102	39.779	0.000	0.000	0.101	0.137	0.000
8	0.002	0.009	0.034	0.094	37.149	0.000	0.015	0.075	0.148	0.000
9	0.005	0.000	0.027	0.117	38.724	0.000	0.016	0.096	0.135	0.000
10	0.008	0.003	0.030	0.112	39.938	0.000	0.013	0.097	0.136	0.001
11	0.002	0.000	0.034	0.114	39.790	0.000	0.003	0.094	0.141	0.000
12	0.003	0.000	0.012	0.119	39.732	0.055	0.004	0.083	0.148	0.000
13	0.007	0.003	0.020	0.099	35.748	0.000	0.013	0.088	0.144	0.000
14	0.004	0.003	0.025	0.133	39.749	0.000	0.008	0.085	0.150	0.000
15	0.010	0.005	0.019	0.118	39.694	0.000	0.000	0.112	0.145	0.000
16	0.004	0.009	0.010	0.125	39.733	0.021	0.001	0.094	0.152	0.005
17	0.002	0.003	0.011	0.119	39.833	0.036	0.000	0.093	0.155	0.000
18	0.006	0.006	0.024	0.097	39.720	0.011	0.003	0.112	0.139	0.000
19	0.003	0.005	0.019	0.099	36.064	0.000	0.000	0.067	0.147	0.000
20	0.000	0.007	0.015	0.104	34.568	0.026	0.000	0.090	0.148	0.000
21	0.004	0.003	0.012	0.107	39.780	0.000	0.012	0.072	0.124	0.001
22	0.002	0.005	0.019	0.145	39.853	0.011	0.014	0.105	0.116	0.001
23	0.001	0.004	0.014	0.125	39.966	0.004	0.000	0.090	0.100	0.002
24	0.006	0.001	0.018	0.127	39.945	0.000	0.013	0.080	0.092	0.000
25	0.004	0.000	0.011	0.138	39.529	0.013	0.032	0.074	0.097	0.006
26	0.005	0.005	0.006	0.151	39.700	0.025	0.004	0.085	0.098	0.004
27	0.000	0.000	0.029	0.157	39.652	0.000	0.000	0.089	0.095	0.001
28	0.001	0.006	0.023	0.142	39.871	0.033	0.016	0.073	0.093	0.001
29	0.001	0.004	0.013	0.113	40.047	0.000	0.000	0.083	0.084	0.004
30	0.003	0.000	0.003	0.113	39.714	0.008	0.015	0.055	0.084	0.000
31	0.006	0.004	0.016	0.127	39.688	0.006	0.012	0.085	0.092	0.000
32	0.005	0.007	0.009	0.116	39.914	0.000	0.005	0.078	0.076	0.000
33	0.004	0.000	0.022	0.121	39.882	0.003	0.000	0.083	0.082	0.001

Point	P	Si	S	Mg	Ca	Mn	Fe	Sr	Na	K
34	0.003	0.003	0.022	0.161	39.631	0.003	0.003	0.086	0.090	0.000
35	0.002	0.000	0.008	0.138	39.343	0.000	0.024	0.075	0.081	0.000
36	0.006	0.004	0.012	0.097	40.073	0.006	0.015	0.062	0.067	0.002
37	0.000	0.000	0.020	0.124	39.511	0.000	0.018	0.056	0.063	0.002
38	0.003	0.008	0.038	0.123	39.849	0.021	0.003	0.076	0.053	0.000
39	0.006	0.009	0.069	0.044	39.121	0.001	0.000	0.167	0.157	0.000
40	0.001	0.002	0.069	0.016	38.699	0.014	0.016	0.262	0.258	0.006
41	0.001	0.000	0.070	0.005	38.702	0.025	0.056	0.137	0.253	0.005
42	0.003	0.005	0.035	0.011	36.892	0.021	0.022	0.327	0.220	0.000
43	0.005	0.002	0.071	0.016	31.351	0.000	0.008	0.190	0.221	0.001
44	0.005	0.000	0.042	0.014	28.657	0.013	0.020	0.216	0.205	0.000
45	0.001	0.000	0.067	0.018	32.010	0.000	0.024	0.204	0.229	0.004
46	0.006	0.002	0.051	0.019	38.585	0.000	0.009	0.306	0.239	0.000
47	0.007	0.029	0.050	0.012	35.445	0.021	0.014	0.160	0.154	0.001
1	0.010	0.001	0.113	0.076	38.785	0.019	0.000	0.129	0.204	0.000
2	0.005	0.000	0.091	0.060	39.447	0.049	0.000	0.115	0.207	0.000
3	0.005	0.003	0.080	0.065	39.418	0.000	0.000	0.132	0.223	0.002
4	0.003	0.011	0.072	0.094	39.235	0.030	0.012	0.110	0.213	0.000
5	0.008	0.000	0.045	0.106	39.569	0.000	0.002	0.107	0.203	0.000
6	0.003	0.002	0.053	0.104	39.546	0.000	0.000	0.086	0.209	0.003
7	0.008	0.008	0.027	0.100	39.084	0.013	0.016	0.126	0.221	0.000
8	0.004	0.009	0.041	0.106	39.351	0.000	0.007	0.081	0.208	0.000
9	0.004	0.003	0.041	0.113	39.453	0.031	0.000	0.080	0.207	0.000
10	0.001	0.011	0.041	0.104	39.430	0.008	0.000	0.102	0.191	0.000
11	0.012	0.010	0.043	0.107	39.780	0.000	0.000	0.113	0.192	0.003
12	0.007	0.000	0.031	0.106	39.538	0.000	0.000	0.113	0.198	0.000
13	0.005	0.004	0.022	0.115	39.656	0.019	0.025	0.115	0.177	0.002
14	0.004	0.004	0.043	0.106	39.541	0.000	0.000	0.124	0.189	0.000
15	0.004	0.004	0.027	0.107	39.505	0.000	0.000	0.089	0.167	0.000
16	0.006	0.007	0.049	0.106	39.563	0.003	0.000	0.099	0.171	0.002
17	0.004	0.005	0.052	0.108	39.439	0.000	0.006	0.122	0.165	0.000
18	0.007	0.010	0.058	0.099	39.545	0.000	0.000	0.087	0.168	0.004
19	0.004	0.000	0.033	0.113	39.652	0.005	0.000	0.083	0.177	0.002
20	0.002	0.016	0.016	0.104	39.794	0.000	0.000	0.086	0.166	0.000
21	0.003	0.000	0.031	0.108	39.645	0.000	0.000	0.106	0.165	0.000
22	0.004	0.006	0.028	0.110	39.684	0.022	0.000	0.104	0.152	0.000
23	0.006	0.000	0.038	0.115	39.510	0.016	0.000	0.124	0.153	0.003
24	0.009	0.013	0.032	0.111	39.744	0.002	0.003	0.088	0.148	0.000
25	0.007	0.001	0.030	0.126	39.841	0.037	0.000	0.104	0.141	0.004
26	0.010	0.000	0.026	0.129	39.983	0.000	0.013	0.074	0.128	0.007
27	0.004	0.008	0.044	0.158	39.773	0.000	0.013	0.084	0.126	0.000
28	0.011	0.007	0.034	0.135	39.982	0.000	0.010	0.101	0.125	0.000
29	0.004	0.000	0.044	0.142	39.858	0.000	0.002	0.093	0.123	0.000
30	0.005	0.007	0.024	0.161	39.859	0.000	0.016	0.091	0.109	0.000
31	0.009	0.006	0.039	0.149	39.730	0.006	0.010	0.077	0.102	0.000
32	0.003	0.010	0.027	0.125	39.865	0.000	0.002	0.099	0.088	0.000
33	0.001	0.010	0.027	0.156	39.994	0.012	0.005	0.098	0.093	0.002
34	0.001	0.009	0.032	0.164	40.078	0.007	0.000	0.088	0.107	0.002
35	0.012	0.000	0.031	0.137	39.894	0.000	0.027	0.078	0.096	0.001
36	0.002	0.001	0.041	0.133	39.949	0.000	0.000	0.083	0.099	0.000
37	0.009	0.005	0.036	0.162	39.806	0.005	0.000	0.066	0.096	0.003
38	0.005	0.013	0.024	0.155	39.774	0.033	0.020	0.077	0.084	0.000
39	0.004	0.000	0.032	0.187	39.730	0.038	0.023	0.069	0.069	0.000
40	0.004	0.004	0.050	0.172	39.776	0.039	0.000	0.104	0.063	0.000
41	0.001	0.001	0.067	0.130	39.835	0.000	0.000	0.090	0.059	0.000
42	0.005	0.007	0.044	0.004	38.771	0.004	0.013	0.125	0.244	0.000
43	0.000	0.000	0.041	0.020	38.034	0.000	0.024	0.248	0.220	0.007

Point	P	Si	S	Mg	Ca	Mn	Fe	Sr	Na	K
44	0.003	0.008	0.036	0.000	33.111	0.001	0.017	0.120	0.242	0.000
45	0.001	0.000	0.035	0.003	30.058	0.000	0.019	0.107	0.220	0.000
46	0.001	0.000	0.044	0.004	29.531	0.000	0.005	0.093	0.222	0.003
47	0.001	0.001	0.034	0.011	27.594	0.034	0.011	0.101	0.212	0.000
48	0.003	0.005	0.037	0.000	26.191	0.011	0.006	0.094	0.213	0.001
49	0.003	0.003	0.048	0.025	27.255	0.000	0.023	0.098	0.217	0.003
50	0.003	0.000	0.051	0.007	26.455	0.003	0.015	0.127	0.204	0.001
51	0.003	0.002	0.043	0.013	26.414	0.000	0.001	0.245	0.221	0.003
52	0.004	0.000	0.053	0.016	25.892	0.026	0.016	0.122	0.212	0.000
53	0.000	0.000	0.050	0.001	25.070	0.003	0.000	0.080	0.216	0.000
54	0.000	0.003	0.031	0.020	23.741	0.000	0.021	0.144	0.197	0.000
55	0.002	0.009	0.029	0.022	24.813	0.000	0.001	0.187	0.203	0.001
56	0.001	0.000	0.041	0.015	24.786	0.000	0.000	0.159	0.199	0.004
57	0.001	0.009	0.049	0.016	24.629	0.000	0.001	0.123	0.207	0.000
58	0.004	0.001	0.040	0.023	23.680	0.014	0.014	0.148	0.194	0.000
59	0.002	0.006	0.036	0.017	24.966	0.000	0.001	0.175	0.203	0.000
60	0.002	0.000	0.029	0.019	23.329	0.002	0.000	0.139	0.198	0.000
61	0.002	0.000	0.027	0.011	24.447	0.004	0.005	0.199	0.207	0.002
62	0.000	0.006	0.056	0.024	24.595	0.000	0.000	0.158	0.205	0.001
63	0.003	0.000	0.018	0.042	25.432	0.003	0.000	0.215	0.216	0.000
64	0.004	0.004	0.038	0.030	31.721	0.019	0.008	0.326	0.217	0.002
65	0.001	0.001	0.033	0.026	30.074	0.000	0.019	0.154	0.207	0.007
66	0.001	0.001	0.037	0.018	32.806	0.000	0.005	0.144	0.235	0.000
67	0.001	0.004	0.068	0.022	38.990	0.000	0.022	0.212	0.216	0.005

1	0.001	0.009	0.072	0.057	39.901	0.005	0.001	0.097	0.166	0.000
2	0.003	0.004	0.035	0.050	40.220	0.008	0.012	0.119	0.192	0.003
3	0.002	0.000	0.047	0.057	34.019	0.000	0.000	0.083	0.166	0.007
4	0.007	0.005	0.057	0.061	40.194	0.008	0.000	0.082	0.169	0.003
5	0.001	0.001	0.042	0.076	40.257	0.012	0.004	0.097	0.154	0.003
6	0.005	0.001	0.041	0.088	40.346	0.017	0.007	0.103	0.149	0.001
7	0.002	0.005	0.050	0.087	40.311	0.000	0.000	0.102	0.144	0.000
8	0.003	0.004	0.048	0.102	40.176	0.022	0.006	0.103	0.159	0.006
9	0.004	0.005	0.024	0.112	39.796	0.014	0.000	0.084	0.152	0.000
10	0.004	0.008	0.034	0.136	40.097	0.023	0.004	0.090	0.138	0.000
11	0.005	0.000	0.018	0.112	39.607	0.000	0.032	0.085	0.154	0.002
12	0.001	0.004	0.022	0.115	39.988	0.000	0.011	0.104	0.140	0.000
13	0.005	0.000	0.020	0.114	32.364	0.000	0.000	0.080	0.152	0.001
14	0.002	0.014	0.024	0.086	40.315	0.000	0.000	0.083	0.142	0.002
15	0.006	0.247	0.032	0.132	39.742	0.000	0.078	0.081	0.149	0.006
16	0.002	0.004	0.009	0.121	39.734	0.029	0.031	0.061	0.159	0.000
17	0.004	0.001	0.028	0.128	40.026	0.000	0.007	0.085	0.148	0.007
18	0.003	0.014	0.024	0.109	40.100	0.000	0.007	0.064	0.133	0.000
19	0.000	0.006	0.016	0.113	40.193	0.000	0.017	0.084	0.135	0.000
20	0.004	0.009	0.028	0.120	40.388	0.069	0.013	0.078	0.146	0.000
21	0.004	0.004	0.028	0.116	40.519	0.036	0.018	0.091	0.143	0.000
22	0.003	0.002	0.000	0.129	40.412	0.004	0.008	0.085	0.128	0.000
23	0.004	0.000	0.005	0.123	38.353	0.002	0.000	0.083	0.126	0.000
24	0.005	0.003	0.023	0.123	40.056	0.046	0.016	0.084	0.113	0.003
25	0.007	0.004	0.015	0.114	40.276	0.003	0.000	0.075	0.108	0.000
26	0.003	0.000	0.027	0.119	40.412	0.003	0.000	0.074	0.119	0.000
27	0.003	0.000	0.023	0.112	40.068	0.016	0.000	0.070	0.117	0.000
28	0.000	0.000	0.008	0.144	40.209	0.014	0.013	0.113	0.107	0.004
29	0.004	0.006	0.014	0.128	40.237	0.000	0.001	0.088	0.099	0.000
30	0.000	0.000	0.022	0.138	40.458	0.014	0.000	0.081	0.096	0.000
31	0.006	0.004	0.029	0.165	40.272	0.000	0.013	0.082	0.090	0.002
32	0.004	0.005	0.028	0.171	40.293	0.000	0.011	0.075	0.089	0.000
33	0.002	0.004	0.021	0.146	40.399	0.047	0.008	0.095	0.077	0.000

Point	P	Si	S	Mg	Ca	Mn	Fe	Sr	Na	K
34	0.002	0.000	0.019	0.107	34.179	0.000	0.000	0.085	0.076	0.000
35	0.002	0.003	0.014	0.112	40.360	0.022	0.023	0.050	0.080	0.003
36	0.005	0.007	0.020	0.127	40.366	0.002	0.000	0.082	0.074	0.000
37	0.007	0.011	0.017	0.121	40.344	0.021	0.001	0.062	0.065	0.000
38	0.001	0.004	0.024	0.142	40.374	0.000	0.000	0.089	0.075	0.002
39	0.008	0.006	0.026	0.135	40.327	0.036	0.006	0.065	0.073	0.000
40	0.007	0.004	0.025	0.107	40.331	0.000	0.034	0.089	0.060	0.004
41	0.007	0.015	0.062	0.073	39.497	0.037	0.000	0.113	0.149	0.001
42	0.005	0.005	0.069	0.012	39.016	0.009	0.001	0.354	0.242	0.001
43	0.001	0.004	0.071	0.012	37.944	0.000	0.000	0.146	0.241	0.003
44	0.000	0.005	0.060	0.015	29.671	0.016	0.019	0.201	0.218	0.000
45	0.002	0.006	0.040	0.001	29.418	0.000	0.008	0.195	0.223	0.002
46	0.005	0.002	0.036	0.010	27.773	0.015	0.020	0.229	0.208	0.000
47	0.002	0.004	0.035	0.014	28.513	0.000	0.009	0.217	0.225	0.003
48	0.004	0.000	0.050	0.013	33.693	0.007	0.000	0.223	0.219	0.005
49	0.007	0.010	0.047	0.010	38.500	0.000	0.000	0.305	0.223	0.000
50	0.001	0.002	0.057	0.014	38.796	0.000	0.000	0.264	0.230	0.006
1	0.006	0.002	0.044	0.060	39.292	0.000	0.000	0.134	0.151	0.000
2	0.007	0.004	0.052	0.071	39.479	0.000	0.000	0.102	0.157	0.000
3	0.003	0.004	0.045	0.072	39.189	0.016	0.000	0.093	0.170	0.000
4	0.005	0.006	0.048	0.063	39.225	0.008	0.000	0.090	0.183	0.000
5	0.003	0.001	0.080	0.086	39.260	0.022	0.000	0.083	0.173	0.000
6	0.007	0.000	0.043	0.066	39.359	0.023	0.000	0.115	0.159	0.000
7	0.000	0.008	0.033	0.085	39.405	0.000	0.022	0.110	0.177	0.005
8	0.001	0.003	0.038	0.087	34.180	0.000	0.015	0.106	0.177	0.006
9	0.004	0.003	0.042	0.096	39.491	0.000	0.003	0.114	0.161	0.002
10	0.006	0.011	0.041	0.121	39.507	0.009	0.000	0.109	0.138	0.000
11	0.004	0.004	0.044	0.138	39.562	0.051	0.001	0.101	0.135	0.005
12	0.004	0.011	0.042	0.131	39.561	0.000	0.007	0.096	0.135	0.000
13	0.006	0.002	0.032	0.135	39.823	0.000	0.014	0.101	0.142	0.000
14	0.010	0.004	0.025	0.121	39.823	0.033	0.005	0.105	0.128	0.008
15	0.001	0.000	0.045	0.116	39.559	0.043	0.003	0.078	0.134	0.000
16	0.002	0.005	0.015	0.113	39.839	0.011	0.000	0.085	0.139	0.000
17	0.005	0.011	0.020	0.109	39.949	0.000	0.000	0.080	0.126	0.002
18	0.006	0.001	0.022	0.125	39.751	0.023	0.013	0.097	0.130	0.001
19	0.001	0.006	0.023	0.144	39.568	0.029	0.031	0.092	0.129	0.005
20	0.007	0.010	0.037	0.151	40.059	0.005	0.012	0.087	0.128	0.003
21	0.004	0.000	0.021	0.133	39.748	0.004	0.008	0.106	0.115	0.000
22	0.004	0.005	0.034	0.159	39.666	0.018	0.000	0.084	0.108	0.005
23	0.005	0.004	0.019	0.130	39.722	0.023	0.000	0.088	0.107	0.004
24	0.001	0.005	0.010	0.124	39.750	0.004	0.003	0.078	0.105	0.005
25	0.004	0.009	0.030	0.139	39.676	0.014	0.000	0.088	0.111	0.000
26	0.004	0.005	0.005	0.159	39.886	0.022	0.006	0.083	0.121	0.000
27	0.004	0.011	0.023	0.124	39.489	0.000	0.010	0.063	0.106	0.003
28	0.003	0.000	0.014	0.127	39.786	0.000	0.014	0.090	0.102	0.000
29	0.002	0.000	0.030	0.153	40.078	0.002	0.002	0.090	0.095	0.000
30	0.005	0.010	0.009	0.146	39.980	0.000	0.000	0.077	0.097	0.000
31	0.004	0.008	0.028	0.156	40.061	0.034	0.000	0.083	0.089	0.004
32	0.003	0.001	0.024	0.167	40.053	0.009	0.006	0.084	0.087	0.003
33	0.004	0.011	0.020	0.128	40.344	0.005	0.000	0.051	0.063	0.000
34	0.007	0.003	0.018	0.114	40.104	0.005	0.024	0.062	0.062	0.002
35	0.003	0.005	0.078	0.161	40.342	0.033	0.005	0.060	0.049	0.001
36	0.005	0.002	0.058	0.012	38.601	0.003	0.027	0.277	0.207	0.003
37	0.007	0.006	0.062	0.018	35.731	0.000	0.021	0.191	0.220	0.004
38	0.001	0.000	0.064	0.009	34.918	0.020	0.017	0.176	0.248	0.005
39	0.005	0.000	0.049	0.009	30.617	0.036	0.010	0.124	0.241	0.000
40	0.003	0.009	0.048	0.031	28.043	0.001	0.009	0.201	0.207	0.001

Point	P	Si	S	Mg	Ca	Mn	Fe	Sr	Na	K
41	0.001	0.000	0.061	0.010	29.302	0.009	0.008	0.184	0.234	0.004
42	0.001	0.006	0.052	0.016	27.754	0.003	0.015	0.235	0.215	0.007
43	0.004	0.014	0.040	0.020	32.334	0.000	0.012	0.224	0.225	0.000
44	0.002	0.007	0.048	0.019	38.939	0.016	0.034	0.188	0.221	0.003
45	0.007	0.002	0.049	0.025	38.624	0.006	0.001	0.281	0.236	0.003
46	0.008	0.007	0.052	0.016	38.671	0.000	0.000	0.280	0.225	0.005

Sample 2

1	0.067	0.019	0.086	0.079	39.143	0.001	0.000	0.042	0.298	0.007
2	0.060	0.016	0.068	0.064	39.738	0.000	0.025	0.109	0.258	0.000
3	0.058	0.018	0.076	0.105	40.331	0.004	0.000	0.112	0.272	0.005
4	0.061	0.006	0.052	0.135	39.326	0.009	0.008	0.108	0.288	0.000
5	0.056	0.012	0.114	0.114	40.140	0.000	0.000	0.128	0.257	0.000
6	0.059	0.007	0.089	0.136	40.240	0.000	0.007	0.145	0.275	0.000
7	0.059	0.005	0.059	0.148	39.850	0.000	0.000	0.117	0.302	0.000
8	0.058	0.006	0.072	0.146	40.026	0.008	0.003	0.102	0.279	0.007
9	0.058	0.014	0.067	0.156	39.821	0.000	0.016	0.125	0.293	0.000
10	0.058	0.006	0.089	0.163	40.137	0.000	0.029	0.110	0.276	0.002
11	0.057	0.006	0.089	0.161	40.122	0.013	0.025	0.100	0.268	0.001
12	0.057	0.009	0.075	0.163	39.676	0.000	0.017	0.104	0.257	0.007
13	0.059	0.018	0.052	0.150	39.883	0.011	0.037	0.100	0.259	0.005
14	0.057	0.024	0.065	0.156	39.435	0.005	0.000	0.129	0.269	0.004
15	0.058	0.013	0.061	0.159	39.751	0.004	0.025	0.109	0.245	0.007
16	0.060	0.010	0.049	0.132	39.974	0.000	0.003	0.087	0.249	0.008
17	0.058	0.009	0.049	0.131	39.943	0.000	0.000	0.126	0.227	0.000
18	0.060	0.009	0.035	0.112	39.863	0.000	0.000	0.088	0.197	0.000
19	0.062	0.004	0.035	0.074	39.890	0.000	0.005	0.105	0.154	0.003
20	0.059	0.001	0.024	0.000	39.013	0.000	0.018	0.100	0.297	0.003
21	0.058	0.008	0.035	0.000	39.531	0.011	0.000	0.152	0.280	0.000
22	0.059	0.014	0.047	0.000	39.283	0.000	0.009	0.113	0.289	0.002
23	0.055	0.019	0.057	0.000	39.786	0.024	0.011	0.088	0.303	0.000
24	0.055	0.013	0.034	0.000	39.454	0.000	0.006	0.101	0.278	0.006
25	0.058	0.004	0.059	0.020	39.390	0.004	0.012	0.095	0.266	0.000
26	0.057	0.001	0.064	0.013	39.223	0.000	0.013	0.081	0.269	0.004
27	0.024	0.089	0.104	0.014	11.936	0.000	0.066	0.073	0.130	0.018
28	0.035	0.013	0.041	0.001	25.690	0.021	0.000	0.078	0.192	0.003
29	0.055	0.001	0.050	0.000	38.258	0.000	0.030	0.088	0.290	0.002
30	0.056	0.017	0.050	0.000	38.826	0.000	0.035	0.093	0.310	0.003
31	0.058	0.002	0.038	0.000	39.150	0.000	0.000	0.002	0.283	0.000
32	0.057	0.015	0.057	0.000	38.751	0.000	0.012	0.001	0.285	0.003
33	0.055	0.012	0.052	0.000	38.850	0.014	0.025	0.007	0.321	0.002

Avian Eggshell (*Gallus gallus*)

Sample 1

1	0.105	0.024	0.021	0.593	37.219	0.013	0.013	0.057	0.045	0.033
2	0.057	0.016	0.024	0.548	37.520	0.019	0.000	0.055	0.036	0.031
3	0.037	0.002	0.014	0.587	37.938	0.005	0.015	0.043	0.030	0.020
4	0.025	0.001	0.015	0.545	37.994	0.000	0.000	0.059	0.029	0.017
5	0.023	0.009	0.012	0.463	38.434	0.009	0.000	0.066	0.028	0.019
6	0.021	0.124	0.007	0.503	36.768	0.014	0.044	0.045	0.026	0.022
7	0.026	0.020	0.025	0.371	38.328	0.000	0.000	0.031	0.032	0.014
8	0.015	0.028	0.019	0.337	38.081	0.000	0.000	0.043	0.026	0.018
9	0.016	0.005	0.019	0.337	38.773	0.000	0.000	0.022	0.034	0.021
10	0.018	0.087	0.013	0.214	36.978	0.013	0.014	0.000	0.027	0.012
11	0.007	0.253	0.026	0.233	31.769	0.000	0.023	0.042	0.041	0.005
12	0.008	0.003	0.007	0.151	39.584	0.000	0.007	0.033	0.042	0.006
13	0.010	0.267	0.086	0.096	33.211	0.014	0.006	0.014	0.044	0.003
14	0.005	0.000	0.016	0.089	39.143	0.012	0.000	0.023	0.067	0.004
15	0.001	0.014	0.017	0.136	39.046	0.000	0.000	0.022	0.069	0.006

Point	P	Si	S	Mg	Ca	Mn	Fe	Sr	Na	K
16	0.001	0.002	0.013	0.250	38.462	0.000	0.000	0.033	0.096	0.000
17	0.000	0.029	0.027	0.393	37.798	0.000	0.000	0.018	0.110	0.003
1	0.099	0.006	0.013	0.584	37.799	0.000	0.026	0.045	0.038	0.030
2	0.053	0.005	0.016	0.609	37.965	0.003	0.000	0.067	0.030	0.019
3	0.034	0.009	0.017	0.520	37.977	0.019	0.000	0.039	0.031	0.029
4	0.009	0.032	0.029	0.198	14.830	0.011	0.010	0.029	0.012	0.009
5	0.022	0.005	0.016	0.464	37.946	0.011	0.000	0.045	0.027	0.012
6	0.018	0.009	0.035	0.390	38.051	0.017	0.000	0.051	0.033	0.026
7	0.020	0.008	0.024	0.359	38.394	0.000	0.000	0.051	0.026	0.016
8	0.019	0.014	0.027	0.343	38.085	0.002	0.013	0.030	0.028	0.014
9	0.016	0.003	0.012	0.312	38.642	0.019	0.000	0.034	0.027	0.023
10	0.013	0.006	0.018	0.313	38.212	0.019	0.007	0.004	0.033	0.020
11	0.018	0.073	0.009	0.258	38.823	0.000	0.000	0.028	0.033	0.012
12	0.010	0.024	0.009	0.156	39.145	0.033	0.000	0.018	0.044	0.008
13	0.010	0.010	0.001	0.116	38.959	0.003	0.011	0.026	0.057	0.006
14	0.005	0.324	0.039	0.087	34.785	0.000	0.065	0.021	0.060	0.009
15	0.005	0.004	0.022	0.188	39.135	0.009	0.000	0.038	0.080	0.009
16	0.001	0.011	0.007	0.238	37.850	0.010	0.011	0.034	0.070	0.000
17	0.008	0.014	0.119	0.437	35.937	0.002	0.001	0.020	0.148	0.000
1	0.118	0.023	0.028	0.588	37.683	0.020	0.000	0.037	0.036	0.025
2	0.052	0.006	0.009	0.597	37.926	0.000	0.012	0.044	0.036	0.023
3	0.036	0.009	0.000	0.569	38.421	0.000	0.012	0.056	0.038	0.027
4	0.028	0.002	0.015	0.528	38.132	0.014	0.000	0.042	0.032	0.025
5	0.026	0.012	0.027	0.442	38.337	0.008	0.000	0.039	0.038	0.029
6	0.022	0.001	0.031	0.419	38.103	0.000	0.026	0.028	0.033	0.018
7	0.023	0.014	0.016	0.344	37.551	0.000	0.000	0.033	0.027	0.018
8	0.017	0.006	0.005	0.377	38.688	0.000	0.000	0.040	0.027	0.021
9	0.007	0.004	0.009	0.341	38.508	0.024	0.006	0.014	0.032	0.022
10	0.007	0.027	0.036	0.146	18.161	0.000	0.003	0.020	0.015	0.007
11	0.009	0.004	0.009	0.328	39.314	0.000	0.000	0.042	0.027	0.016
12	0.008	0.000	0.017	0.236	39.303	0.034	0.000	0.029	0.031	0.005
13	0.012	0.002	0.011	0.191	39.492	0.006	0.003	0.012	0.042	0.003
14	0.005	0.001	0.028	0.146	39.779	0.005	0.002	0.052	0.048	0.008
15	0.002	0.064	0.000	0.149	39.590	0.000	0.002	0.046	0.042	0.002
16	0.004	0.019	0.024	0.176	39.058	0.000	0.016	0.022	0.085	0.005
1	0.106	0.006	0.027	0.621	37.680	0.013	0.000	0.053	0.038	0.021
2	0.058	0.010	0.031	0.589	37.466	0.000	0.000	0.052	0.043	0.028
3	0.017	0.008	0.032	0.297	20.130	0.000	0.000	0.044	0.018	0.009
4	0.033	0.768	0.001	0.505	37.051	0.002	0.000	0.033	0.037	0.018
5	0.028	0.006	0.020	0.448	38.326	0.027	0.003	0.039	0.036	0.030
6	0.031	0.005	0.023	0.441	38.034	0.005	0.000	0.037	0.029	0.021
7	0.015	0.007	0.019	0.384	38.229	0.004	0.007	0.034	0.022	0.025
8	0.025	0.005	0.019	0.357	38.320	0.020	0.000	0.016	0.028	0.025
9	0.019	0.004	0.015	0.317	38.369	0.000	0.000	0.025	0.032	0.014
10	0.018	0.012	0.024	0.261	38.535	0.009	0.000	0.023	0.026	0.010
11	0.011	0.002	0.016	0.234	38.898	0.009	0.000	0.028	0.027	0.011
12	0.009	0.013	0.004	0.196	39.211	0.003	0.003	0.004	0.049	0.010
13	0.010	0.017	0.023	0.133	39.017	0.000	0.011	0.020	0.042	0.005
14	0.009	0.047	0.026	0.113	37.445	0.000	0.029	0.004	0.061	0.001
15	0.001	0.040	0.022	0.157	38.824	0.000	0.018	0.024	0.042	0.000
16	0.006	0.109	0.020	0.288	36.912	0.000	0.009	0.004	0.056	0.002
17	0.000	0.000	0.009	0.304	39.078	0.005	0.000	0.046	0.091	0.000
Sample 2										
1	0.123	0.015	0.018	0.557	39.369	0.000	0.000	0.024	N/A	0.029
2	0.072	0.031	0.021	0.513	38.548	0.000	0.015	0.039	N/A	0.033

Point	P	Si	S	Mg	Ca	Mn	Fe	Sr	Na	K
3	0.046	0.006	0.033	0.593	38.217	0.000	0.000	0.000	N/A	0.025
4	0.031	0.001	0.018	0.501	38.637	0.035	0.000	0.030	N/A	0.029
5	0.032	0.009	0.037	0.593	38.329	0.018	0.000	0.035	N/A	0.027
6	0.041	0.008	0.022	0.561	38.425	0.000	0.017	0.015	N/A	0.025
7	0.035	0.014	0.004	0.579	38.000	0.045	0.014	0.006	N/A	0.022
8	0.034	0.009	0.025	0.484	38.241	0.027	0.000	0.021	N/A	0.019
9	0.033	0.017	0.027	0.489	38.089	0.024	0.000	0.021	N/A	0.027
10	0.031	0.015	0.031	0.410	38.091	0.012	0.000	0.022	N/A	0.022
11	0.022	0.021	0.034	0.344	38.601	0.048	0.012	0.024	N/A	0.008
12	0.027	0.017	0.028	0.287	38.499	0.009	0.017	0.032	N/A	0.012
13	0.020	0.015	0.037	0.285	38.083	0.018	0.005	0.026	N/A	0.021
14	0.017	0.004	0.023	0.229	38.447	0.000	0.000	0.023	N/A	0.008
15	0.015	0.007	0.013	0.229	38.818	0.000	0.001	0.023	N/A	0.015
16	0.011	1.118	0.016	0.215	37.850	0.015	0.046	0.019	N/A	0.033
17	0.013	0.010	0.010	0.212	39.088	0.000	0.007	0.012	N/A	0.013
18	0.006	0.004	0.018	0.171	39.606	0.018	0.000	0.030	N/A	0.009
19	0.007	0.009	0.009	0.173	39.516	0.055	0.008	0.036	N/A	0.000
20	0.000	0.012	0.019	0.132	39.237	0.007	0.023	0.018	N/A	0.006
21	0.010	0.010	0.018	0.098	39.062	0.010	0.012	0.000	N/A	0.007
22	0.006	0.009	0.017	0.106	39.267	0.058	0.013	0.009	N/A	0.010
23	0.003	0.000	0.017	0.119	39.706	0.000	0.021	0.028	N/A	0.001
24	0.007	0.000	0.003	0.172	39.492	0.000	0.000	0.017	N/A	0.006
25	0.003	0.012	0.008	0.273	39.018	0.028	0.006	0.023	N/A	0.004
26	0.009	0.018	0.017	0.243	36.011	0.005	0.009	0.011	N/A	0.001
27	0.000	0.005	0.005	0.320	39.326	0.042	0.027	0.008	N/A	0.001
1	0.324	0.022	0.081	0.754	36.547	0.000	0.016	0.006	N/A	0.034
2	0.114	0.007	0.018	0.509	38.974	0.000	0.023	0.002	N/A	0.031
3	0.058	0.000	0.030	0.554	38.543	0.000	0.002	0.018	N/A	0.028
4	0.041	0.012	0.038	0.560	38.091	0.035	0.000	0.017	N/A	0.027
5	0.029	0.008	0.027	0.488	38.352	0.016	0.005	0.018	N/A	0.025
6	0.029	0.005	0.022	0.562	37.910	0.000	0.010	0.000	N/A	0.029
7	0.026	0.007	0.010	0.589	37.891	0.000	0.026	0.015	N/A	0.029
8	0.031	0.000	0.043	0.546	38.105	0.026	0.000	0.011	N/A	0.016
9	0.035	0.014	0.046	0.489	38.028	0.039	0.022	0.012	N/A	0.021
10	0.027	0.005	0.015	0.390	38.384	0.000	0.006	0.000	N/A	0.023
11	0.026	0.002	0.013	0.346	38.085	0.012	0.022	0.020	N/A	0.018
12	0.028	0.004	0.032	0.325	38.576	0.017	0.002	0.000	N/A	0.014
13	0.019	0.005	0.020	0.274	38.590	0.000	0.006	0.007	N/A	0.012
14	0.024	0.010	0.021	0.257	38.891	0.000	0.014	0.002	N/A	0.011
15	0.012	0.009	0.007	0.232	39.111	0.020	0.026	0.001	N/A	0.007
16	0.012	0.005	0.006	0.159	39.379	0.034	0.000	0.008	N/A	0.000
17	0.009	0.005	0.011	0.167	39.125	0.001	0.000	0.006	N/A	0.009
18	0.006	0.013	0.022	0.126	39.356	0.000	0.011	0.018	N/A	0.005
19	0.008	0.008	0.021	0.098	38.727	0.013	0.017	0.033	N/A	0.002
20	0.003	0.001	0.014	0.106	38.963	0.000	0.000	0.004	N/A	0.000
21	0.000	0.005	0.018	0.103	39.200	0.044	0.000	0.003	N/A	0.002
22	0.000	0.000	0.000	0.150	39.644	0.000	0.000	0.024	N/A	0.000
23	0.001	0.015	0.009	0.192	39.534	0.007	0.002	0.018	N/A	0.005
24	0.003	0.002	0.035	0.341	37.766	0.022	0.006	0.006	N/A	0.000
25	0.003	0.006	0.092	0.423	37.493	0.000	0.007	0.012	N/A	0.008

Appendix C Gel Protein Data

SDS Polyacrylamide Gel Loadings

***Terebratulina retusa* (Figure 4.2)**

	Concentration (mg/μl)	Loading (μl)
Lane 1 Unstained protein standards	-	5
Lane 2 <i>T. retusa</i> GnHCL extract	204	10
Lane 3 <i>T. retusa</i> EDTA extract	228	10

***Novocrania anomala* (Figure 4.3)**

	Concentration (mg/μl)	Loading (μl)
Lane 1 Unstained protein standards	-	5
Lane 2 <i>N. anomala</i> GnHCl extract	73	10
Lane3 <i>N. anomala</i> EDTA extract	63	10

***Mytilus edulis* (Figure 4.4)**

	Concentration (mg/μl)	Loading (μl)
Lane 1 Unstained protein standards	-	5
Lane 2 <i>M. edulis</i> GnHCL extract	541	10
Lane 3 <i>M. edulis</i> EDTA extract	208	10

***Gallus gallus* (Figure 4.6)**

	Concentration (mg/μl)	Loading (μl)
Lane 1 Unstained protein standards	-	5
Lane 2,3&4Eggshell EDTA extract	171	10

